Synthesis and Properties of Chemically Modified Carbon Nanotubes

MUSTAFA KEMAL BAYAZIT

Synthesis and Properties of Chemically Modified Carbon Nanotubes

A thesis submitted for the partial fulfilment of the requirement for the Degree of

Doctor of Philosophy

In the faculty of Science of

Durham University

By

Mustafa Kemal BAYAZIT

Durham University

Department of Chemistry

University Science Laboratories

South Road

Durham

2010

Copyright

Declaration

This work was conducted in the Department of Chemistry at Durham University between October 2007 and July 2010. The work has not been submitted for a degree in this, or any other university. It is my own work, unless otherwise indicated.

Dedication

This PhD thesis is dedicated to my dearest wife Dr. Esra Gümüş BAYAZIT

Acknowledgements

I genuinely thank my supervisor, Dr. Karl S. Coleman, and would like to extend my sincere gratitude to him for his encouragement, time, support, patience and knowledge during my whole study period. I am grateful to the Scientific and Technological Research Council of Turkey (TUBITAK) who provided me with generous financial support (Grant Number: 2213) to pursue my PhD degree. I would also like to thank Prof. Dr. Nihat Celebi and Prof. Dr. Ozdemir Ozarslan for encouraging me to do PhD abroad. I acknowledge Department of Chemistry, Durham University who helped fund part of my tution fee. I would like to give a special thanks to the former head of department, Prof. Judith A.K. Howard, who believed in me and supported me during my PhD endeavor.

I would also like to thank my first year dissertation committee members Dr Philip W. Dyer and Dr Lian Hutchings, my co-supervisor and head of department Prof. John S.O. Evans who followed my progression, Prof. Martin R. Bryce who allowed me to use his laboratory facilities, Dr Nigel Clarke and Dr Lars-Olof Palsson for their insights and helpful discussions on my thesis and Dr Richard Thompson for tutoring.

I thank Dr. Graham Beamson of the National Centre for Electron Spectroscopy and Surface Analysis (NCESS) at Daresbury Laboratory for technical assistance and useful discussions on the XPS measurements, Doug Carswell for recording the TGA data, and Dr Alan Kenwright for his discussion on NMR data. I also thank Dr. A.S. Jombert for her friendship and my best British friend Chris Herron who looked after me since the beginning of my UK life.

I am especially grateful to my parents (Esme&Orhan BAYAZIT) and sisters (Fatoş&Gonca BAYAZIT) for their support throughout every stage of my life.

Finally, I wish to thank my dearest wife, Dr. Esra Gümüş BAYAZIT for her love, encouragement and support throughout my PhD study.

Table of Contents

Table of Contents

Table of Contents

Figures

Figures

Figures

Figures

Abbreviations

AFM	Atomic force microscopy
ATR	Attenuated total reflection
ATR-IR	Attenuated total reflection infrared
BCF	Benzylchloroformate
BE	Binding energy
BWF	Breit-Wigner-Fano
CNTs	Carbon nanotubes
Conc	Concentration
CVD	Chemical vapor deposition
DMAD	Dimethyl acetylenedicarboxylate
DMAP	4-dimethylaminopyridine
DMF	*N*,*N*-Dimethylformamide
DMSO	Dimethylsulfoxide
DNA	Deoxyribo nucleic acid
DNT	2,4-Dinitrotoluene
DOS	the density of electronic states
EDS	Energy dispersive spectrometry
EtOH	Ethanol
FG	Functional group
FIR	Far-infrared
FTIR	Fourier transform infra-red
FTSC	Fluorescein-5-thiosemicarbazide
HiPco	High-pressure carbon monoxide
HOMO	Highest occupied molecular orbital

HPLC	High-performance liquid chromatography
LUMO	Lowest unoccupied molecular orbital
MCF	Methylchloroformate
MWNTs	Multi-wall carbon nanotubes
NCESS	The National Centre for Electron Spectroscopy and Surface Analysis
NEMS	Nanoelectromechanical systems
NEt_3	Triethylamine
NHFA	Nitronium hexafluoroantimonate
NFP	*N*-Formylpiperidine
NMR	Nuclear magnetic resonance
2NP	2-Nitrophenol
3NP	3-Nitrophenol
4NP	4-Nitrophenol
4NT	4-Nitrotoluene
NT	Nitrosotoluene
P	Phenol
PAA	Poly(acrylic acid)
PDMS	Poly(dimethylsiloxane)
PEG	Poly(ethylene glycol)
PEI	Poly(ethyleneimine)
PLQY	Photoluminescence quantum yield
PSS	Poly(styrene sulphonate)
PTFE	Poly(tetrafluoroethylene)
PVP	Poly(4-vinylpyridine)
PVPy	Poly(vinyl pyrrolidone)

RBMs	The radial breathing modes
SDS	Sodium dodecyl sulfate
STM	Scanning tunneling microscopy
SWNTs	Single-walled carbon nanotubes
TEM	Transmission electron microscopy
TGA-MS	Thermogravimetric analysis-Mass spectrometry
THF	Tetrahydrofuran
TMS	Tetramethylene sulfone
TUBITAK	The Scientific and Technological Research Council of Turkey
UV-vis-NIR	Ultraviolet visible near infrared
VTP-EIMS	Variable temperature pyrolysis-electron ionization mass spectrometry
XPS	X-ray photoelectron spectroscopy

Abstract

Since their discovery single-walled carbon nanotubes (SWNTs) have gained the interest of many scientists and engineers due to their prominent structural, mechanical and electronic properties which make them applicable in various areas including electronics, chemical and biological sensing and reinforced composite materials. Although SWNTs have many application areas their use can be limited since they are synthesised as a mixture of metallic and semiconducting species with different diameters and helicities and they have limited solubility in aqueous and non-aqueous solvents. Covalent modification of SWNTs is an important tool to introduce new functional groups onto the surface of nanotubes to improve their solubility and processability. It can also be used to separate metallic from semiconducting nanotubes.

The work presented here has concentrated on the non-disruptive covalent modification of SWNTs using pyridine diazonium salt addition, 1,3-dipolar cycloaddition and reductive alkylation.

The selectivitiy of the addition was probed by UV-vis-NIR and Raman spectroscopy where the metallic were found to be more selective than semiconducting SWNTs. The location and distribution of the functional groups was determined by AFM using electrostatic interactions with gold nanoparticles.

Rheological data showed that the pyridine modified SWNTs were able to act as crosslinkers and hydrogen bond to poly(acrylic acid) to form SWNT hydrogels. The indolizine modified SWNTs, emitted blue light when excited *ca.* 330 nm, were capable of sensing 4-nitrophenol, 3-nitrophenol, 2-nitrophenol, 2-nitrosotoluene and 2,4-dinitrotoluene with a detection limit of *ca.* 10^{-8} M.

The modified SWNTs were further characterised using FTIR, XPS, TGA-MS and optical microscopy.

1. STRUCTURES AND PROPERTIES OF CARBON NANOTUBES (CNTs)

1.1. Introduction: Discovery of Carbon Nanotubes

Since the discovery of closed graphite shells dubbed buckminsterfullerene by Kroto *et al.*[1] in 1985, carbon has started to gain importance in nanoscale science including chemistry, biology and engineering. CNTs were first discovered around 1952 by Radushkevich *et al.* and perhaps have been around for much longer.[2,3] However it is only after Iijima's observation of CNTs[4] in 1991 that CNTs began to receive so much attention by scientists all around the world from many wide-ranging disciplines. They have since been shown to have extraordinary electrical, mechanical and thermal properties.[5-7]

1.2. Bonding of Carbon Atoms in Carbon Nanotubes

The structure of a carbon nanotube can be conceptualized by wrapping a graphene sheet into a seamless cylinder as shown in Figure 1-1.

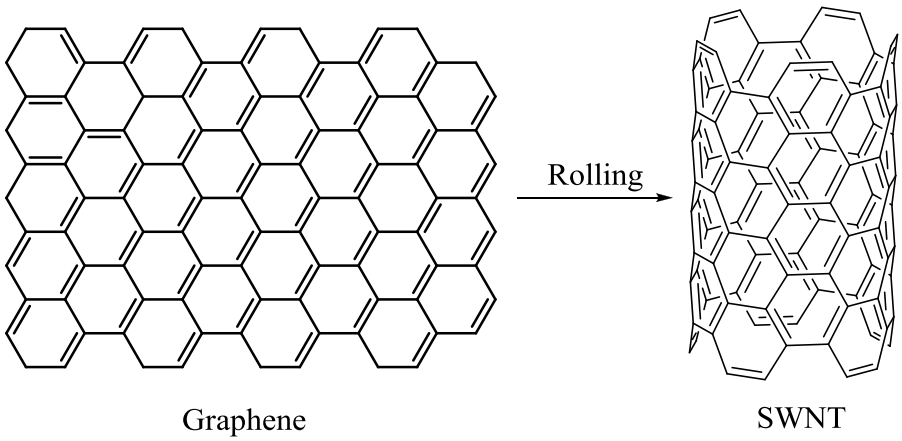

Figure 1- 1 Schematic view of carbon nanotube structure derived from a graphene sheet.

Thus, CNTs can be considered as long seamless cylinders made of a hexagonal honeycomb lattice of carbon atoms, the ends of which can either be capped by two halves of fullerene or left open.

A carbon atom has six electrons, two are accommodated in the 1s orbital and the remaining four electrons occupy the 2s and 2p orbitals, which are responsible for bonding.

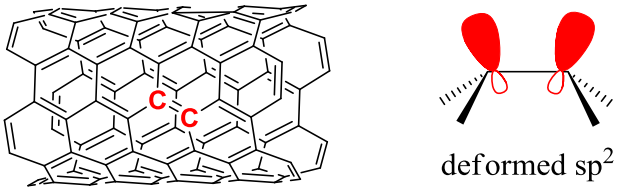

Figure 1- 2 Schematic representation of C-C bond in single-walled carbon nanotube framework

CNTs have deformed sp^2 hybridization due to the circular curvature.[7] Deformation in sp^2 hybridization causes the shifting of the three σ bonds, which lie in the sp^2 plane, to out of plane. As a result the π orbital is more delocalized outside to compensate as shown in Figure 1-2. This type of symmetry change in the sp^2 orbital makes nanotubes chemically more reactive, mechanically more strong, and electrically and thermally more conductive than graphite.[7] Additionally, they produce topological defects such as pentagons and heptagons in the hexagonal network to form capped, bent, toroidal, and helical nanotubes where electrons are localized in pentagons and heptagons because of redistribution of π electrons.[7] There can also be sp^3 hybridized carbons, formed from the carbon framework due to oxidation, which also results in the formation of terminal esters, anhydrides and carboxylic acid groups at the open end of nanotubes, Figure 1-3.

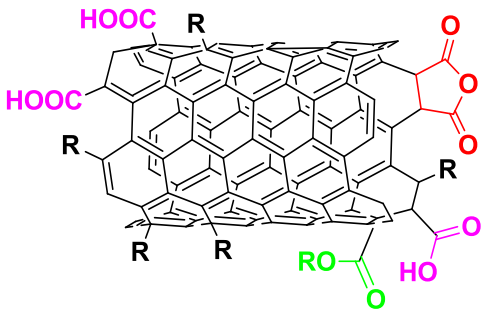

Figure 1- 3 A schematic representation of possible surface defects in a SWNT (R=alkyl)

1.3. Types of Carbon Nanotubes

In general, nanotubes can form in two distinct categories.[8-10] One of them, single-walled carbon nanotubes (SWNTs) which consist of a single cylinder, and which have been used in this work, have a diameter of close to 1.0 nm, with a tube length that can be many thousands of times longer. A SWNT can be represented using a vector **C** with two integers (*n*,*m*) related to graphite vectors $\boldsymbol{a_1}$ and $\boldsymbol{a_2}$, Figure 1-4.[7,11] For unique definition of the structure of a particular nanotube, one needs to define a chirality vector, in terms of integer multiples of two primitive lattice parameters of graphene, that exactly maps the circumference of the carbon nanotube. This chirality vector can be defined as $\mathbf{C_h = n a_1 + m a_2}$, where '*n*' and '*m*' are integers,[12,13] Figure 1-4. The tubes with $m = n$ are generally referred to as armchair tubes and $m = 0$ as zigzag tubes. Others are named as chiral tubes in general with the chiral angle q, Figure 1.4.[7]

The other type of nanotubes are multi-walled carbon nanotubes (MWNTs),[4] which are made of multiple concentric cylinders of increasing diameter placed around a central axis with spacing between each shell of the order of the spacing between two adjacent layers in graphite (3.4 Å) and diameter in the range of 10-20 nm.[14]

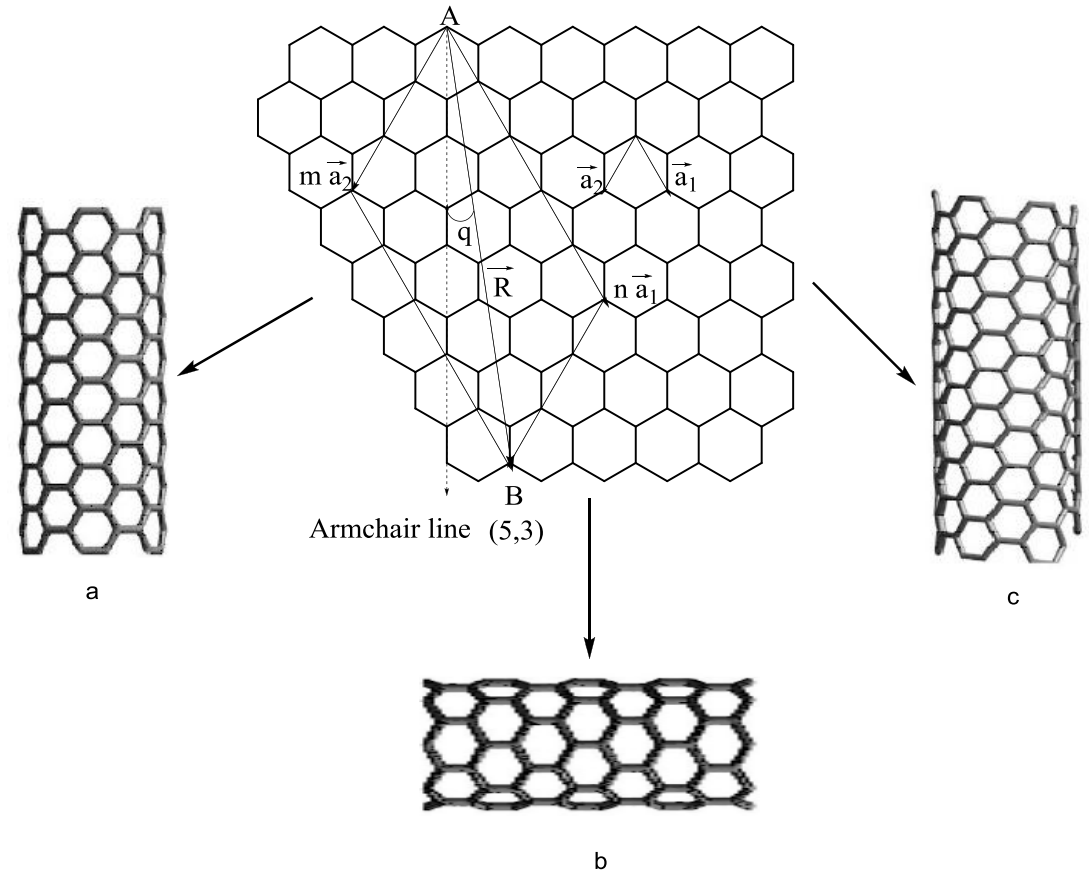

Figure 1- 4 A schematic representation of nanotube formation via rolling graphite sheet along the chiral vector $C = na_1 + ma_2$ where the n and m are integers and a_1 and a_2 are graphite lattice vector. The diagram is for a (5,3) nanotube. (a), (b) and (c) represent armchair (*m*, *m*), zigzag (*n*,0) and chiral (*n*,*m*) nanotubes, respectively.

1.4. Electronic Properties of Carbon Nanotubes

The electronic properties of nanotubes have received much attention in carbon nanotube research and applications. According to both experimental and theoretical results SWNTs can be considered as either metallic or semiconducting depending on the wrapping angle of the graphene sheet with regards to the tube axis.[12,13,15-18] Figure 1-5 displays the chirality map which shows the various types of SWNTs that can be formed. The extraordinary and unique dependence of electronic structure on chirality vector arises from the fact that, in a single graphene sheet, the conduction and valence bands just

touch each other at the six corner points, called as Fermi points which are one particular electron state, of the hexagonal first Brillouin zone. The Fermi point refers to an event chirality of electrons is involved and the diameter of a carbon nanotube for which the nanotube becomes metallic. This unusual band structure has a direct consequence on the electronic properties of graphene making it a zero band gap semiconductor. When a graphene sheet is rolled into a SWNT, periodic boundary conditions are imposed in the circumferential and as a result, each band of graphene splits into a number of 1-D sub bands. The allowed energy states of the tube are the cuts of the graphene band structure. When these cuts pass through a Fermi point, the tube is metallic whereas if no cuts pass through a Fermi point, the tube is semiconducting.[19]

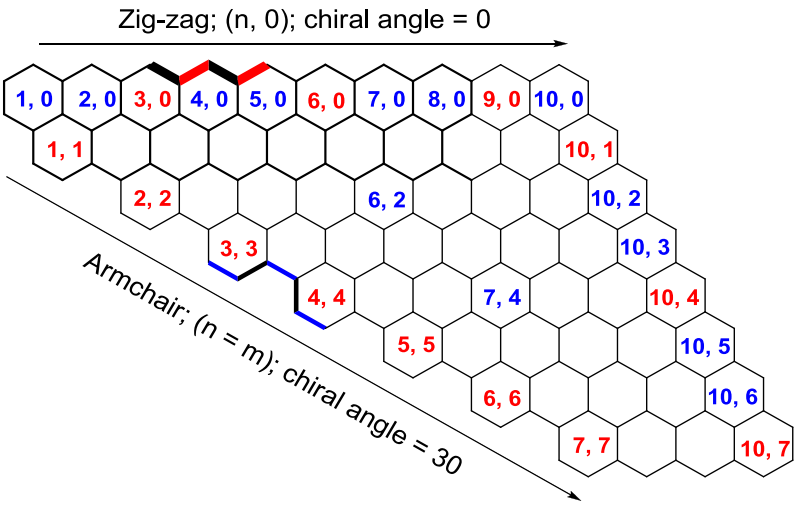

Figure 1-5 Graphical representation of chirality map which displays the different types of SWNTs that can be formed via rolling a graphene sheet. SWNTs denoted by blue (n, m) are semiconducting and red (n, m) are metallic.

Moreover, calculations[12,13,15-17] reveal that all armchair tubes (n=m) are conducting, while the other tubes, which are zigzag and chiral, are either small band gap semiconductors (as a consequence of curvature-induced mixing of π and σ states) if

n-m=3i or otherwise truly semiconducting with larger band gaps if n-m≠3i, where '*i*' is a non-zero integer. Theoretical calculations also predict that one third of the tubes are metallic and two thirds are semiconducting.[13] Scanning tunneling microscopy (STM) studies on SWNTs, by Wildöer *et al.*[18] and Odom *et al.*[20] confirm these predictions experimentally. However, carbon nanotubes (CNTs) are always produced as a mixture with a distribution of diameters and chirality and no method has so far been discovered to synthesize individual carbon nanotubes having the same chirality.

1.5. Synthesis of Carbon Nanotubes

There have been numerous published review articles[21-24] available on the synthesis of carbon nanotubes. Several methods have been used to synthesize SWNTs including arc discharge, laser ablation, chemical vapor deposition (CVD), high-pressure carbon monoxide (HiPco) and flame methods. These methods are summarized in Table 1-1.[25]

Method/Date	Authors	Procedure	Comments
Arc discharge/ 1993	Iijima[10] Bethune[9]	Produced at more than 2500 ^{o}C applying 50–500 Torr CH_4/Ar or He in the presence of Fe or Co catalyst in carbon	First method for SWNTs
Laser ablation /1996	Thess *et al.*[26]	Produced at 1200 ^{o}C in furnace introducing 500 Torr Ar in the presence of Ni/Co catalyst in carbon	First laser ablation
CVD/1996	Dai *et al.*[27]	Produced at 1200 ^{o}C applying 1.1 atm CO in the presence of Mo, Co/Ni catalysts	First CVD growth
CVD (HiPco)/1999	Nikolaev *et al.*[28]	Produced at 1200 ^{o}C applying 10 atm CO in the presence of $Fe(CO)_5$ vapor	Synthesis of HiPco SWNTs

Flame/ 2000	Vander Wal *et al.*[29,30]	Produced at 900–1400 in flame introducing N_2/Ar/air + C_2H_2 or C_2H_4 in the presence of metallocene	First flame synthesis

Table 1-1 List of methods to produce carbon nanotubes[25]

1.6. Applications of Carbon Nanotubes

Since the discovery of carbon nanotubes, they have attracted much interest due to their small dimensions, strength and their exceptional physical properties. Thus, they have been accepted as a unique material with a wide range of favorable scientific and industrial applications and have already been applied successfully for field-effect transistors,[31-33] nano-tweezers,[34] high resolution atomic probes,[35] chemical probes,[36] mechanical actuators,[37] hydrogen storage,[38] non-volatile random access memory,[39] field-emission displays,[40] data storage devices,[41] and chemical sensors.[42]

Moreover, single walled carbon nanotubes are among the strongest and most resistive materials known to exist in nature due to their mechanical properties. SWNTs have a Young's modulus approximately 1 TPa and tensile strength nearly 50 GPa, which are greater than Young's modulus (200 GPa) and tensile strength (400 MPa) of stainless steel.[43] These values are in accord with with the in-plane values for graphite and with that of diamond, and also agree with theoretical estimates for CNTs.[44,45] Direct measurements performed by an AFM set-up in a scanning electron microscope (SEM) also showed similar values of Young's modulus, and tensile strengths of the order of 20 GPa.[46,47] Hence, nanotubes can tolerate large strain before mechanical failure.[42,48,49] Together with their light weight, their strength makes nanotubes an ideal candidate for reinforcement in polymer composite materials,[50-60] which have applications in many

areas such as the construction of aircraft, space-craft and earthquake-resistant houses[61] and nanoelectromechanical systems (NEMS).[62-68]

1.7. Purification of Carbon Nanotubes

CNTs synthesised by any of the methods given in Section 1.5 contain considerable amounts of impurities, mostly metal catalyst particles and other forms of carbon such as metal catalyst-containing carbon nanospheres and polyaromatic carbons including fullerenes. Although producing CNTs, as pure as possible, is the main goal of many researchers, many post purification techniques have been developed to date. Most common techniques involve thermal oxidation in air,[26] hydrothermal treatment,[69] H_2O-plasma oxidation,[70] acid oxidation,[71] dispersion separation by microfiltration,[72] high-performance liquid chromatography (HPLC).[73] In addition to those techniques, a non-destructive purification technique has been reported by Murphy *et al.*[74] including the use of a polymer host system to extract the graphitic impurities without the use of any oxidation steps.

Although there are many purification methods, it is not possible to produce a specific type of nanotube without contamination. Even after multiple purification techniques, purified material always contains small amounts of impurity such as catalyst particles and any other carbonaceous materials. Generally people working with CNTs apply more than one technique for the removal of all undesirable materials that appear during the synthesis. However, many purification techniques harm the nanotubes causing defect sites, either on sidewalls or on the open ends of the nanotube. Although defects cause many changes in physical, mechanical and electronic properties, they can be very useful reactive sites for further reactions to functionalize the nanotubes.

1.8. Functionalisation of Carbon Nanotubes

CNTs are both highly polarizable and smooth-sided compounds. Individual tubes attract each other with an attractive force of 0.5eV/nm. Due to high cohesive interactions, CNTs having large molecular weights appear as bundled structures or ropes.[75] This characteristic of CNTs gives rise to low solubility and poor dispersion in common organic solvents, aqueous solutions and polymeric matrices. Another factor affecting dispersion quality is the lack of interfacial interactions between the nanotube and the solvent. On account of these two factors, it is difficult to process the pristine carbon nanotubes, especially SWNTs, in ordinary medium without altering their surface properties. In order for the full potential of CNTs to be realized much effort has focused on their surface chemistry. The introduction of surface groups has the obvious advantage of introducing extra functionality to the CNTs which can be important for sensing, self assembly in electronic devices or even as points of attachment for polymers or biomolecules. Also the surface groups have the added advantage of interrupting the strong van der Waals forces that cause aggregation or bundling of the material, particularly problematic for single-walled carbon nanotubes (SWNTs) and thus aid dispersion in both aqueous and non-aqueous solvents.[76] Several strategies including covalent and non-covalent techniques have been developed to overcome the solubility problem and to produce reactive side groups which could interact with different systems, Figure 1-6.[8] Methods for noncovalent[8,77,78] and covalent[8,78-80] functionalisation of SWNTs have recently been reviewed.

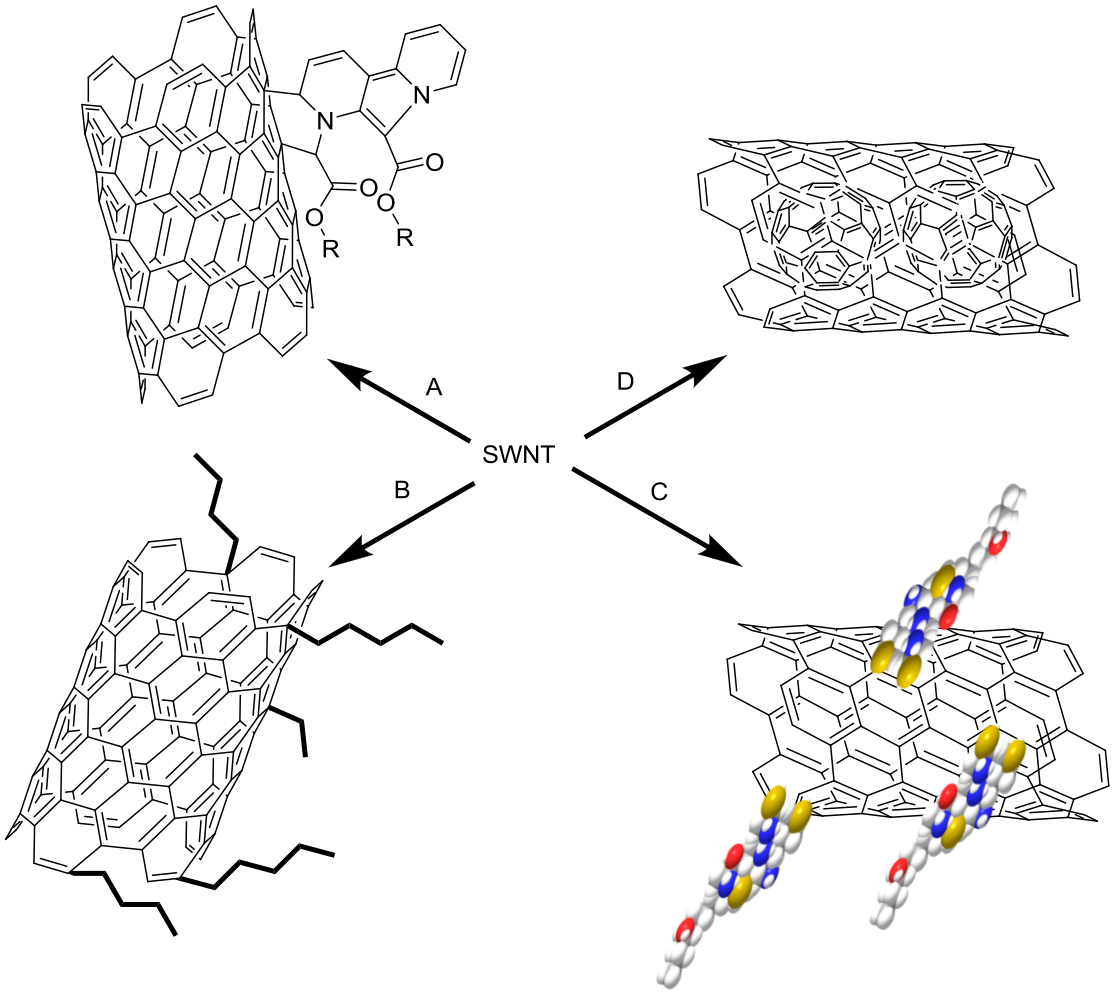

Figure 1-6 Functionalisation possibilities for SWNTs: A) covalent sidewall functionalisation, B) defect-group functionalisation, C) non-covalent exohedral functionalisation with surfactants or polymers, D) endohedral functionalisation with, for example, C_{60} . For methods B-C, the groups attached to nanotube surface are representative.

1.8.1. Non-covalent Sidewall Functionalisation of Carbon Nanotubes

Non-covalent functionalisation increases the solubility of CNTs in solutions without harming the side wall and the electronic properties of tube. Here, the interaction between tube surface and the wrapped materials is mainly π-π stacking or van der Waals forces. The major disadvantage of non-covalent routes for the modification of CNTs is that they can make large portions of the CNT surface inaccessible, which

could be a disadvantage for applications such as electronics. Non-covalent functionalisation of CNTs using surfactants such as sodium dodecyl sulphate,[81,82] sodium dodecylbenzene sulphonate,[83,84] cationic surfactants such as benzalkonium chloride,[72] and non-ionic surfactants such Triton-X[81] has widely been used to prepare stable dispersions of de-bundled CNTs. Treatment of CNTs with polymer matrixes including polystyrene sulphonate (PSS) and polyvinyl pyrrolidone (PVPy) resulted in highly soluble CNTs.[75] Solubility of CNTs has also been enhanced using different polymers such as poly(acrylic acid) (PAA),[85] polyethylene,[86] poly(dimethylsiloxane) (PDMS),[87] and natural polymers, such as Gum Arabic[88] and starch.[89] It has been reported that CNTs could be non-covalently modified to increase solubility and processability in water using proteins and DNA.[90-92] It has also been shown that biomolocules[93-95] for biosensor development and large aromatic compounds[96-99] such as pyrene could be used for the non-covalent functionalisation of CNTs.

1.8.2. Covalent Sidewall Functionalisation of Carbon Nanotubes

Covalent functionalisation of SWNTs produces sp^3 hybridized carbon atoms on the side wall. The common aspect of each functionalisation method is the use of highly reactive species to attack nanotube sidewalls. Functionalisation occurs at defect sites along the sidewalls and tube ends, which are also easily oxidized to form open tubes. Hence, covalent functionalisation increases the solubility and processability of carbon nanotubes. However, it may distort or destroy the unique properties of the nanotube network. Several covalent functionalisation methods are available such as defect site production using acids[81,100] and functionalisation from the defects,[101] producing carboxylic acid groups on the end caps and subsequent reactions from the acids,[36,102] and direct covalent sidewall functionalisation.[80] Chen *et al.* have further functionalised

the oxidized nanotubes (acid-cut nanotubes) using long chain alkylamines via acylation, and the modified material showed enhanced solubility in organic solvents, Figure 1-7.[103] Homon *et al.* have reported that direct thermal mixing of oxidized nanotubes and alkylamines produced soluble modified material through the formation of zwitterions, Figure 1-7.[104]

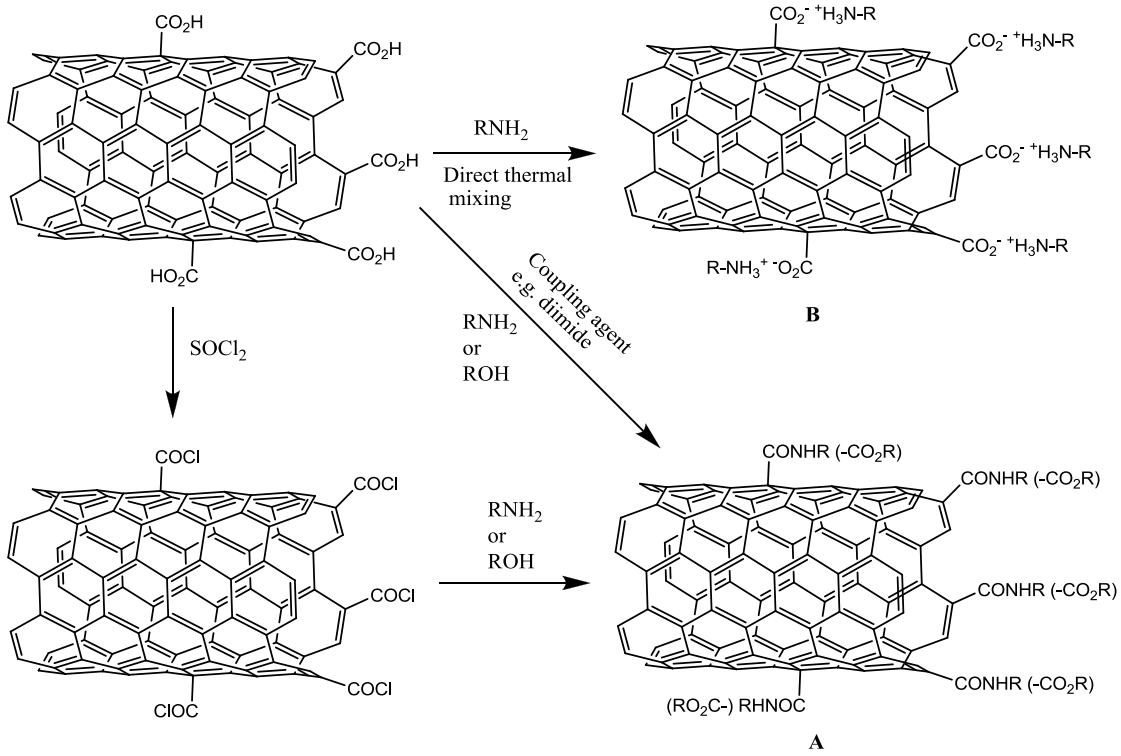

Figure 1-7 Amidation/esterification (A) and zwitterions formation (B) reactions of oxidized nanotubes through the defect sites of the surface

In addition to defect site chemistry several methodologies for the covalent sidewall functionalisation have been reported to date, Table 1-2.[25] Substituted benzene diazonium salts have widely been used to functionalise surface of SWNTs. This method can be carried out with both electrochemical reduction of the salt[105] and treating the surfactant-wrapped nanotubes[29,83,106-108] with the reactive salt intermediate in aqueous solutions.[109] In addition, it is possible to use arene diazonium intermediates

directly or prepared *in situ* using organic solvents[110] or oleum,[111] or without solvent.[112] Another interesting method is fluorination that was first used by Mickelson and coworkers.[113] Fluorinated SWNTs can be reacted with many other organic species such as organolithium and Grignard reagents to diversify the nanotubes.[114] Another technique includes the formation of alkyl radicals and reaction with the tube surface.[115] The Billups reaction was developed by Liang *et al.* to lithiate the nanotube surface in the presence of liquid ammonia.[116] Prato *et al.*[117] used a 1,3-dipolar cycloaddition of an azomethine ylide generated *in situ* from an amino acid and aldehyde to form lightly functionalised but highly soluble SWNTs. Four other methods that use highly reactive intermediates to functionalise carbon nanotubes are nitrene decomposition, the Bingel reaction, dichlorocarbene formation, and pyridinium ylide cycloaddition as developed by Holzinger,[118] Coleman,[119] and Kamaras[120] respectively. Covalent sidewall modification of SWNTs via diazonium, cyloaddition and reductive alkylation pathways shall be described in detail in Chapter III, IV and VI.

Methodology	**Functional Group (FG)**	**Characterization Techniques**	**Degree of Functionalisation**	**Highest Solubility**
Diazonium[105,109,110,112]	Aryl	UV-vis-NIR, TGA, Raman, XPS, ATR-IR, AFM, TEM	1 FG in every 10 carbons in SDS/water and 1 FG in every 25 carbons in organic solvent or neat	0.8 mg/mL in DMF
Diazonium in Oleum[111]	Aryl	UV-vis-NIR, Raman, TGA, XPS, ATR-IR, AFM, TEM	1 FG in every 20 carbons	0.25 mg/ mL in H2O
Fluorination[113]	Fluorine	ATR-IR, AFM, STM, VTP-EIMS, UV-vis-NIR, Raman, TGA	1 FG in every 2 carbons	1 mg/mL in 2-propanol
Radical	Alkyl	Raman, ATR-IR,		Not given

Chemistry[115]		UV-vis-NIR, TGA	1 FG in every 6 carbons	
Billups reaction[116]	Alkyl, aryl	TEM, AFM, Raman, ATR-IR, TGA-MS	1 FG in every 17 carbons	Not given
Azomethine ylides (Prato reaction)[117]	Pyrrolidine	UV-vis-NIR, Raman, TEM	1 FG in every 100 carbons	50 mg/mL in $CHCl_3$
Nitrene[118]	Aziridene	XPS, AFM, TEM, NMR, Raman UV-vis-NIR	1 FG in every 50 carbons	1.2 mg/ mL in DMSO
Bingel reaction[119]	Cyclopropane	AFM, ^{19}F-NMR, XPS	1 FG in every 50 carbons	Not given
Dichlorocarbene[120,121]	Cyclopropane	Mid-IR, Raman, EDS, TGA, UV-vis-NIR,AFM	1 FG in every 25 carbons	Not given
Free-radical additions[122,123]	Perfluorooctyl	AFM, UV-vis-NIR, ^{19}F-NMR	Not given	Not given
Reductive alkylation[116,124-131]	Alkyl	Raman, TGA, XPS, STM	1 FG in every 31 carbons	Not given

Table 1-2 Common SWNT Sidewall Functionalisation Methodologies (adapted from Ref. 25)

1.9. Selectivity of the addition reactions

Application of carbon nanotubes in electronics[31-33,40,41,132] has gained much interest due to the extraordinary electronic properties of the material. Since the nanotubes have been produced as a mixture of metallic and semiconducting species with different diameters and helicities and no method has been developed for the production of single type nanotube, selective covalent functionalisation of the nanotube sidewall as a method of separation has become increasingly important. However both experimental and theoretical studies show that introducing new groups on nanotube sidewall via addition reactions is more difficult than the classical organic chemistry on a

conjugated π-system.[8,78,130,133-136] It is also very important to use the most versatile spectroscopic technique for the identification of the electrically distinct nanotubes. Although the original mapping of the electronic transitions of carbon nanotubes in terms of their diameters has been done by Kataura[137] there are also several experimentally interesting examples studied to assign the optical features of the semiconducting and metallic nanotubes using band-gap fluorescence,[108,138] UV-vis-NIR[108,139] and Raman spectroscopy.[106,139,140] Since it has been noticed that the functionalisation of SWNTs might be a tool for the separation of metallic and semiconducting nanotubes several strategies have been suggested for the modification of SWNTs including diazonium salt addition, cycloaddition and reactive organometallic compound additions.

Diazonium salt addition to SWNTs has been extensively studied by Bahr and co-workers.[80,105,110] The authors have reported that the small-diameter SWNTs could be derivatized using the electrochemical reduction of aryl diazonium salt. Saini *et al.* have shown that the small-diameter HiPco nanotubes could be alkylated following the fluorination.[141] However no information of the reactivity/selectivity of the metallic and semiconducting nanotubes has been reported in those publications.

Kamaras *et al.* have shown that the pristine SWNTs with strong far-infrared (FIR) absorption, characteristic of metal, are not changed following the introduction of octadecylamine groups which make nanotubes soluble in organic solvents. However it was reported that the introduction of cyclopropane groups using dichlorocarbene generated from $PhHgCCl_2Br$ resulted in a change in far-infrared absorption bands revealing the sensitivity of the metallic properties to the introduction of defects.[120]

Strano *et al.* have reported that metallic rather than semiconducting SWNTs suspended in SDS solution could be functionalised using diazonium reagents under carefully controlled conditions, Figure 1-8.[139] It has also been reported that the semiconducting

nanotubes could be separated from the metallic ones controlling the nanotube reaction pathways. They have also pointed out that the reactivity of the metallic nanotubes was inversely proportional to their diameter.

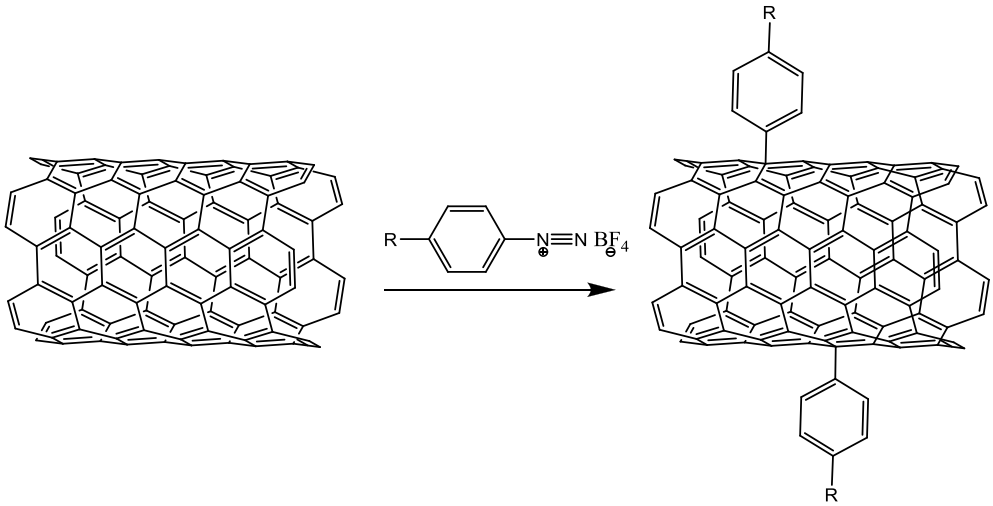

Figure 1-8 Schematic representation of diameter-selective diazonium reaction (R=Cl,[139,142] Br,[143] OH[144-146])

The selective addition of the diazonium salts to SWNTs surface has been probed using UV-vis-NIR and solution-phase Raman spectroscopy (532 nm) to monitor valence-to-conduction electronic transitions of metallic and semiconducting nanotubes and the change in low-frequency Raman modes assigned to semiconducting and metallic SWNTs, respectively. Proposing a reaction mechanism where the diazonium reagent produces a charge transfer complex on nanotube sidewall the preference of the addition to metallic nanotubes has been explained by the electronic states, Figure 1-9, close to Fermi level which causes the stabilisation of the transition states by electron donation from nanotube to diazonium salt while covalent attachment takes place.[139]

Selectivity of the 4-chlorobenzenediazonium salt addition to SWNTs surface has been further investigated by Strano *et al.* using solution phase resonance Raman spectroscopy with a range of laser excitation wavelengths (532, 633, 785 and 830 nm)

to produce experimental mapping of electronic transitions, Figure 1-8.[142] The author has again shown that the addition to SWNTs favored metallic species over semiconducting ones. Electronic transition maps provided by Strano have opened the way for discussing the selectivity of the addition reactions using the radial breathing modes (RBMs) in the Raman spectra of modified SWNTs.

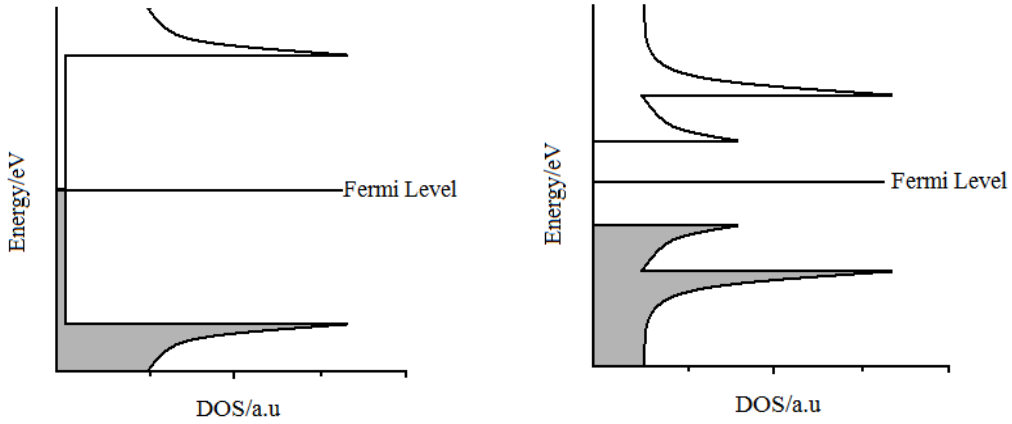

Figure 1-9 Schematic representation of the density of electronic states (DOS) for a metallic (left) and a semiconducting (right) nanotube.

Wang *et al.* have compared the electrical and Raman spectral responses of the pristine and 4-bromobenzene modified SWNTs to explain and optimize the effects of the diazonium chemistry on the electrical conductivity of random networks of SWNTs with different transistor channel lengths, Figure 1-8.[143] Pristine SWNTs have been grown on a silicon substrate using a CVD method and, the diazonium reaction has been carried out using low reagent concentrations. Results have concluded that there was a preference for metallic tubes to react with 4-bromobenzene diazonium showing a small suppression of metallic tube conductivity. Moreover the authors have pointed out that is was possible to observe significant suppression of the metallic tube conductivity when high concentrations of the diazonium reagent, which reacts with semiconducting nanotubes, were used.

Kim *et al.* have described a new protocol for the enrichment of one electronic-type SWNT applying the selective functionalisation of SWNTs using 4-hydroxybenzene diazonium salt followed by free solution electrophoresis, Figure 1-8.[144] Raman and UV-vis-NIR results revealed that the electrophoresis could be a versatile technique for the separation of metal-enriched SWNTs from semiconductor-enriched SWNTs due to their differences in electrophoretic mobilities. The same author has also demonstrated that the selective functionalisation of the metallic SWNTs with 4-hydroxybenzenediazonium salts could change the density of the individual SWNT and, the change in densities could be used for the selective separation of metallic SWNTs from semiconducting ones, Figure 1-8.[145]

Nair *et al.* have described the electronic structure-selective chemistry on nanotubes performing reactions of SWNTs with 4-hydroxybenzenediazonium salt at various diazonium concentrations and temperatures, with or without illumination of visible light, Figure 1.8.[146] Results assessed using UV-vis-NIR spectroscopy revealed that rate of diazonium salt addition to metallic nanotubes were greater than semiconducting ones and the selectivity of the addition could be controlled using the low concentration of reactive diazonium reagent.

Fantini *et al.* have stated that the functional groups on aryldiazonium salts have a significant effect both on selectivity and reactivitiy.[147] Raman and UV-vis-NIR results revealed that the modification of metallic SWNTs via *p*-nitrophenyl groups was more reactive than *p*-chlorophenyl groups, whereas the *p*-chlorophenyl addition was more sensitive to the tube diameter.

Doyle *et al.* have studied the structure-dependent relative reactivities of 4-substituted benzene dizonium salts, Ar-R (Ar = N_2^+-C_6H_4 and R = Cl, NO_2, $N(CH_3)_2$, OCH_3, COOH and OH) towards SWNTs in both acidic (pH 5.5) and basic (pH 10) conditions using near-infrared fluorescent spectroscopy for semiconducting species and UV-vis-

NIR for metallics.[148] Results revealed that the reactivities of the salts at pH 10 were the greatest for SWNTs having the largest band gaps (small diameter) and, the magnitude of this band gap dependence varied according to the R-group attached, with R = OMe showing the strongest variation. In contrast acidification of the sample to pH 5.5 resulted in a reverse reactivity order for R = OH and COOH showing affinity towards smaller band gap (large diameter) SWNTs.[148]

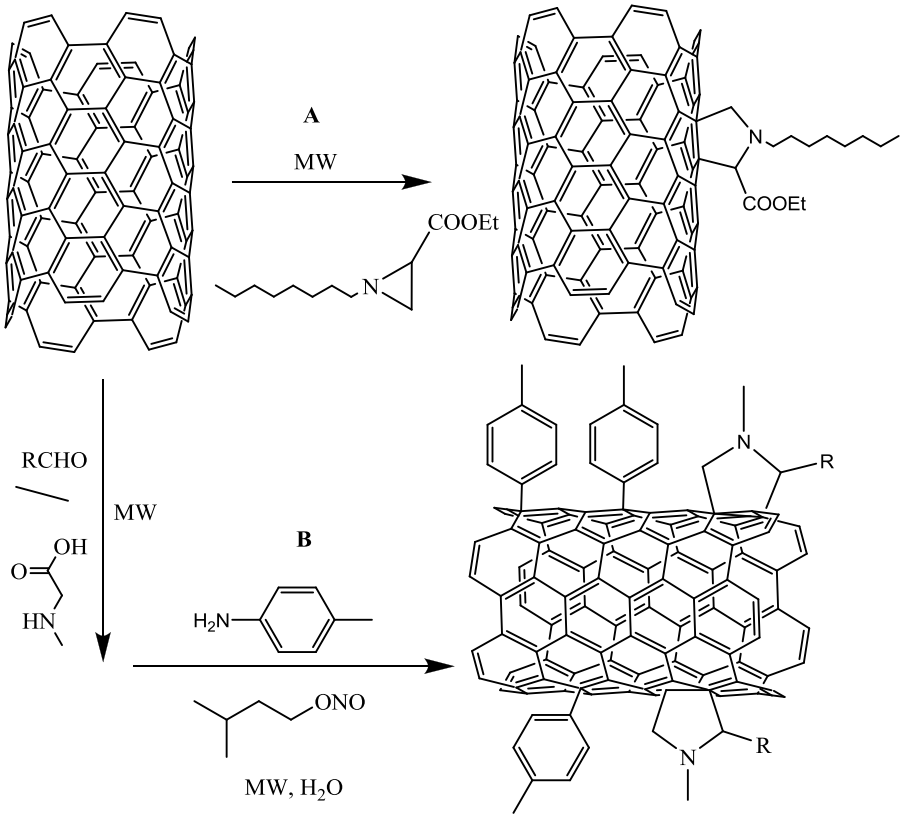

Figure 1-10 Schematic representation of the microwave-assisted cycloaddition of aziridines to SWNTs[149] (**A**) and microwave-induced multiple functionalisation of SWNTs via 1,3-dipolar cycloaddition of substituted azomethine ylides[150] (**B**) (R= hexyl, undecyl, 3,5-dimethoxyphenyl and 3,4,5-dodecoxyphenyl)

Raman spectroscopy results of the microwave-assisted cycloaddition of aziridines to SWNTs and microwave-induced multiple functionalisation of SWNTs via 1,3-dipolar cycloaddition of substituted azomethine ylides (R = hexyl, undecyl, 3,5-

dimethoxyphenyl and 3,4,5-dodecoxyphenyl) followed by the addition of 4-methylbenzenediazonium salts reported by Brunetti *et al.* have revealed that the metallic nanotubes could be more easily functionalised compared with semiconducting ones, Figure 1-10.[149,150]

An alternative method for the covalent functionalisation of SWNTs using azomethine ylides generated by double deprotonation of the trialkylamine-*N*-oxides bearing pyrenepropyl and anthraceneethyl groups has been reported by Ménard-Mayon *et al.*.[151] Results provided using Raman spectroscopy have revealed that the addition of the pyrrolidine ring to SWNT surface was selective for semiconducting nanotubes.

Hamon *et al.* have demonstrated that the SWNTs could be functionalised using singlet oxygen most likely producing either the [2 + 2] or [4 + 2] cycloaddition product on nanotube sidewall and the addition was selective for metallic nanotubes over semiconducting ones.[152]

An example for the chiral selective addition to SWNTs framework has been demonstrated by Banerjee and group.[153] Their protocol has included osmylation of the SWNTs in the presence of solution phase OsO_4 using a photochemical reaction pathway. Selectivity of the addition has been probed by Raman spectroscopy using different laser excitations revealing the reactivity of the metallic versus semiconducting nanotubes. It has also been reported that the driving force for the metallic selectivity was the large electron density of the metallic nanotubes near Fermi level which stabilizes the intermediate charge transfer complex formed by OsO_4. The authors have also stated that the dissociation of the charge transfer complex has resulted in both covalent sidewall functionalisation and templating of OsO_2, formed by reduction of OsO_4, on the nanotube sidewall. In a separate article the same author discusses the diameter-selective reactivity of the solution phase ozonolysis of SWNTs.[154] In contrast to osmylation, results have revealed that the ozonation of

SWNTs was a diameter dependent reaction where the smaller diameter nanotubes reacted more extensively than larger diameter tubes, which was explained by the pyramidalization and π-orbital misalignment.[79,136]

An *et al.* have shown a scalable method for a diameter-selective removal of metallic SWNTs from semiconducting ones by dispersing pristine SWNTs in tetramethylene sulfone (TMS)/chloroform solution with nitronium ions (NO_2^+) produced from nitronium hexafluoroantimonate (NHFA).[155] Results evaluated using resonance Raman spectroscopy have revealed that the small diameter nanotubes (less than 1.1 nm) were completely destroyed and removed while semiconducting remained intact. The reason for the metallic nanotube reactivity has again been explained by the strong electron transfer from metallic nanotubes to nitronium ions.

Yang *et al.* have reported another technique for the selective removal of small diameter metallic SWNTs using the nitronium ions (NO_2^+) which can form a charge transfer complex with nanotubes.[156] In general this technique can be considered as a continuation of the method defined by An *et al.* where the nitronium hexafluoroantimonate (NHFA) has been used as a source for nitronium ions (NO_2^+) formation. In this case they have used HNO_3/H_2SO_4 solution as a source of nitronium ions (NO_2^+) which can attack π electrons on the carbon nanotube surface. Results confirmed by resonant Raman and optical absorption spectra have revealed that metallic nanotubes with a diameter range of 0.9-1.1 nm were completely destroyed and removed due to the more electron density at the Fermi level while semiconducting nanotubes remained intact.

Density functional calculations on NO_2 adsorption reported by Seo and co-workers have also stated that adsorption of NO_2 molecule on nanotube surface was an electronic structure-dependent and a strain-dependent process and preferably occured on metallic nanotubes rather than semiconducting.[157] Calculations have also revealed

that charge density at Fermi level had a very important role for the adsorption of acceptor type adsorbate.

Hemraj-Benny *et al.* have shown that the photochemical adddition of silyl groups on a nanotube surface was possible using trimethoxysilane and hexaphenyldisilane.[158] Selectivity profile analysis of trimethoxysilane and hexaphenyldisilane addition reaction was carried out using resonance Raman spectroscopy and UV-vis-NIR. In trimethoxysilane addition the smaller diameter semiconducting nanotubes, in the range of 0.79-0.84 nm, were more reactive than the metallic nanotubes. In contrast, hexaphenyldisilane addition was less-diameter selective compared with trimethoxysilane.

A new reaction sequence for the covalent modification of SWNTs including the nucleophilic addition of *tert*-butyllithium to nanotube surface followed by re-oxidation using bubbling oxygen has been described by Graupner *et al.*, Figure 1-11.[159] Raman spectroscopy revealed that the addition of *tert*-butyl groups to SWNT sidewall was selective for metallic nanotubes over semiconducting ones.

Wunderlich *et al.* have reported the covalent addition of organolithium and organomagnesium compounds (*n*-Buli, *t*BuLi, EtLi, *n*HexLi, *n*BuMgCl, *t*BuMgCl) to SWNTs, Figure 1-11.[130] Modified SWNTs were characterised using NIR-fluoresence and Raman spectroscopies and results revealed that the reaction of organometallic compounds with SWNTs exhibited more selectivity towards smaller diameter metallic nanotubes than semiconducting ones.

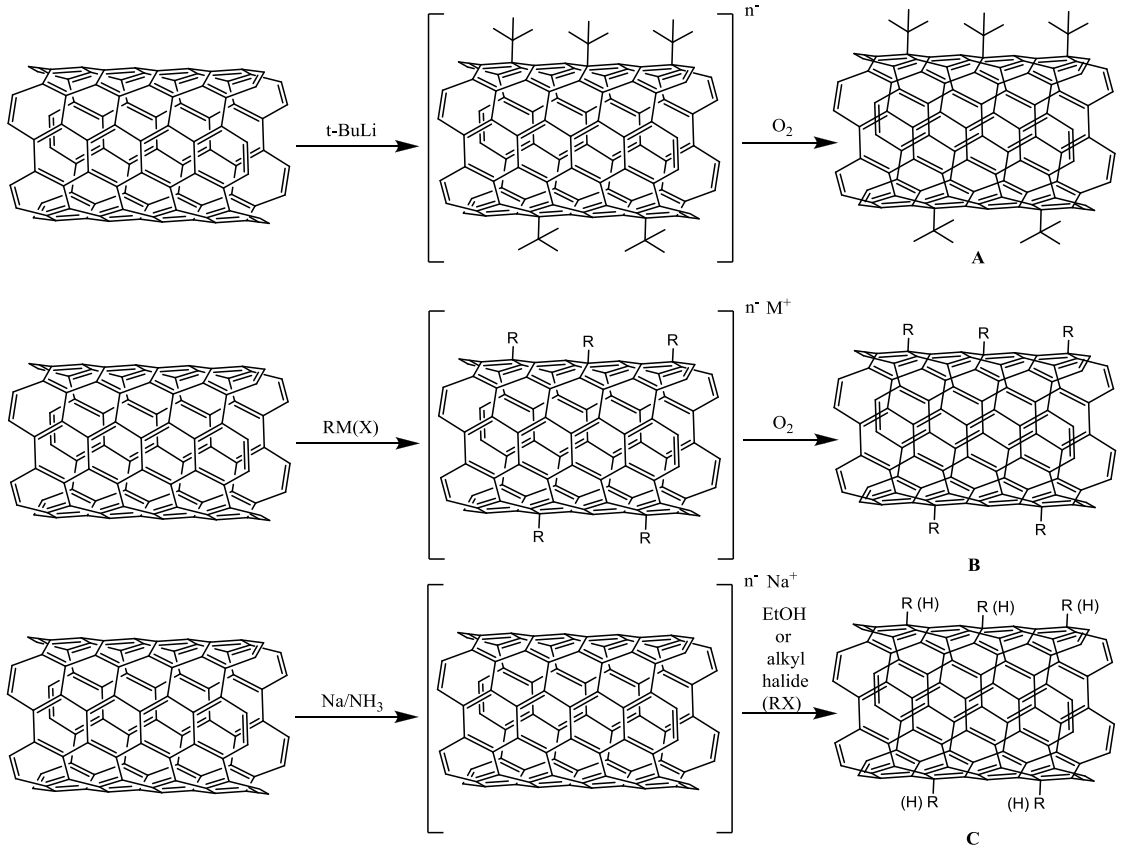

Figure 1-11 Schematic representation of (**A**) *tert*-butyllithium to nanotube surface followed by re-oxidation,[159] (**B**) covalent addition of organolithium and organomagnesium compounds (R= *n*Bu, *t*-Bu, Et, or *n*Hex; M=Li or Mg; X=Cl (for M=Mg),[130] (**C**) the covalent sidewall modification of SWNTs by the reduction with sodium (Billups reaction) followed by alkylation with butyl iodide.[131]

In a separate article Wunderlich and colleagues have also shown that the covalent sidewall modification of SWNTs by the reduction with sodium (Billups reaction) followed by alkylation with butyl iodide was selective for smaller diameter metallic nanotubes over semiconducting ones using UV-vis-NIR, NIR emission and Raman spectroscopic techniques, Figure 1-11.[131]

Muller *et al.* have demonstrated the diameter dependence of the pentyl and dodecyl addition to SWNTs following the Billups reduction using the resonance profiles of the radial breathing modes (RBMs).[160] Results showed that the addition was selective and

inversely proportional to the tube diameter where both smaller diameter metallic and semiconducting nanotubes were more reactive than larger ones and, the chain lengths did not influence this trend.

Pekker *et al.* have shown that the *n*Buli and *t*BuLi addition to SWNTs is preferred by small diameter nanotubes calculating the optical conductivites of the electronic transitions in the range of 0-50000 cm^{-1}.[161]

Fernando *et al.* have shown that the SWNTs could be functionalised repeatedly using diamine-terminated oligomeric poly(ethylene glycol).[162] Diameter selectivity analysis performed using UV-vis-NIR and Raman showed that the reaction was selective for smaller diameter nanotubes, regardless of their being semiconducting or metallic.

It has also been reported that the metallic and semiconducting nanotubes could be selectively separated each other using electric fields[163] and non-covalent attachments including the use of surfactants and single-stranded DNA.[95,164]

Selectivity of the addition reactions to the SWNTs sidewall has theoretically been investigated by Niyogi *et al.*[79] and Chen *et al.*[136] revealing that the metallic tubes having smaller diameters are preferrable due to misallignment of π-orbitals and sp^2 C atoms exhibiting a higher degree of pyramidalisation.

Joselevich *et al.* have also theoretically discussed the electronic structure and chemical reactivity of carbon nanotubes.[165,166] It has been pointed out that the diameter selective additions to SWNTs could be explained by the curvature-induced local strain due to the sp^2-hybridized carbon atoms.[79,136] The author has also commented that the selectivity of metallic nanotubes over semiconducting ones was dependent on the electronic band structure of the nanotubes. The reason for this trend has been explained by the reduced aromaticity of the metallic nanotubes which have a smaller HOMO-LUMO gap.[165,166]

In this work chemically modified SWNTs have been synthesised using known organic reactions (diazonium reactions, 1,3-dipolar cycloaddition reactions and reductive alkylation), and the properties of the modified SWNTs have been investigated. The structures of functionalised SWNTs have been characterised using spectroscopic (eg. FTIR, XPS, Raman, luminesence, UV-vis-NIR), thermal (eg. TGA-MS) and microscopic (eg. AFM, optical microscopy) methods.

2. CHARACTERISATION OF COVALENTLY FUNCTIONALISED SWNTS

2.1. Overview

Characterisation of covalently modified CNTs has been a major issue since the chemistry of CNTs started more than a decade ago. It has been pointed out in almost every publication by nanotube researchers that the characterisation of modified nanotubes specifies a constant issue in nanotube research. Since the discovery of nanotubes, several techniques have been applied for adequate characterization of the functionalised nanotubes including FTIR,[167-170] Raman,[171-173] UV-vis-NIR,[108,118,138,174] fluorescence and X-ray photo electron spectroscopies, thermogravimetric analysis (TGA)[175,176] and atomic force microscopy (AFM),[177-181] scanning tunneling microscopy (STM),[177] scanning electron microscopy (SEM)[81,113,168,182] and transmission electron microscopy (TEM).[109,113,116,118,127,168,183,184] It has been noted that a combination of many if not all of these should be sufficient to fully characterise the modified nanotubes.[8,78,80,114,118,177,183,185-189] Table 2-1 displays commonly used techniques with their limitations and a brief explanation for sample preparation and the characterisation of the chemically modified carbon nanotubes.

Technique	Typical Sample Form	Outcomes	Limitations
FTIR	Solid, liquid	Functional group analysis	No direct evidence for covalent functionalisation and degree of functionalisation
Raman	Solid, liquid	Shows the change in D band indicating the covalent functionalisation	Gives limited evidence for degree of functionalisation

			Continue
UV-vis-NIR	Solution	Gives a direct evidence for covalent modification	No evidence for degree of functionalisation
Fluorescence Spectroscopy	Solution	Shows the tagged fluorescence groups on nanotube surface or the directly produced fluorescence groups on nanotube surface confirming the covalent functionalisation	No evidence for degree of functionalisation
XPS	Solid	Shows elements present in sample and gives an idea about degree of functionalisation	No direct evidence for covalent functionalisation and degree of functionalisation
TGA	Solid	gives an idea about degree of functionalisation	No direct evidence for covalent functionalisation
SEM	Solid	Shows the change in morphology	No direct evidence for covalent functionalisation
TEM	Solid	Gives the image of the sample but sometimes gives direct evidence of covalent functionalisation when the groups tagged with nanoparticles	No evidence for degree of functionalisation
STM	Solid	Displays the distribution of the nanotube	No evidence for degree of functionalisation, needs conductive material
AFM	Solid	Gives information about the topography of raw modified material but sometimes gives direct evidence of covalent functionalisation when the groups tagged with nanoparticles	No evidence for degree of functionalisation

Table 2-1 Commonly used techniques with their limitations and a brief explanation for sample preparation and the characterisation of the chemically modified carbon nanotubes.

2.2. Fourier-transform infrared spectroscopy (FTIR)

Infrared spectroscopy is a versatile tool for studying pure rotational, pure vibrational, and rotation-vibration energy changes in the ground state of molecules.[190] Infrared spectroscopy deals with the interaction between a molecule and radiation from the IR region (IR region = 4000 - 400 cm^{-1}) of the electromagnetic spectrum spectrum. The

appearance of a vibrational transition in the infrared region depends on an overall change of the electric dipole moment during the vibration, and the intensity of the bands are dependent on the magnitude of the dipole moment change.[190] Infrared method gives information on vibrational frequencies which have been extensively used to fingerprint certain groups in different molecules.

In nanotube research FTIR is used to provide information of the functional groups present on SWNT surface. Figure 2-1 shows the FTIR spectrum of the pristine SWNTs recorded using ATR.

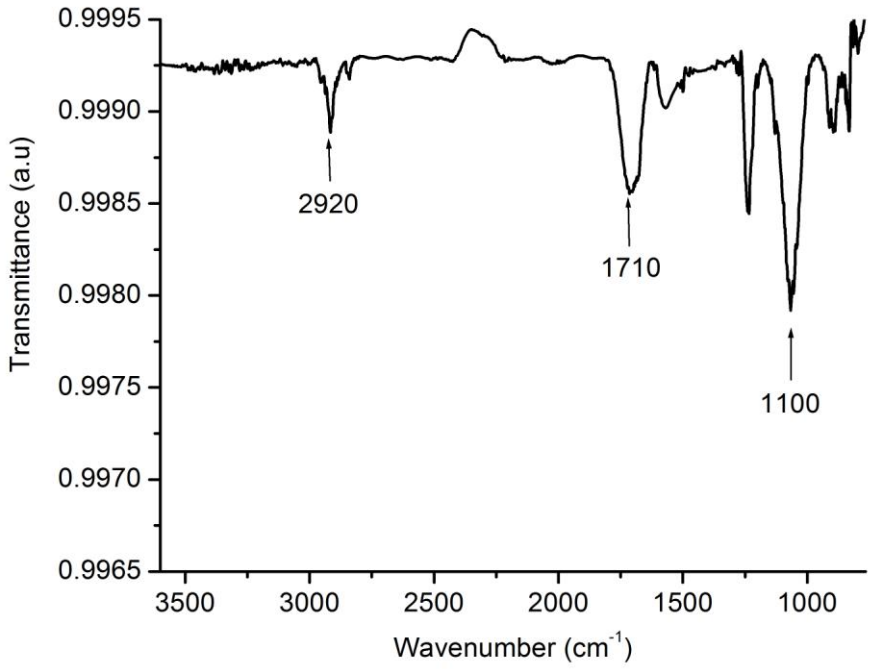

Figure 2- 1 FTIR spectrum of the purified SWNTs recorded using ATR technique.

Although direct information of the covalent functionalisation can not be provided it is possible to elucidate the presence of various organic functional groups including COOH(R), $-NO_2$, $-SO_3$, $-NH_2$, -OH and $-CH_n$ using FTIR.[116,167,191,192] Spectra have been recorded either preparing a thin film of the CNT material or using ATR technique. It has been reported that CNTs showed three main bands which are

attributable to C=O stretching, C-O-C stretching and C-H stretching at *ca.* 1710, 1100 and 2920 cm^{-1}, respectively.[193] It is thought that the bands appeared due to the presence of the carboxylic acid produced during the purification period. Thereafter, it has been widely used for characterising modified SWNTs.[102,103,105,115,116,168,169,194,195]

2.3. Raman Spectroscopy

Raman spectroscopy is concerned with the frequency of the light scattered by molecules as they undergo rotations and vibrations. The theory of Raman scattering depends on the collision of incident light with a molecule where the molecule is induced by the collision to undergo a pure rotational, or a vibrational, or a rotation-vibration change.[190] When monochromatic light of frequency ν_0 strikes a cell containing a transparent substance, most of the light passes through unaffected. However some of the light is scattered by the sample in all directions, Figure 2-2.[190]

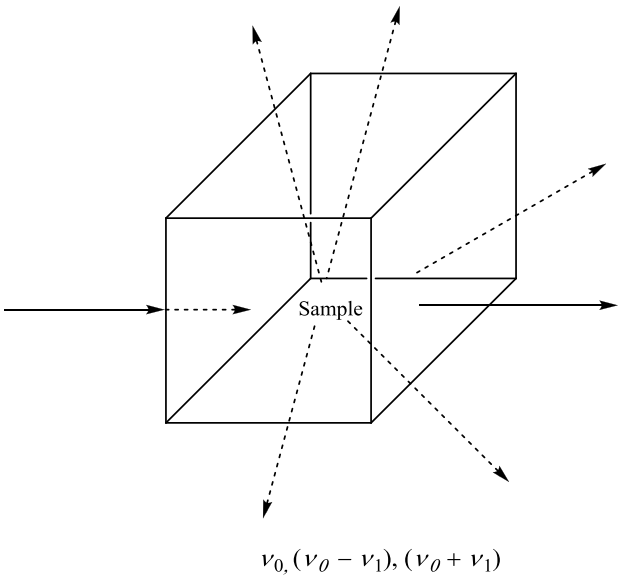

Figure 2- 2 Occurrance of scattered light with frequencies ν_0 , (ν_0 - ν_1) and (ν_0 + ν_1).

The scattered light contains photons having the same frequency ν_0 as the incident light (elastic scattering) and different frequencies from that of the incident light such as

(v_0 - v_1) and (v_0 + v_1). The difference corresponds to the energy change which has taken place within the molecule. The lines having lower frequency than the incident light (v_0 - v_1) are termed as Stokes lines (red shifted), while the high-frequency lines (v_0 + v_1) are known as anti-Stokes lines (blue shifted), Figure 2-3. For vibrational transitions the anti-Stokes lines are usually weaker than the Stokes lines. In contrast to infrared spectroscopy, Raman spectroscopy is dependent on a change in the polarizability during the vibration, and the Raman intensity is concerned with the polarizability of the vibrating atoms and their bonds present.[190]

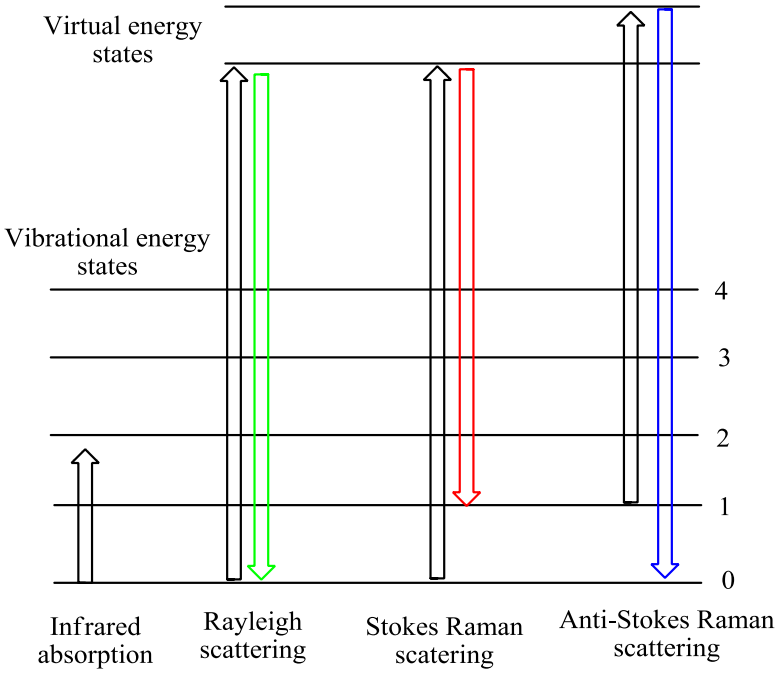

Figure 2- 3 Energy level diagram of states in Raman signal.

Resonance Raman spectroscopy has been used extensively for determining a wealth of information regarding the nanotube chirality, electronic type and degree of chemical functional groups (or defects) present.[131,142,146,154,164,196,197] Figure 2-4 shows the representative Raman spectrum of the purified SWNTs excited at 632.8 nm. A typical Raman spectrum of SWNTs can be divided into four regions; the RBM (radial breathing mode) typically 100 – 400 cm^{-1}, the disorder or D band from 1280 – 1320

cm^{-1}, the graphene or G band (tangential mode) 1500 – 1600 cm^{-1} and the G´ (or D*) band ca. 2600 cm^{-1}. The RBM is inversely proportional to the diameter of the nanotube [$\omega_{RBM} = A + (B/d_t)$, where A = 223.5 nm cm^{-1}, B = 12.5 cm^{-1} and d_t is the nanotube diameter in nm] which in turn can be related to the chirality of the SWNT as $d_t = (a\sqrt{(n^2+m^2+nm)})/\pi$, where *n* and *m* are the chiral integers and *a* is the lattice vector of graphene (= $d_{(c\text{-}c)}\sqrt{3}$, where $d_{(c\text{-}c)}$ is the C-C bond length in nm). The RBM mode is used to consider the selectivity of the addends towards the different diameter nanotubes.[131,191] The D band is dispersive (shifts to higher frequency as the excitation energy increases) and is linked to the reduction in symmetry of the SWNTs as result of functionalisation or the presence of defects. The ratio of this band with the tangential band (G) is widely used to assess the degree of chemical modification in SWNTs.[103,113,115,116,124,168,169,182,194,198-201] The tangential mode can be split into two components ω^{+}_{G} and ω^{-}_{G} associated with vibrations along the nanotube axis and vibrations perpendicular to the nanotube axis.

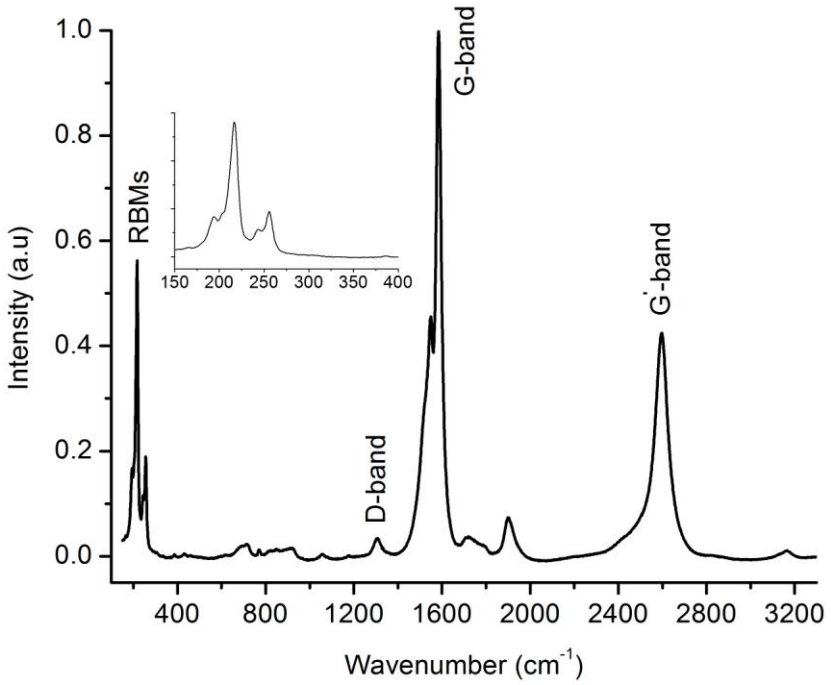

Figure 2-4 Resonance Raman spectrum of purified SWNTs excited at 632.8 nm and normalized at G-band. Inset: RBMs region.

The ω^{+}_{G} component, at higher wavenumbers, has Lorentzian line shape for both metallic and semiconducting SWNTs and is diameter independent whereas the ω^{-}_{G} mode exhibits diameter dependence and is asymmetrical in metallic SWNTs and best described by a Breit-Wigner-Fano (BWF) lineshape.[202]

The G´ (or D*) band is a two-phonon second order Raman scattering process that is pressure dependent and has been used to monitor stress transfer in carbon nanotube composites.[203]

Raman spectroscopy is also a powerful tool to probe the selectivity of the reactions applied for functionalisation.[204] In general small changes in RBMs can be used as a measure of selectivity since they are diameter dependent modes. It is important to note that, to provide a complete picture of the chiralities present, several lasers of different excitation frequency must be used. RBM region Raman spectra interpretations carried

out for the aryl diazonium salt addition, nitrene cycloaddition and reductive alkylation reactions has revealed a preference for metallic over semiconducting SWNTs.[118,130,131,142,159] It has also been noted that the intensity of the G-band relative to RBM could change as a result of covalent modification.[105,109,110,159,183]

Raman spectroscopy has also been used for deducing the reversibility of the chemical modification method used. It has been observed that thermal annealing of the cyclopropanated SWNTs was unable to restore the disrupted CNTs structure.[169] It has also been shown that it was possible to restore the properties of the aryl diazonium modified SWNTs by annealing at high temperatures under inert atmosphere.[109]

2.4. Ultraviolet-visible-near infrared (UV-vis-NIR) spectroscopy

Electronic spectroscopy (uv = 200-400 nm, visible = 400-800 nm) is corresponded to electronic transitions between the energy levels that correspond to the molecular orbitals of the systems.[205] When an atom or molecule absorbs energy, electrons are excited from their ground state to an excited state, Figure 2-5.

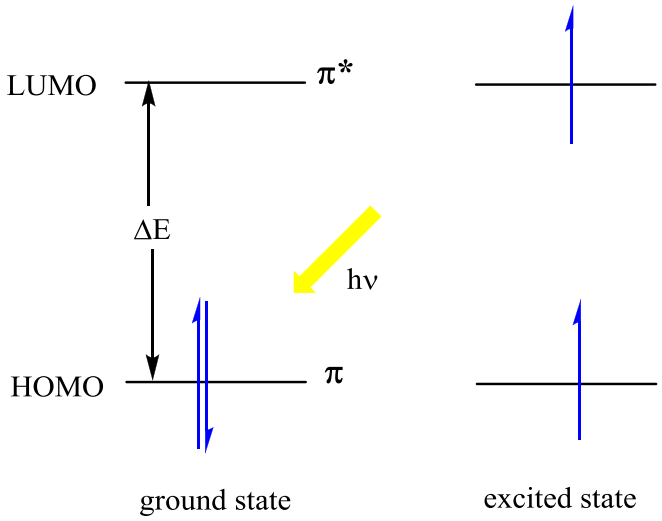

Figure 2- 5 Schematic representation of the electronic transitions between π and π* orbitals.

Transitions involving π orbitals and lone pairs (non-bonding) are important and so UV-vis spectroscopy is of most use for identifying conjugated systems which are in energetically more accesible.[205]

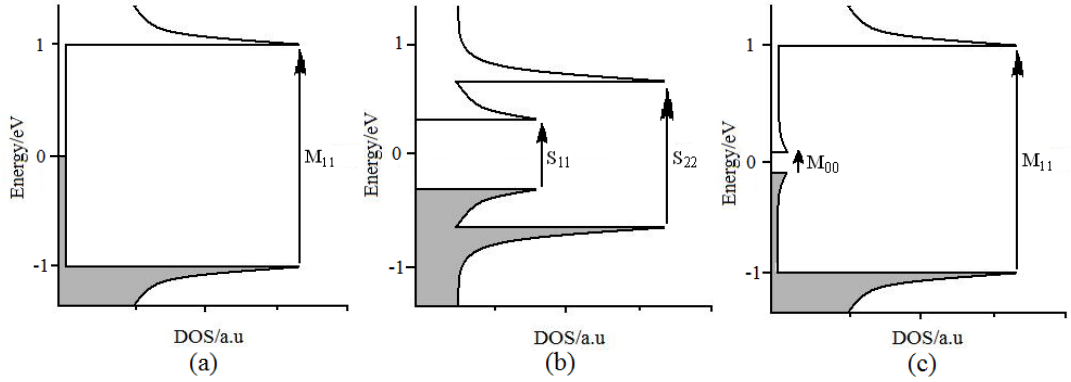

Figure 2- 6 Schematic illustration of the density of states of SWNTs. (a) Metallic SWNT (M_{11} represents the first metallic transition). (b) Semiconducting SWNT (S_{11} and S_{22} represent the first and second semiconducting transitions, respectively). (c) Small gap semiconducting SWNT (M_{00} represents the transition in chiral and zigzag metallic SWNTs).

The electronic structure of the SWNTs can be explained by the electronic properties of 2-D graphene sheet representing a continuous electronic density of states (DOS) which splits into series of spikes in SWNTs called van Hove singularities, Figure 2-6.[206]

Optical absorption measurements in the UV-vis-NIR region show the transitions between the electronic densities of state in SWNTs which appear as absorption bands.[103,137] Figure 2-7 displays the electronic spectrum of the purified SWNTs recorded in DMF.[134,139,144,145,152,161]

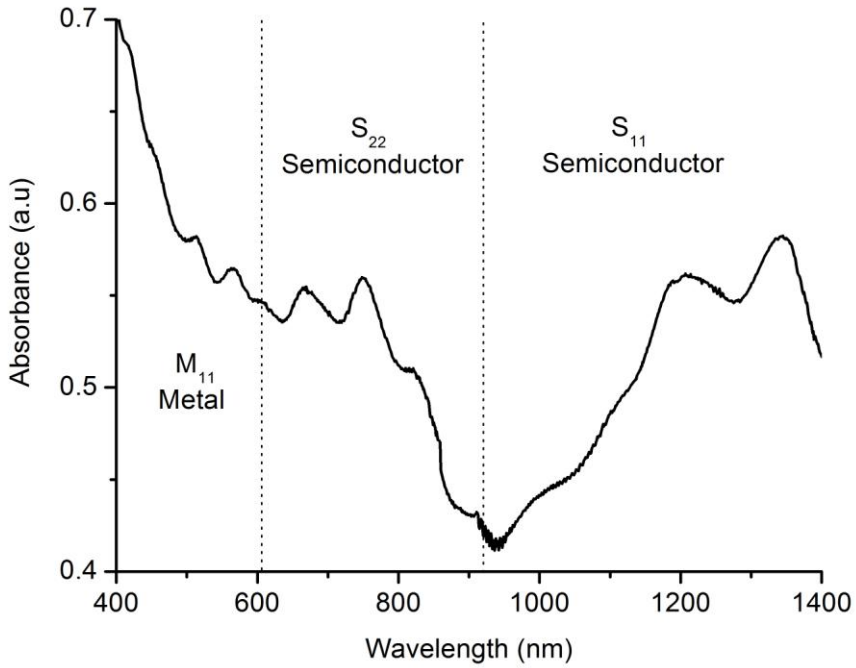

Figure 2- 7 Normalised (at 400 nm) UV-vis-NIR spectrum of purified SWNTs recorded in DMF. M_{11}, S_{22} and S_{11} denote the metallic, semiconducting and semiconducting transitions, respectively.

From the figure, it is seen that the first metallic transitions (M_{11}), the second semiconducting (S_{22}) and the first semiconducting (S_{11}) transitions occur in 400-600, 600-900 and 900-1400 nm regions, respectively.[206] It has been reported that any disruption in electronic structure caused by the covalent modification induces the suppression of the electronic transition bands.[103] This finding has favoured the use of UV-vis-NIR spectroscopy as a common technique to provide direct evidence of covalent modification.[105,109,110,117,168,184,194,207]

Besides direct evidence for covalent modification, UV-vis-NIR spectroscopy can also be used as a versatile tool for providing information on reactivity and/or selectivity of the modification technique. Strano and co-workers have followed the aryl diazonium addition to SWNT surface using UV-vis-NIR spectroscopy and reported that the

addition is selective for metallic over semiconducting SWNTs.[139] Moreover it is also possible to get the information on the reversibility of the modification technique by thermally annealing the modified SWNTs at high temperatures. A few articles have been published on reversibility of modified SWNTs stating that the pristine SWNTs could be restored.[198] Electronic spectra of the restored SWNTs have displayed the characteristic van Hove singularities as an indication of reversibility.[208]

Absorption spectroscopy has been widely used to calculate the solubility of the pristine and modified SWNTs using Beer's law and an extinction coefficient of 30 mL mg^{-1} cm^{-1} and absorption values at λ=700 nm.[209] It is known that the modification of SWNTs leads to an increase in solubility. Thus, a dispersion of modified CNTs will have a higher absorbance than that of pristine CNTs, and this can also be taken as proof of CNT derivatisation.[194]

2.5. Fluorescence Spectroscopy

Emission of light by a substance is known as luminesence, and it occurs when an electron returns to the electronic ground state from an excited state and loses its excess energy as a photon. When a molecule absorbs UV radiation it is excited from a vibrational level in the electronic ground state to one of the many vibrational levels in the electronic excited state which is usually the first excited singlet state where all electrons in the molecule are spin-paired, Figure 2-8.[205]

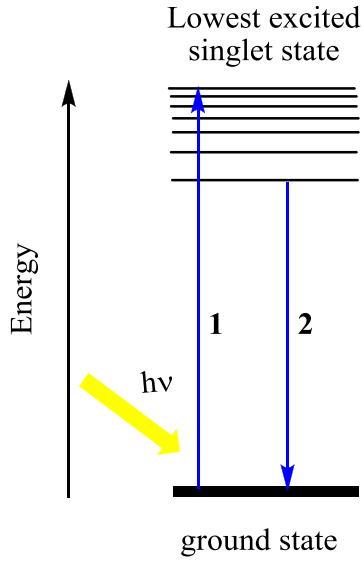

Figure 2- 8 Schematic representation of fluorescence process following absorption of a photon by a molecule

A molecule in a high vibrational level of the excited state loses energy to other molecules through collision and falls to the lowest vibrational level of this state. The molecule also partitions the excess energy to other possible modes of vibration and rotation. Fluorescence occurs when the molecule returns to the electronic ground state, from the excited singlet state, by emission of a photon.[205]

Fluorescence spectroscopy can be applied for characterizing the modified SWNTs if the material has the fluorescent groups on surface. It has been reported that the light emitting groups could be introduced to SWNT sidewall by either tagging a fluorescent group[210,211] or producing the group on surface.[191] Prato and his group have shown that pyrene, porphyrin, quinoline and phthalocyanine chromophores could be tagged to CNTs.[212-214] Furthermore they have reported that enough emission signals could be determined from chromophore group functionalised SWNTs.[212-214]

2.6. X-ray photoelectron spectroscopy (XPS)

XPS is a very informative surface chemical analysis technique that can be used to analyze the surface chemistry of the material. It provides a wealth of information related to elemental composition, empirical formula, chemical state and electronic state of the elements present in sample. The theory behind this technique is the photoelectric effect which is the ejection of electrons from atoms or molecules by electromagnetic radiation. The photoelectric effect was explained by Einstein in 1905 using the quantum theory from which he derived the relationship:[205]

$$\text{K.E. (ejected electrons)} = h\nu - \text{BE}$$

where ν is the frequency of the ultraviolet light and BE is the energy of the electronic level from which the electron was ejected measured as a core binding energy. The binding energies of core electrons are highly characteristic of the element present in sample. Small 'chemical shifts' in binding energies give information about the surrounding chemical environment of an atom, allowing deductions to be made about the chemical structure of the sample.[205]

When a solid sample is bombarded with X-rays of sufficiently high energies (in excess of 1000 eV) to stimulate (photo)emission of electrons from the core energy levels of atoms, several processes (either photoelectric process where the sample loses a photoelectron to yield excited ion S^{*+}, or the sample undergoes an electronic transition to produce an excited state of the atom or molecule S*) occur depending on the energy of source, Figure 2-9.[205]

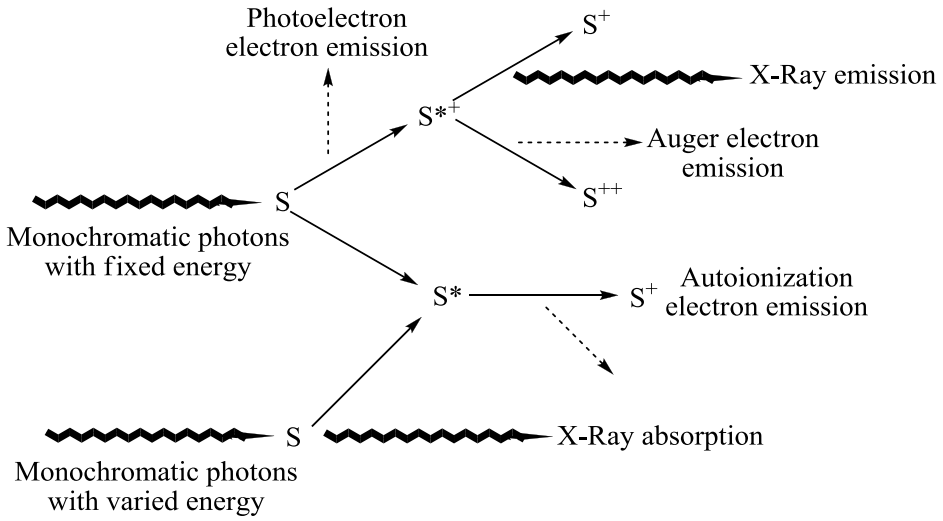

Figure 2- 9 Schematic representation of the processes occured when sample is bombarded with a monochromatic beam of photons (S represents one type of sample atom).

The main requirements for X-ray photoelectron spectrometers are high resolution and monochromatic X-radiation, UHV pumping equipment, collision and preparatory chambers, an electron energy analyser, and counting and recording equipment, Figure 2-10.[205]

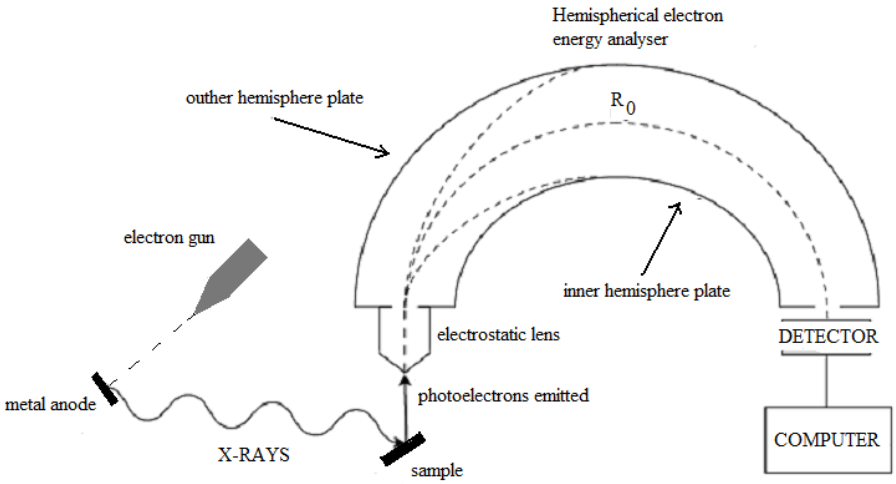

Figure 2- 10 Schematic diagram illustrating the basic design of an X-ray photoelectron spectrometer.

XPS has been extensively used to monitor the surface chemistry of functionalised SWNTs.[76,118,119,182,184,191,201,215-218] It has generally been used to identify the heteroatom elements (F, I, N and S). Although no direct evidence of covalent functionalisation has been provided it is useful for the quantification of degree of modification. However, quantification can be complicated by overlapped binding energies. Deconvoluted XPS bands in a spectrum can be used to study fine structures on SWNTs. Chakraborty and co-workers have recently published the electronic fine structures of 4-nitrophenyl modified SWNTs confirming the covalent modification.[218] It has also been reported that the C1s XPS spectrum of oxidized SWNTs can be deconvoluted to find the oxygen-containing functional groups present.[201] Several articles have been reported for the identification of the hetero atoms in modified SWNTs including the fluorination/de-fluorination of CNTs,[182,215,217] fluorinated chains introduced via the Bingel reaction,[119] iodine addition,[184] cycloadditions with nitrogen containing groups[118] and covalent addition of sulfur.[216]

2.7. Thermo gravimetric analysis (TGA)

TGA, is a weight- and temperature-sensitive technique, which has been used extensively to determine the characteristic of carbon nanotubes (purity), degradation temperature, absorbed moisture content, the level of metal particles which are used as catalysts in the production of the nanotubes and solvent residues. TGA plot of the purified SWNTs recorded under inert atmosphere in the range of 100-900 ^{o}C shows a mass loss attributable to various components in the nanotube material, including amorphous carbon, groups produced by oxidation during the purification, and graphitic particles. TGA analysis of modified SWNTs has been performed under inert atmospheres (He, Ar or N_2) to determine the weight loss upon heating and the degree of functionalisation and TGA coupled with gas phase mass spectrometry (MS) has

been used for the identification of the groups fragmented during heating process.[105,109,115,116,124,168,175,176,183,184,189,191,198] The temperature at which the groups come off can be used as indicative of covalent functionalisation since the attached groups will come off considerably at high temperatures compared to the adsorbed groups.[127]

2.8. Atomic force microscopy (AFM)

AFM technique is based on the use of a cantilever with a tip or probe (typically 10 - 20 nm in radius) at the end, which is used to monitor the sample surface as it is raster scanned across it, Figure 2-11. The probe movement in the x- , y- and z-directions is controlled using x - , y- and z-piezoceramic elements respectively, by applying voltage across them. The probe is maintained at a constant vertical force which is controlled by the voltage applied to the z-piezoceramic element. A laser (typically HeNe, 632.8 nm) reflected from the top of the cantilever onto a four-segment, position sensitive photodetector is used to monitor deflections of the cantilever (in the z-direction). Three-dimensional map of the sample is built using the changes in the position of the laser along the photodetectors y-axes. A constant vertical force exerted upon the sample is maintained using a feedback loop by adjusting the height of the sample relative to the probes z-position to compensate for surface features encountered.

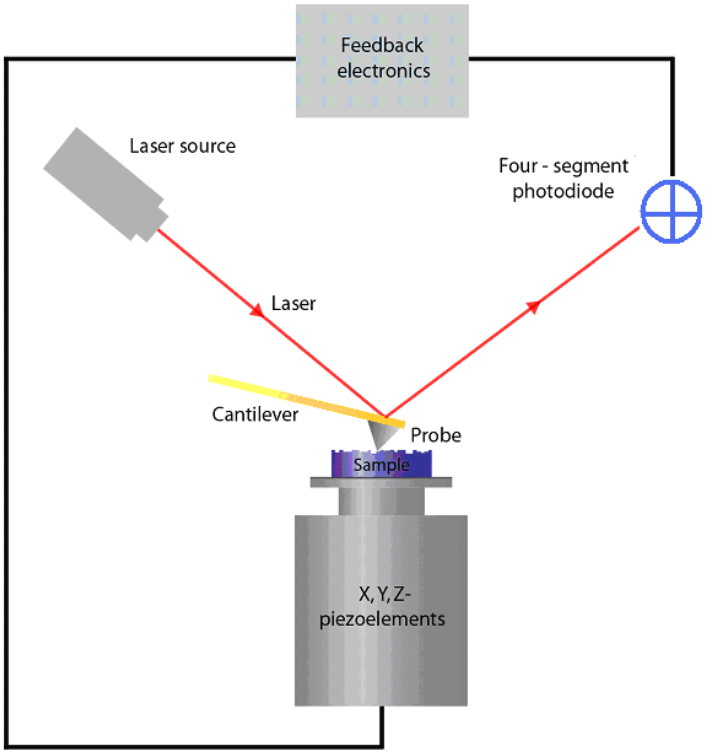

Figure 2- 11 Block diagram of principle operation of a (multimode) AFM.

AFM is used as a powerful imaging technique for the characterization of the SWNTs representing the "visual image" of the material. Height image of individual SWNTs provides information of morphology of SWNTs, the functional groups present on nanotube surface (if the functional group is large enough to change the height along an individual SWNT) and diameter/length, dispersion and exfoliation of bundles.[102,109,116,118,124,169,179,183,194,198,207,219] Fan *et al.* have pointed out that the AFM could be used to identify the location of chemical defects.[178] Coleman *et al.* have reported that the gold tagged thiol groups on SWNT surface could be imaged by tapping mode AFM and used for the direct evidence of covalent modification of SWNTs.[119,180] AFM height image of the gold nanoparticle decorated SWNTs has revealed that the gold tagging on SWNTs is an effective method showing the location and the distribution of the gold nanoparticles.[119,180] Thereafter, gold tagging has been used for characterizing the modified SWNTs.[177]

3. PYRIDINE FUNCTIONALISED CARBON NANOTUBES (CNTs)

3.1. Introduction

The covalent attachment of aryl groups to the surface of CNTs following the addition and activation of the corresponding diazonium salts is a well utilized reaction in nanotube chemistry. This chemistry was first described by Tour and co-workers for the derivatization of small diameter nanotubes via electrochemical reduction of *p*-substituted benzene diazonium tetrafluoroborates bearing Br, F, Cl, *tert*-butyl, nitro, methoxy carbonyl, tetradecyl and 2-(2-(2-methoxyethoxy)ethoxy)ethyl) groups in acetonitrile.[105] The authors reported that there was nearly 1 functional group for every 20 carbons in the nanotube framework and nanotubes with *tert*-butyl benzene moiety had significantly improved solubility in organic solvents. Strano *et al.* and Stephenson *et al.* have also shown that the addition of benzene diazonium tetrafluoroborates could also be carried out in the presence of surfactants[139] and ionic liquids,[220] respectively. Thereafter Tour *et al.* reported a new method for the direct treatment of SWNTs with aryl diazonium salts which is more scalable and flexible than the electrochemical method.[110] The protocol for this method includes the thermally induced reaction of SWNTs in *o*-dichlorobenzene/acetonitrile with diazonium compounds generated *in situ* by the action of isoamyl nitrite on aniline derivatives with Cl, tert-butyl, methoxy carbonyl, nitro and carboxylic acid groups or aryl diazonium tetrafluoroborate salts.[105] Dyke *at al.* expanded the use of aryl diazonium salts showing that SWNTs could be functionalised by the substituted aryl diazonium salts generated using isoamyl nitrite or $NaNO_2/H^+$ in solvent free conditions at 60 ^oC.[112] The authors have stated that this method had several advantages including being scalable, cost-effective, and

evironmentally benign when compared with the functionalisation of SWNTs using electrochemical reduction of diazonium salts[105] and thermally generated diazonium salts.[110] The mechanism and kinetics of the reaction have been studied and the reaction has been shown to be selective for metallic single-walled carbon nanotubes (SWNTs) with the reactivity of the semi-conducting SWNTs, which react concurrently but typically more slowly, depending on the diameter of the nanotube and the substituents attached to the aryl ring.[139,146,148] The detailed mechanism of the reaction is complex and it was only very recently that Chenevier and co-workers showed that it involved a free-radical chain reaction with metallic SWNTs having an unexpected catalytic role.[221] Interestingly, although the diazonium reaction has been used for the introduction of aryl substituents to CNTs it has so far not been used to introduce heterocycles to the nanotube surface. This is surprising as the heteroatom introduced could be used to extend CNT chemistry.

In this chapter the synthesis and characterisation of pyridine functionalised SWNTs produced via diazonium based reaction pathway and their interaction with poly(acrylic acid) (PAA) (MW= 250.000) were reported. The functionalised SWNT material was characterized by X-ray photoelectron spectroscopy (XPS), thermo gravimetric analysis – mass spectrometry (TGA-MS), UV-vis-NIR, FTIR and Raman spectroscopy and the location and distribution of the functional groups determined using atomic force microscopy (AFM). Rheometer was used to investigate the SWNT/PAA interaction.

3.2. Synthesis of pyridine modified SWNTs

Purified SWNTs were reacted with a pyridine diazonium salt generated in-situ by the oxidation of 4-aminopyridine with $NaNO_2$ in HCl to afford pyridine functionalised SWNTs (**1**) using the modified literature procedure reported by Tour *et al.*,[112] Scheme 3-1.

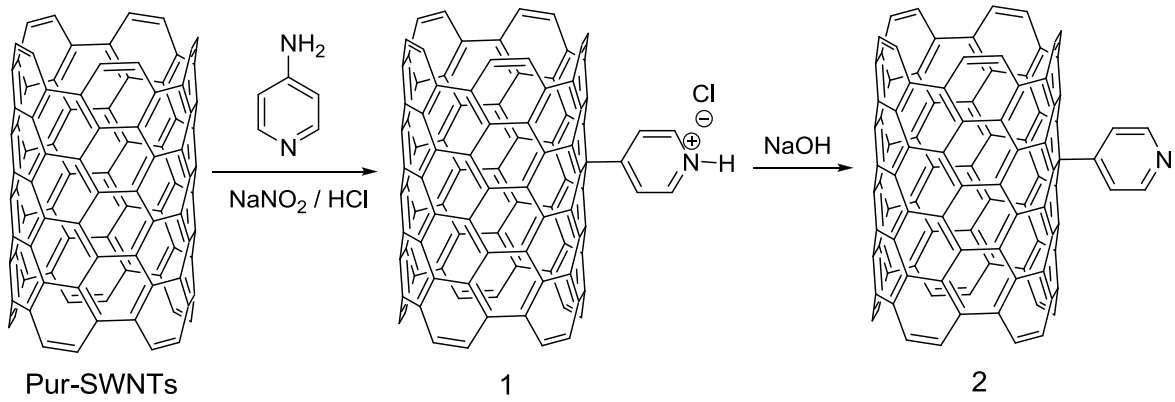

Scheme 3-1 Schematic representation of the diazonium reaction pathway for pyridine functionalised SWNTs (**2**)

In order to prevent the reaction of pyridine heterocycle with nitrosonium cation (NO^+), pyridine nitrogen was protected by dissolving in 4 M HCl solution prior to generation of pyridine diazonium salt. The acidic conditions of the reaction ensure that the pyridine nitrogen is protonated. Therefore, before the isolation of pyridine modified SWNTs it is curucial to de-protonate the pyridinium hydrochloride salt formed using sodium hydroxide. Since aryl diazonium chlorides are unstable at high temperatures pyridine diazonium chloride addition to SWNTs surface was carried out at low temperatures (0-5 ^oC) to prevent the decomposition of the reactive salts. DMF was preferred as reaction solvent due to its miscibility with water and high solubility of nanotubes. The disadvantage of the DMF usage was its basicity due to the presence of the ammonia as it increased the temperature of the reaction mixture reacting with hydrochloric acid. Therefore DMF was added dropwise not to cause high temperature increases that could decompose the pyridine diazonium salts. Formation of stable nanotube dispersion was observed following the addition of SWNTs to the pyridine diazonium salt as indicative of the covalent attachment of pyridine group to SWNT surface.

3.3. Characterisation and properties of pyridine modified SWNTs

3.3.1. Effect of pyridine surface functionalisation on nanotube solubility

The pyridine modified SWNTs (**2**) were characterised using UV-vis-NIR spectroscopy. SWNTs display characteristic bands in the region of 300-1800 nm.[108,200] It is known that the surface functionalisation produces sp^3 hybridised carbon atoms on nanotube framework altering the electronic properties of the SWNTs.[118] This alteration causes a decrease in the intensity of the electronic bands observed in absorption spectrum revealing the sidewall functionalisation.

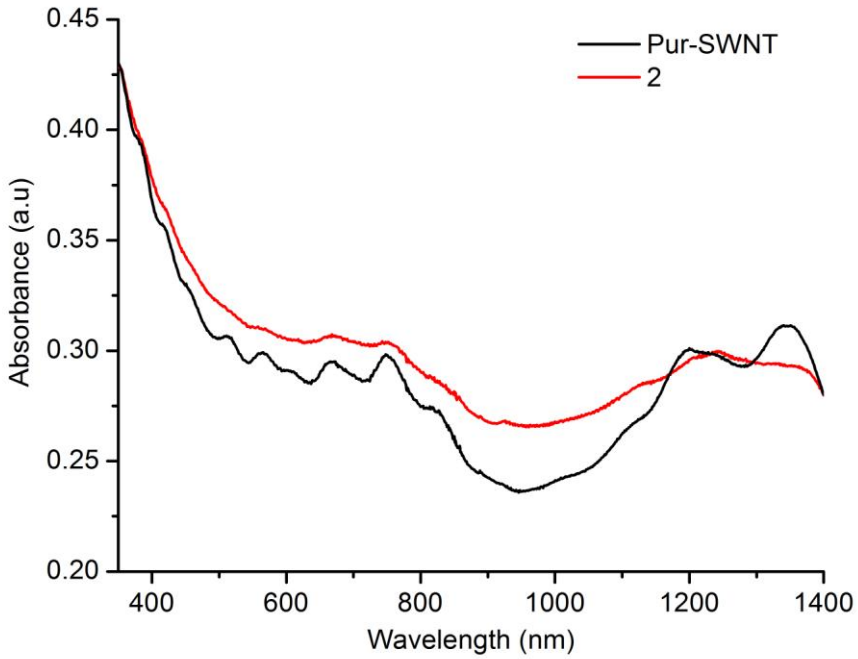

Figure 3-1 Normalized (at 350 nm) UV-vis-NIR spectra, recorded in DMF, of purified SWNTs (black) and pyridine functionalised SWNTs (**2**) (red).

UV-Vis-NIR spectrum of (**2**) confirmed the covalent attachment of the pyridine functional group to the surface of the nanotube as the characteristic absorption bands

corresponding to the electronic transitions between the van Hove singularities were suppressed upon functionalisation,[198] Figure 3-1.

The solubility of the modified SWNTs was recorded in DMF, ethanol and water. A stable dispersion of the pyridine functionalised material (**2**) in DMF and ethanol had a concentration of 163 μg mL^{-1} and 73 μg mL^{-1} respectively, calculated using Beer's law and an extinction coefficient of 30 mL mg^{-1} cm^{-1} and absorption values at λ = 700 nm.[209] Protonation of the pyridine functionalised SWNTs (**2**) by HCl results in a decrease in dispersibility with values reduced to 77 μg mL^{-1} and 1 μg mL^{-1} for DMF and ethanol, respectively, whereas the solubility of the pyridine functionalized SWNTs in water improved upon protonation. The solubility of the protonated material (**1**) in H_2O was 8 μg mL^{-1} where the purified and un-protonated SWNTs (**2**) were close to ~1 μg mL^{-1}. Optial pictures of purified, pyridine functionalised (**2**) and pyridinium hydrochloride functionalised SWNTs in water are given in Figure 3-2.

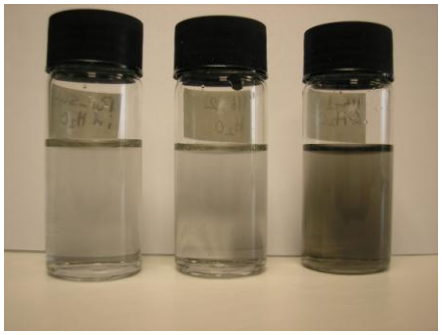

Figure 3- 2 Optical picture of the stable dispersions of purified (left), pyridine functionalised (**2**) (middle) and pyridinium hydrochloride functionalised (**1**) (right) SWNTs in water.

It was possible to observe the deprotonation of the pyridinium hydrochloride functionalised SWNTs in water by mixing the stable dispersion of the protonated pyridine functionalised SWNTs in water with $CHCl_3$ followed by NaOH treatment

(0.5 M). Since the water is immiscible with $CHCl_3$ formation of two layers which are aqueous (top) and organic (bottom), were observed upon mixing with $CHCl_3$. It was observed that the pyridinium salt modified SWNTs preferred aqueous layer (top layer) due to the strong ion-dipole interactions between protonated pyridine modified SWNTs and water. Deprotonation of pyridinium salt modified SWNTs using NaOH formed the pyridine modified SWNTs which moved into $CHCl_3$ phase (bottom layer). Figure 3-3 shows the optical images of the pyridinium hydrochloride functionalised SWNTs in water-$CHCl_3$ (left) and pyridinium hydrochloride functionalised SWNTs in water-$CHCl_3$ after NaOH addition (right) followed by shaking.

Figure 3- 3 Optical images of the pyridinium hydrochloride functionalised SWNTs (**1**) in water-$CHCl_3$ (left) and pyridinium hydrochloride functionalised SWNTs (**1**) in water-$CHCl_3$ after NaOH addition (right).

3.3.2. Diameter selectivity of pyridine diazonium salt addition

Raman spectroscopy has been used extensively to study SWNTs with the D-band at *ca.* 1300 cm^{-1} linked to the reduction in symmetry of the SWNTs, the intensity of which offers an approximation of the degree of functionalisation when compared with the tangential band (G-band) at *ca.* 1590 cm^{-1}.[131,169,222] The Raman spectra (632.8 nm excitation) of (**2**) and purified SWNTs, for comparison, are shown in Figure 3-4.

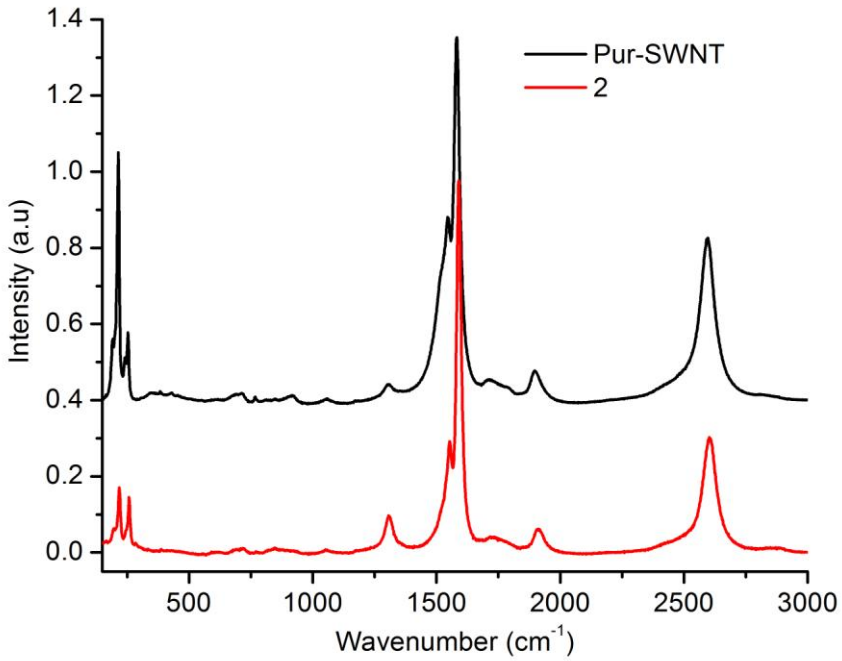

Figure 3-4 Offset Raman spectra (632.8 nm, 1.96 eV) of purified SWNTs (black) and pyridine functionalised SWNTs (**2**) (red) normalized at the G-band.

The pyridine modified SWNTs (**2**) have an enhanced D-band at *ca.* 1306 cm^{-1} when compared with unmodified SWNTs, with an A_D/A_G ratio of $0.146\pm5.07\times10^{-4}$ versus 0.044±0.002 for purified pristine SWNTs, indicative of groups attached to the surface of the nanotubes. The Raman spectra of the purified and pyridine modified (**2**) SWNTs excited at 532 nm (2.33 eV) and 785 nm (1.58 eV) are shown in Appendix A (Figure A1 and Figure A2) for comparison. The Raman spectrum of the pyridine modified SWNTs (**2**) excited at 532 nm displayed an enhanced and slightly shifted D-band *ca.* 1335 cm^{-1} when compared with the Raman spectrum of purified SWNTs. Excitation at 785 nm caused a shift of D-band to 1290 cm^{-1} for modified SWNTs (**2**). A_D/A_G ratio was 0.414±0.015 (unmodified SWNT: 0.142±0.004) and 0.134±0.006 (unmodified SWNT: 0.054±0.006) at 532, 785 nm excitation, respectively.

Detailed study of the selectivity and reactivity of the pyridine diazonium salt addition towards SWNTs was performed using 632.8 nm (1.96 eV), 532 nm (2.33 eV) and 785 nm (1.58 eV) laser excitation sources. The rate of reaction of substituted aryl diazonium salts with CNTs has been shown to be fast for metallic SWNTs with the reactivity of the semi-conducting SWNTs exhibiting a more complex relationship with nanotube diameter and the substituents present on the aryl diazonium salt.[139,146,148] Strano *et al.* has described the selectivity mechanism of the 4-chlorobenzene tetrafluoroborate addition to SWNTs.[223] It was shown that the selectivity proceeded by two distinct and long-lived steps including a selective noncovalent adsorption followed by a slower covalent reaction that need not be selective. The reactivity of the pyridine diazonium salts appears to be no different. Examination of the radial breathing modes (RBMs) in the Raman spectra at 632.8 nm excitation, known to excite both metallic and semi-conducting SWNTs, shows some differences between the chemically functionalised and pristine SWNTs, Figure 3-5.

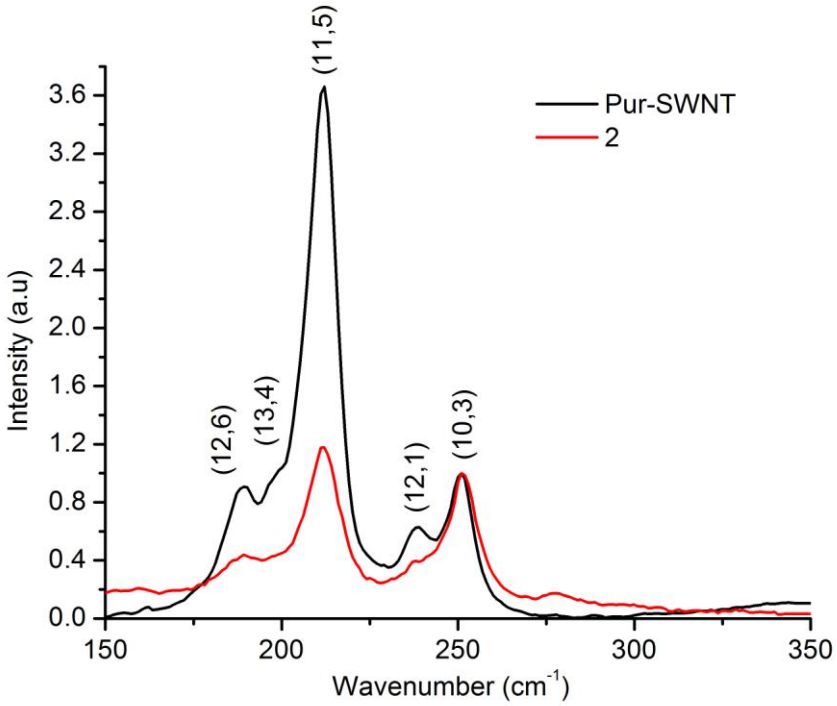

Figure 3-5 RBM region of the Raman spectra (632.8 nm, 1.96 eV) of purified SWNTs (black) and pyridine functionalised SWNTs (**2**) (red) normalized at 251cm^{-1}.

The Raman spectrum of purified SWNTs shows five peaks at *ca.* 189, 197, 212, 238 and 251 cm^{-1} in the RBM region which can be assigned to (12,6) (13,4), (11,5), (12,1) and (10,3) SWNTs with diameters of 1.26, 1.21, 1.12, 0.99 and 0.94 nm respectively, using the modified Kataura plots of Strano,[142] the first three being metallic and the remaining two semiconducting nanotubes. Following normalization at 251 cm^{-1} which remained relatively unchanged during the reaction, the band most influenced by the addition of the pyridine diazonium salt was the one at 189 cm^{-1} which corresponds to metallic (12,6) SWNTs.

Excitation at 532 nm (2.33 eV) predominantly affects the metallic nanotubes. In the RBM region of the spectrum of the purified SWNTs excited at 532 nm two bands at 189 and 273 cm^{-1} which are assigned to (12,6) and (9,3) SWNTs with diameters of 1.26 and 0.85 nm, respectively are observed, Figure 3-6. It is clear to see that the band

intensity at 273 cm^{-1} decreases in the pyridine functionalised SWNTs (**2**) when the spectra normalized are at 189 cm^{-1}.

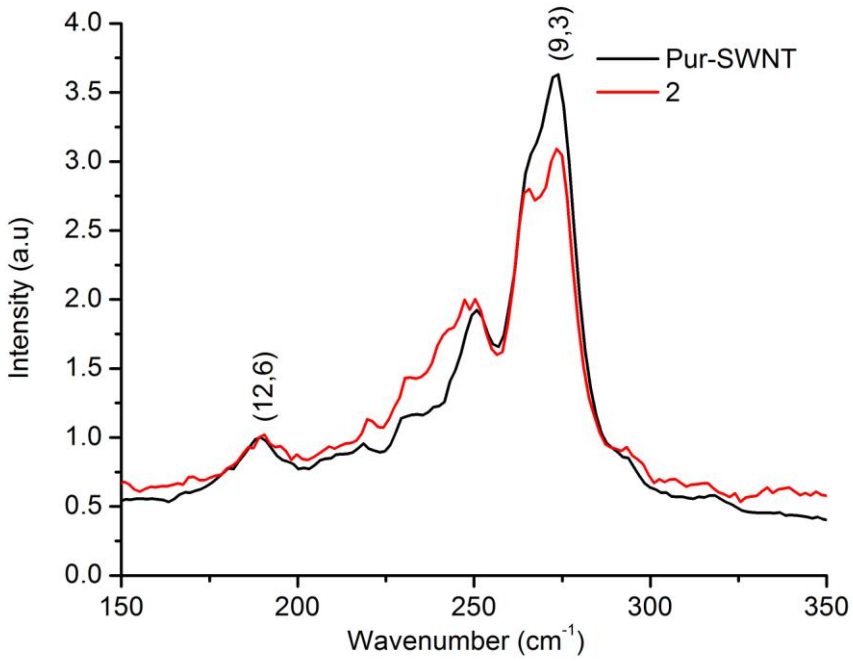

Figure 3-6 RBM region of the Raman spectra (532 nm, 2.33 eV) of purified SWNTs (black) and pyridine functionalised SWNTs (**2**) (red) normalized at 189 cm^{-1}.

In contrast, excitation at 785 nm (1.58 eV) brings into resonance predominantly semiconducting SWNTs. The RBM spectrum of unmodified SWNTs excited at 785 nm (1.58 eV), Figure 3-7, show five bands at 202, 212, 222, 230 and 265 cm^{-1} which can be assigned to (9,8), (9,7), (10,5), (11,3) and (10,2) SWNTs with diameters of 1.18, 1.12, 1.06, 1.02 and 0.85 nm respectively. The Raman spectrum of the pyridine functionalised SWNTs (**2**), normalized at 265 cm^{-1}, shows a significant decrease in the band at 202 cm^{-1} assigned to larger diameter semiconducting.

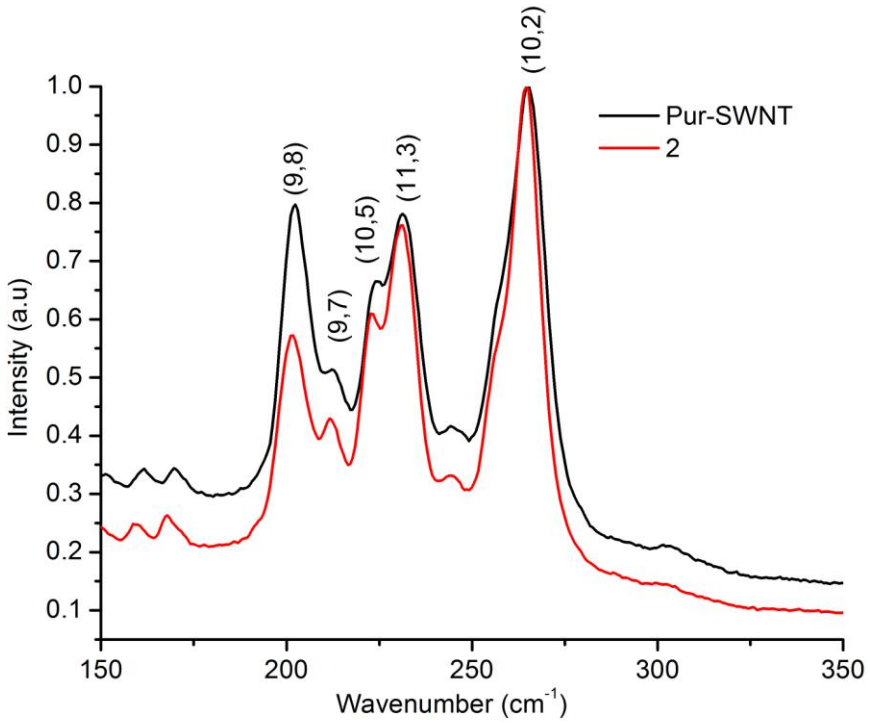

Figure 3-7 RBM region of the Raman spectra (785 nm, 1.58 eV) of purified SWNTs (black) and pyridine functionalised SWNTs (**2**) (red) normalized at 265 cm^{-1}.

The use of resonance Raman for the assessment of selectivity in reactions with SWNTs is crucial. As a SWNT becomes functionalised the electronic properties of the material change and the nanotube moves off resonance and an apparent decrease in intensity is observed. RBM region spectrum provided by 632 nm laser excitation revealed that the pyridine diazonium salt addition to SWNT sidewall was selective for metallic SWNTs over semiconducting ones. The reason for this trend can be explained by the electronic states of the metallic nanotubes close to Fermi level which causes the stabilisation of the transition states via electron donation from nanotube to diazonium salt while covalent attachment takes place.[139] In addition 532 excitation showed that selectivity was towards smaller diameter metallic SWNTs since they have misallignment of π-orbitals and sp^2 C atoms exhibiting a higher degree of pyramidalisation.[79,136] On the other hand, 785 nm excitation displayed that larger

diameter semiconducting SWNTs were more reactive than smaller diameter SWNTs due to the latter having a larger band-gap and thus a large region where the density of states (DOS) of the SWNT is zero.[146] Overall data showed that the metallic is more reactive than semiconducting and large diameter semiconducting is more reactive than small diameter SWNTs.

3.3.3. Determination of surface modification density via thermal and X-ray analysis

The degree of functionalisation of pyridine modified SWNTs (**2**) was probed by thermogravimetric analysis - mass spectrometry (TGA-MS) which showed a weight loss of 25 ± 0.005 % at 600 °C compared to *ca.* 7 ± 0.005 % for purified SWNTs, Figure 3-8.

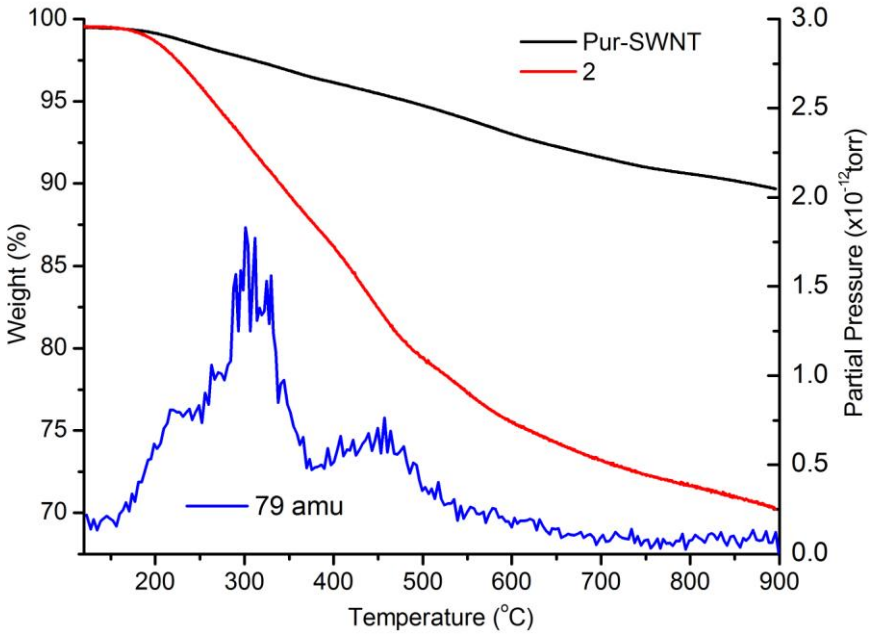

Figure 3-8 TGA-MS data (10 °C min^{-1}) of purified SWNTs (black) and pyridine functionalised SWNTs (**2**) (red). MS trace (blue) of pyridine (79 amu) given off during heating.

This corresponds to the presence of approximately 1 functional group for every 30 nanotube carbon atoms (3.33 atomic%). The peak of mass loss is *ca.* 310 °C and corresponds to the pyridine fragment (79 amu) which was detected by mass spectrometry. The mass spectrum of the modified SWNTs showed another peak *ca.* 450 ^{o}C, which is considerably less intense than the peak *ca.* 310 ^{o}C revealing the presence of two different pyridine groups having different environments (pyridine attached to sidewalls or end caps).

The level of functionalisation was also confirmed by XPS measurements where elemental composition analysis showed the presence of *ca.* 2.90±0.39 atomic per cent (at.%) of nitrogen in SWNT-pyridine (**2**) equivalent to approximately 1 pyridine group per 33 nanotube carbon atoms which is in close agreement with the TGA-MS data. XPS of pyridine modified SWNTs (**2**), Figure 3-9, displays the presence of four distinct C 1s contribution peaks at a binding energy of 284.6, 285.5, 286.5 and 287.7 eV, two O 1s peaks at a binding energy of 532.5 eV and 534.7 and three N 1s peaks at a binding energy of 398.9, 400.0 and 402.0 eV.

No change was observed in binding energy of C 1s and O 1s for pyridine modified SWNTs (**2**), Figure 3-9, when compared with the binding energies for purified SWNTs (see Appendix A, Figure A8). However broadening of the O1s XPS spectrum was observed presumably as a result of introducing new hydroxyl groups during free pyridyl radical addition. The fitted N1s XPS spectrum, Figure 3-9, with three components at 398.9, 400.0 and 402.0 eV were attributed to pyridine,[224] diazo group (-N=N-)[225,226] or the pyridine radical cation ($N^{\bullet}$) formed during X-ray excitation in the analysis chamber[227] and adsorbed N_2,[228] respectively.

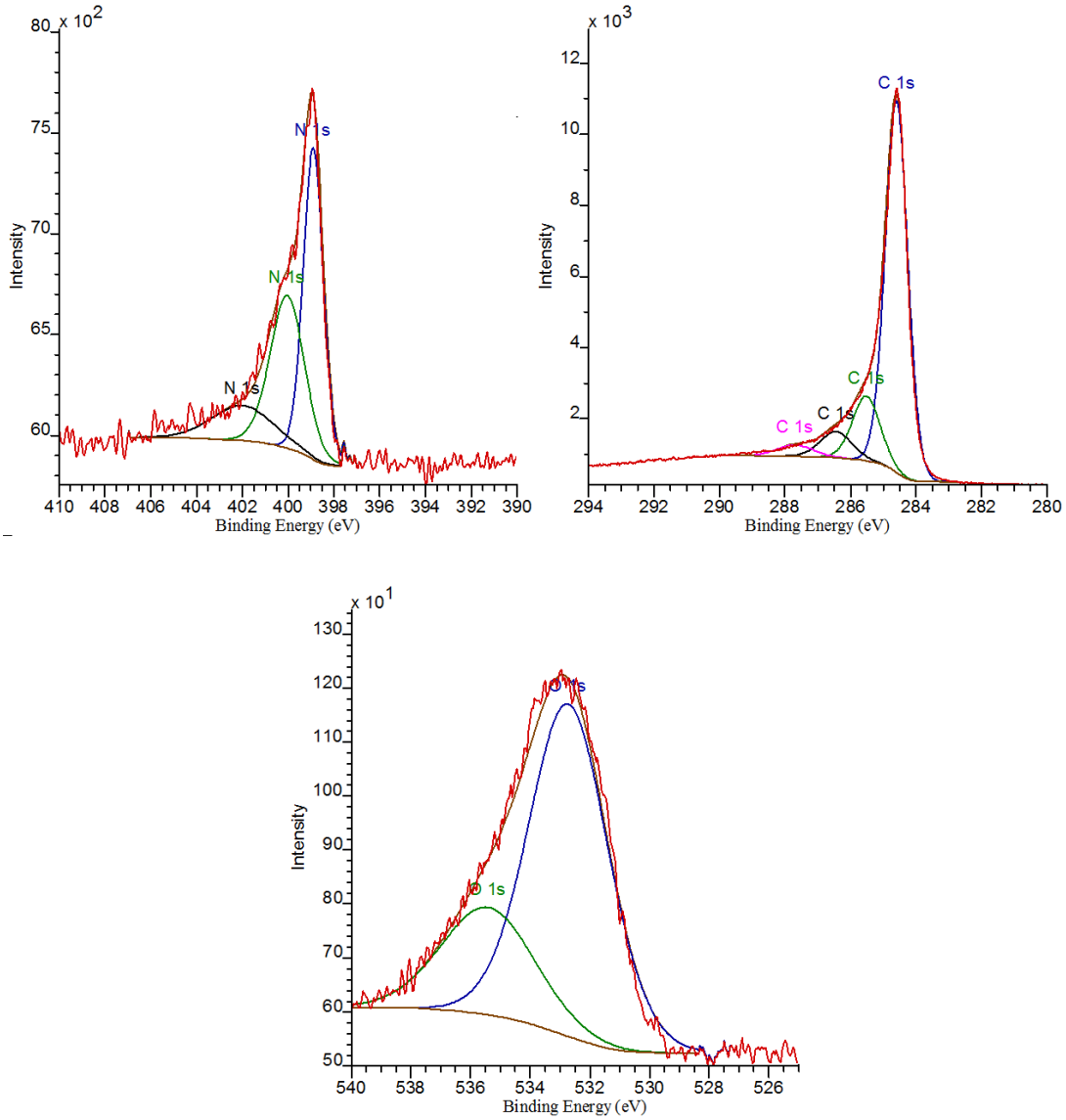

Figure 3-9 Top Left: N1s XPS spectrum of the pyridine modified SWNTs (**2**) with three components *ca.* 398.9 (blue), 400.0 (green) and 402.0 (black) eV; Top Right: C1s XPS spectrum of the pyridine modified SWNTs (**2**) with four components *ca.* 284.6 (blue), 285.5 (green), 286.5 (black) and 287.7 (magenta) eV; Bottom Middle: O1s XPS spectrum of the pyridine modified SWNTs (**2**) with two components *ca.* 532.5 (blue) and 534.7 (green) eV.

3.3.4. Reversibility of pyridine surface addition

Reversibility of the pyridine addition to SWNT sidewall was observed heating a few miligrams of pyridine modified SWNTs (**2**) till 900 ^{o}C by 10 ^{o}C/min under He atmosphere followed by cooling down to the room temperature. Raman (632 nm, 1.96 eV) and UV-vis-NIR spectroscopies were performed to monitor the changes after heating and the results were compared with pristine SWNTs. Raman (632 nm, 1.96 eV) and UV-vis-NIR spectra of the heat-treated pyridine-modified and the pristine SWNTs are shown in Appendix A (Figure A3 and Figure A4). UV-vis-NIR and Raman spectra of the annealed pyridine modified SWNTs reveals that the addition of pyridine heterocycles to SWNTs sidewall is a reversible process restoring the electronic and structural properties of pristine SWNTs.

3.2.5. Effect of sodium nitrite on surface oxidation

In order to elucidate the possible nanotube sidewall oxidation that could be resulted by the reagents used to generate diazonium salt, a control experiment has also been performed by subjecting the pristine SWNTs to acidic solution of sodium nitrite in the absence of *p*-aminopyridine in DMF at room temperature. SWNTs were isolated using the same procedure given for pyridine modified SWNTs, except NaOH treatment. Resulting material was characterised using Raman, UV-vis-NIR and thermogravimetric anaylsis. The Raman and UV-vis-NIR spectra and TGA plot are shown in Appendix A (Figure A5-A7). Overall data showed that the acidic sodium nitrite solution had no effect on modification of SWNTs in the absence of *p*-aminopyridine.

3.3.6. Gold nanoparticle tagging for AFM visualisation

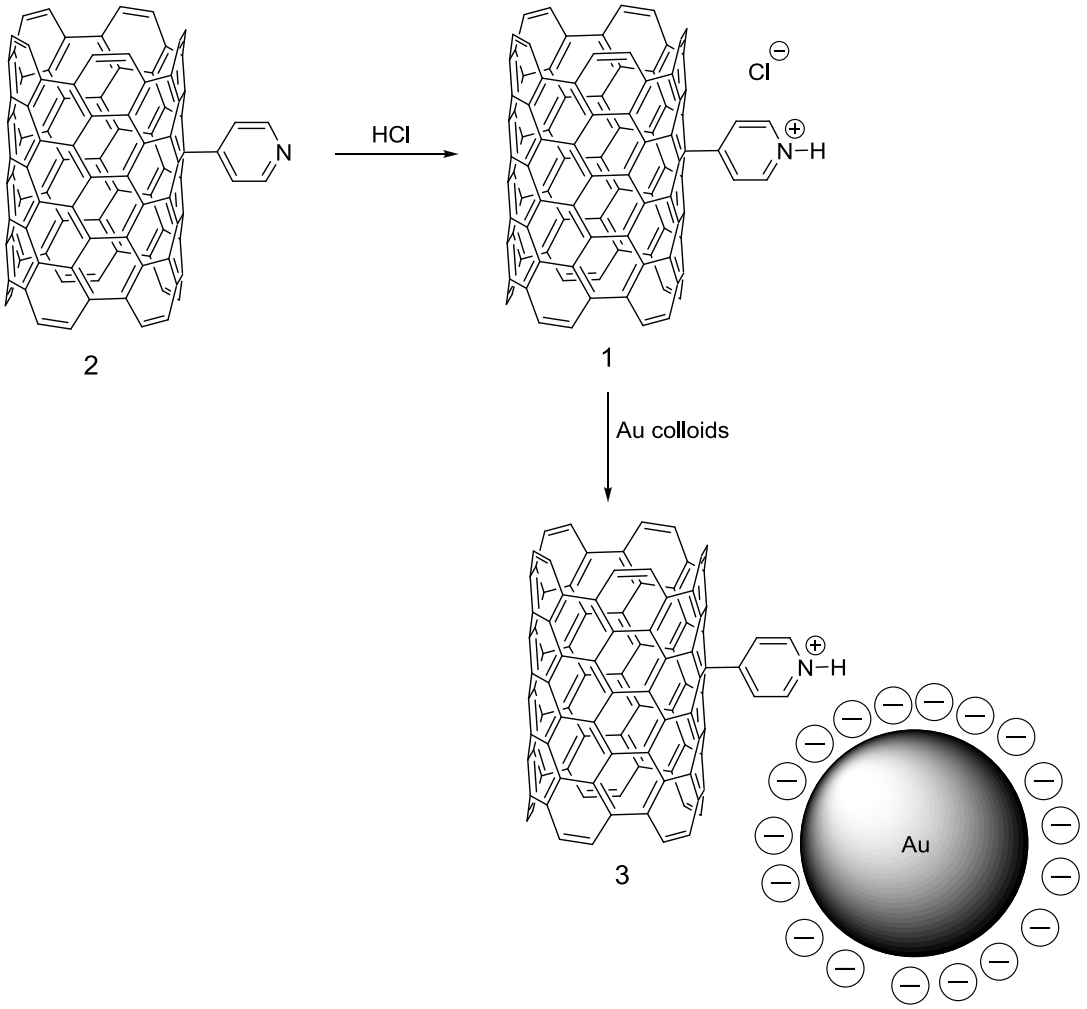

Scheme 3-2 Schematic representation of the electrostatic interaction of gold colloids with pyridine functionalised SWNTs (**2**) following the HCl treatment for AFM functional group tagging experiments.

Characterisation of SWNTs, functionalised with organic groups, using conventional spectroscopy can be difficult and requires extensive use of control experiments to rule out physical adsorption. However using chemical tagging techniques it has been shown in the past[119,180,191] that it is possible to exploit the chemistry of the attached organic group to anchor nanoparticles to the surface of the SWNTs. This allows the functional groups to be visualized by atomic force microscopy (AFM) and provides

information on distribution and localisation of functional groups on the nanotube surface. For the pyridine functionalised SWNTs (**2**) the methodology is relatively simple and doesn't require extensive functional group conversion, Scheme 3-2.

Using a strong acid, HCl, it was possible to protonate the pyridine nitrogen to make the corresponding pyridinium salt. Exposing the positively charged pyridinium functionalised SWNTs (**1**), deposited on a freshly cleaved mica surface, to negatively charged citrate stabilised gold colloids 4 – 6 nm in diameter results in an electrostatic interaction of the gold nanoparticles with the functionalised SWNTs (**3**), Figure 3-10.

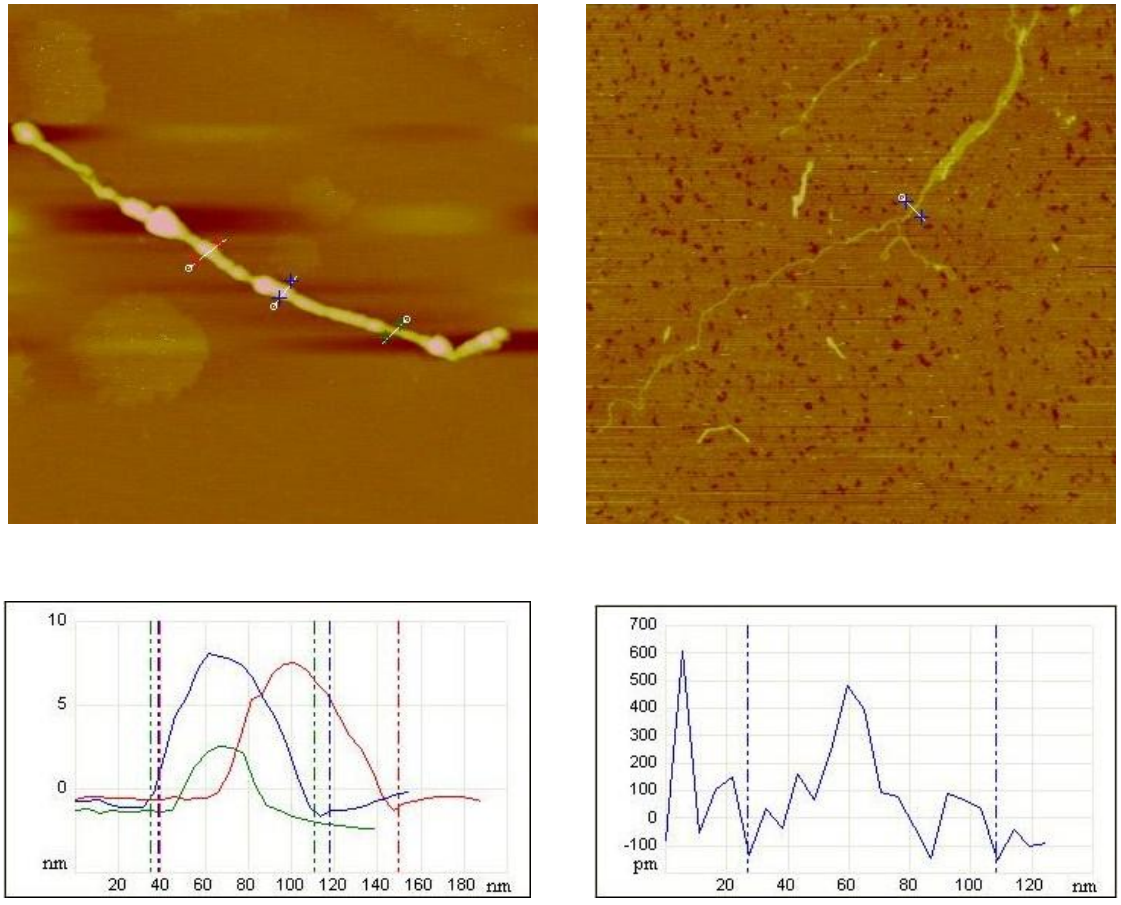

Figure 3-10 A typical tapping mode AFM height image of a protonated pyridine functionalised SWNT (**3**) (2.0 μm by 2.0 μm) (Top left) and purified SWNT (2.0 μm by 2.0 μm) (Top right) after exposure to citrate stabilized Au colloids (4 – 6 nm). The section analysis of the individualized gold decorated pyridinium modified SWNT (**3**) (Bottom left) and purified SWNT (Bottom right). The image shown is with a z scale of 0 – 5 nm.

It is clear from the figure that gold particles, visible as light features on the AFM height image, decorate the entire length of the SWNT. Control experiments where purified SWNTs, that have not undergone any chemical functionalisation, are exposed to gold colloids show no significant presence of nanoparticles on the SWNT surface, Figure 3-10. Section analysis of the AFM image for the gold decorated pyridine modified SWNTs (**3**) reveals that the diameter of the nanotube where gold nanoparticle anchored (~7-8 nm) are greater than the non-decorated parts (~2 nm) confirming the interaction of positively charged SWNTs (**1**) with gold nanoparticles.

3.3.7. Pyridine modified SWNTs as gelators for Poly(acrylic acid)s

Since the pristine SWNTs, producing bundles held strongly together, are poorly suspended in water their use and processing in composites, films or fibers in aqueous medium are very limited. In order to exfoliate bundles and prepare individual SWNTs several non-covalent wrapping strategies including the use of polyelectrolytes have been performed.[78,84,85,229,230] Grunlan *et al.* showed that poly(acrylic acid) (PAA), which is a weak polyelectrolyte with a pH responsive behaviour, could be used for the preparation of stable aqueous dispersions of nanotubes at relatively high pH (5.6 to 7.4) due to the strong repulsive forces between negatively charged PAA wrapped nanotubes.[231] This interaction was explained by the formation of the highly negatively charged extended polymer chains at high pH via deprotonation of PAA which has highly coiled conformation at low pH due to the strong intramolecular hydrogen bonding.[231-234] They also pointed out that the solubility of the nanotubes decreased in more basic conditions and the viscosity of the SWNT/PAA system increased upon pH increase due to the highly exfoliated SWNTs.[231] However, later the same author reported that the viscosity of SWNT/PAA system was not depend on the exfoliation quality of nanotubes comparing the viscosities and the cryo-TEM micrographs of the

vitrified SWNT/PAA solutions at pH 2.9 and 9.2, respectively. Results revealed that the nanotubes were exfoliated better in 1% PAA solution at pH 2.9 than pH 9.2 although the viscosity of the SWNT/PAA solution at pH 9.2 was greater than pH 2.9.[233]

It is known that the pyridine has an accessible heteroatom donor group which is capable of making hydrogen bonding with carboxylic acid groups. In order to find out the effect of the pyridine functionalisation on the solubility of SWNTs in 1% PAA/water solution, the interaction between the pyridine functionalised SWNTs (**2**) and the poly(acrylic acid) (PAA) (MW=250.000) was investigated, Scheme 3-3.

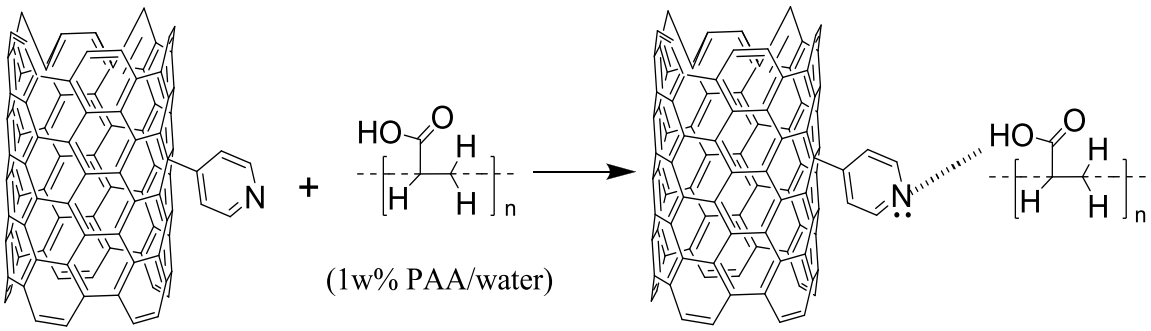

2

Scheme 3-3 Possible interaction of the pyridine modified SWNTs (**2**) with poly(acrylic acid)

In order to obtain accurate values for the maximum dispersibility of the pyridine modified SWNTs (**2**) in PAA/water solution (1%) the molar absorptivity of pyridine modified SWNTs (**2**) in 1% PAA was determined constructing a calibration curve (absorbance versus concentration) preparing 1, 2, 3, 4, 5, 6, 7, 8, 9, 10 μg/mL solutions (infinitely soluble) of pyridine modified SWNTs in PAA/water solution (1w%, pH 2.8). Absorbances were recorded at 700 nm as reported in literature.[209] Figure 3-11 shows the absorbance versus concentration linear fitted line of the pyridine modified

SWNTs using the linear regression in excel. In agreement with the Beer-Lambert's law the molar absorptivity of the pyridine functionalised SWNTs in PAA/water solution (1w%) was calculated as ~25 mL mg^{-1} cm^{-1} from the gradient of the linear line.

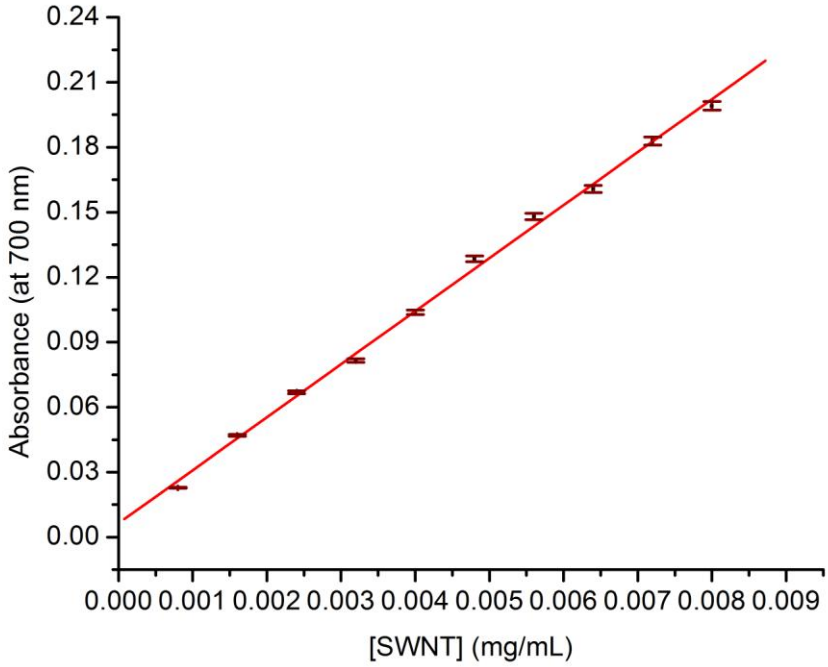

Figure 3-11 Absorbance versus concentration linear fitted line of the pyridine modified SWNTs for molar absorptivity calculation (1w% PAA, pH 2.8)

Solubility of the pyridine modified SWNTs (**2**) in 1% PAA/water was calculated at different pH using the molar absorptivity of ~25 mL mg^{-1} cm^{-1}. Stable dispersions of the pyridine modified SWNTs (~25 mg) in PAA/water solution (~1w%, 3 mL) having a pH 2.8, 4.3, 5.8, 7.5, 8.8 and 10.3, respectively were prepared sonicating the SWNT/PAA/water mixture using an ultrasonic probe sonication (40 W) for 30 min in an ice cooled bath. The pH of the PAA/water solutions was adjusted adding concentrated sodium hydroxide solution (10M) to the aqueous solution. The absorption spectra of the supernatant were recorded after allowing the dispersions to stand for 2 h. Figure 3-12 displays the spectra of the pyridine modified SWNTs in PAA/water

solution (~1w %) at different pH values. The absorption spectrum of modified SWNTs at pH 5.8 revealed that the modified SWNTs were individually dispersed as the bands due to the van Hove singularities were observed.

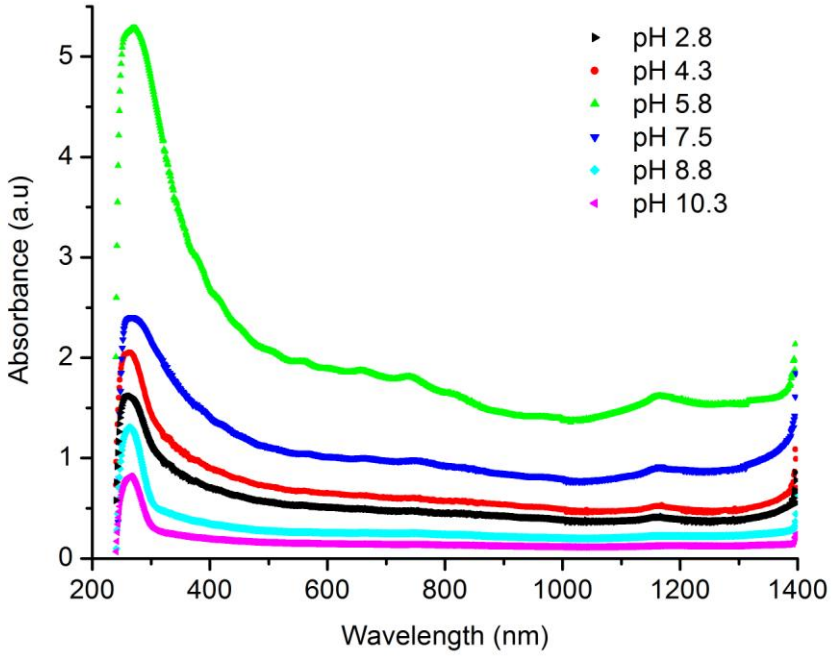

Figure 3-12 UV-vis-NIR spectrum of the pyridine modified SWNTs (**2**) in PAA solution (~1w %) at pH 2.8, 4.3, 5.8, 7.5, 8.8 and 10.3.

The solubility of the pyridine modified SWNTs (**2**) in PAA/water solution (1w %) at different pH values are given in Table 3-1.

pH	2.8	4.3	5.8	7.5	8.8	10.3
Solubility of (**2**) (mg/mL)	1.9	2.41	7.17	3.91	1.00	0.56

Table 3-1 Solubility data for the pyridine modified SWNTs (**2**) in PAA (~1%) at pH 2.8, 4.3, 5.8, 7.5, 8.8 and 10.3.

From the Table 3-1, it is clear that the solubility of the pyridine functionalised SWNTs increases with pH and reaches its maximum value at pH 5.8 resulting in the formation of hydrogel that was able to withstand the upturned container test and, it starts to decrease after pH 5.8. Wheras, the pristine SWNTs dispersed in 1% PAA failed the test and flowed more like a viscous liquid. Figure 3-13 displays the optical picture of the pyridine modified SWNT-PAA hydrogel and pristine unmodified SWNT-PAA dispersion at pH 5.8.

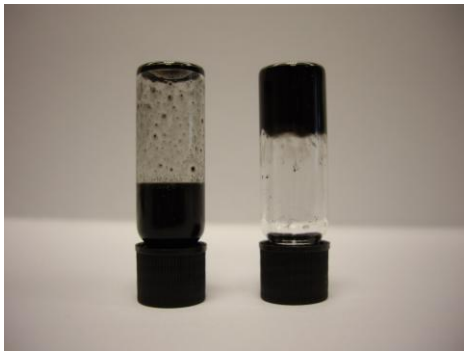

Figure 3-13 The optical picture of the pyridine modified SWNT-PAA hydrogel (right) and pristine unmodified SWNT-PAA dispersion (left) at pH 5.8

This can be explained by the pH responsive behaviour of the poly(acrylic acid). At high pH values the carboxylic acid groups are deprotonated to carboxylates increasing the negative charge density on PAA which causes repulsion between polymer chains resulting in a more extended conformation. It is known that the charge density of PAA changes from 30 to 80% between pH 6 and pH 8.[233] Therefore it is not surprising to get well dispersed pyridine modified SWNTs/PAA dispersions in aqueous solutions at pH 5.8. The driving force for the formation of the stable nanotube dispersion can be thought as hydrogen bonding, Scheme 3-3, between the carboxylic acid groups and the pyridine nitrogen lone pairs. The strength of the hydrogen bonding between carboxylic

acid and pyridine groups has been reported by Tian *et al.* showing that the nanotubes of the poly(4-vinylpyridine) (PVP) and poly(acrylic acid) (PAA) could be fabricated on polycarbonate template using the layer-by-layer assembly technique.[235] In contrast, at low pH values PAA is a neutral weak polyelectrolyte exhibiting intramolecular hydrogen bonding and highly coiled conformation which causes a decrease in the dispersibility of nanotubes.[233]

Rheology measurements also confirmed the formation of the hydrogel. In general gel is defined as the substantially dilute crosslinked system, which exhibits no flow when in the steady-state.[236] Measurement of the rheological properties can provide micro structural information, enabling a better understanding of the application and end use characteristics. A frequency sweep test is one of the best techniques, providing the viscoelastic properties (like Storage (Elastic) Modulus (G'), the Viscous (Loss) Modulus (G"), and the Complex Viscosity (η*)) of a sample as a function of timescale, for determination of sample microstructure . The storage modulus is known as a measure of the elastic component of the sample and the loss modulus is the viscous component of the sample. If the storage modulus (G') is greater than the loss modulus (G") and both are independent of frequency, the material is named as "gel".[237] The use of carbon nanotubes as gelators has recently been shown by Vaysse *et al.* fabricating carbon nanotube reinforced porous organogels of the poly(methyl methacrylate) using water, methanol, propanol and cyclohexane as parogens.[238] Shi *et al.* has developed an actuator hydrogelating nanotubes with poly(vinyl alcohol).[239] Homenick *et al.* has shown that the poly(ethyleneimine) (PEI) functionalized SWNTs could be used as a crosslinker to produce collagen hydrogels exhibiting higher Young's moduli than collagen gels cross-linked with just nanotubes or PEI.[240] Cyclodextrin modified SWNTs has also been used for the formation of supramolecular SWNT hydrogels with poly(acrylic acid) having dodecyl groups via host-guest interaction.[241] Figure 3-14

shows the complex viscosity (η*), storage modulus (G') and loss modulus (G") of the pyridine modified SWNTs/PAA and unmodified SWNT/PAA system versus frequency plots.

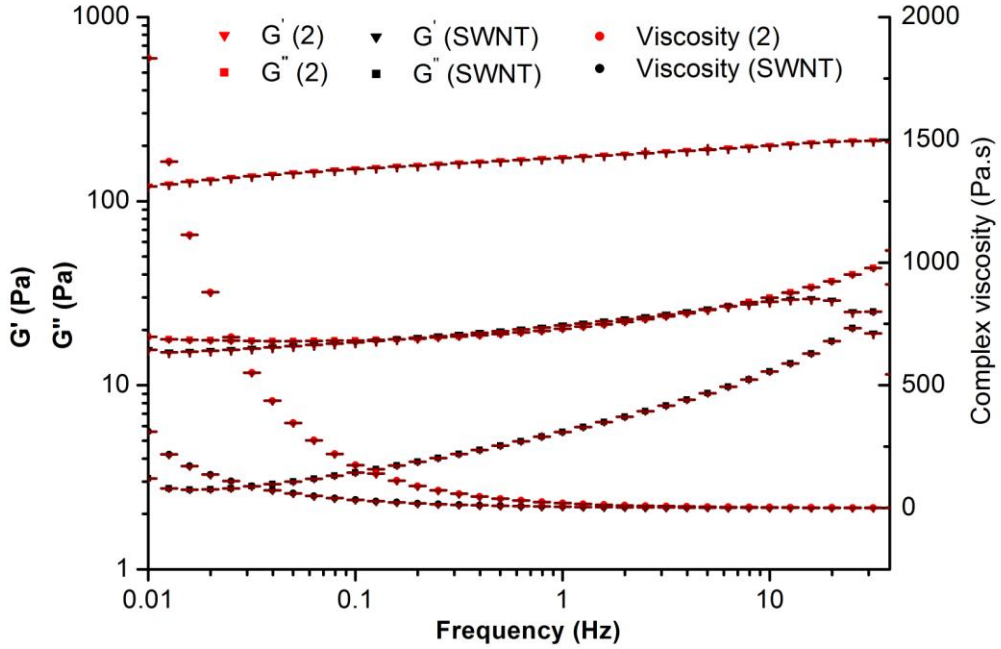

Figure 3-14 Plots of the dynamic viscosity (η'), storage modulus (G') and loss modulus (G") of the pyridine modified SWNTs (**2**)/PAA and unmodified SWNT/PAA system versus frequency.

Results revealed that both pyridine modified SWNT/PAA and unmodified SWNT/PAA systems behaved like a gel since the storage modulus (G') was greater than loss modulus (G"). However it was observed that the G' and G" values for unmodified SWNT/PAA system were less independent of frequency change. This showed that the gel-like material produced by unmodified SWNT/PAA system was less stable than the gel produced by pyridine modified SWNT/PAA system due to the strong interaction of pyridine side groups with PAA. This behaviour was also confirmed by the dynamic viscosity values of both systems. It was observed that the viscosity of the pyridine modified SWNT/PAA system was higher than the viscosity of

the unmodified SWNT/PAA system at low frequencies although both of them are independent of frequency at high frequency values. This shows that the flow rate of the pyridine modified SWNT-PAA system is less than unmodified SWNT/PAA system confirming the strong interaction of pyridine modified SWNTs with PAA and the formation of well-structured (gelled) system.

3.4. Conclusion

Attachment of the pyridine groups to the surface of SWNTs has been achieved by *in situ* generated pyridine diazonium salts prepared using *p*-aminopyridine and $NaNO_2$/HCl solution. In order to extend the chemistry, pyridine nitrogen has been protected by protonating prior to the diazonium salt formation and deprotonated after introducing to SWNTs. As pyridine has a heteroatom donor group which is capable of doing hydrogen bonding with a variety of functional groups (*e.g.* carboxylic acids) and reacting or coordinating with a lot of chemical substrates (*e.g.* metals, alkyl halides) it is clear that several non-covalent and covalent strategies can be developed to increase the solubility and processability of SWNTs. Pyridine functionalised SWNTs show remarkable exfoliation in DMF and ethanol as well as in water upon protonation. We have also shown that the pyridine modified SWNTs could be used as a gelator to produce hydrogels with poly(acrylic acid) interacting through hydrogen bonding. This type of interaction can be extended using protonated or deprotonated form of the pyridine modified SWNTs with different polymers having accessible side groups.

Selectivity of the addition was monitored applying resonance Raman spectroscopy with three different laser excitation sources. Results revealed that the pyridine diazonium salt addition to SWNTs was selective for smaller diameter metallic SWNTs over semiconductings ones, raising the possibility that it can be exploited for the separation of nanotubes by electronic type which is of great importance for

applications such as nanoelectronics. The findings were in close agreement with those reported to date. When the pyridine modified SWNTs were annealed the pristine SWNTs properties were restored revealing that the pyridine addition to nanotube surface was a reversible process. By deliberately protonating the pyridine nitrogen and exploiting the electrostatic interaction with negatively charged citrate stabilized gold nanoparticles we have been able to show by AFM the location and distribution of the functional groups on the nanotube surface. AFM also revealed that the pyridine diazonium salt addition was a non-disruptive modification method showing the nanotubes having ~2μm lengths.

4. INDOLIZINE MODIFIED CARBON NANOTUBES (CNTs)

4.1. Introduction

One of the most versatile routes to the covalent chemical modification of carbon nanotubes is perhaps 1,3 dipolar cycloadditions which were pioneered by Prato *et al.*[117] using azomethine ylides, typically generated *in situ* by the thermal condensation of aldehydes and α-amino acids, that produce pyrrolidine rings containing solubilising triethylene glycol chains or octyl groups.[242] In order to use in biomedical applications Prato's group has also modified the nanotubes using the *N*-functionalised glycine derivatives bearing a Boc(*tert*-butyloxycarbonyl)-protected amino end group which could be deprotected to yield amine functionalities suitable to further transformations.[243] The introduction of pyrrolidines to the surface of CNTs has been used extensively to aid the transfection of CNTs into mammalian cells and for the delivery of pharmacologically active molecules such as peptides, MTX and amphotericin B.[244,245] 1,3-Dipolar cyloaddition of azomethine ylides to SWNTs was expanded introducing phenol groups to SWNTs by Georgakilas *et al.*.[246] The resulting modified SWNTs showed enhanced dispersibility in common organic and aqueous solvents allowing the preparation of nanotube composite films or gels. An alternative method for the functionalisation of SWNTs using the azomethine ylides derived from trialkylamine-*N*-oxides has been reported by Ménard-Mayon and co-workers.[151] They have pointed out that the semiconducting nanotubes could be separated from the metallic ones when *N*-oxides bearing pyrene groups were used. Swager *et al.* have described the formation of cyclopentyl rings on nanotube surface using zwitterions formed by the reaction of 4-dimethylaminopyridine (DMAP) with dimethyl

acetylenedicarboxylate (DMAD).[247] 1,3-Dipolar cycloaddition of nitrile imines and nitrile oxides has been carried out to attach 2,5-diarylpyrazoline or pyridyl-isoxazoline rings, respectively on nanotube surface.[248,249] Microwave induced functionalisation of carbon nanotubes has also been described by Wang *et al.* showing that 1,3-dipolar cycloaddition of nitrile imines to SWNT sidewall under microwave conditions was faster than thermal conditions.[250] Brunetti *et al.* reported the microwave-assisted rapid cycloaddition to pristine nanotubes in solvent free conditions using octyl substituted aziridines.[149] It was shown that the microwave assisted cycloaddition of aziridines were much more efficient than the classical thermal conditions for azomethine ylides.[117] The same group also described a new approach for the multiple functionalisation of non-oxidized carbon nanotubes under microwave conditions using the combination of two techniques, 1,3-dipolar cycloaddition of hexyl, undecyl, 3,5-dimethoxyphenyl and 3,4,5-dodecoxypheyl substituted azomethine ylides in solvent free conditions and addition of *p*-methylbenzene diazonium salt addition in water.[150] Although the derivativization of CNTs is highly desirable the challenge remains to achieve sufficient functionalisation of the CNT surface to ensure ease of processing or facilitate the attachment of active molecules or particles, whilst avoiding significant degradation of the structure which could compromise the exciting properties of the material.[103]

In this chapter two different approaches for the preparation of indolizine modified SWNTs have been described. Indolizine derivatives are particularly interesting as they are well known for exhibiting a variety of pharmacologically desirable properties, including cardiovascular, anti-inflammatory and antioxidant properties,[251] as well as having known fluorescent properties and being used in sensor applications.[191,252-254]

The first method, Scheme 4-1, includes a simple and convenient non-destructive direct modification of SWNTs using 1,3-dipolar cycloaddition of pyridinium ylides,

readily prepared from simple Kröhnke salts *N*-(ethoxycarbonylmethyl)-pyridinium bromide (**4**), *N*-(4-methyl sodium benzenesulfonate)- pyridinium bromide (**5**) and *N*-(4-nitrobenzyl)-pyridinium bromide (**6**), respectively and, the second, Scheme 4-6, describes the generation of pyridinium ylides using the pyridine modified SWNTs (see Chapter III) and its subsequent 1,3-dipolar cycloaddition reaction (click reaction) via dimethyl acetylenedicarboxylate (DMAD) to yield indolizines.

Kröhnke salts (**4**), (**5**) and (**6**) have been characterised by nuclear magnetic resonance spectroscopy (NMR) and fourier transform infrared spectroscopy (FTIR). XPS, TGA-MS, AFM, UV-vis-NIR, FTIR and Raman spectroscopy have been employed to characterise the functionalised SWNTs.

4.2. Synthesis of indolizine modified SWNTs

4.2.1. Indolizine formation via 1,3-dipolar cycloaddition of pyridinium ylides

Purified SWNTs were reacted with pyridinium ylides generated *in-situ* via the addition of triethylamine (NEt_3) to the Kröhnke salts *N*-(ethoxycarbonylmethyl)-pyridinium bromide (**4**), *N*-(4-methyl sodium benzene sulfonate)-pyridinium bromide (**5**) and *N*-(4-nitrobenzyl)-pyridinium bromide (**6**) to afford SWNT with indolizine groups covalently bound to the nanotube surface **7a-b**, **8** and **9**, Scheme 4-1. Kröhnke salts (**4**), (**5**) and (**6**) were easily prepared using a modified literature procedure[255] by the addition of ethyl 2-bromoacetate, sodium 4-(bromomethy1)benzenesulfonate[256] and 4-nitrobenzylbromide, respectively, to pyridine at room temperature. The resulting crude salts were washed with either ether (**4**) or acetone/ethanol (**5** and **6**) to remove excess pyridine, ethyl 2-bromoacetate, sodium 4-(bromomethyl) benzenesulfonic acid and 4-nitrobenzylbromide to afford the pyridinium bromide salts (**4**) (92%), (**5**) (88%) and

(**6**) (90%). Isolated salts (**4-6**) were characterized using FTIR, ^{1}H and ^{13}C NMR and all data is listed in Chapter VII.

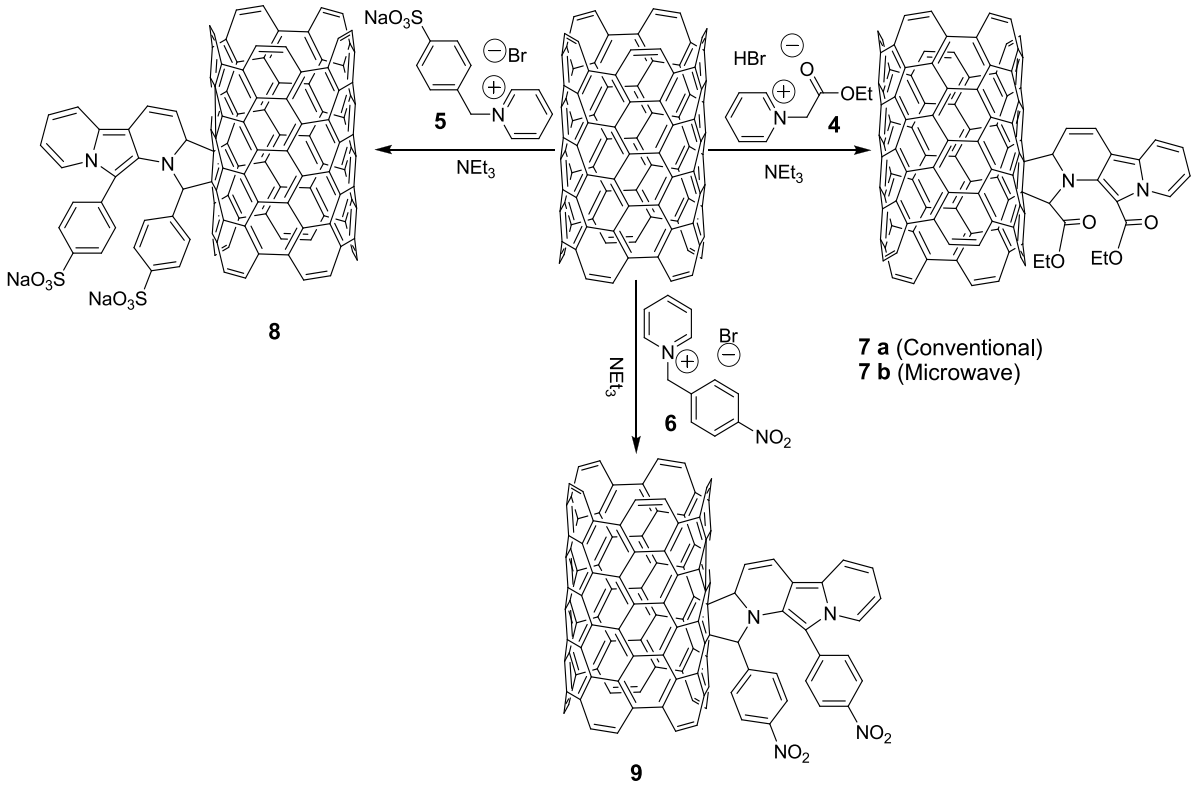

Scheme 4- 1 Schematic representation of the 1,3-dipolar cycloaddition of a pyridinium ylide, generated by the action of base on the Kröhnke salt (**4**), (**5**) and (**6**) to the sidewalls of the SWNTs to form an indolizine (**7a**, **b**), (**8**) and (**9**).

The ylides produced via the addition of NEt_3 to the corresponding pyridinium bromide salts (**4-6**) were not isolated due to the unstable nature of the pyridinium ylides and all reactions were carried out *in situ*.

The indolizine formation on SWNT surface reaction can be carried out using both conventional (**7a**) and microwave heating (**7b**), (**8**) and (**9**) with the latter resulting in significantly shorter reaction times (5 days versus 1 h). The use of microwaves to accelerate cycloaddition reactions on a carbon nanotube surface was recently reported for the cycloaddition of aziridines.[149] The 1,3-dipolar cycloaddition of the pyridinium

ylide to the SWNT surface with the nanotube acting as the dipolarphile, is believed to occur with the pyridinium ylide first adding to the nanotube surface to form a pyrrolidine ring closely followed by the addition of a second ylide to the addendum on the nanotube surface to afford an indolizine, Scheme 4-1. The driving force for the double addition of the ylide is likely to be aromatisation of the resulting indolizine formed. A similar result occurs in the absence of SWNTs with the pyridinium ylide generated from (**4**) undergoing a 1,3-dipolar cycloaddition with a second pyridinium ylide followed by water washing and extracting by dichloromethane as evidenced by electrospray mass spectrometry, Figure 4-1.

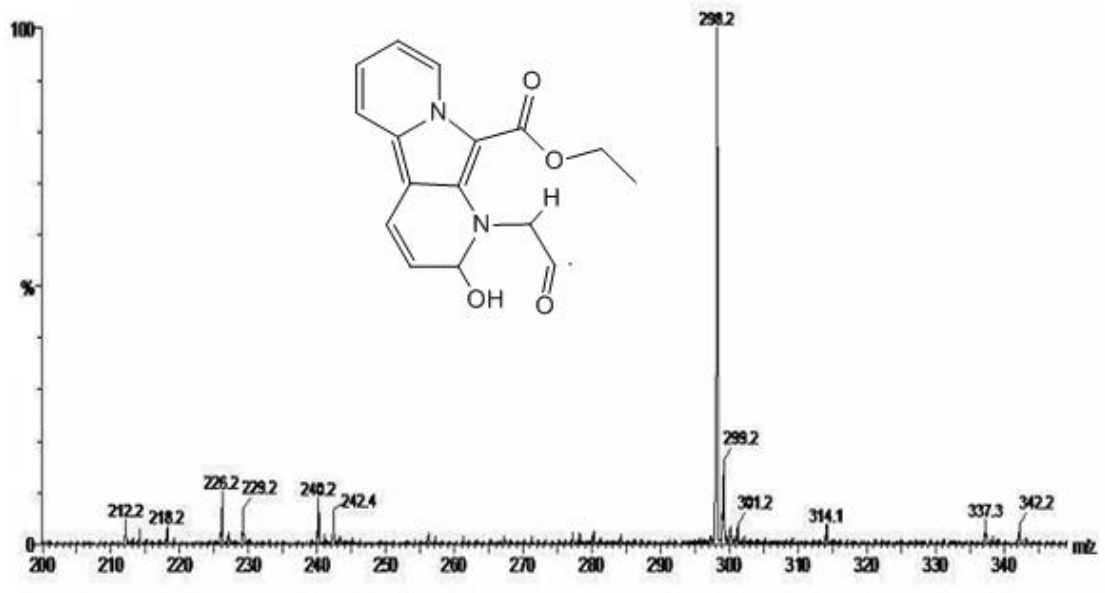

Figure 4- 1 Mass spectrum (ES+) of the crude reaction mixture (**b**) produced after microwave heating of *N*-(ethoxycarbonylmethyl)-pyridinium bromide (**4**) in the presence of triethylamine (NEt_3) in DMF followed by water treatment.

Figure 4-1 shows the mass spectrum of the crude product (**b**) (see Scheme 4-2) after microwave heating of *N*-(ethoxycarbonylmethyl)-pyridinium bromide (**4**) in the presence of triethylamine (NEt_3) in DMF. It is clearly seen that the crude product

fragments mainly into 298.2 amu (100 %) which represents the molecular ion of the corresponding indolizine product. This fragmentation (298.2 amu) can simply be explained by the given scheme for the fragmentation of the possible cycloadduct afforded by the reaction of pyridinium ylide (**4**) with another one, Scheme 4-2. Self reaction of two pyridinium ylides produces an unstable zwitterionic product (**a**) (MW: 326.13 amu) and the treatment of the corresponding unstable adduct with water causes both the protonation of the negatively charged methylene carbon atom and the hydroxylation of the positively charged carbon atom on pyridine ring yielding product (**b**) (MW: 344.14 amu). The new adduct (**b**) converts into the product (**c**) (MW: 299.10) upon heating by losing the ethoxy (OEt, 45 amu) group.

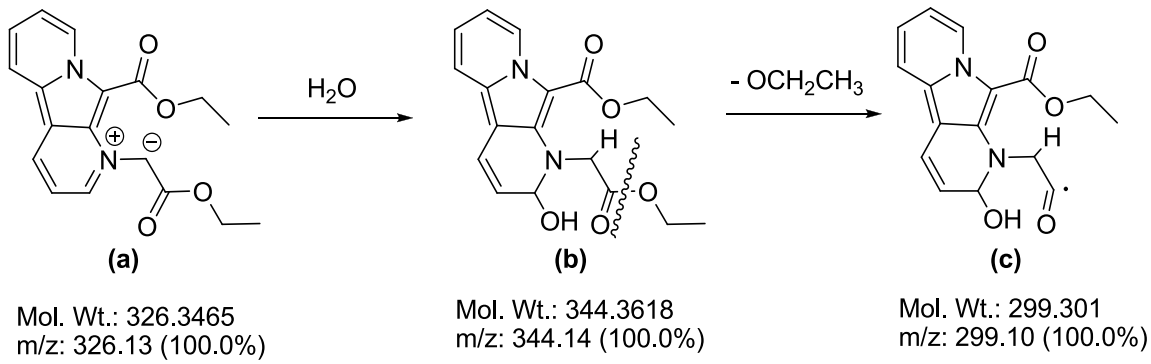

Scheme 4-2 Schematic representation of mass fragmentations of the crude material produced after microwave heating of *N*-(ethoxycarbonylmethyl)-pyridinium bromide (**4**) in the presence of triethylamine (NEt_3) in DMF followed by water treatment.

4.2.1.1. Characterisation and properties of indolizine modified SWNTs prepared via direct 1,3-dipolar cycloaddition of pyridinium ylides

Vibrational spectroscopy was used to identify the characteristic functional groups found on indolizine functionalised SWNTs. FTIR of the indolizine functionalised SWNTs (**7a-b**), Figure 4-2, shows the presence of the ester group ($\nu_{(CO)}$ 1730 cm^{-1}) and two bands characteristic of an indolizine at 1632 and 1541 cm^{-1}.[253]

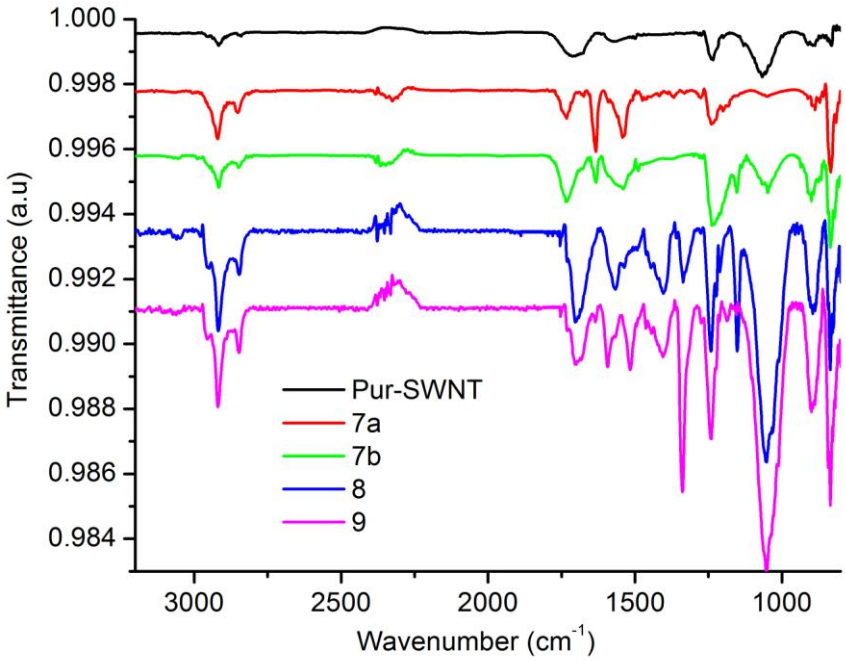

Figure 4- 2 Normalised and offset FTIR spectra of purified SWNTs (black), indolizine functionalised SWNTs (**7a**) prepared by conventional heating using *N*-(ethoxycarbonylmethyl)-pyridinium bromide (**4**) (red), indolizine functionalised SWNTs (**7b**) prepared by microwave heating using *N*-(ethoxycarbonylmethyl)-pyridinium bromide (**4**) (green), indolizine functionalised SWNTs (**8**) prepared by microwave heating using *N*-(4-methyl sodium benzenesulfonate)-pyridinium bromide (**5**) (blue) and indolizine functionalised SWNTs (**9**) prepared by microwave heating using *N*-(4-nitrobenzyl)-pyridinium bromide (**6**) (magenta).

FTIR spectra of the indolizine functionalised SWNTs (**8**) and (**9**) are also shown in Figure 4-2. FTIR spectrum of (**8**) displays the characteristic SO_2 symmetric stretching ($\nu_{(SO)}$ 1150 cm^{-1}) and SO_2 asymmetric stretching ($\nu_{(SO)}$ 1338 cm^{-1}) as an indication of sulfoxy group.[257] The band at 1520 cm^{-1} in FTIR spectrum of (**9**) indicates the presence of NO_2 asymmetric stretching ($\nu_{(NO)}$ 1520 cm^{-1}) confirming the availability of nitro groups.[258,259] Two bands at *ca.* 1580 and 1400 cm^{-1} in both spectra (**8** and **9**) can be assigned as characteristic stretchings of an indolizine.[253]

Direct evidence for the covalent functionalisation of SWNTs with pyridinium ylides was provided by Raman spectroscopy. The Raman spectra (excited at 632.8 nm and normalized to the G-band intensity) of pristine SWNTs and the cycloaddition products (**7a**, **7b**, **8** and **9**) are shown in Figure 4-3. As expected the modified SWNTs (**7a**, **7b**, **8** and **9**) have an enhanced D-band at *ca.* 1350 cm^{-1} when compared with unmodified SWNTs (A_D/A_G=0.086±0.003), with an A_D/A_G ratio of 0.173±0.006, 0.275±0.002, 0.166±0.005 and 0.136±0.001 respectively, indicative of groups attached to the surface of the nanotubes.[13, 44-46] The Raman spectra of the purified and modified (**7a**, **7b**, **8** and **9**) SWNTs excited at 532 nm (2.33 eV) and 785 nm (1.58 eV) are given in Appendix B (Figure B-1 and Figure B-2). From the spectra it is clear to see that the D band is shifted in frequency with changing laser excitation energy as the D band is dispersive. A_D/A_G ratio of the modified (**1a**, **1b**, **2b** and **3b**) SWNTs, Table 4-1, was also greater than purified SWNTs as an indication of covalent modification.

	Pur-SWNT	**7a**	**7b**	**8**	**9**
532 nm	0.061±0.001	0.158±0.005	0.152±0.001	0.194±0.005	0.14±0.004
785 nm	0.026±0.01	0.068±0.005	0.077±0.003	0.088±0.002	0.059±0.004

Table 4- 1 A_D/A_G of the modified SWNTs at 532 and 785 nm excitation.

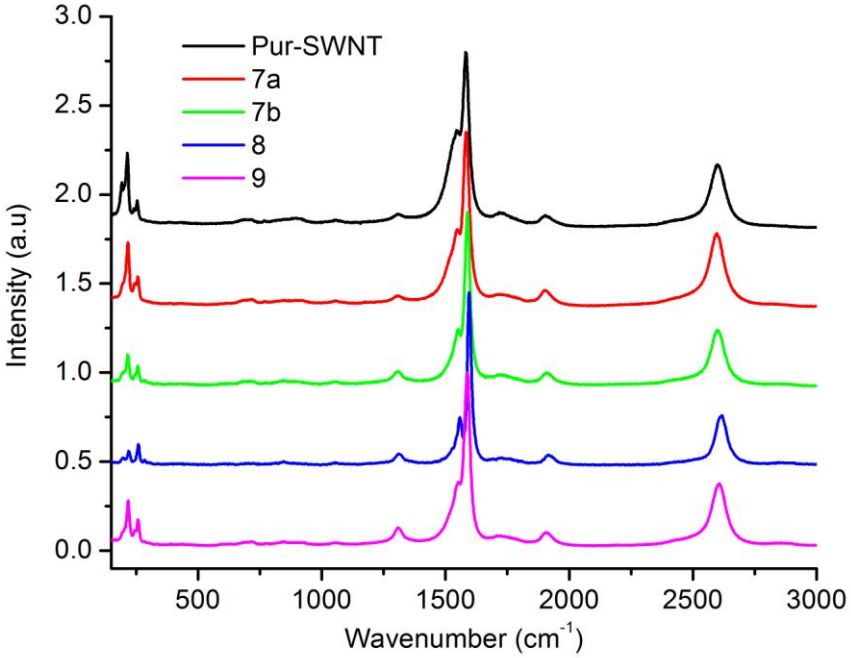

Figure 4- 3 Raman spectra (632.8 nm, 1.96 eV) of purified SWNTs (black), indolizine functionalised SWNTs (**7a**) prepared by conventional heating using *N*-(ethoxycarbonylmethyl)-pyridinium bromide (**4**) (red), indolizine functionalised SWNTs (**7b**) prepared by microwave heating using *N*-(ethoxycarbonylmethyl)-pyridinium bromide (**4**) (green), indolizine functionalised SWNTs (**8**) prepared by microwave heating using *N*-(4-methyl sodium benzenesulfonate)-pyridinium bromide (**5**) (blue) and indolizine functionalised SWNTs (**9**) prepared by microwave heating using *N*-(4-nitrobenzyl)-pyridinium bromide (**6**) (magenta) normalised at the G-band.

The UV-vis-NIR spectra of the modified SWNTs (**7a**, **7b**, **8** and **9**), Figure 4-4, showed the expected suppression of the bands in the region 400-1400 nm, present due to the van Hove singularities, indicating that functionalisation has taken place.[169,198-200]

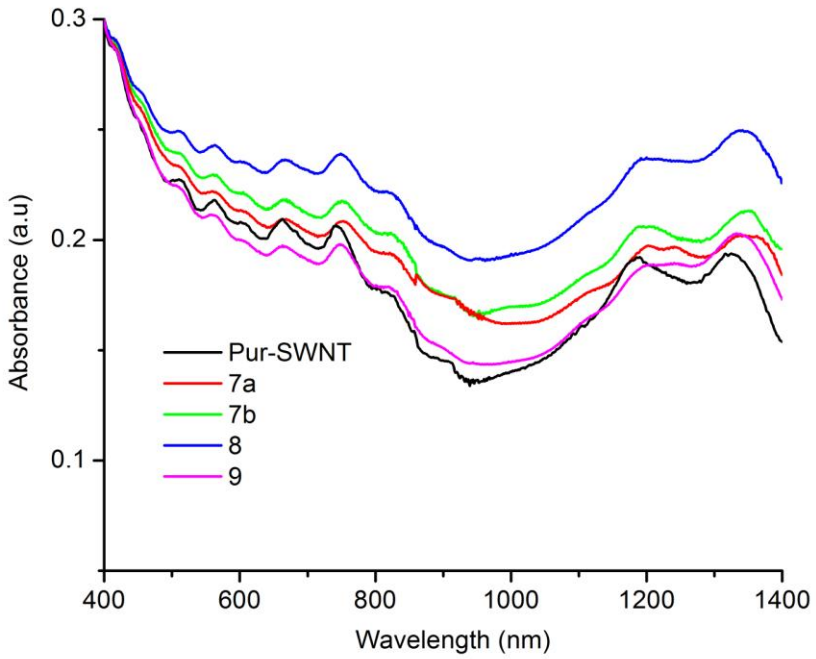

Figure 4- 4 Normalized (at 400 nm) UV-vis-NIR spectra, recorded in DMF, of purified SWNTs (black), indolizine functionalised SWNTs (**7a**) prepared by conventional heating using *N*-(ethoxycarbonylmethyl)-pyridinium bromide (**4**) (red), indolizine functionalised SWNTs (**7b**) prepared by microwave heating using *N*-(ethoxycarbonylmethyl)-pyridinium bromide (**4**) (green), indolizine functionalised SWNTs (**8**) prepared by microwave heating using *N*-(4-methyl sodium benzenesulfonate)-pyridinium bromide (**5**) (blue) and indolizine functionalised SWNTs (**9**) prepared by microwave heating using *N*-(4-nitrobenzyl)-pyridinium bromide (**6**) (magenta).

4.2.1.1.1. Effect of indolizine addition on solubility of SWNTs

The solubility of the indolizine modified SWNTs (**7b**, **8** and **9**) in DMF increased when compared with the purified SWNTs. Table 4-2 shows the infinite solubility of the indolizine modified SWNTs (**7b**, **8** and **9**) in DMF calculated using the extinction coefficient of 30 mL mg^{-1} cm^{-1}.[209]

SWNTs	Solubility in DMF (μg/mL)
Pur-SWNTs	4.3
7b	24.2
8	23.0
9	20.0

Table 4- 2 The solubility of indolizine modified (**7b**, **8** and **9**) and pristine SWNTs in DMF. (μg/mL)

The indolizine modified SWNTs (**7b**) were further derivatized using decyl alcohol to yield decanol-indolizine modified SWNTs (**10**) as it has been reported that the solubility of the SWNTs bearing long alkyl chains was enhanced in common organic solvents.[150,242] Scheme 4-3 shows the trans-esterification reaction of the indolizine modified SWNTs (**7b**) with decanol. Ethoxy groups on indolizine modified SWNTs (**7b**) were converted into the decoxy groups via the addition of excess decanol (0.5 mL) to the dispersion of 3 mg of (**7b**) in DMF (15 mL).

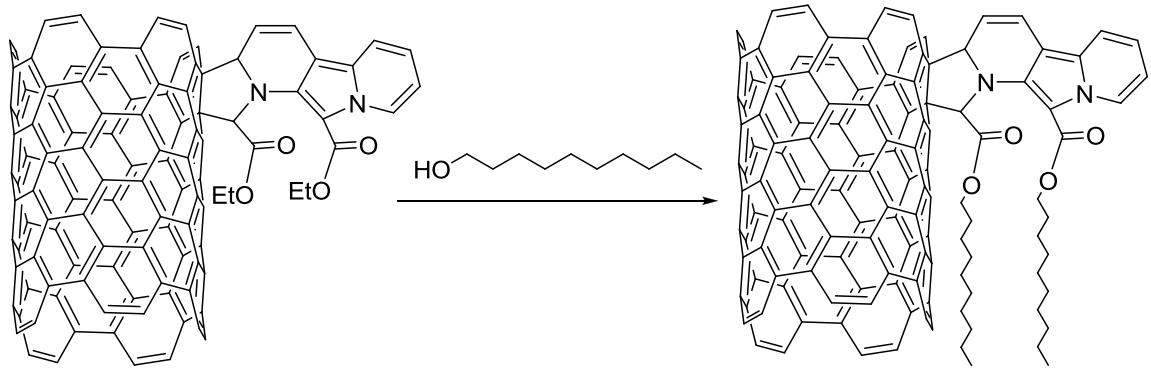

7b 10

Scheme 4-3 Schematic representation of the trans-esterification reaction of indolizine modified SWNTs (**7b**) with decanol.

A stable dispersion of the indolizine modified SWNTs (**7b**) in DMF had a concentration of 24.2 μg mL^{-1} which increased to 48.4 μg mL^{-1} when the indolizine modified SWNTs trans-esterified using decyl alcohol (**10**).

It was also possible to enhance the water solubility of the indolizine modified SWNTs (**7b**) by generating quaternary salts of them. Therefore we have converted the ester group on the indolizine functionalised SWNTs (**7b**) to an amide with a terminal tertiary amine, by reaction with *N,N*-dimethylethylenediamine, which was subsequently quaternarized by reaction with iodomethane to afford quaternary ammonium salts of indolizine-SWNTs (**11**), Scheme 4-4. Basiuk *et al.* have reported that surface of nanotubes especially MWNTs could be functionalised in the presence of long chain amines such as octadecylamine, nonylamine and dodecylamine at 150-170 ^{o}C and reduced pressure employing the gas-phase solvent-free procedure.[260,261] Results revealed that the addition was taken place on pyracylene units or C-C bonds of pentagons and they also showed that ideal nanotube sidewalls composed of solely benzene rings were found to be inert with respect to amines.[260]

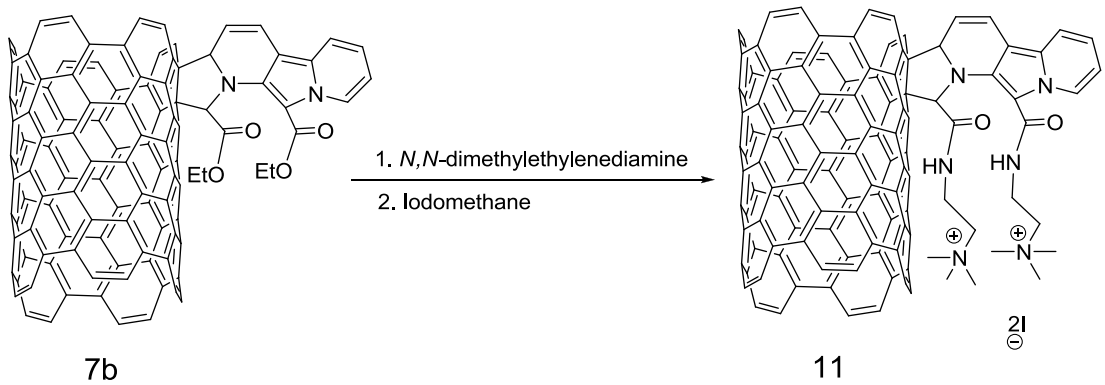

Scheme 4-4 Schematic representation of the amide and quaternary ammonium salt formation on SWNT surface

In contrast to their procedure amide formation reaction for gold tagging was carried out at 100 ^{o}C and 1 atm to reduce the possibility of the direct amine addition. A stable

dispersion of indolizine modified SWNTs (**7b**), in high purity water, had a concentration of 2.1 μg mL^{-1} which increased to 7.4μg mL^{-1} after the preparation of quaternary salt of indolizine-SWNTs (**11**).

4.2.1.1.2. Gold colloid tagging for AFM visualisation

Formation of the positively charged indolizine modified SWNTs (**11**) allowed us to visualise the functional groups by depositing them on a mica surface where they were exposed to citrate stabilised gold colloids 4 – 6 nm in diameter, Scheme 4-5.

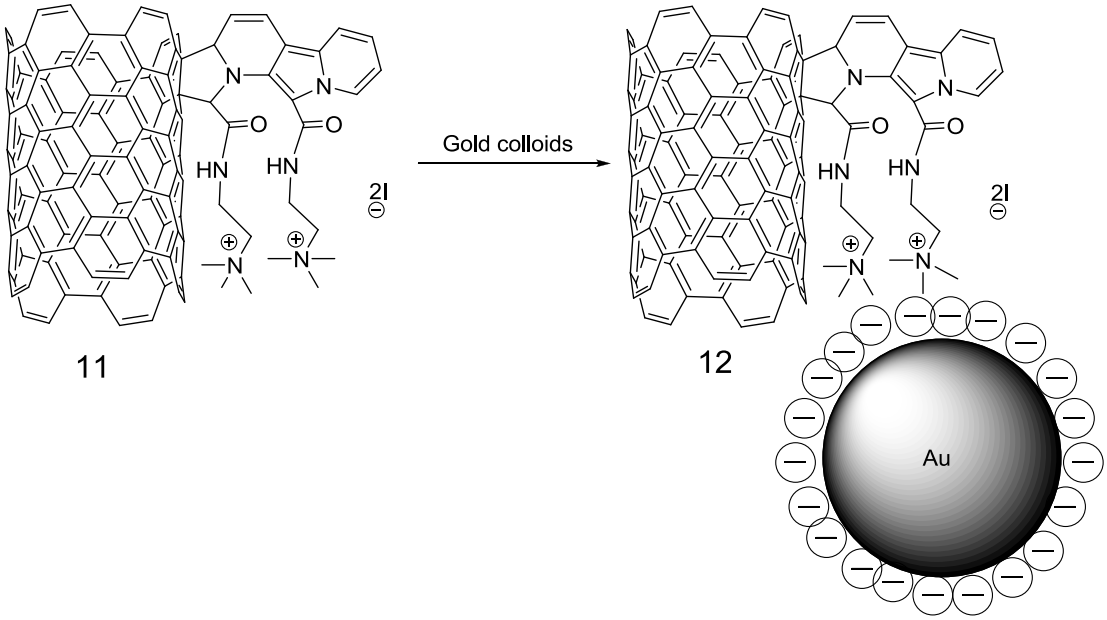

Scheme 4-5 Schematic representation of the electrostatic interaction of gold colloids with indolizine functionalised SWNTs (**7b**) for AFM functional group tagging experiments.

The electrostatic interaction of the negatively charged gold nanoparticles with the positively charge functionalised SWNTs is clear with the gold particles, Figure 4-5, visible as light features on the AFM height image, showing the presence and distribution of the indolizine functional groups on the nanotube surface. Control

experiments where purified SWNTs, that have not undergone any chemical functionalisation, are exposed to gold colloids showed that Au nanoparticles was not adsorbed on the surface of unmodified SWNTs, Figure 4-5. AFM section analysis for gold decorated indolizine modified SWNTs (**12**) revealed that the functionalisation of the SWNTs with pyridinium ylides was a non-destructive method which produces individualized long SWNTs without damaging.

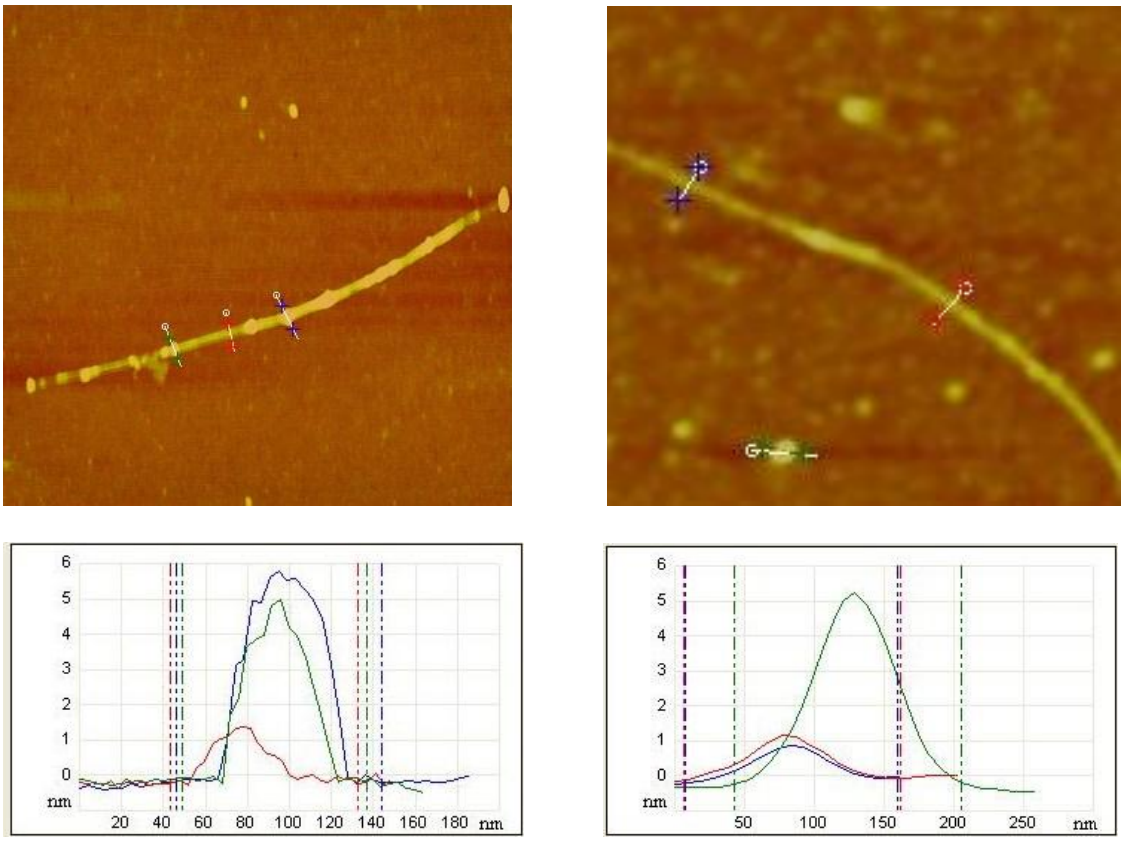

Figure 4- 5 A typical tapping mode AFM height image of an indolizine functionalised SWNT with positively charged tertiary amines (**11**) (1.9 μm by 1.9 μm) (Top left) and purified SWNT (2.0 μm by 2.0 μm) (Top right) after exposure to citrate stabilized Au colloids (4 – 6 nm). The section analysis of the individualized gold decorated quaternary salt of modified SWNT (**12**) (Bottom left) and purified SWNT (Bottom right). The image shown is with a z scale of 0 – 5 nm.

4.2.1.1.3. X-ray and thermal analysis of indolizine modified SWNTs

The level of functionalisation was confirmed by XPS measurements. Here, representative XPS spectra of the indolizine modified SWNTs are presented and, the rest of the spectra, including XPS survey spectra, are attached to Appendix B (Figure B3-B6). Table 4-3 displays the elemental compositions in the modified (**7a**, **7b**, **8** and **9**) and pristine SWNT sample and their binding energies.

SWNTs	Element	C1s	O1s	N1s	Na1s	S2p	Si2p	F1s
Pristine	BE (eV)	284.4	532.4	-	-	-	-	-
	Conc(%)	95.55 ±0.41	4.45 ±0.24	-	-	-	-	-
7a	BE (eV)	284.6	531.2	399.40	-	-	-	688.2
	Conc(%)	93.91 ±0.70	3.28 ±0.19	1.60 ±0.27	-	-	-	1.21 ±0.13
7b	BE (eV)	284.6	532.1	398.8	1072.0	-	102.0	-
	Conc (%)	90.27 ±0.69	6.83 ±0.26	1.98 ±0.30	0.12	-	0.80	-
8	BE (eV)	284.5	532.9	399.9	1071.8	165.9	-	-
	Conc (%)	89.38 ±0.68	8.39 ±0.34	1.48 ±0.41	0.40 ±0.12	0.35 ±0.07	-	-
9	BE (eV)	284.5	532.9	399.7, 405.8	-	-	-	-
	Conc (%)	91.36 ±0.72	6.55 ±0.31	2.09 ±0.29	-	-	-	-

Table 4- 3 Elemental composition and the binding energies of the elements present in purified SWNTs and the indolizine modified SWNTs (**7a**, **7b**, **8** and **9**).

According to the data provided by XPS, purified SWNTs contain 95.55±0.41 % C and 4.45±0.24 % O atoms. Figure 4-6 shows the deconvoluted C1s and O1s XPS spectra of purified SWNTs.

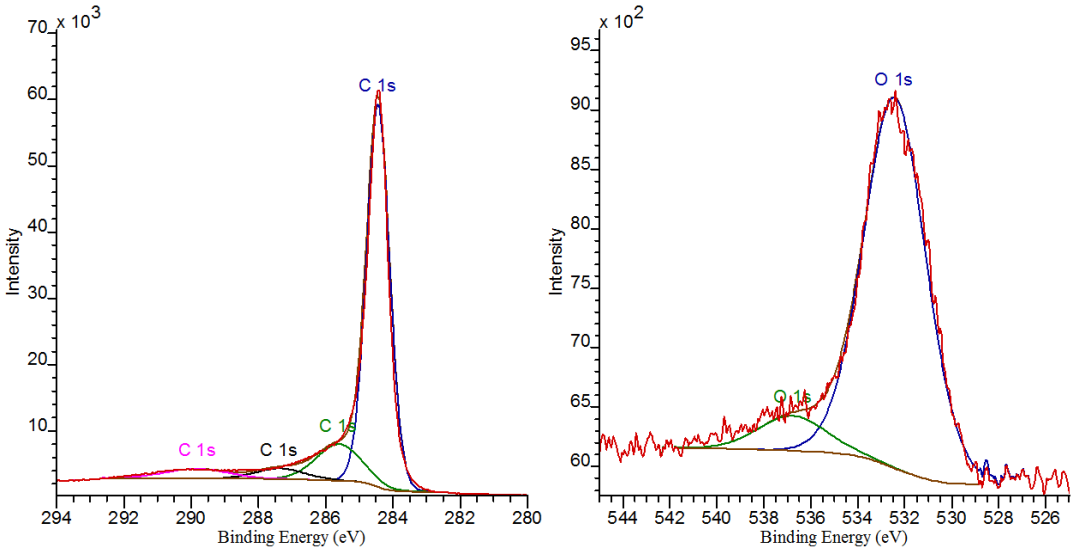

Figure 4- 6 Left: C1s XPS spectrum of the purified SWNTs and the position of components, Right: O1s XPS spectrum of the purified SWNTs and the position of components.

Analysis of C 1s XPS spectrum of purified SWNTs shows four components having binding energies at 284.4, 285.4, 287.2 and 289.8 eV atributable to graphitic carbon (C=C),[262] σ*(-C*-C*(H)) transition due to the contamination or the remaining C-H bonds on the surface,[263,264] carbonyl (or ether)[265] and carboxyl group (-O-C*=O),[264,266] respectively. O1s XPS spectrum consists of two main components at 532.4 and 536.7 eV corresponded to carboxyl (-O-C=O*)[264] and hydroxyl (-C-O*H),[267] respectively. The presence of O atom in purified SWNT sample can be due to either atmospheric oxygen and carbon dioxide contamination[268] or the oxidized SWNTs produced during purification period.[262] Composition (%) of each component in C1s and O1s XPS spectra of pristine SWNTs is given in Table 4-4.

	Peak position/eV				Composition %
C1s	284.4 (C=C)[262]	285.4 *(-C*-C*(H))[263,264]	287.2 (>C=O or C-O-C)[265]	289.8 (-O-C*=O)[264,266]	75.89/14.23/4.56/5.32
O1s	532.4 (-O-C=O*)[264]	536.7 (-C-O*H)[267]	-	-	90.71/9.29

Table 4- 4 Peak positions (eV) and the composition (%) of each component in C1s and O1s XPS spectra of pristine SWNTs

In addition to C and O atoms, indolizine modified SWNTs (**7a**, **7b**, **8** and **9**) show the presence of 1.60±0.27, 1.98±0.30, 1.48±0.41 and 2.09±0.29 atomic per cent (at.%) nitrogen which are equal to one indolizine group per 95, 76, 86 and 130 CNT carbon atom, respectively (see Table 4-3). It was also noticed that the elemental composition of the carbon atom in indolizine modified SWNTs decreased due to the covalently attached O and N containing indolizine groups. Figure 4-7 displays the N1s and O1s XPS spectra of the indolizine modified SWNTs (**7b**). From the Figure 4-7, it is clear to see that N1s XPS spectrum consists of two main components positioned at 398.8 and 401.2 eV and, O1s XPS spectrum consists of three main components positioned at 530.1, 531.7 and 535.2 eV, respectively.

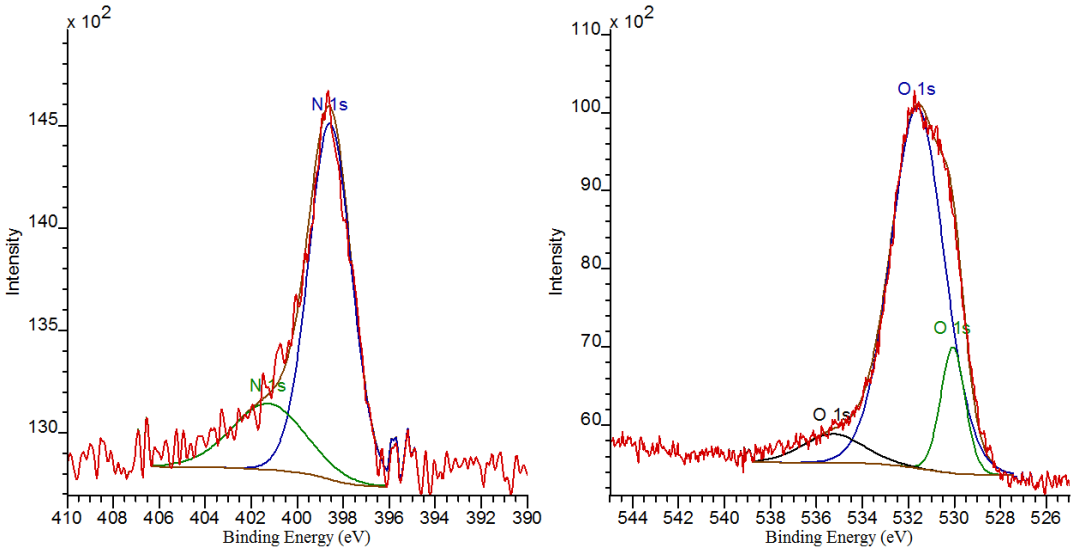

Figure 4- 7 Left: N1s XPS spectrum of the indolizine modified SWNTs (**7b**) and the position of components, Right: O1s XPS spectrum of the indolizine modified SWNTs (**7b**) and the position of components.

Table 4-5 shows the position (eV) and the composition % of each component in N1s and O1s XPS spectra of indolizine modified SWNTs (**7b**).

	Peak position/eV				Composition %
N1s	398.8 (pyridine) [269,270]	401.2 (quaternary pyridine)[271]	-	-	76.02/23.98
O1s	530.1 (Fe_2O_3)[272]	531.7 (isolated –OH, C=O, O-C=O)[273]	535.2(carbonates)[274]	-	12.69/80.07/7.24

Table 4- 5 Peak positions (eV) and the composition (%) of each component in N1s and O1s XPS spectra of indolizine modified SWNTs (**7b**).

N1s component at 398.8 eV is characteristic of sp^2 hybridised pyridine nitrogen[269,270] and the component at 401.2 eV is attributed to quaternary pyridine.[271] Moreover O1s XPS spectrum of indolizine modified SWNTs (**7b**) shows a broadened line shape as an indication of new oxygen containing group attachment on nanotube surface when compared with XPS spectrum of O 1s for purified SWNTs.

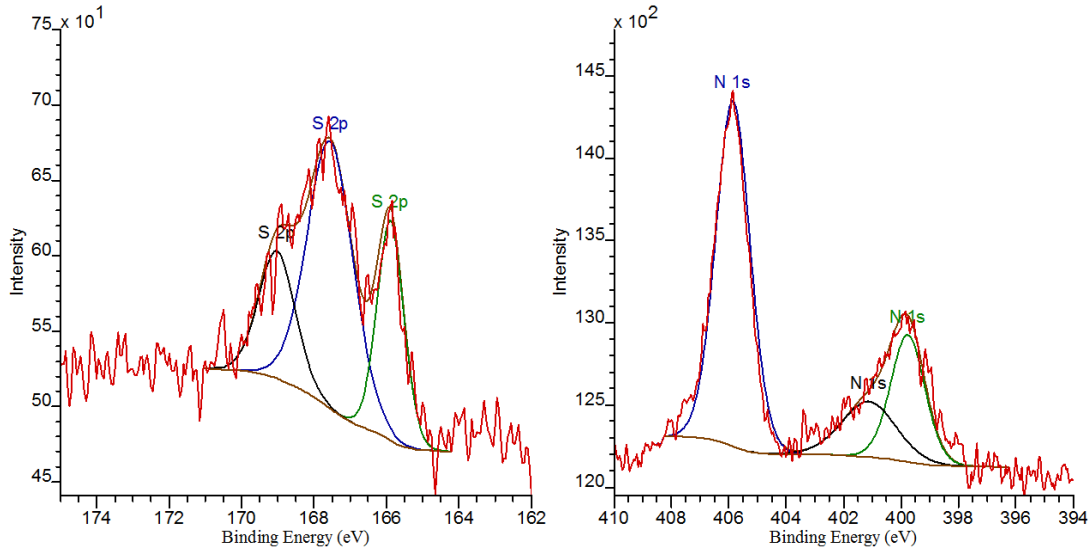

Figure 4- 8 Left: S2p XPS spectrum of the indolizine modified SWNTs (**8**) with three components *ca.* 165.8 (green), 167.5 (blue) and 169.0 (black) eV; Right: N1s XPS spectrum of the indolizine modified SWNTs (**9**) with three components *ca.* 399.7 (green), 401.1 (black) and 405.8 (blue) eV.

Since the indolizine modified SWNTs (**8** and **9**) contain sulfonate and nitro groups it was possible to assign S and N atoms using XPS. Analysis of the indolizine modified SWNTs (**8** and **9**) displayed, Figure 4-8, the presence of sulfonate group in (**8**) and nitro group in (**9**) showing the characteristic S2p[98,275,276] with three components *ca.* 165.8, 167.5 and 169.0 eV attributable to $-SO_3Na$,[277] O=S=O[278,279] (2p1/2) and O=S=O[278,279] (2p3/2), respectively and, N1s[280-282] at 405.8 eV attributable to $-NO_2$ group.

TGA-MS of modified SWNTs (**7a**, **7b**, **8** and **9**) shows a weight loss of 17±0.005, 22±0.005, 20±0.005 and 25±0.005 % respectively, at 600 °C compared to *ca.* 7±0.005% for purified SWNTs, Figure 4-9.

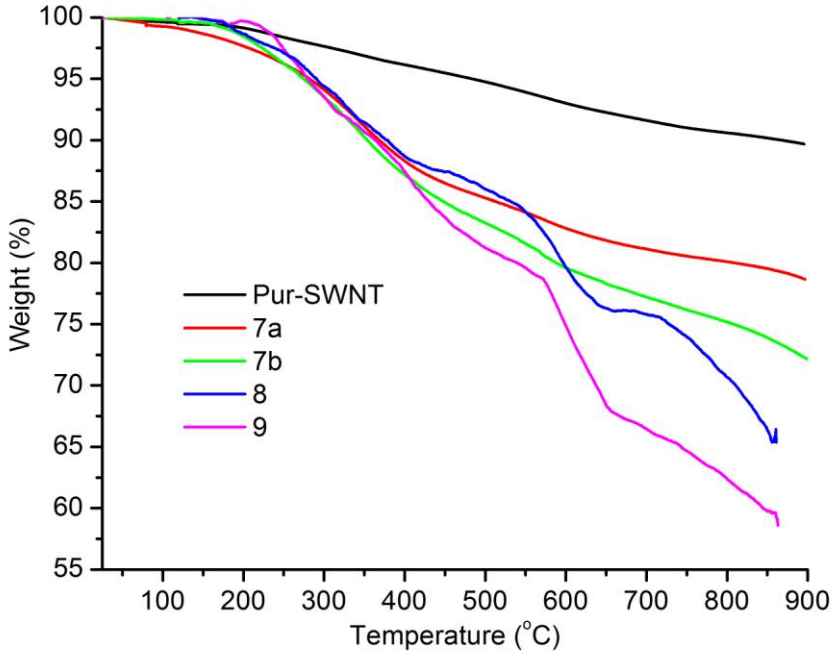

Figure 4- 9 TGA-MS data (10 °C min^{-1}) of purified SWNTs (black), indolizine functionalised SWNTs (**7a**) prepared by conventional heating using *N*-(ethoxycarbonylmethyl)-pyridinium bromide (**4**) (red), indolizine functionalised SWNTs (**7b**) prepared by microwave heating using *N*-(ethoxycarbonylmethyl)-pyridinium bromide (**4**) (green), indolizine functionalised SWNTs (**8**) prepared by microwave heating using *N*-(4-methyl sodium benzenesulfonate)-pyridinium bromide (**5**) (blue) and indolizine functionalised SWNTs (**9**) prepared by microwave heating using *N*-(4-nitrobenzyl)-pyridinium bromide (**6**) (magenta).

This corresponds to the presence of approximately 1 functional group for 133 (1.54 N% and 96 (2.08 N%), 179 (1.12 N%) and 106 (1.89 N%) carbon atoms respectively. When the conventional heating (**7a**) and the microwave heating (**7b**) processes were compared it was observed that the microwave conditions give slightly higher levels of

functionalisation. The results provided by TGA were in close agreement with the values determined by XPS. Mass spectrometry results, Figure 4-10, suggested that the peak of mass loss is between 200 and 600 ^{o}C for the indolizine modified SWNTs (**7b**, **8** and **9**).

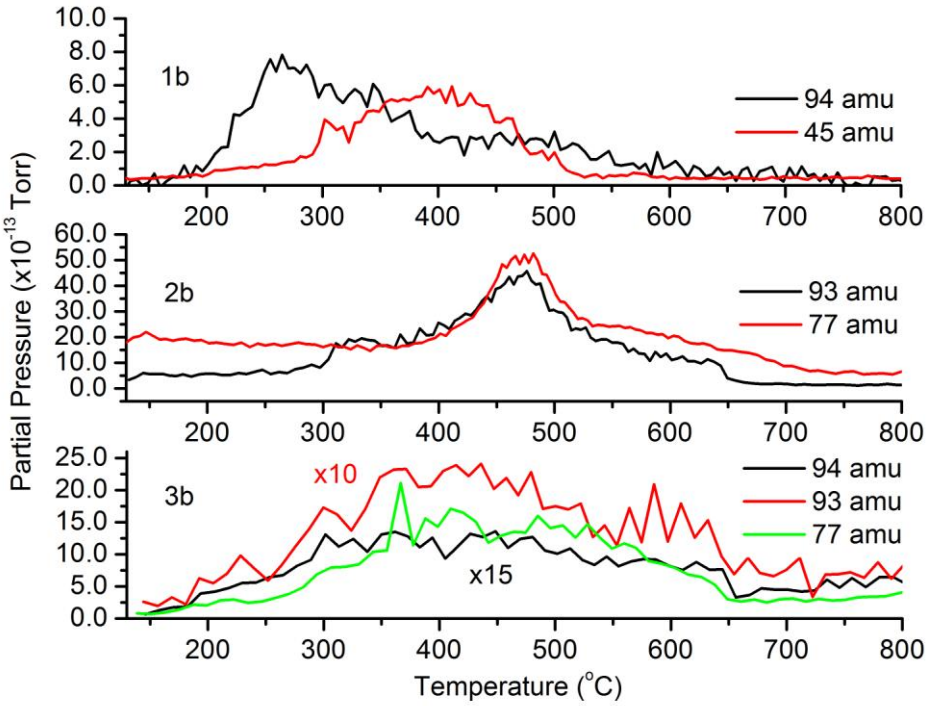

Figure 4- 10 Top: MS trace (black) of N-methylpyridinium (94 amu) and (red) ethyl ester fragment (OEt, 45 amu) given off during heating of (**1b**). Middle: MS trace (black) of N-methylpyridinium (94 amu) and (red) phenyl fragment (C_6H_5, 77 amu) given off during heating of (**2b**). Bottom: MS trace (black) of N-methylpyridinium (94 amu), (red) phenoxy fragment (C_6H_5O, 93 amu) and (green) phenyl fragment (C_6H_5, 77 amu) given off during heating of (**3b**).

However it was not possible to observe the parent ion of the indolizine due to its high molecular mass. Although the parent ion of the indolizine was not observed, fragments relating to the ethyl ester group (OEt, 45 amu) and *N*-methylpyridinium (94 amu) for (**7b**), *N*-methylenepyridinium (93 amu) and phenyl (77 amu) for (**8**) and, *N*-

methylpyridinium (94 amu), phenoxy (C_6H_5O, 93 amu) and phenyl (C_6H_5, 77 amu) for (**9**) were detected by mass spectrometry.

4.2.1.1.4. Metallic versus semiconducting selectivity in 1,3-dipolar cycloaddition of pyridinium ylides

Detailed study of the selectivity and reactivity of the pyridinium ylide addition towards SWNTs was performed using 632.8 nm (1.96 eV), 532 nm (2.33 eV) and 785 nm (1.58 eV) laser excitation sources. Raman spectroscopy at 632.8 nm (1.96 eV), Figure 4-11, of the unmodified SWNT material in the RBM region shows five peaks at *ca.* 187, 197, 209, 236 and 251 cm^{-1} the latter two being significantly less intense.

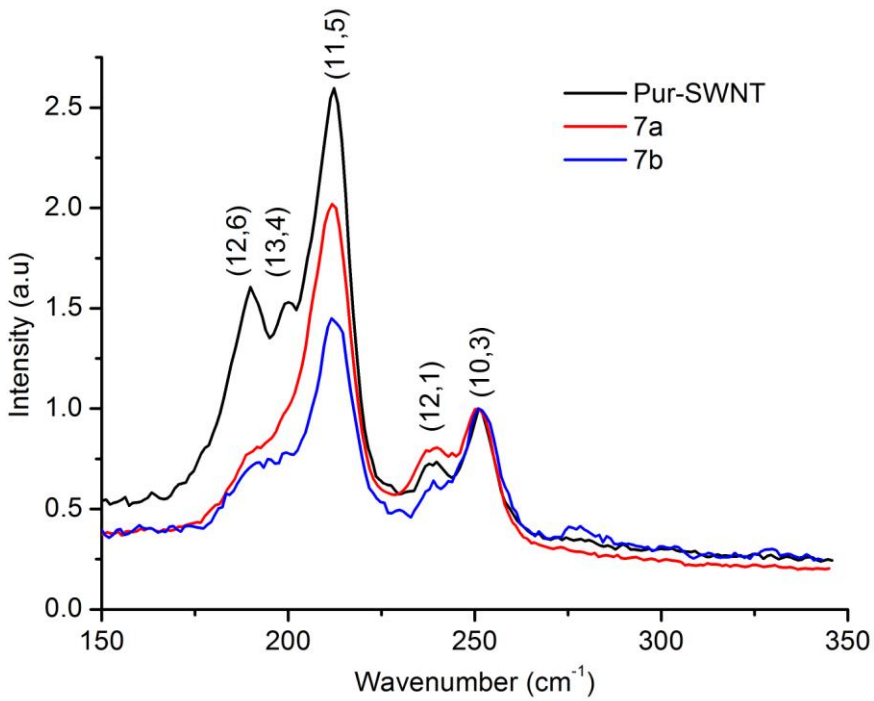

Figure 4- 11 RBM region of the Raman spectra (632.8 nm, 1.96 eV) of purified SWNTs (black), indolizine functionalised SWNTs (**7a**) prepared by conventional heating using *N*-(ethoxycarbonylmethyl)-pyridinium bromide (**4**) (red) and indolizine functionalised SWNTs (**7b**) prepared by microwave heating using *N*-(ethoxycarbonylmethyl)-pyridinium bromide (**4**) (blue) normalized at 251 cm^{-1}.

Using modified Kataura plots[142] these bands are assigned to (12,6), (13,4), (11,5), (12,1) and (10,3) SWNTs with diameters of 1.28, 1.21, 1.14, 1.00 and 0.94 respectively, the first three being metallic and the remaining two semiconducting nanotubes. Cycloaddition to form (**7a**) and (**7b**) results in changes in intensity of some of the bands. By normalizing the spectra to the band at 251 cm^{-1} (which is essentially unchanged after reaction) it is clear that the semiconducting SWNTs are relatively unchanged upon functionalisation whereas the bands assigned to metallic SWNTs are significantly reduced in intensity, Figure 4-11.

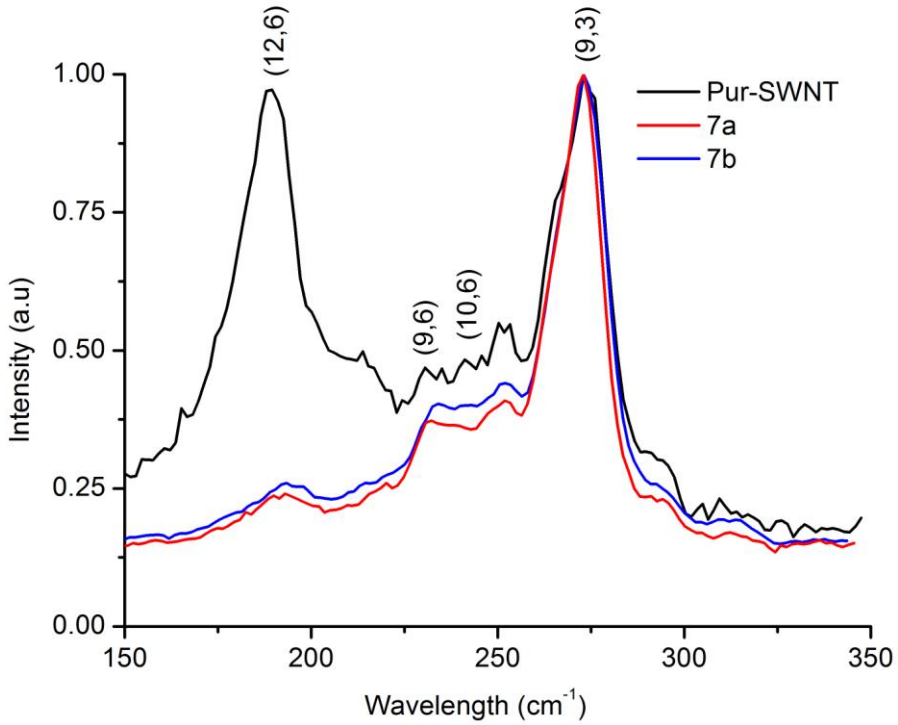

Figure 4- 12 RBM region of the Raman spectra (532 nm, 2.33 eV) of purified SWNTs (black), indolizine functionalised SWNTs (**7a**) prepared by conventional heating using *N*-(ethoxycarbonylmethyl)-pyridinium bromide (**4**) (red) and indolizine functionalised SWNTs (**7b**) prepared by microwave heating using *N*-(ethoxycarbonylmethyl)-pyridinium bromide (**4**) (blue) normalized at 273 cm^{-1}.

Excitation at 532 nm (2.33 eV), Figure 4-12, shows two bands at 187 and 273 cm^{-1} which can be assigned to (12,6) and (9,3) SWNTs with diameters of 1.28 and 0.86 nm respectively, the two possible weak bands at 234 and 253 cm^{-1} are ignored. The assignment of the (12,6) SWNTs is tentative as this nanotube chirality would be expected to be just off resonance using 2.33 eV excitation. Raman spectra, normalized at 273 cm^{-1}, of the functionalised SWNTs (**7a**) and (**7b**), Figure 4-12, show a significant decrease in the band at 187 cm^{-1} assigned to larger diameter metallic SWNTs.

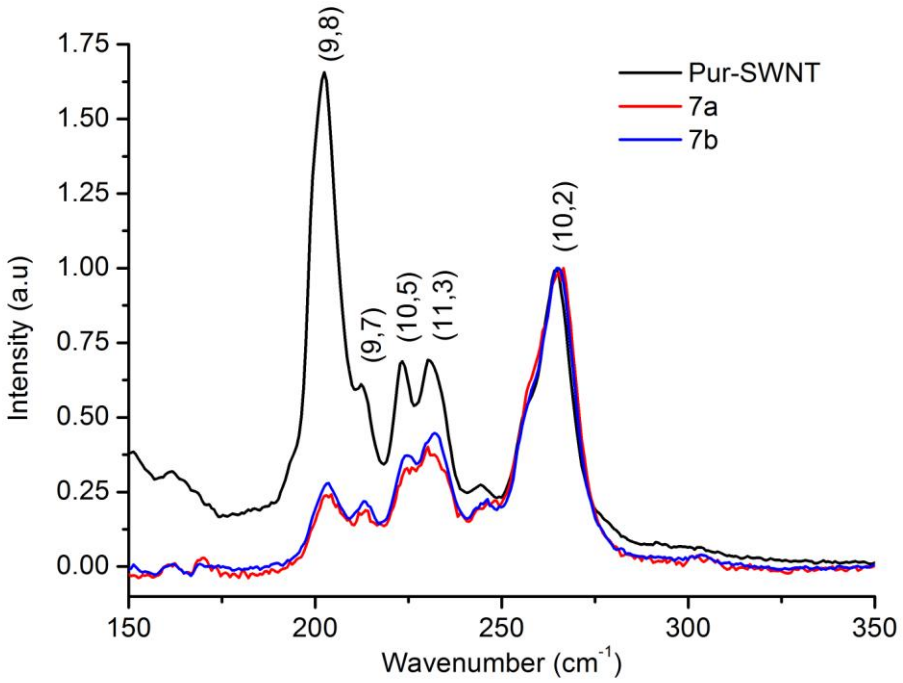

Figure 4- 13 RBM region of the Raman spectra (785 nm, 1.58 eV) of purified SWNTs (black), indolizine functionalised SWNTs (**7a**) prepared by conventional heating using *N*-(ethoxycarbonylmethyl)-pyridinium bromide (**4**) (red) and indolizine functionalised SWNTs (**7b**) prepared by microwave heating using *N*-(ethoxycarbonylmethyl)-pyridinium bromide (**4**) (blue) normalized at 265 cm^{-1}.

Excitation at 785 nm (1.58 eV), Figure 4-13, shows five bands at 202, 212, 222, 230 and 265 cm^{-1} which can be assigned (9,8), (9,7), (10,5), (11,3) and (10,2) SWNTs with diameters of 1.18, 1.12, 1.06, 1.02 and 0.85 nm respectively, the possible weak band at 245 cm^{-1} is ignored. Note the (10,2) assignment, although the best fit, is tentative as this nanotube chirality would be just off resonance when excited at 1.58 eV.

The Raman spectra of the functionalised SWNTs (**7a**) and (**7b**), normalized at 265 cm^{-1}, show a significant decrease in the band at 202 cm^{-1} assigned to larger diameter semiconducting SWNTs and a somewhat smaller decrease in the bands at 212, 222 and 230 cm^{-1}, Figure 4-13.

RBM region of the Raman spectra of the modified SWNTs (**8** and **9**) excited at 632.8 (1.96 eV), 532 (2.33 eV) and 785 nm (1.58 eV) are also given in Appendix B (Figure B7-B9) for comparision. From the results shown here it is clear that excitation at 632.8 nm shows that the cycloaddition reaction is selective for metallic SWNTs where 532 nm excitation shows that selectivity is towards larger diameter metallic SWNTs. Interestingly, 785 nm excitation shows that the reaction is not limited to metallic SWNTs as larger diameter semiconducting SWNTs react. Thus from the resonance Raman data it is clear that the 1,3 dipolar cycloaddition of pyridinium ylides is selective for larger diameter SWNTs. This is interesting as typically smaller diameter SWNTs are often predicted to be more reactive than their larger counterparts due to the greater degree of curvature and π-orbital misalignment present.[79] However, larger diameter semiconducting SWNTs have been shown to be more reactive than smaller diameter SWNTs to diazonium salts due to the latter having a larger band-gap and thus a large region where the density of states (DOS) of the SWNT is zero.[146] The selectivity displayed by the 1,3-dipolar cycloaddition reaction discussed here is similar, metallic more reactive than semiconducting and large diameter semiconducting more reactive than small diameter SWNTs, and thus the reactivity is

likely to be correlated with band-gap. This fits with a mechanism that first involves electron transfer from the SWNT which is in agreement with metallic SWNTs, which have a finite DOS at the Fermi level, being more reactive than semiconducting SWNTs.

4.2.1.1.5. Fluorescent properties of indolizine modified SWNTs

Since indolizines are known to be florescent compounds[32, 33] they emit light upon excitation. Figure 4-14 displays the emission spectra of the indolizine modified SWNTs (~10^{-4} M) (**7a**, **7b**, **8** and **9**) recorded in DMF.

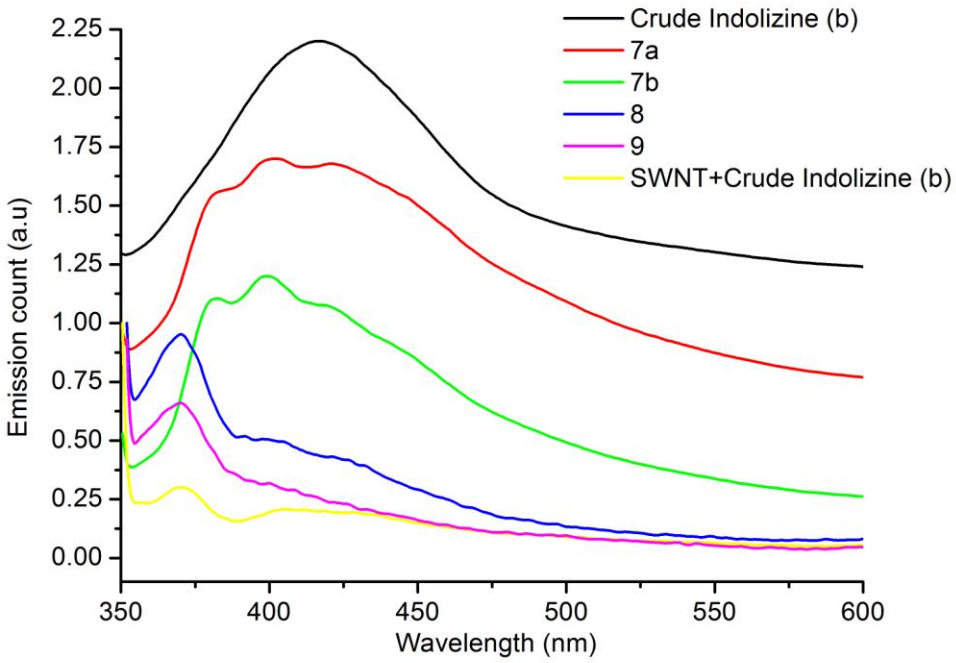

Figure 4- 14 Normalized and offset fluorescence spectra of the indolizine formed from the 1,3-dipolar cycloaddition of the pyridinium ylide, generated from the pyridinium salt (**4**), with a second pyridinium ylide in the absence of SWNTs (black), (**7a**) (red), (**7b**) (green), (**8**) (blue), (**9**) (magenta) and the control experiment of mechanically mixing purified SWNTs with the indolizine generated from the cycloaddition of one pyridinium ylide to another (yellow).

Whilst excitation of (**7a**) and (**7b**) at 335 nm results in a blue emission at 416 nm, modified SWNTs (**8** and **9**) show no sign of fluorescence. This could be owing to the quenching effect of the strong electron withdrawing groups (-NO_2 and -$SO_3^-Na^+$) attached to the indolizine system. A similar effect was observed by Vlahovici *et al.* on molecular indolizine system.[283] Unfortunately, quantum yields were not determined due to the strong scattering and absorption of the SWNTs which made it difficult to compare absolute emission intensities and true quantum efficiencies. Control experiments mechanically mixing the crude reaction product (**b**) (see Scheme 4-2), prepared via the 1,3-dipolar addition of the pyridinium ylide to a second pyridinium ylide under microwave conditions, with purified SWNTs followed by washing showed no sign of fluorescence.

Since the emission spectrum of the indolizine modified SWNTs (**7b**) had a significant tail in the green it was also possible to look at green emission using an optical microscope. Figure 4-15 shows the white light optical image (left) and the epi-fluoresence image (right) of indolizine modified SWNTs (**7b**). Fluorescence images were recorded using excitation light transmitted through a 420 to 480 nm excitation filter and fluorescence observed after passage through a 500 nm emission filter (Olympus CX-DMB-2 cube). It is clear to see the green spots on the epi-fluoresence image (right) of indolizine modified SWNTs as an indicatorof covalent functionalisation of SWNTs via light emitting groups. Efficiency of the green spots also reveals that the light emitting indolizine functionalised SWNTs could be used for imaging.

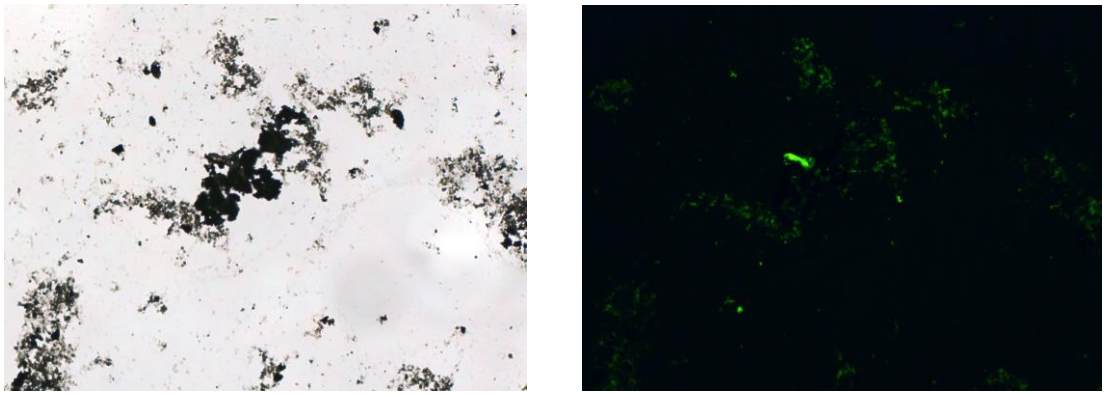

Figure 4- 15 White light optical image (left) and epi-fluorescence image (right) of the indolizine modified SWNTs (**7b**) (718 x 533 μm).

4.2.2. Indolizine formation via click reaction

In this section it has been demonstrated that it is possible to introduce light emitting indolizine groups[251,252,283-285] purposely to the surface of CNTs using 'click' chemistry. 'Click' chemistry, defined as a modular reaction bringing together two simple units to generate a more complex substance, is gaining momentum in materials science.[286] For CNTs 'click' chemistry is predominantly based around the Huisgen cycloaddition of azides to alkynes and has been used to attach polystyrene,[287] beta-cyclodextrin[288] and phthalocyanines[289] to the surface of nanotubes. In addition, other simple 1,3-dipolar cycloaddition reactions fit the criteria of 'click' chemistry such as the reaction described here. The pyridinium ylide, rather than reacting with the CNT surface directly, is covalently bonded to the nanotube which then undergoes 1,3-dipolar cycloaddition with dimethyl acetylenedicarboxylate (DMAD), Scheme 4-6.

Pyridine functionalised SWNTs (**2**) described in Chapter III were used to generate the pyridinium salts. Indolizine functional groups were formed on the surface of the SWNTs by first generating the simple Kröhnke salts followed by reaction with NEt_3 and DMAD, Scheme 4-6. PEG_{400}-yl 2-bromoacetate and PEG_{2000}-yl 2-bromoacetate

were synthesised using a literature procedure[285] and characterised using FTIR, ^{1}H NMR and ^{13}C NMR spectroscopy.

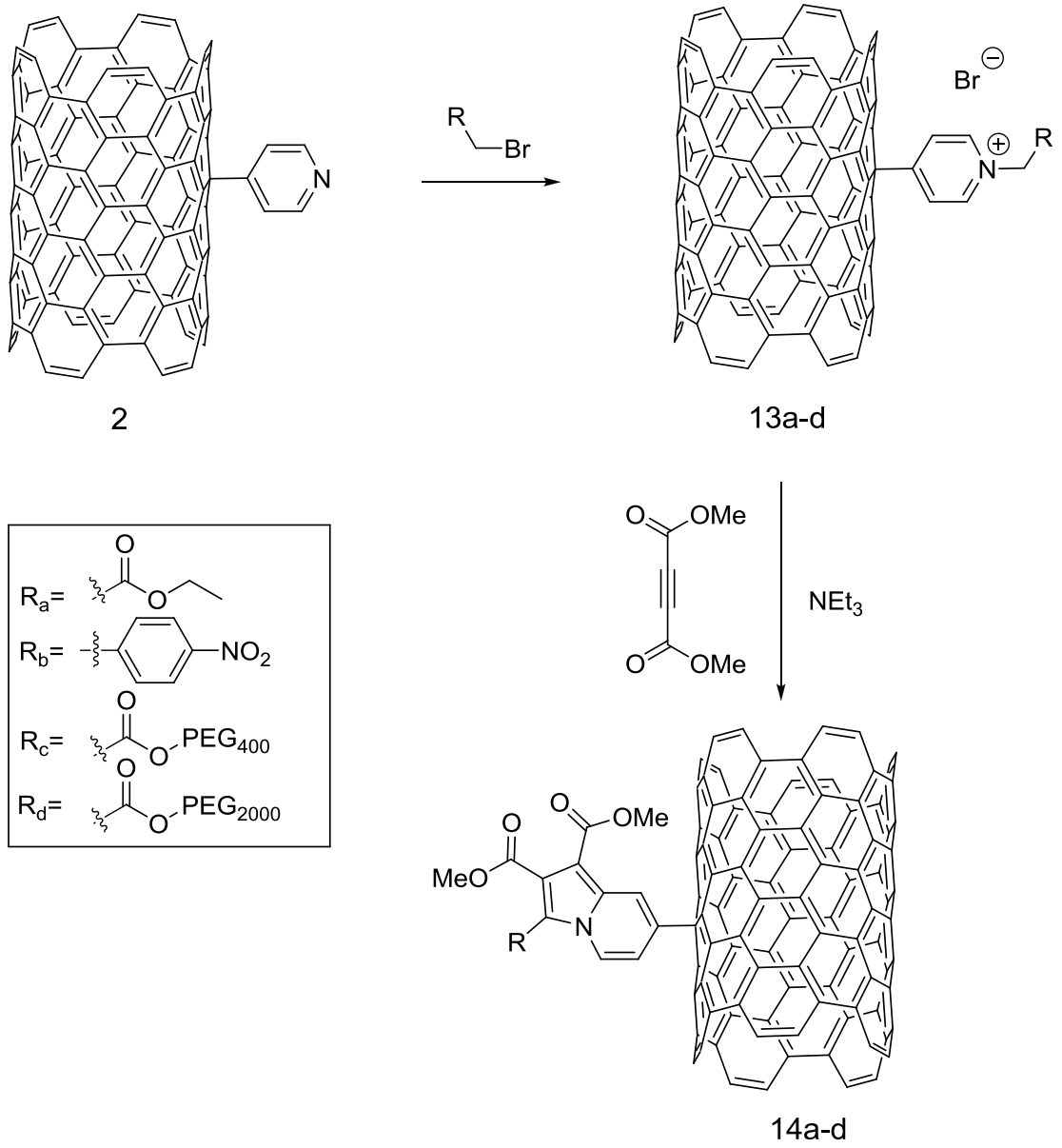

Scheme 4-6 Schematic representation of the pyridine functionalised SWNTs (**2**) and the 1,3-dipolar cycloaddition of pyridinium salts (**13a-d**) with DMAD in the presence of NEt_3 to form corresponding indolizine modified SWNTs (**14a-d**).

4.2.2.1. Characterisation and properties of indolizine modified SWNTs prepared via click reaction

All reactions were carried out in DMF and it was possible to follow the progress by monitoring the dispersion of the SWNT material using UV-vis-NIR. A stable dispersion of the pyridine functionalised material had a concentration of ~163 μg mL^{-1}, which decreased dramatically to 0.2 μg mL^{-1} upon the addition of ethyl-2-bromoacetate to form the Kröhnke salt (**13a**) which increased to 40 μg mL^{-1} following cycloaddition to form the indolizine functionalised SWNTs (**14a**). Table 4-6 shows the solubility of the stable dispersion of Kröhnke salts (**13a-d**), indolizine functionalised SWNTs (**14a-d**) and pyridine functionalised SWNTs (**2**) in both DMF and ethanol (EtOH). Before recording the UV-vis-NIR spectra of modified SWNTs stable dispersions of them were prepared by sonicating in an ultrasonic bath for 10 min and left for settling overnight. Supernatant solutions of the corresponding materials were used to calculate the solubility of each of the modified SWNTs.

	2	**13a**	**13b**	**13c**	**13d**	**14a**	**14b**	**14c**	**14d**
DMF	162.6	0.2	8.4	8.8	3.9	40.0	47.4	32.3	10.1
EtOH	72.4	34.0	28.5	7.3	3.1	16.4	19.3	6.0	1.26

Table 4- 6 Solubility data (μg/mL) of the Kröhnke salts (**13a-d**), indolizine functionalised SWNTs (**14a-d**) and pyridine functionalised SWNTs (**2**) in both DMF and EtOH.

The solubility, Table 4-6, of the pyridine functionalised SWNTs (**2**) in DMF decreased after generating Kröhnke salts (**13a-d**) which increased by the formation of indolizine groups. Wheras, the solubility of the Kröhnke salts (**13a-d**) in EtOH decreased after generating Kröhnke salts (**13a-d**) which again decreased by the formation of indolizine

groups. It was also observed that the solubility of Kröhnke salts (**13a-b**) were higher in EtOH than in DMF.

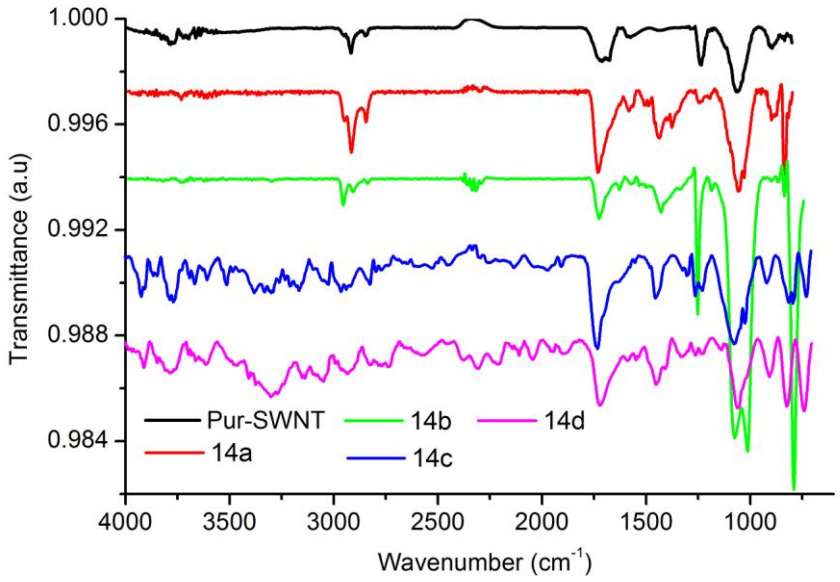

Figure 4- 16 FTIR spectra of purified SWNTs (black), indolizine functionalised SWNTs (**14a**) prepared by ethyl-2-bromoacetate (red), indolizine functionalised SWNTs (**14b**) prepared by 4-nitrobenzyl bromide (green), indolizine functionalised SWNTs (**14c**) prepared by PEG_{400}-yl 2-bromoacetate (blue) and indolizine functionalised SWNTs (**14d**) prepared by PEG_{2000}-yl 2-bromoacetate (magenta).

FTIR spectroscopy was used to characterize functional groups attached to indolizine on nanotube surface. The FTIR spectra of indolizine modified SWNTs (**14a-d**), Figure 4-16, show the presence of the ester groups attached to the indolizine ring as a broad band ($\nu_{(CO)}$) centered around 1730 cm^{-1} (along with multiple bands between 1600-1300 cm^{-1}, presumably from the formation of the indolizine). The bands *ca.* 2850-2990 cm^{-1} in the spectrum of (**14b**) that are upshifted compared with (**14a**) are attributed to the

aromatic C-H strectchings and the band at 1270 cm^{-1} indicates the NO_2 symmetric stretching ($\nu_{(NO)}$ 1270 cm^{-1}) confirming the availability of nitro groups.[258,259]

TGA-MS of the indolizine functionalised SWNTs (**14a-d**), Figure 4-17, showed a weight loss of 38±0.005, 35±0.005, 48±0.005 and 64±0.005 % respectively, at 600 °C compared with *ca.* 7±0.005 % for purified SWNTs.

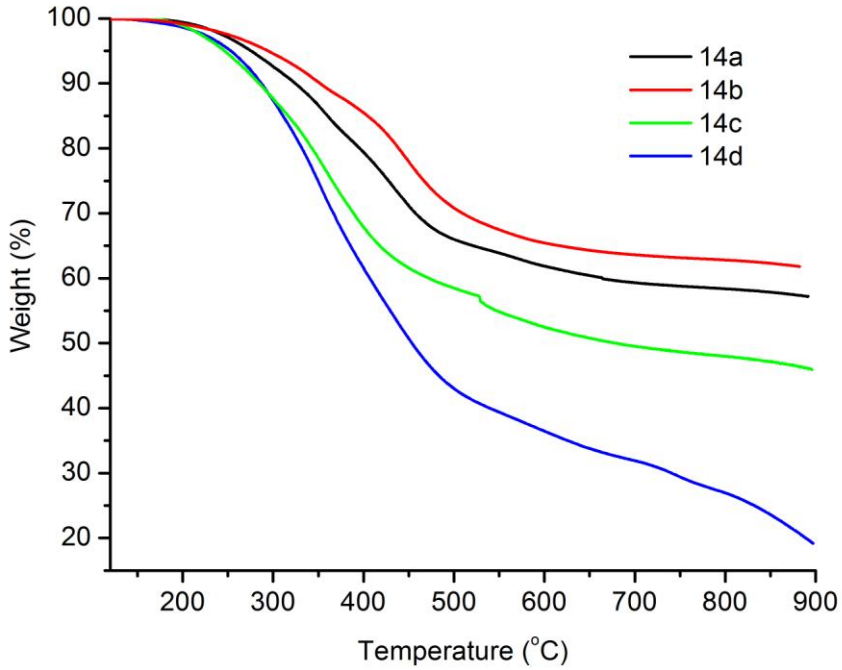

Figure 4- 17 TGA data (10 °C min^{-1}) of indolizine functionalised SWNTs (**14a**) prepared by ethyl-2-bromoacetate (black), indolizine functionalised SWNTs (**14b**) prepared by 4-nitrobenzyl bromide (red), indolizine functionalised SWNTs (**14c**) prepared by PEG_{400}-yl 2-bromoacetate (green) and indolizine functionalised SWNTs (**14d**) prepared by PEG_{2000}-yl 2-bromoacetate (blue).

Weight losses of the indolizine modified SWNTs (**14a-d**) correspond to the presence of approximately 1 functional group for every 56 (1.77 N%), 76 (1.32 N%), 79 (1.27 N%) and 142 (0.70 N%) nanotube carbon atoms, respectively. Mass spectrometry results revealed that the indolizine groups were covalently attached to nanotube

surface showing common fragments at high temperatures for the indolizine modified SWNTs. The mass fragments detected by mass spectrometry showed that the indolizine modified SWNTs (**14a**) fragmented into methyl ester group (OMe, 31 amu), ethyl ester group (OEt, 45 amu) and N-methylpyridinium (94 amu) *ca.* 300-500 ^{o}C, Figure 4-18 (left), although the parent ion of the indolizine was not observed. Figure 4-18 (right) shows that methyl ester group (OMe, 31 amu), N-methylpyridinium (94 amu), phenyl group (C_6H_4, 76 amu), nitroso group (NO, 30 amu) and phenoxy group (C_6H_4O, 93 amu) evolved confirming the presence of a nitro phenyl group attached on the indolizine modified SWNTs (**14b**).

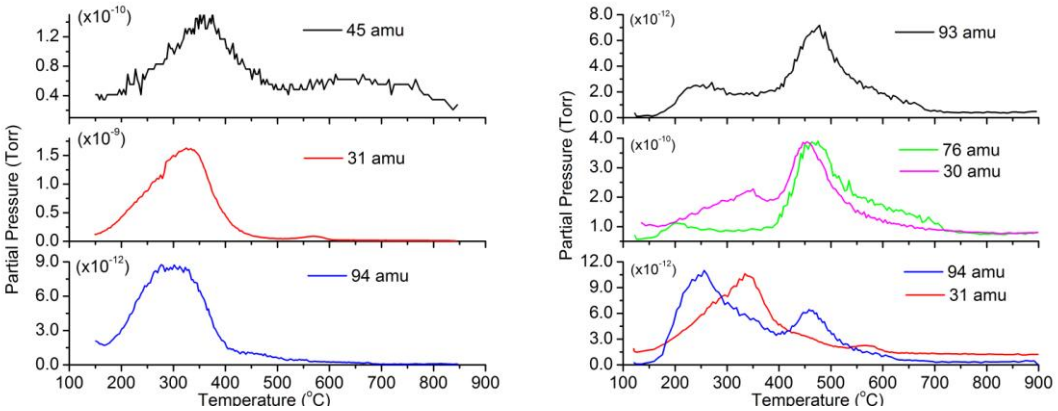

Figure 4- 18 Left: Mass trace (black) of ethoxy (45 amu), (red) methoxy (31 amu) and (blue) methylpyridinium (94 amu) fragment given off during the heating of indolizine modified SWNTs (**14a**). Right: Mass trace (black) of phenoxy (93 amu), (red) methoxy (31 amu), (blue) methylpyridinium (94 amu), (green) phenyl (76 amu) and (magenta) nitroso (30 amu) fragment given off during the heating of indolizine modified SWNTs (**14b**).

Mass spectrometry data recorded for the poly(ethyleneglycol) containing indolizine modified SWNTs (**14c-d**), Figure 4-19, display the presence of methyl ester (OMe, 31 amu), N-methylpyridinium (94 amu) and ethyl formyl group ($COOCH_2CH_3$, 73 amu) as an indicative of the pegylated indolizine modified SWNTs.

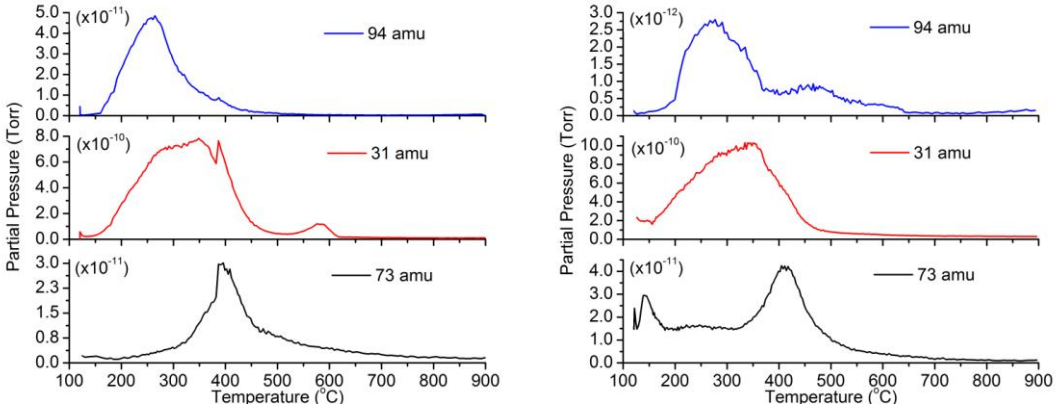

Figure 4- 19 Left: Mass trace (black) of ethyl formyl (73 amu), (red) methoxy (31 amu) and (blue) methylpyridinium (94 amu) fragment given off during the heating of indolizine modified SWNTs (**14c**). Right: Mass trace (black) of ethyl formyl (73 amu), (red) methoxy (31 amu) and (blue) methylpyridinium (94 amu) fragment given off during the heating of indolizine modified SWNTs (**14d**).

4.2.2.1.1. Fluorescent properties of indolizine modified SWNTs

The presence of the indolizine groups on nanotube surface was confirmed using fluorescence spectroscopy where the studies showed that the indolizine functionalised SWNTs (**14a, 14c** and **14d**) emitted light upon excitation, Figure 4-20. Excitation of (**14a**), (**14c**) and (**14d**) at 330 nm resulted in a blue emission at *ca.* 404 nm. For comparision, free indolizine, 3-ethyl 1,2-dimethyl indolizine-1,2,3-tricarboxylate (**15a**) and dimethyl 3-(4-nitrophenyl)indolizine-1,2-dicarboxylate (**15b**), were synthesised via the addition of ethyl-2-bromoacetate and 4-nitrobenzyl bromide to pyridine to afford N-(ethoxycarbonylmethyl)-pyridinium bromide and (4-nitrobenzyl)pyridinium bromide, respectively which undergo the 1-3-dipolar cycloaddition reaction with DMAD in the presence of base (NEt_3), Scheme 4-7. The free indolizine (**15b**) was further reduced to afford dimethyl 3-(4-aminophenyl)indolizine-1,2-dicarboxylate (**16**)

using a literature method.[290] Isolated compounds (**15a-b and 16**) were characterized using FTIR, mass spectrometry, ^{1}H and ^{13}C NMR and all data is listed in Chapter VII. Control experiments mechanically mixing the free indolizine (**15a**), (Figure 4-20), with purified SWNTs followed by washing with THF, acetone and ethanol showed no sign of luminescence.

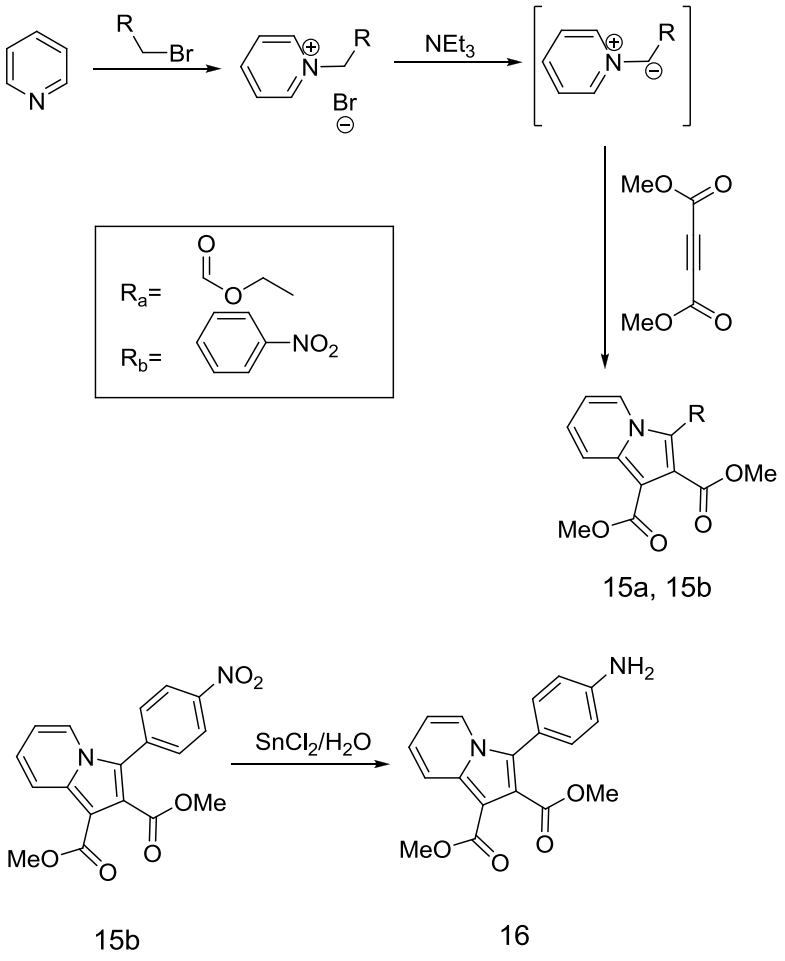

Scheme 4-7 Schematic representation of the synthesis of 3-ethyl 1,2-dimethyl indolizine-1,2,3-tricarboxylate (**15a**), dimethyl 3-(4-nitrophenyl)indolizine-1,2-dicarboxylate (**15b**) and dimethyl 3-(4-aminophenyl)indolizine-1,2-dicarboxylate (**16**).

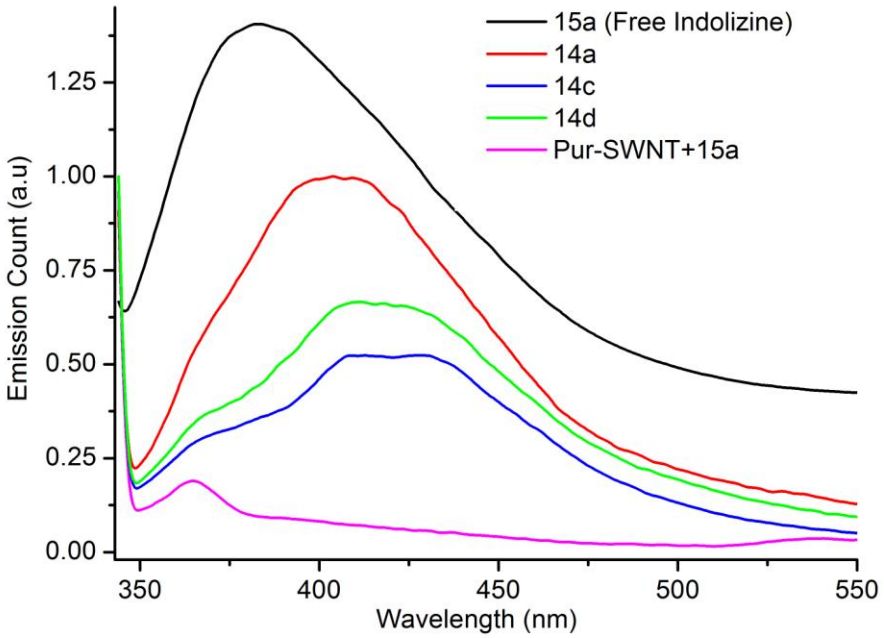

Figure 4- 20 Normalized and offset fluorescence spectra of the indolizine formed from the 1,3-dipolar cycloaddition of the pyridinium ylide to DMAD (**15a**) (black), indolizine functionalised SWNTs (**14a**) (red) prepared by ethyl-2-bromoacetate, indolizine functionalised SWNTs (**14c**) (blue) prepared by PEG_{400}-yl 2-bromoacetate and indolizine functionalised SWNTs (**14d**) (green) prepared by PEG_{2000}-yl 2-bromoacetate and the control experiment of mechanically mixing purified SWNTs with the indolizine (**15a**) generated from the cycloaddition of one pyridinium ylide to DMAD (magenta).

In contrast to (**14a**, **14c** and **14d**), excitation of (**14b**) at 330 nm showed no sign of fluorescence, Figure 4-21. It was no surprise since the modified SWNTs (**14b**) bear strong electron withdrawing groups ($–NO_2$) having ability to quench the fluoresence.[283] Reduction of the nitro groups on modified SWNTs (**14b**) using a literature method[290] yielded the modified SWNTs (**17**) having NH_2 groups, Scheme 4-8.

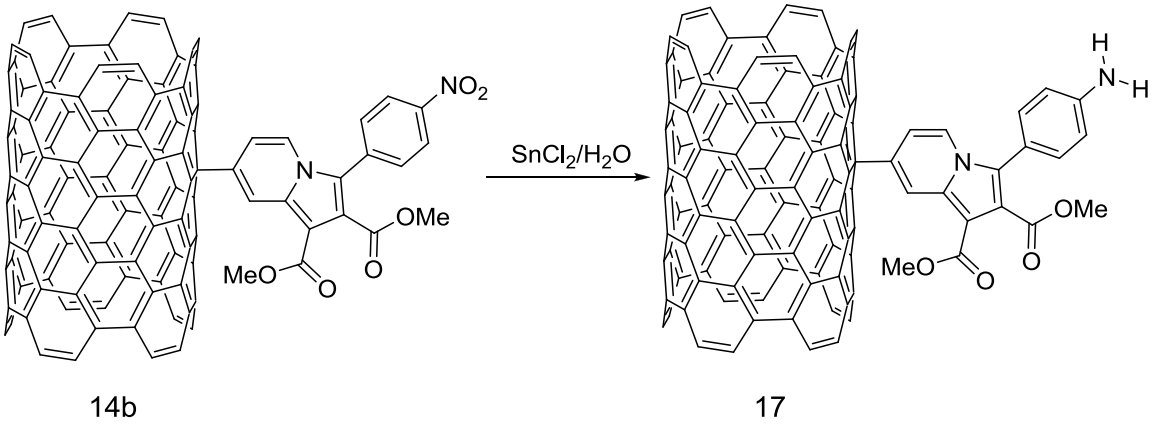

14b 17

Scheme 4-8 Schematic representation of the nitro groups reduction on SWNT surface in the presence of $SnCl_2$/HCl.

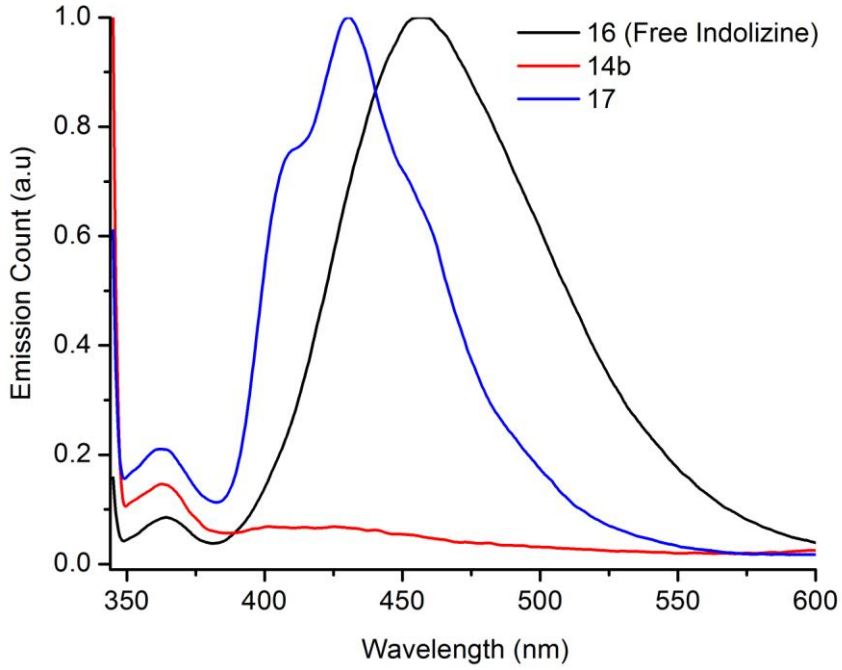

Figure 4- 21 Fluorescence spectra of the indolizine formed from the 1,3-dipolar cycloaddition of the pyridinium ylide to DMAD followed by nitro reduction (**16**) (black), indolizine functionalised SWNTs (**14b**) (red), indolizine functionalised SWNTs (**17**) (blue).

Following the reduction of indolizine modified SWNTs (**15b**) it was recorded that excitation of the modified SWNTs (**17**) at 330 nm emited light at 430 nm, Figure 4-21.

Control sample was prepared by mechanically mixing the free indolizine, dimethyl 3-(4-aminophenyl)indolizine-1,2-dicarboxylate (**16**), with purified SWNTs followed by washing with THF, acetone and ethanol. Excitation of control SWNT at 330 nm showed no sign of fluorescence, Figure 4-21. XPS was used to confirm the reduction of nitro groups on indolizine modified SWNTs (**14b**). Figure 4-22 shows the N1s and Sn3d XPS spectra of the indolizine modified SWNTs (**17**).

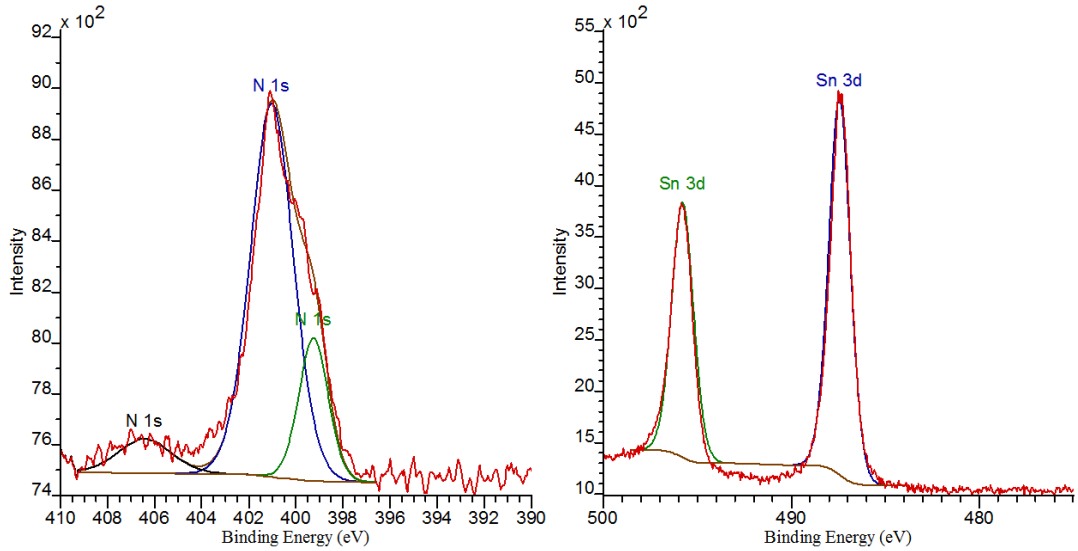

Figure 4- 22 N1s XPS spectra of the indolizine modified SWNTs (**17**) (left) and Sn3d XPS spectrum of indolizine modified SWNTs (**17**) (right) and, the position of components.

The N1s XPS spectrum shows three components positioned at 406.4, 401.0 and 399.2 eV, respectively due to the residual nitro group (-NO_2) [218,281,282] when compared to indolizine modified SWNTs (**14b**) (see Figure 4-26), the indolizine ring nitrogen (-N<)[291] and unreacted pyridine.[292] The composition of the each component at 406.4, 401.0 and 399.2 eV was 8.26, 72.67 and 16.06 %, respectively. The suppression of the peak at *ca.* 406.4 eV suggested that the nitro groups were almost reduced when compared to the N1s XPS spectrum of (**14b**) (see Figure 4-26). Residual Sn was also

detected *ca.* 487.4 and 495.7 eV with an atomic percentage of 1.5 presumably due to the $SnCl_2$ used.

The presence of a significant tail in the green region in the emission spectra of modified SWNTs (**14a**, **17**, **14c**, and **14d**) allowed us to optically image them as a solid material. Figure 4-23 shows the white light optical image (left) and the epi-fluoresence image (right) of indolizine modified SWNTs (**14a**, **17**, **14c** and **14d**). Fluorescence images were recorded using excitation light transmitted through a 420 to 480 nm excitation filter and fluorescence observed after passage through a 500 nm emission filter (Olympus CX-DMB-2 cube). It is clear to see the green spots on the epi-fluoresence image (right) of modified SWNTs (**14a**, **17**, **14c** and **14d**) as an indicator of covalently attached light emiting indolizine groups. This suggested that the quantum efficiency of the emitted light could be sufficiently high for practical applications. We were unable to calculate the absolute quantum efficiencies of the indolizine modified SWNTs (**14a**, **17**, **14c** and **14d**) due to the strong scattering and absorption of the SWNTs. However it was possible to determine the quantum yields of the free indolizines (**15a** and **16**). The fluorescence quantum yields (Φ_f) were determined from the corrected fluorescence spectra, using anthracene dissolved in ethanol as a standard ($\Phi^{st}_f = 0.27$ at 25 ^oC).[283] Φ_f of the unknown samples (un) were estimated by means of the formula:

$$\phi^{un}_f = \phi^{st}_f \frac{A_{st}\,\text{Area}_{(un)}\,n^2_{(un)}}{A_{un}\,\text{Area}_{(st)}\,n^2_{(st)}}$$

where A_{st} and A_{un} are the absorptivities corresponding to the wavelength of 330 nm, $\text{Area}_{(st)}$ and $\text{Area}_{(un)}$ are the areas of the corresponding corrected fluorescence spectra, of the standard and the indolizines, and n_{st}, n_{un} are the refractive indices of the solvents. Quantum yields of the free indolizines (**15a** and **16**) were calculated as 0.055 and 0.035, respectively.

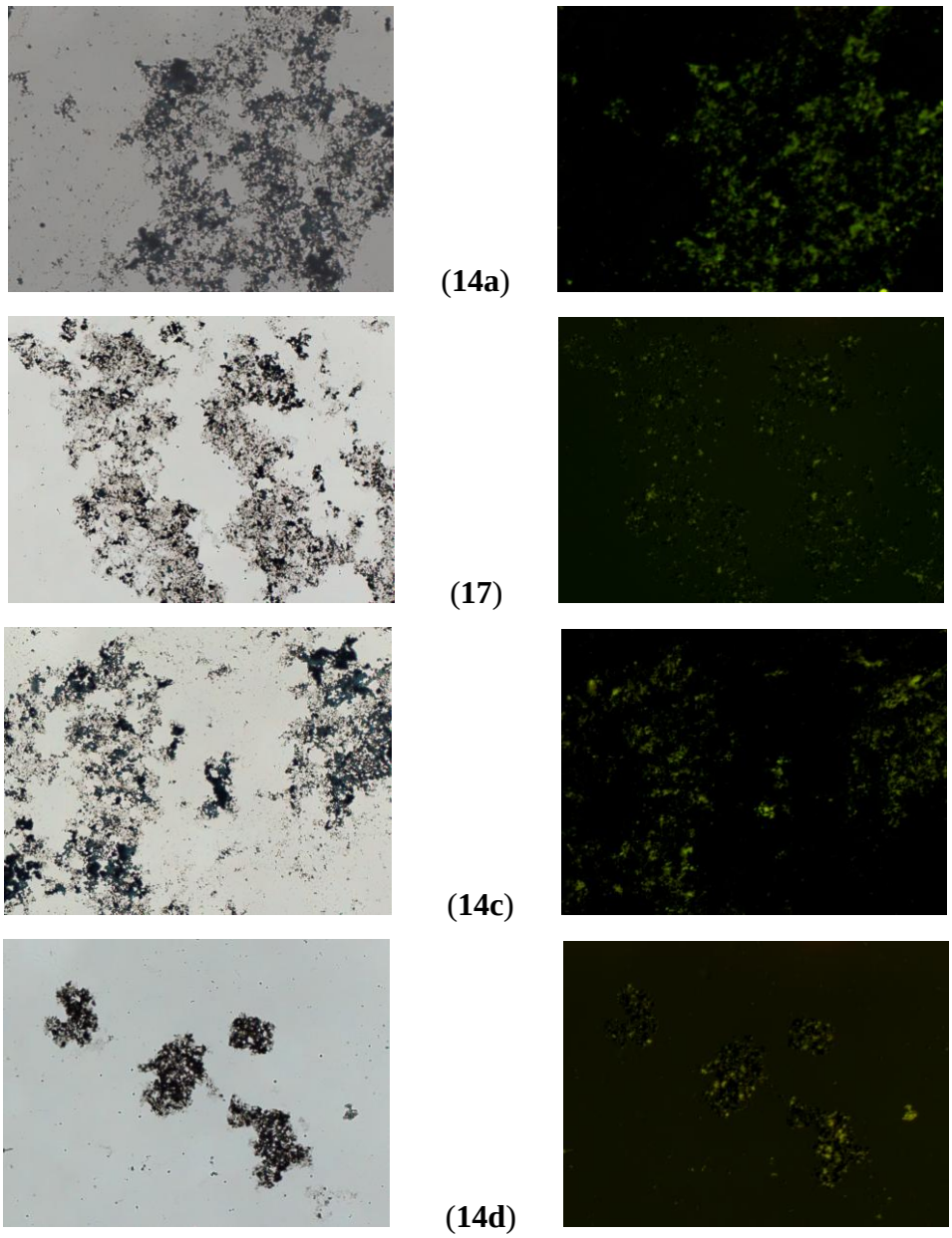

Figure 4- 23 Unmodified white light transmission image (left) and fluorescence image (right) of indolizine functionalised SWNTs (**14a**, **17**, **14c and 14d**) taken using an Olympus CX41 optical microscope, field of view 718 x 533 μm.

4.2.2.2. Monitoring indolizine formation using X-ray analysis

The success of the functionalisation of the SWNTs with pyridinium bromide salts (**13a-c**) and indolizines (**14a-d** and **17**) was investigated using XPS. Results were

evaluated using representative XPS spectra and, the remaining XPS spectra are given in Appendix B (Figure B10-B14).

SWNTs	Element	C1s	O1s	N1s	Br3d	Sn3d
Pristine	BE (eV)	284.4	532.4	-	-	-
	Conc (%at)	95.55 ±0.39	4.45 ±0.39	-	-	-
13a	BE (eV)	284.5	533.5	402.3, 400.0 and 398.9	67.7, 68.7 and 69.6	-
	Conc (%at)	84.95 ±1.04	11.21 ±0.51	2.47 ±0.36	1.47 ±0.20	-
14a	BE (eV)	284.6	533.6	398.9 and 401.4	-	-
	Conc (%at)	80.67 ±0.83	17.11 ±0.57	2.22 ±0.33	-	-
13b	BE (eV)	284.5	533.1	406.1, 404.0, 402.4 and 399.8	-	-
	Conc (%at)	84.97 ±0.71	11.61 ±0.94	3.42 ±0.15	-	-
14b	BE (eV)	284.6	533.5	406.0, 401.3, 400.0 and 398.7	-	-
	Conc (%at)	83.77 ±1.02	14.07 ±0.82	2.16 ±0.56	-	-
17	BE (eV)	284.6	531.7	406.4, 401.0 and 399.2	-	487.50
	Conc (%at)	72.76 ±1.15	23.40 ±0.91	2.32 ±0.38	-	1.51 ±0.06
13c	BE (eV)	284.5	532.9	401.9, 400.4 and 398.9	70.7 and 68.2	
	Conc (%at)	83.34 ±0.41	14.05 ±0.24	1.32 ±0.19	1.29 ±0.04	
14c	BE (eV)	284.6	533.7	401.5	70.90	
	Conc (%at)	80.14 ±0.37	17.43 ±0.23	2.18 ±0.12	0.26 ±0.03	
14d	BE (eV)	284.6	533.7	401.20	71.15	
	Conc (%at)	81.08 ±0.63	17.26 ±0.41	1.60 ±0.22	0.06 ±0.03	

Table 4- 7 Elemental composition and the binding energies of the elements in the pyridinium bromide salts of the modified SWNTs (**13a-c**) and the indolizine modified SWNTs (**14a-d** and **17**).

Table 4-7 shows the elemental composition (%) of the C, O, N, Br and Sn in the modified SWNTs (**13a-d**, **14a-d** and **17**), pristine SWNTs and their binding energies in eV. From the table it is clear that all of the modified nanotubes contain N atom as an indication of the nitrogen containing group attachment to the SWNT surface. The C1s XPS spectra of the indolizine modified SWNTs (**14a-d**), Figure 4-24, showed a strong graphitic component at *ca*. 284.6 eV.[281,293]

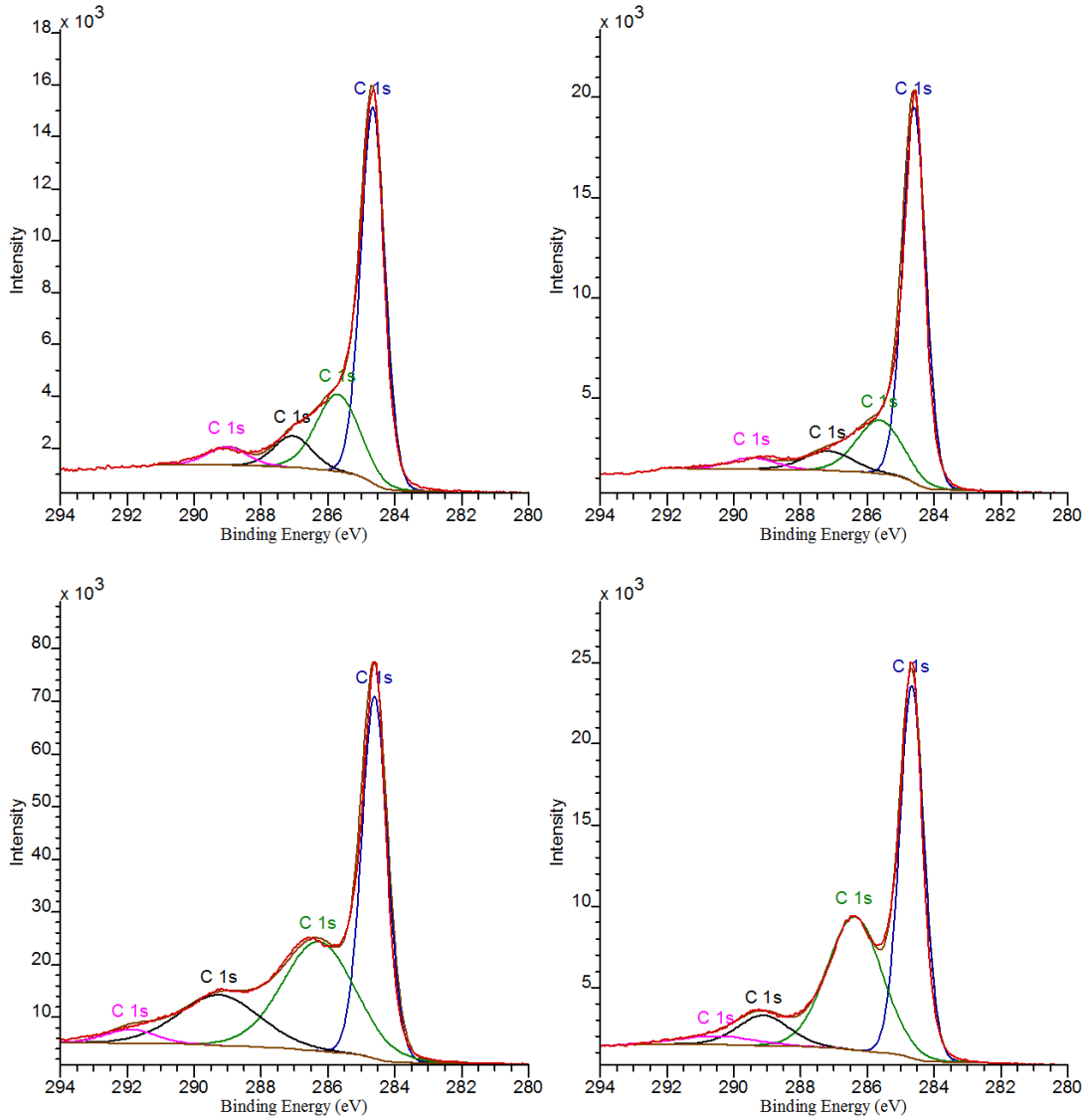

Figure 4- 24 C1s XPS spectra of the indolizine modified SWNTs (**14a**) (Top left), **(14b**) (Top right), (**14c**) (Bottom left) and (**14d**) (Bottom right) and, the position of components.

Table 4-8 displays the peak positions and the relative intensity of the each C1s component found in modified SWNTs (**14a-d**). It was observed that the composition of the graphitic carbon in modified SWNTs (**14a-b**) was greater than the modified SWNTs (**14c-d**), Table 4-8. Moreover pegylated indolizine functionalised SWNTs (**14c-d**) showed the appearance of another peak at *ca.* 286.3 eV that is due to the ether group (C-O-C) of the PEG chain.[294] Intensity of the ether peak in PEG_{2000} indolizine modified SWNTs (**14d**) was greater than the intensity of the PEG_{400} modified (**14c**) indicating the presence of more ether groups.

	C1s Peak position/eV				Composition %
14a	284.6 (C=C)[262]	285.6 (-C*-C*(H))[263,264]	287.0 (>C=O)[265]	289.0 (R-O-C*=O)[295,296]	62.99/23.49/8.39/5.12
14b	284.6 (C=C)[262]	285.6 (-C*-C*(H))[263,264]	287.1 (>C=O)[265]	289.4 (R-O-C*=O)[295,296]	68.68/19.51/7.72/4.10
14c	284.6 (C=C)[262]	286.3 (C-O-C)[294]	289.2 (R-O-C*=O)[295,296]	291.9 (π-π*)[295,296]	42.46/35.88/18.55/3.12
14d	284.6 (C=C)[262]	286.3 (C-O-C)[294]	289.1 (R-O-C*=O)[295,296]	290.6 (CO_3), CO_2[295,296]	48.76/39.34/8.42/3.48

Table 4- 8 The peak positions (eV) and the composition (%) of each component in C1s XPS spectra of indolizine modified SWNTs (**14a-d**).

The O1s XPS spectra of the indolizine modified SWNTs were analysed in an analogous manner to the C1s XPS spectra. Figure 4-25 shows the O1s XPS spectra of the indolizine modified SWNTs (**14a-d**) and, Table 4-9 shows the peak position and the relative intensity of the each component.

Analysis O1s reveals two photoelectron peaks for (**14a**) and three photoelectron peaks for (**14b-d**) can be resolved. An increase in the percentage of the O atom showed that O containing groups were attached to the nanotube surface (Table 4-9). The peaks at

ca. 531.7 and 533.5 eV correspond to C=O and C-O bonds, respectively.[281,297] In the case of the indolizine modified SWNTs (**14b**) it was noticed that the composition of the peak at 533.5 eV increased as an indicative of the aromatic nitro group (NO_2).[218,280-282,298,299]

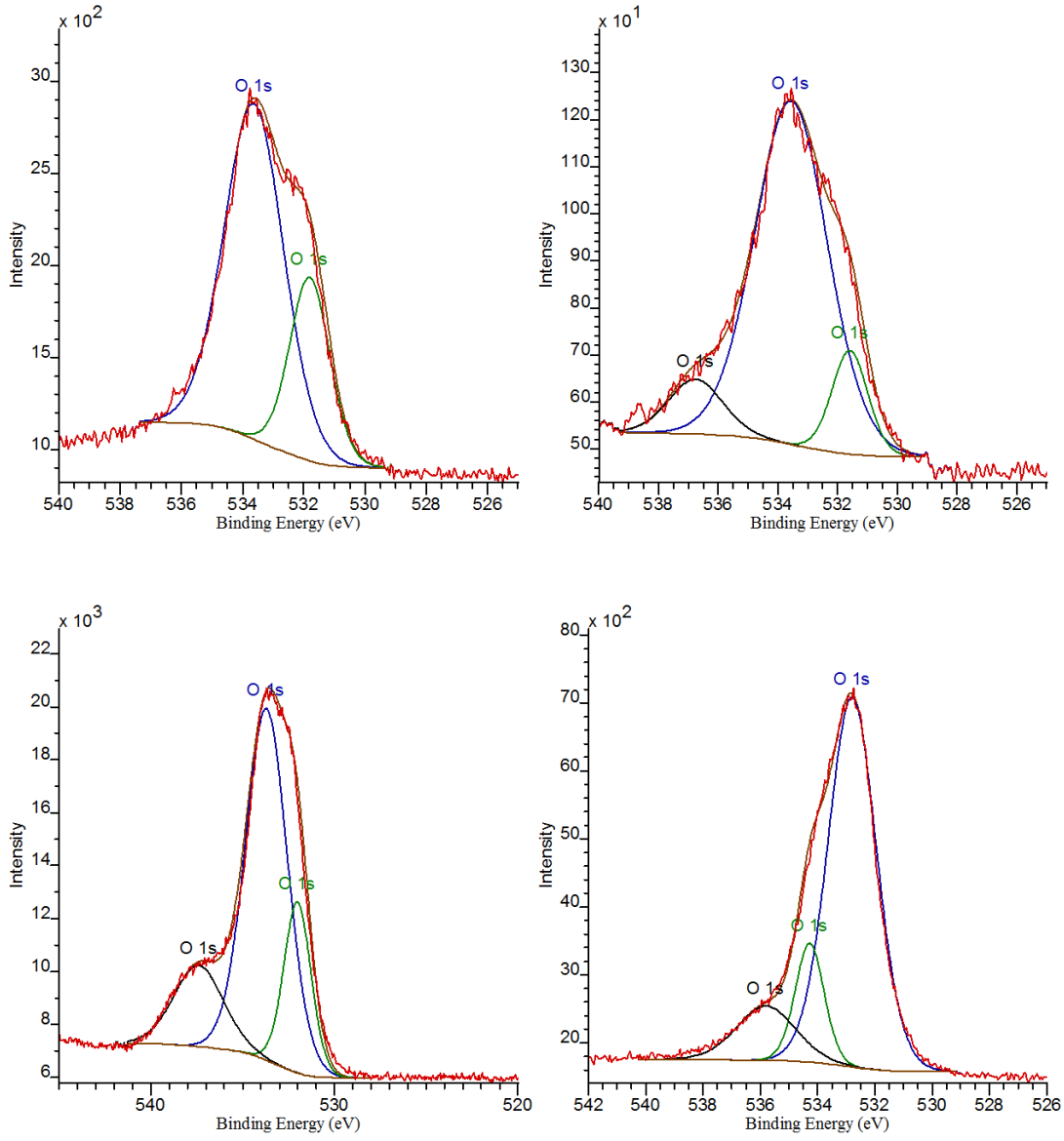

Figure 4- 25 O1s XPS spectra of the indolizine modified SWNTs (**14a**) (Top left), (**14b**) (Top right), (**14c**) (Bottom left) and (**14d**) (Bottom right) and, the position of components.

	O1s Peak position/eV			Composition %
14a	531.8 (isolated –OH, C=O, O-C=O)[273]	533.6 (C-O-C=O)[273]	-	26.97/73.03
14b	531.7 (isolated –OH, C=O, O-C=O)[273]	533.5 (C-O-C=O)[273] or (NO_2)[298]	536.7 (-C-O-H)[267]	11.67/78.99/9.35
14c	531.9 (isolated –OH, C=O, O-C=O)[273]	533.7 (C-O-C=O)[273]	537.4 (Si-O)[300]	19.88/63.00/17.12
14d	532.8 (C=O, O-C=O)[273]	534.2 (C-O-C=O)[301]	535.8 (adsorbed H_2O)[302]	73.03/13.99/12.98

Table 4- 9 Peak positions (eV) and the composition (%) of each component in O1s XPS spectra of indolizine modified SWNTs (**14a-d**).

Since all the reactions have taken place on pyridine N atom it is important to explain the N1s spectra of the pyridinium salt functionalised SWNTs (**13a-d**) and the indolizine modified SWNTs (**14a-d**) to assess the success of pyridinium salt formation and the 1,3-dipolar cycloaddition reaction. Figure 4-26 shows N1s XPS spectra of (**13a-b** and **14a-b**). For comparison the remaining N1s XPS spectra are given in Appendix B (Figure B13). The N1s XPS spectrum of the quaternized pyridine salt modified SWNTs (**13a**) shows a dominant peak component attributable to the quaternized pyridine groups (N^+) at 402.3 eV,[292,303-305] unreacted pyridine groups at 398.9 eV[292] and pyridine radical cation ($N^{\bullet}$) or diazo group at *ca.* 400.0 eV.[225-227] After the 1,3-dipolar cycloaddition reaction of the pyridinium salt modified SWNTs (**13a**) the N1s spectrum of indolizine modified SWNTs (**14a**) showed three main components positioned at 401.4, 399.9 and 398.9 eV, respectively which correspond to the indolizine ring nitrogen (-N<),[291] diazo group (-N=N-),[225,226] and unreacted pyridine.[292]

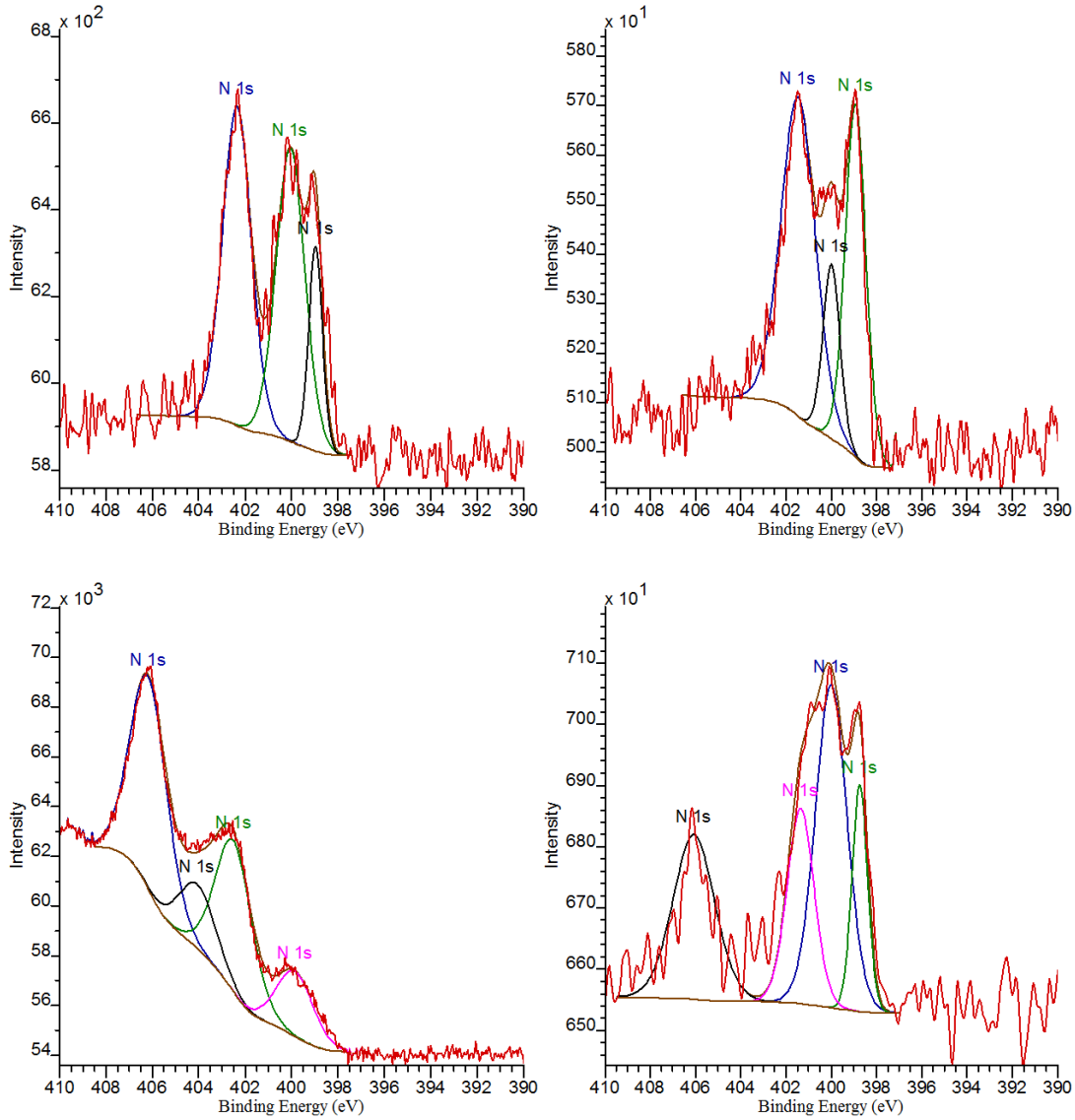

Figure 4- 26 N1s XPS spectra of the pyridinium salt modified SWNTs (**13a**) (Top left), (**13b**) (Bottom left) and indolizine modified SWNTs (**14a**) (Top right), (**14b**) (Bottom right) and the position of components.

The N1s XPS spectrum of the pyridinium salt modified SWNTs (**14b**), Figure 4-26, is fitted with four components due to nitro group ($-NO_2$),[218,281,282] pyridine diazo (-N=N),[306] quaternized pyridine groups (N^+)[292,303-305] and unreacted pyridine groups (-N=)[292] at 406.1, 404.0, 402.4 and 399.8, respectively. Three components were observed in the N1s XPS spectrum of indolizine modified SWNTs (**14b**) at 406.0, 401.3, 400.0 and 398.7 eV, respectively which are attributable to the nitro group (-

NO_2),[218,281,282] the indolizine ring nitrogen (-N<),[291] diazo group (-N=N-),[225,226] and unreacted pyridine.[292]

The component contribution (related to the peak at *ca.* 402.3 eV) of the corresponding N1s XPS spectra of pyridinium salt (**13a**), Table 4-10, revealed that ~40-50 % of the pyridine modified SWNTs (**2**) converted into the pyridinium salt (**13a**) showing the presence of 44.95 % of N1s component. Further evidence for the yield of salt formation was provided by the composition of the nitro group present in pyridinium salt modified SWNTs (**13b**). Analysis showed 43.1 % conversion giving a result very close to (**13a**).

	N1s Peak position/eV				Composition %
13a	398.9 (pyridine)[292]	400.0 ($N^{\bullet}$) or (–N=N-)[225-227]	402.3 (N^{+}) [292,303-305]	-	13.71/41.35/44.95
14a	398.9 (pyridine)[292]	399.9 ($N^{\bullet}$) or (-N=N-)[225-227]	401.4 (-N<)[291]	-	34.35/13.92/51.73
13b	399.8 ($N^{\bullet}$) or (-N=N-)[225-227]	402.4 (N^{+}) [292,303-305]	404.0 (nitrite)[307]	406.1 (-NO_2)[218,281,282]	13.22/30.63/13.05/43.10
14b	398.7 (pyridine)[292]	400.0 ($N^{\bullet}$) or (-N=N-)[225-227]	401.3 (-N<)[291]	406.0 (-NO_2)[218,281,282]	13.59/39.57/20.35/26.48

Table 4- 10 Peak positions (eV) and the composition (%) of each component in N1s XPS spectra of the pyridinium salt modified SWNTs (**13a** and **13b**) and indolizine modified SWNTs (**14a** and **14b**).

Since the pyridinium salt modified SWNTs contain Br atom it was also possible to prove the salt formation by monitoring the Br3d XPS spectrum. Figure 4-27 shows the Br3d XPS spectrum of (**13a**) and the XPS survey spectra of (**13a**) and (**14a**). The Br3d XPS spectrum of (**13a**) confirmed the presence of Br atom showing a peak *ca.* 69.5

eV.[226] Quantification analysis for the pyridinium salt modified SWNTs (**13a**) showed the presence of 1.47±0.20 % Br atom (see Table 4-7) which is nearly equal to the half of the nitrogen atom (2.90±0.39 % N) present in pyridine modified SWNTs (**2**). This suggests approximately 50 % conversion of (**2**) into (**13a**). From the XPS survey spectra of (**13a**) and (**14a**), it is clear that the Br atom is no longer present on the formation of (**14a**).

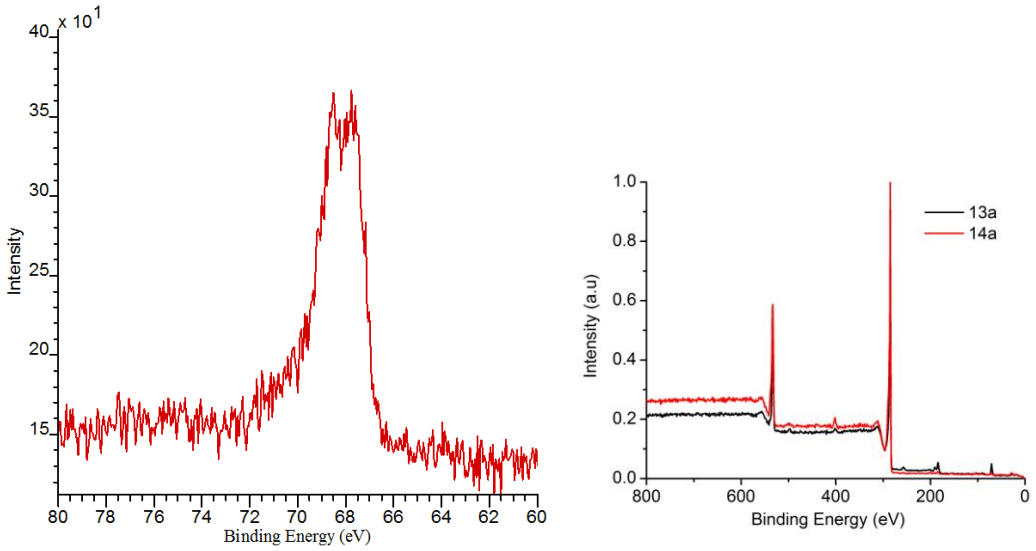

Figure 4- 27 Br3d XPS spectra of the pyridinium salt modified SWNTs (**13a**) (left) and XPS survey spectrum of pyridinium salt (**13a**) (black) and indolizine (**14a**) (red) modified SWNTs (right).

Overall XPS analysis of the indolizine modified SWNTs (**14a-d**) displayed the presence of 2.22±0.33, 2.16±0.56, 2.18±012 and 1.60±0.22 atomic per cent (at.%) nitrogen, respectively (see Table 4-7), which are less than the atomic per cent nitrogen (2.90 %) in pyridine modified SWNTs (**2**), confirming that the new groups were attached to the nanotube surface. However XPS results were not in close agreement with TGA data since the gravimetric analysis was performed considering all pyridine groups were converted into indolizine.

4.2.2.3. Gold colloid tagging for AFM visualisation

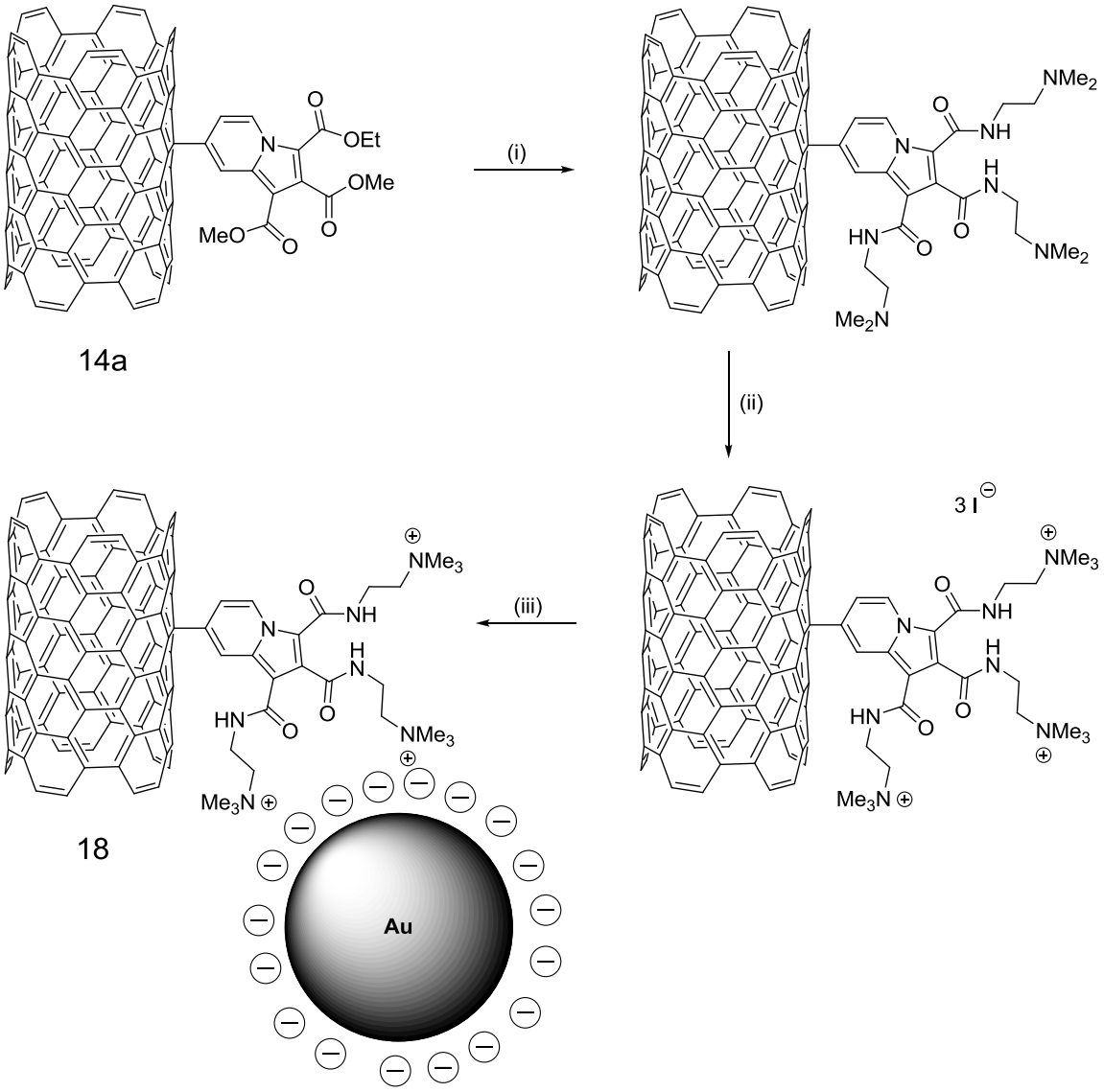

Scheme 4-9 Schematic representation of the electrostatic interaction of gold colloids with indolizine functionalised SWNTs (**14a**) for AFM functional group tagging experiments. (i) *N*,*N*-Dimethylethylenediamine, 100 °C, 15h. (ii) MeI, room temperature, 15h. (iii) Aqueous solution of citrate stabilized gold colloids.

AFM tagging experiments were used to confirm the location and distribution of the functional groups. A positive charge, which undergoes an electrostatic interaction with citrate stabilized gold nanoparticles that are visible by AFM (Figure 4-28), can be

added to the indolizine groups by converting the ester groups on the indolizine functionalised SWNTs (**14a**) to an amide with a terminal tertiary amine, by reaction with *N*,*N*-dimethylethylenediamine, followed by quaternarization with iodomethane, Scheme 4-9. Amide formation was performed at 100 ^{o}C to prevent direct amination of nanotube surface since the treatment of nanotubes with amines could result in formation of amine groups on either sidewalls or endcaps.[260] However, it is worth nothing that any unreacted pyridine / pyridinium functional groups that may be present on the SWNT surface could also be labeled under these reaction conditions.

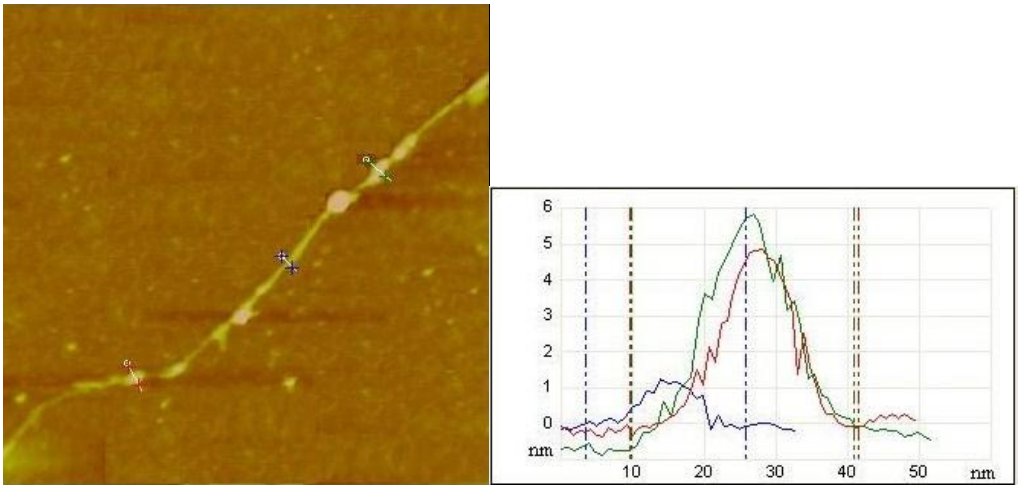

Figure 4- 28 A typical tapping mode AFM height image of an indolizine functionalised SWNT (**14a**) with positively charged tertiary amines after exposure to citrate stabilized Au colloids (4 – 6 nm) (**18**) (left) and the section analysis of the individualized gold decorated quaternary salt of modified SWNT (**18**) (right). The image shown is 720 nm by 720 nm with a z scale of 0 – 5 nm.

4.3. Conclusion

In this chapter two methods for direct and indirect modification to prepare indolizine functionalised fluorescent SWNTs were described. In both cases the potential reactivity of the pyridine nitrogen lone pairs that allows the preparation of several

pyridinium salts was used to produce various indolizine functionalised SWNTs. Raman spectroscopy results for the direct SWNT modification via pyridinium ylides showed that the 1,3-dipolar cycloaddition was selective for metallic over larger diameter semiconducting tubes offering a possible way to separate metallic from semiconducting. The reactivity of the pyridine heterocycle can open the way to fuctionalisation of the SWNTs with well-defined side groups including polymers and cyclodextrins that could be useful for further composite and sensor applications. Due to the planar 10-π electron system of the indolizines they are known as fluorescent compounds. The indolizine functionalised fluorescent SWNTs (**7a-b**, **14a, 14c-d** and **17**) are no exception and were shown to emit in the blue (400-450 nm) when excited *ca.* 330-335 nm. However no fluorescence has been observed for the indolizine functionalised SWNTs (**8**, **9** and **14b**) due to the strong electron withdrawing nitro and sulfonate groups which quench the fluoresence. Fluoresence spectroscopy results together with optical microscopy images revealed that the indolizine modified fluorescent SWNTs with ester side groups can be a potential functional material for cell transfection and drug delivery due to their quantum effficieny that are enough for imaging. AFM tagging experiments involving the electrostatic interaction of citrate stabilized gold nanoparticles with indolizines (**7b, 14a**) that were deliberately positively charged confirmed the presence of ester groups which are available for further reactions on the entire length of the carbon nanotubes. UV-vis-NIR revealed that the solubility of the pristine SWNTs in common organic solvents was increased introducing indolizine groups, which was further increase by derivatising the indolizine modified SWNTs using long alkyl chains via trans-esterification.

5. PHOTO CHEMICAL SENSING PROPERTIES OF THE INDOLIZINE MODIFIED CARBON NANOTUBES (CNTs)

5.1. Introduction

Many potential applications of CNTs including sensors, electronics, opto-electronics, field emission devices, batteries/fuel cells, fibers, reinforced composites, drug delivery, catalysis and gas storage have been proposed. In particular much effort has been spent on designing and fabricating analytical,[308-315] mechanical[316-320] and optical sensors.[321-325] The potential applications of chemical sensors are to monitor environmental pollution; to develop detection of warfare and security threats; to produce diagnostics for medical care; and to provide efficient and sensitive tools for quality control in industrial applications. Due to their interesting chemical and physical properties carbon nanotubes have been used for chemical sensor applications, each based on alterations in a particular property: chemiresistors and back gate field effect transistors,[42,326-331] depending on the conductivity change in the nanotube, and photo chemical or optical sensors,[309,332-336] owing to the scattered light resulted by the adsorption of chemical species. A SWNT based sensor was firstly reported by Dai and co-workers in 2000. They proved that small concentrations of NO_2 caused large changes in SWNT conduction.[42] O'Connell *et al.* reported that the one-dimensional direct band gap semiconducting tubes could fluoresce brightly in the 800- to 1600 nm wavelength range of the near infrared proposing the use of SWNTs in fiber optic communications and bioimaging.[108] Barone *et al.* fabricated a SWNT based near-infrared optical sensor for glucose detection by assembling a monolayer of the enzyme on nanotube surface followed by ferricyanide functionalisation.[321] The authors

revealed that the intensity of fluorescence increased with increase in glucose concentration. Zhao and co-workers showed that a pyrene-modified *β*-cyclodextrin-decorated SWNT field-effect transistor device which works as a photosensor could be fabricated to detect a fluorescent adamantyl-modified Ru complex. The working principle of the device was explained by a charge-transfer process from pyrenecyclodextrin-SWNT hybrids to adamantyl-modified Ru complex.[337] A chemiresistive sensor based on SWNT and hexafluoroisopropanol functionalised polythiophene for chemical warfare agents including sarin gas and dimethyl methylphosphonate has been fabricated by Wang *et al.* using a simple spin-casting technique.[326] The sensory response was investigated measuring the conductance of the SWNT deposition. They also suggested that carbon nanotubes dispersed with receptor containing polymers that could make strong H-bonding interactions were a promising approach for the production of low cost chemiresistive sensors.[326] A quinoline grafted nanotube based fluorescent chemosensor has been reported by Dong *et al.* to sense Cu^{2+} and Zn^{2+} ions since the quinoline derivatives effectively coordinate with specific metal ions.[338,339] Zhang *et al*. has shown that a fluorescent sensor could be fabricated via the non covalent interaction between a nanotube and DNA with 6-carboxyfluorescein groups used to detect Hg^{2+}.[340]

In chapter IV it has been shown that it was possible to produce simple Kröhnke salts (**13a** and **14b**) reacting pyridine functionalised SWNTs with ethyl-2-bromoacetate and 4-nitrobenzylbromide and, indolizine functionalised fluorescent SWNTs (**14a** and **17**) by the 1,3-dipolar cycloaddition reaction of pyridinium ylides, generated from the Kröhnke salts with DMAD. Indolizines, the simplest hetero-aromatic molecules containing both a π-excessive pyrrole and a π-deficient pyridine ring, have attracted special attention due to their luminescent properties[191] with potential sensing applications[284,341-343] and interesting chemical and biological activity.[254,344,345]

Unsubstituted indolizines are considered as planar, electron-rich 10 π-electron aromatic heterocycles. Due to the electron rich planar geometry indolizines with carboxyl ester groups, like fluorescent molecular clips bearing accessible carbonyl moeities, can be capable of π-π interactions and H-bonding with suitable guest molecules.[346]

In this chapter the interaction of the indolizines (host) on SWNT surface (**14a** and **17**) and the free indolizines (control host) (**15a** and **16**, see chapter IV) with aromatic compounds (**19-25**) (guest) has been investigated in order to determine the photochemical sensing properties of the indolizine functionalised SWNTs in both solution and solid state, Scheme 5-1 and 5-2.

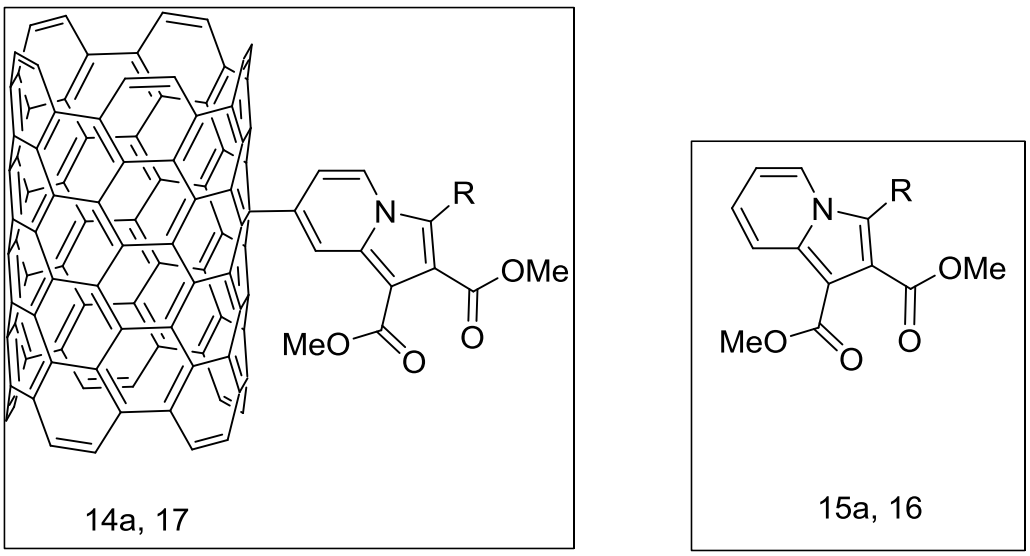

Scheme 5-1 Schematic representation of the chemical structures of indolizine modified SWNTs (**14a** and **17**) and free indolizines (**15a** and **16**)

5.2. Photochemical sensing in solution phase

There is an increasing demand to develop sensing devices to monitor trace amount of nitroaromatics especially nitrophenols due to their toxicity upon inhalation and ingestion since they have been listed as potential pollutants by U.S. Environmental Protection Agency.[331,347] Moreover the detection of nitroaromatics is very important in terms of homeland security as the home-made explosives such as trinitrotoluene (TNT) and ammonium picrate (dunnite) have usually been developed using the derivatives of the nitroaromatic compounds.[326,348]

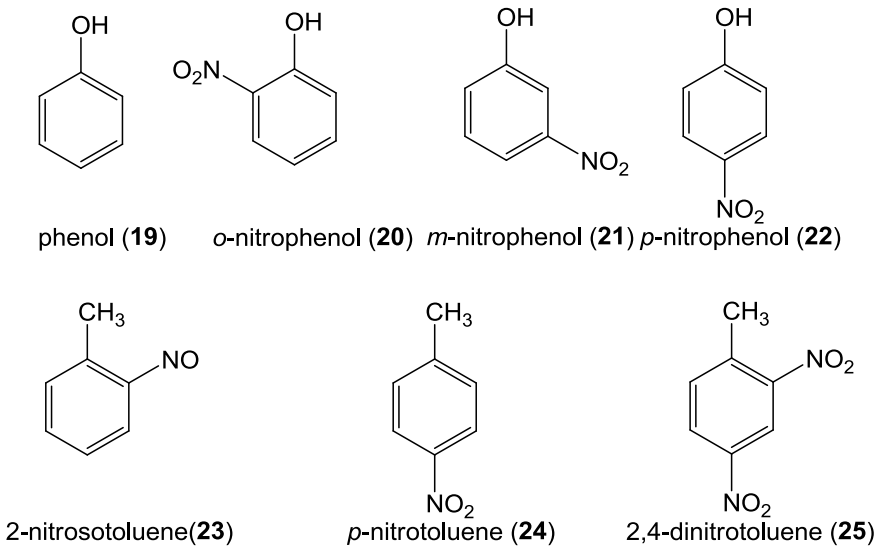

Scheme 5-2 Schematic representation of the guest molecules (**19**-**25**)

In order to evaluate the sensing capabilities of the indolizine modified SWNTs (**14a** and **17)** phenol (**19**), 2-nitrophenol (**20**), 3-nitrophenol (**21**), 4-nitrophenol (**22**), 2-nitrosotoluene (**23**), 4-nitrotoluene (**24**) and 2,4-dinitrotoluene (**25**) were selected as guest molecules, Scheme 5-2. A literature method reported by She *et al.* has been followed to evaluate the solution phase photochemical sensing properties of indolizine modified SWNTs.[346] A stock solution of **14a** and **17** (~1.50 μg/mL, ~1.25 x 10^{-4} M in

terms of carbon) and the guest molecules (**19-25**) (1 x 10^{-4} M) were prepared in acetonitrile (CH_3CN) for fluorescence spectral analysis. Each time a 3 mL solution of **14a** or **17** was filled in a quartz cell of 1cm optical path length, and different stock solutions of guest molecules (**19-25**) were added into quartz cell portion wise (2, 2, 2, 2, 2, 5, 5, 5, 25, 25, 25, 100 μL) using a micropipette. An excitation wavelength of 330 nm and a temperature of 25 ^{o}C were employed in all experiments. Concentration of the guest molecules after the addition of 2 μL has been calculated as 6.66 x 10^{-8} M. Table 5-1 shows the resulting concentration of the guest molecules following each addition.

Total volume of guest molecule solution (μL)	2	4	6	8	10	15	20	25	50	75	100	200
Concentration (x 10^{-7} M)	0.66	1.33	1.99	2.65	3.32	4.97	6.62	8.26	16.39	24.39	32.25	62.50

Table 5- 1 Final concentration of the guest molecules (**19-25**)

Figure 5-1 shows the emission spectra of indolizine functionalised SWNTs (**14a** and **17**, see chapter IV) excited at 330 nm in CH_3CN and free indolizines (**15a** and **16**, see chapter IV) as comparision.

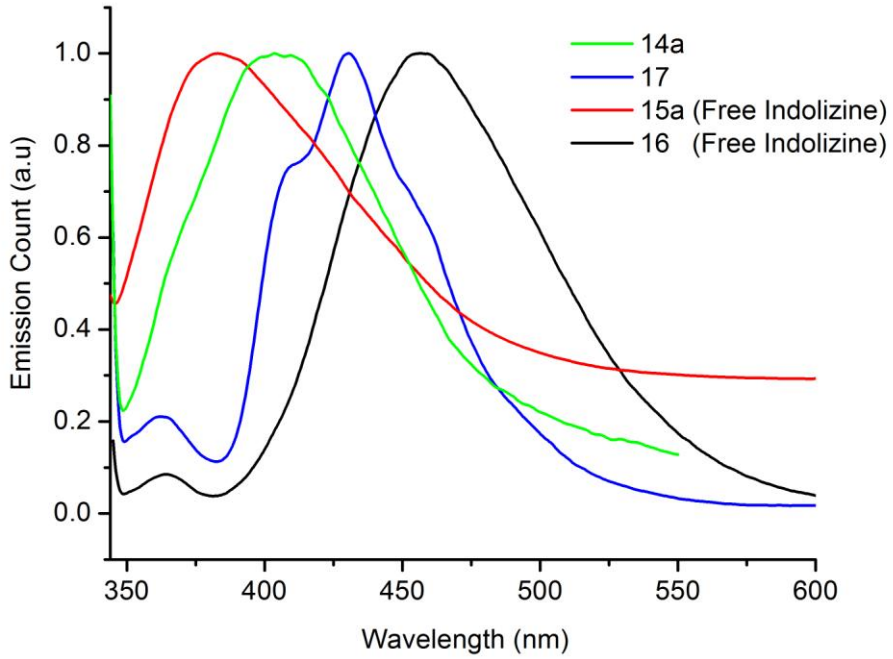

Figure 5- 1 Emission spectra of indolizine functionalised SWNTs (**14a** and **17**) and free indolizines (**15a** and **16**) excited at 330 nm in CH_3CN.

5.2.1. Photochemical sensing properties of indolizine modified SWNTs with ester side groups (14a)

Analysis of the indolizine functionalised SWNTs (**14a**) after the addition of corresponding guest molecules (62.50 x 10^{-7} M) showed that the guest compounds (**20-23**) caused a significant decrease in the fluorescence intensity of the host molecule while the compounds (**19**, **24** and **25**) had no considerable effect on system. Figure 5-2 displays the percentage decrease in fluorescence intensity of the indolizine functionalised SWNTs (**14a**) upon the addition of 200 µL (62.50 x 10^{-7} M) of guest molecules (**19-25**). The percentages were calculated considering the correction factor

due to the dilution via the addition of guest molecules (200 μL) which increase the total volume to 3.2 mL.

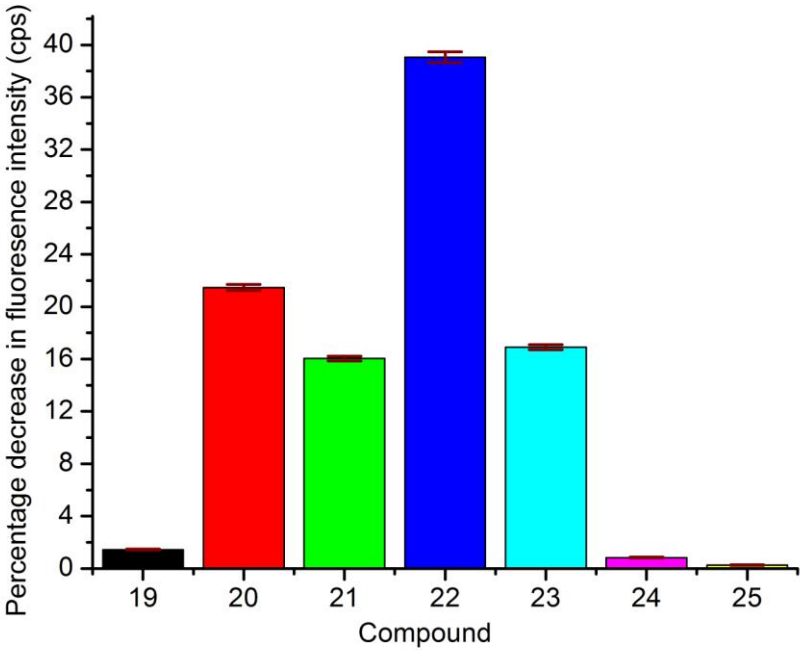

Figure 5- 2 Percentage decrease in fluorescence intensity of indolizine functionalised SWNTs (**14a**) (1.25 x 10^{-4} M) upon the addition of (200 μL, 1 x 10^{-4} M) phenol (**19**), 2-nitrophenol (**20**), 3-nitrophenol (**21**), 4-nitrophenol (**22**), 2-nitrosotoluene (**23**), 4-nitrotoluene (**24**) and 2,4-dinitrotoluene (**25**).

Results showed that the guest compound (**22**) had the most quenching impact when compared with the remaining guest molecules (**19-21**, **23-25**). This could be due to a variety of more effective intermolecular processes between guest compound **22** and indolizine group than the other guest molecules (**19-21**, **23-25**) such as excited state reactions, energy transfer, complex-formation and collisional quenching. These processes can occur during the excited state lifetime such as excited state reactions, energy transfer or collisional quenching or they may appear due to formation of complexes in the ground state (static quenching).[349-351]

Emission spectra of the guest molecules (**19-25**), dissolved in CH_3CN and excited at 330 nm, were also recorded separately to evaluate their contribution to the real fluorescence intensity of the host system (**14a**). Figure 5-3 shows the emission spectra of the guest molecules (**19-25**) and the host system (**14a**) for comparison indicating that the guest compounds do not display significant emission upon excitation at 330 nm and they contribute very little to the total fluorescence of the system.

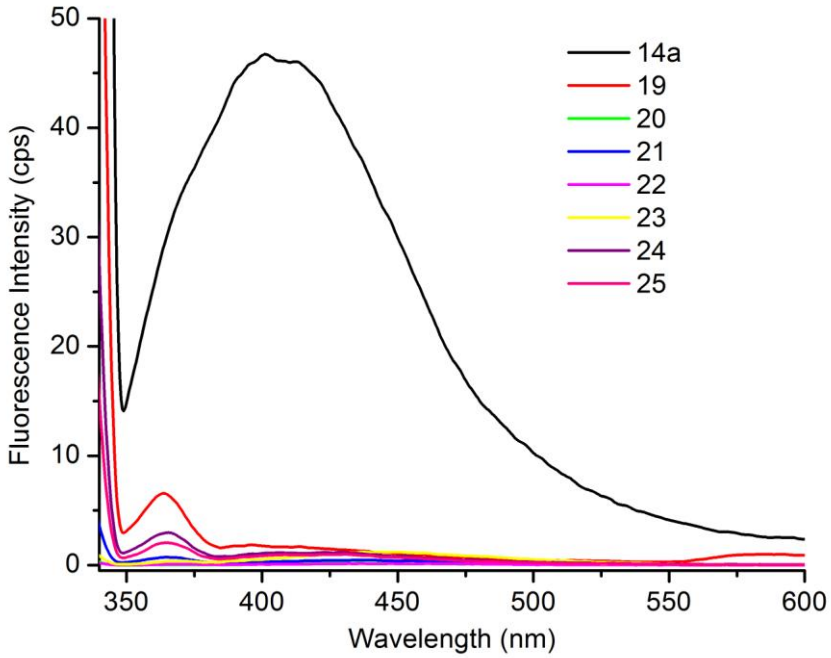

Figure 5- 3 Emission spectra of the individual guest molecules (**19-25**) and indolizine modified SWNTs (**14a**) as comparison dissolved in CH_3CN and excited at 330 nm.

The sensing capability of the indolizine functionalised SWNTs (**14a**) was monitored by titrating them with the guest molecules (**19-25**). Figure 5-4 shows the change in the fluorescence intensity of (**14a**) in the presence of (**22**) with a volume of 2, 4, 6, 8, 10, 15, 20, 25, 50, 75, 100, 200 µL, respectively. The plots revealed that there was a regular decrease in the fluorescence intensity of the host system (**14a**) via the addition of guest molecule (**22**). The spectra showing the change in the fluorescence intensity

of indolizine functionalised SWNTs (**14a**) by titrating with the other guest molecules (**19-21**, **23-25**) are given in Appendix C (Figure C1-C6). Solution phase binding data showed that trace amount of 4-nitrophenol (**22**) (6.60 x 10^{-8} M) could be detected using indolizine functionalised SWNTs (**14a**).

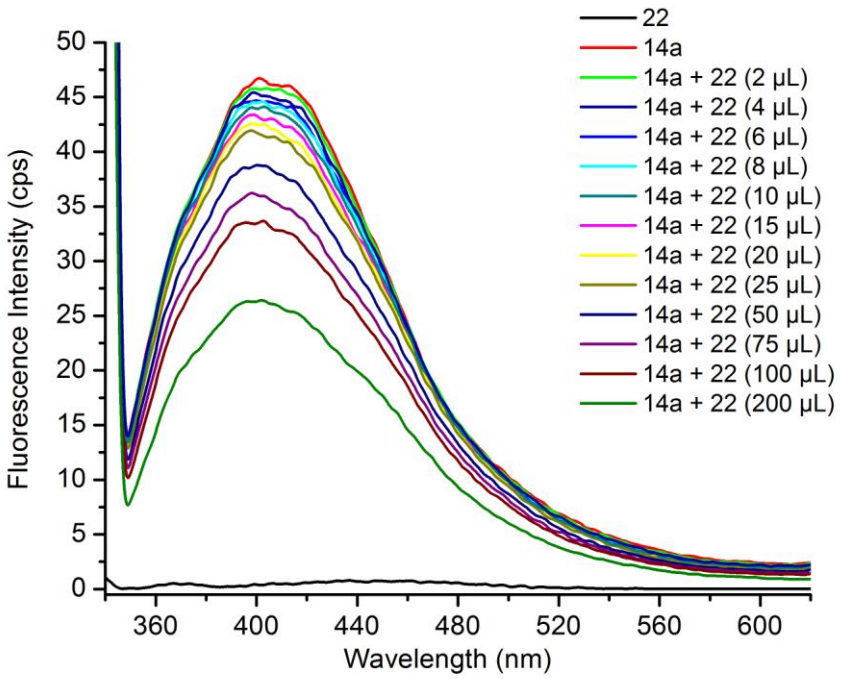

Figure 5- 4 Fluorescence spectra of **14a** (1.25 x 10^{-4} M) excited at 330 nm in the presence of 2, 4, 6, 8, 10, 15, 20, 25, 50, 75, 100, 200 µL equivalent of 4-nitrophenol (**22**) (1 x 10^{-4} M) dissolved in CH_3CN.

However detection limit can be lower than 6.60 x 10^{-8} M since 4-nitrophenol molecules could also be adsorbed by nanotube surface. This has been observed by Liu *et al*. who developed a SWNT based device assembling nanotubes to electrodes using AC dielectrophoresis technique which allows the real-time detection of adsorbed nitrophenols in aqueous solution by measuring the conductance change due to the charge transfer between nitro groups and SWNTs and the metal-nanotube interface modification.[331] Similarly, Zhao *et al.* have shown the use of carbon nanotube-ionic

liquid gel modified glassy carbon electrodes for the voltammetric determination of the nitroaromatics including *p*-nitrophenol, *o*-nitrophenol, *m*-nitrophenol, *p*-nitroaniline and *p*-nitrobenzoic acid.[352]

The Stern-Volmer relationship allows us to investigate the kinetics of a photophysical intermolecular deactivation process. Luminescence in solution obeys the linear Stern-Volmer relationship.[353]

$$F_0 / F = 1 + k_q \tau_0 \, . \, [Q]$$

Where F_0 denotes the initial intensity of the fluorescent species without quencher, F represents the final intensity of the fluorescent species with quencher, k_q is the quencher rate coefficient, τ_0 is the fluorescence lifetime of the fluorescent species without a quencher and [Q] is the concentration of the quencher.

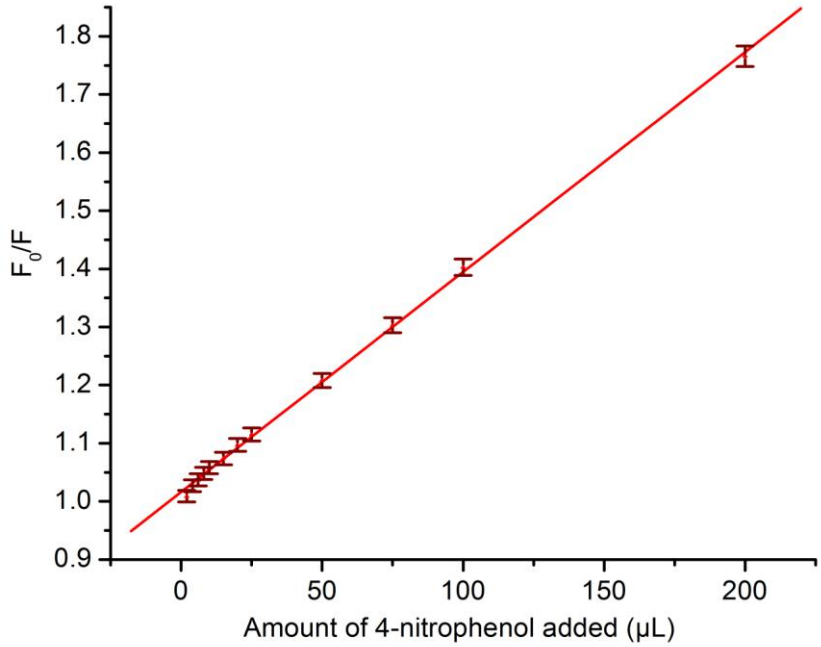

Figure 5- 5 Stern-Volmer plot of the emission data provided by the addition of 2, 4, 6, 8, 10, 15, 20, 25, 50, 75, 100, 200 µL equivalent of 4-nitrophenol (**22**) dissolved in CH_3CN to the indolizine functionalised SWNTs (**14a**).

Figure 5-5 shows the Stern-Volmer plot of the emission data (polynomial fitted) provided via the addition of guest molecule (**22**) to the fluorescent host molecule (**14a**). The linear shape of the Stern-Volmer plot indicates a single class of fluorophores, all equally accessible to quencher.[349] The quenching of indolizine modified SWNTs (**14a**) can be described by either collisional (dynamic) quenching which occurs when the excited indolizine experiences contact with guest molecule (**22**) that facilitate non-radiative transitions to ground state or static quenching where the indolizine can form a stable complex with guest molecule.[349-351] This shows that the fluorescent data provided by fluorescent intensity measurements alone could be explained by either dynamic or static quenching processes unless additional data is provided such as measurement of fluorescence lifetimes and absorption spectra of fluorophores.[349]

5.2.2. Photochemical sensing properties of free indolizine with ester side groups (15a)

Since it is not possible to explore the interactions between indolizine functionalised SWNTs (**14a**) and *p*-nitrophenol (**22**) applying conventional methods including FTIR and NMR, the free indolizine (**15a**) was synthesised using a literature procedure (see chapter IV).[255,259] Fluorescence spectral analysis of the free indolizine (**15a**) in the presence of guest molecules (**19-22**) (200 μL) showed that the results were in close agreement with the results provided for indolizine modified SWNTs (**14a**). Figure 5-6 shows the change in fluorescence intensity of the free indolizine (**15a**) upon the addition of 200 μL of guest molecules (**19-22**) confirming the system has higher affinity towards 4-nitrophenol (**22**) than the other quenchers (**19-21, 23-25**)

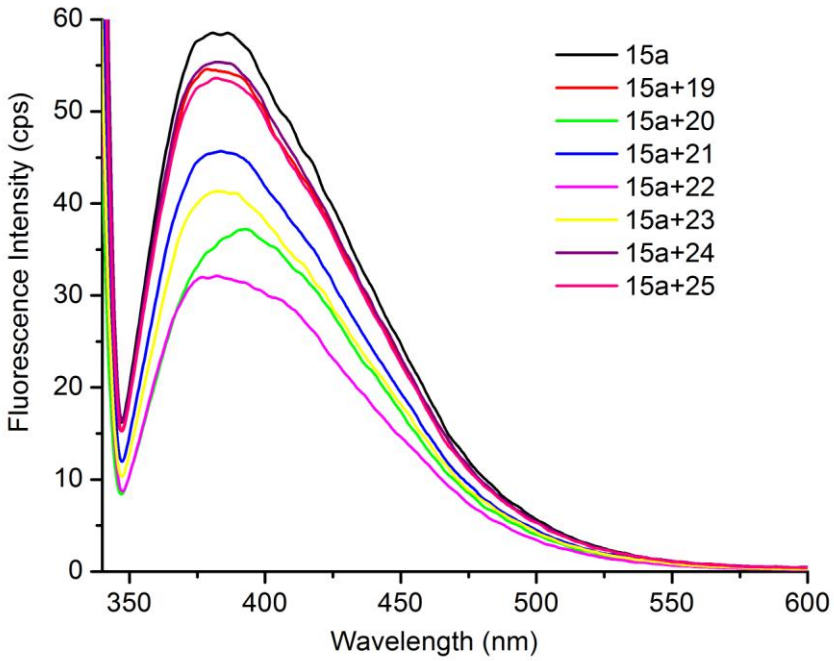

Figure 5- 6 Change in fluorescence intensity of the free indolizine (**15a**) upon the addition of 200 µL of guest molecules (**19-25**)

Free indolizine (**15a**) compound (2.09 x 10^{-7} M) was further titrated with the *p*-nitrophenol (**22**) (1 x 10^{-4} M) to compare the results with the data recorded for indolizine modified SWNT (**14a**). Figure 5-7 shows the change in the fluorescence intensity of (**15a**) in the presence of (**22**) with a volume of 2, 4, 6, 8, 10, 15, 20, 25, 50, 75, 100, 200 µL, respectively. A regular decrease in the fluorescence intensity was observed after the addition of guest molecule (**22**) to the host system (**15a**) confirming the intermolecular interaction between host and guest molecules.

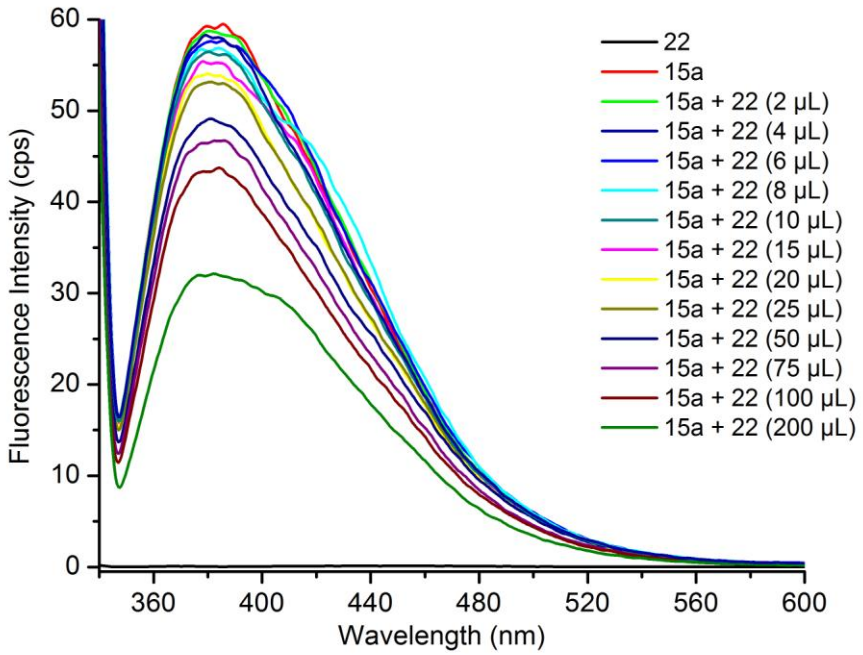

Figure 5- 7 Percent change in fluorescence intensity of (**15a**) in the presence of 4-nitrophenol (**22**) with a volume of 2, 4, 6, 8, 10, 15, 20, 25, 50, 75, 100, 200 µL.

The Stern-Volmer plot of the emission data (polynomial fitted), Figure 5-8, provided by the addition of quencher (**22**) to the fluorescent free indolizine (**15a**) showed nearly a linear line.[349] Data provided by the interaction of the host (**15a**) and the guest (**22**) were very close to the data for the host (**14a**) and the guest (**22**) and, revealed that the SWNTs were functionalised with the fluorescent indolizine groups which are capable of sensing the aromatic nitro and nitroso compounds (**20-23**).

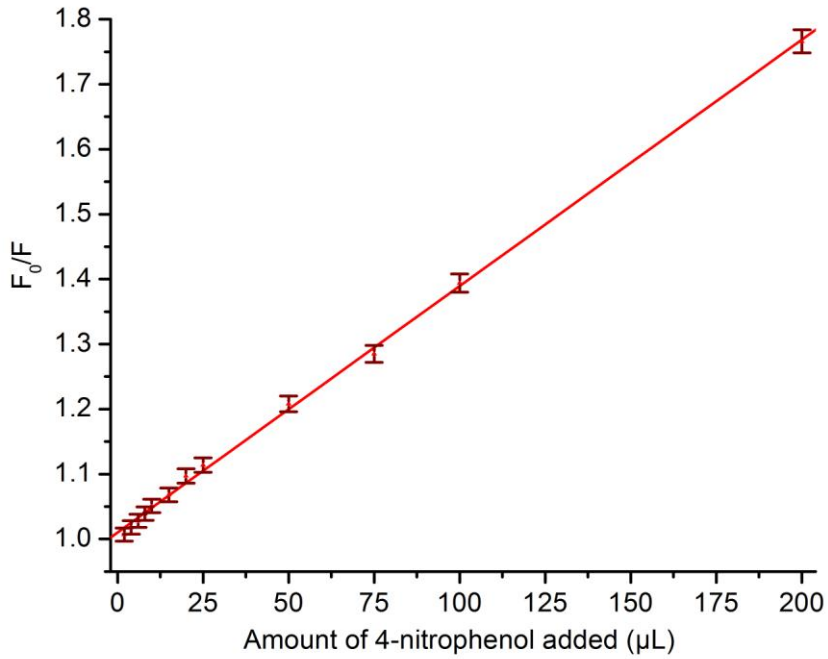

Figure 5- 8 Stern-Volmer plot of the emission data provided by the addition of 2, 4, 6, 8, 10, 15, 20, 25, 50, 75, 100, 200 µL equivalent of 4-nitrophenol (**22**) dissolved in CH_3CN to the free indolizine (**15a**).

FTIR and NMR spectra of the individual compounds (**15a** and **22**) and the mixture of two compounds (**15a:22**) were also recorded in order to evaluate the type of interactions. Stock solutions of (**15a**) (10 mg, 3.28 x 10^{-2} mmol) and (**22**) (4.5 mg, 3.28 x 10^{-2} mmol) in deuterated chloroform ($CDCl_3$, 2 mL) were prepared. ^{1}H NMR was recorded after placing 1 mL aliquots of each solution into an NMR tube and shaking well to ensure a homogeneous solution was formed (**15a:22**). Figure 5-9 shows the ^{1}H NMR spectra of (**15a**), (**22**) and the mixture (**15a:22**). NMR data for guest compound (**22**) after mixing shows that the aromatic protons undergo upfield shifting (H_c, -0.02 ppm; H_b, -0.01 ppm) while the hydroxyl proton (H_a) shifts to downfield by 0.19 ppm. The appearance of the new broad hydroxyl proton signal (at *ca.* 6 ppm) can be explained by H-bonding via ester carbonyls or water present in $CDCl_3$, or

deprotonation of 4-nitrophenol.[354-358] Upfield and downfield shifts indicate that the guest compound (**22**) could interact with the indolizine aromatic ring system via π-π interactions and ethoxy or methoxy ester carbonyl (C=O) groups on indolizine (**15a**) via H-bonding or proton transfer from 4-nitrophenol to ester carbonyl groups.[346,358,359] Since the free indolizine (**15a**) has three different ester carbonyl groups it was difficult to determine the guest molecule position and which ester carbonyl was participating in the H-bonding interaction or proton transfer.

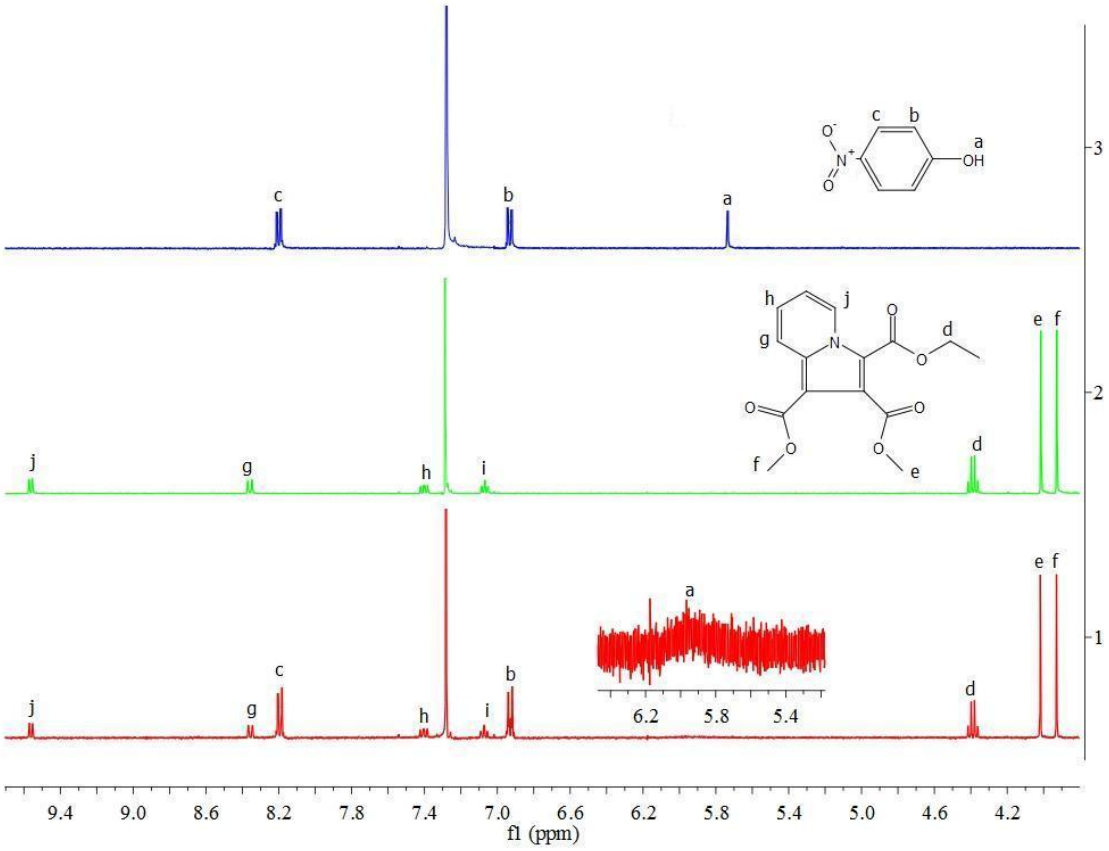

Figure 5- 9 ^{1}H NMR spectra of free indolizine (**15a**), 4-nitrophenol (**22**) and the mixture (**15a:22**).

FTIR spectroscopy was performed to elucidate the H-bonding interaction or proton transfer between ester carbonyls and the hydroxyl group of the guest molecule.[356,358,359] FTIR spectra of compounds were recorded by dropping the stock

solutions of the compounds (**15a** and **22**) and the mixture (**15a:22**) on vacuum dried KBr disk. Figure 5-10 shows the FTIR spectra of free indolizine (**15a**), 4-nitrophenol (**22**) and the mixture (**15a:22**).

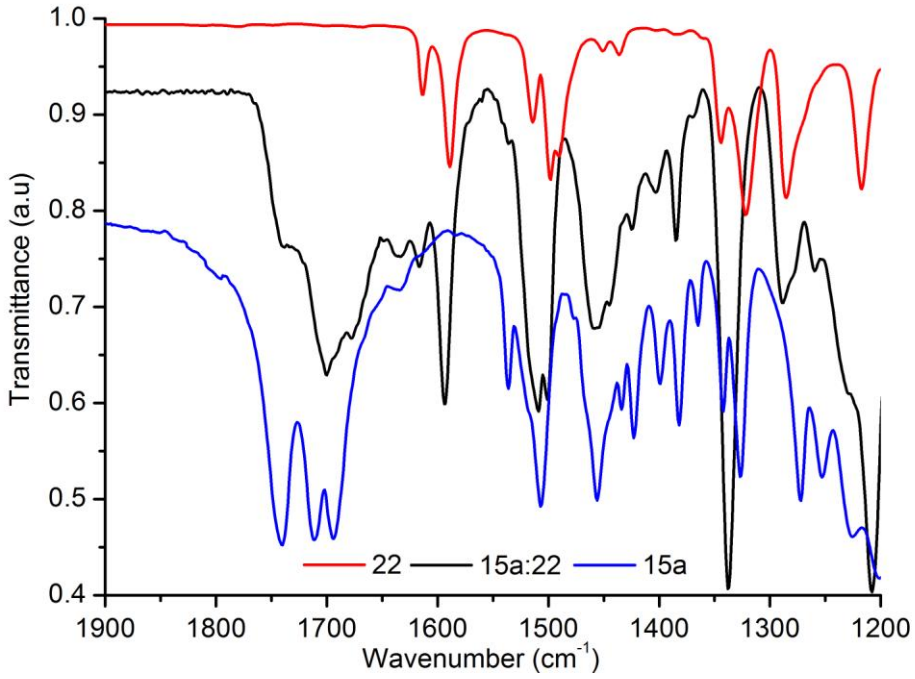

Figure 5- 10 FTIR spectra of free indolizine (**15a**), 4-nitrophenol (**22**) and the mixture (**15a:22**).

FTIR spectrum of the free indolizine (**15a**) displayed three $\nu_{C=O}$ stretching vibrations at 1740, 1710 and 1695 cm^{-1} due to the presence of ethoxy and methoxy ester carbonyl groups. A significant alteration was observed for the $\nu_{C=O}$ stretching bands at 1740 and 1695 cm^{-1} following the complexation as a result of strong interaction like H-bonding or proton transfer.[346,358,359] FTIR spectrum of the mixture (**15a:22**) showed a broad $\nu_{C=O}$ stretching at 1700 cm^{-1} confirming that either the ester carbonyls interacted with hydroxyl groups via H-bonding or carbonyl groups was protonated when compared with the FTIR spectrum of free indolizine (**15a**).[346,358,359] FTIR spectrum of the guest

molecule (**22**) displayed a sharp $\nu_{C=C}$ stretching band at 1589 cm^{-1} which shifts to 1595 cm^{-1} as a result of intermolecular interactions such as π- π stacking.[346]

Overall results provided by ^{1}H-NMR and FTIR revealed that free indolizine (**15a**) interacts the electron deficient aromatic nitro phenolic compounds strongly and selectively by the aid of π-π interactions, H-bonding and/or proton transfer from acidic 4-nitrophenol to indolizine carbonyl resulting in a charge transfer from the electron rich indolizine system to the electron poor guest molecule decreasing the fluorescence intensity of the host system, Scheme 5-3.[346,356,358,359]

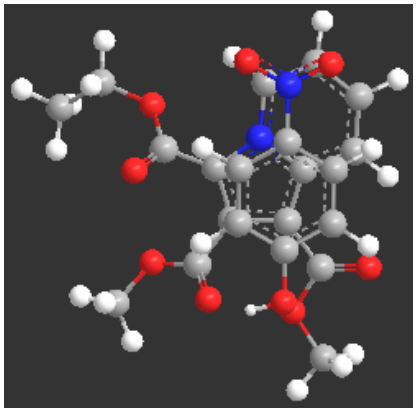

Scheme 5-3 MMFF94- minimized model of free indolizine (**15a**) and guest compound (**22**). Color code: C, gray; H, white; N, blue; O, red.

5.2.3. Photochemical sensing properties of indolizine modified SWNTs with ester and amino phenyl side groups (17)

Indolizine functionalised SWNTs (**17**) having amino phenyl side group (instead of ethoxy carbonyl) have been used to probe the possible interactions between host (**17**) and guest (**19-25**) compounds and to have detailed information of the H-bonding between methoxy ester carbonyls and the hydroxyl group. All experiments were carried out as described above for SWNTs (**14a**). As expected indolizine

functionalised SWNTs (**17**) responded to all the guest compounds (**19-25**) with varying sensitivities. Figure 5-11 displays the percentage decrease in fluorescence intensity of the indolizine functionalised SWNTs (**17**) upon the addition of 200 μL of guest molecules (**19-25**).

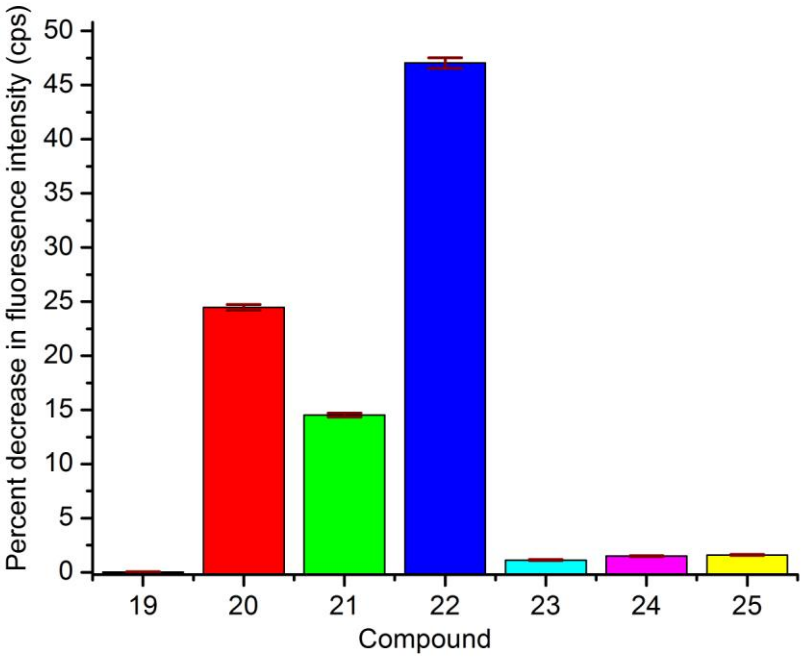

Figure 5- 11 Percentage decrease in fluorescence intensity of the indolizine functionalised SWNTs (**17**) upon the addition of 200 μL of guest molecules (**19-25**).

From the Figure 5-11 it is clear that the decrease in fluorescent intensity of the host molecule (**17**) via the addition of guest molecules (**22, 24-25**) (200 μL) is greater than the indolizine modified SWNTs (**14a**) revealing that the amino substituted benzene ring also interacts with the guest compounds (**22, 24-25**) added via H-bonding, π-π interactions or proton transfer.[346,356,357,359] However the indolizine system (**17**) does not detect the guest compound (**23**) as well as the indolizine system (**14a**). Regular decrease in the fluorescence intensity of (**17**) by the addition of the guest compound (**22**) with a volume of 2, 4, 6, 8, 10, 15, 20, 25, 50, 75, 100, 200 μL, respectively,

Figure 5-12, confirmed the response of the host system (**17**). The spectra showing the change in the fluorescence intensity of indolizine functionalised SWNTs (**17**) by titrating with the other guest molecules (**19-21**, **23**, **24**) are also given in Appendix C (Figure C7-C11).

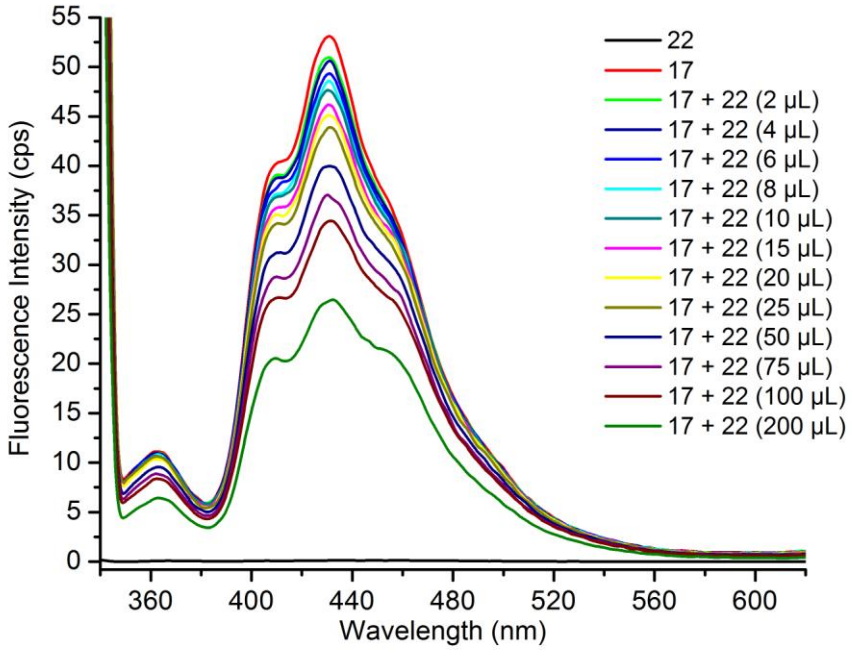

Figure 5- 12 Change in the fluorescence intensity of (**17**) by the addition of the guest compound (**22**) with a volume of 2, 4, 6, 8, 10, 15, 20, 25, 50, 75, 100, 200 µL.

Solution phase binding titration data indicated that trace amount of 4-nitrophenol (**22**) could be detected using indolizine functionalised SWNTs (**17**) with a detection limit of 6.60×10^{-8} M ignoring the adsorbed guest molecules by SWNT surface.

In contrast to the Stern-Volmer plot obtained (polynomial fitted) for the indolizine functionalised SWNTs (**14a**) Stern-Volmer plot of the system formed by (**17**) and (**22**) showed slight upward deviation from the linearity in the range of 15 to 200 µL addition, Figure 5-13. This kind of upward curvature can be best explained by both

static and dynamic quenching processes revealing that there might be a ground-state complex formation.[349,350,360]

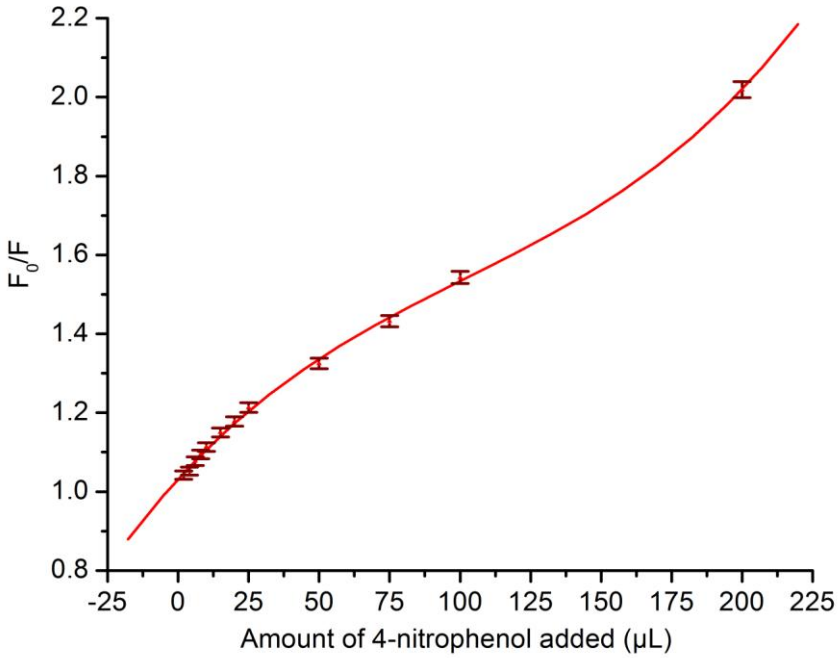

Figure 5- 13 Stern-Volmer plot of the emission data provided by the addition of 2, 4, 6, 8, 10, 15, 20, 25, 50, 75, 100, 200 µL equivalent of 4-nitrophenol (**22**) dissolved in CH_3CN to the indolizine functionalised SWNTs (**17**).

This was an expected result since the host system (**17**) has both methyl esters and the amino substituted benzene ring which might interact with the corresponding guest molecule (**22**) via H-bonding, π-π stacking and proton transfer, Scheme 5-4.[346,357-359,361,362]

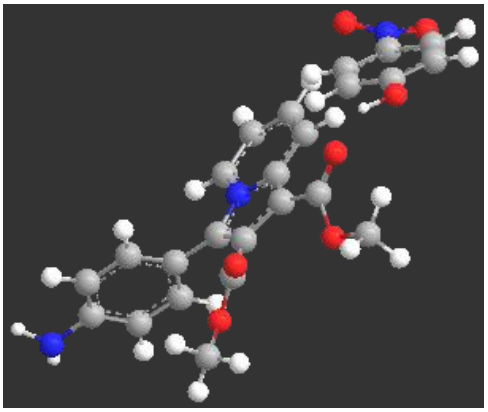

Scheme 5-4 MMFF94-minimized model of free indolizine (**16**) and guest compound (**22**). Color code: C, gray; H, white; N, blue; O, red.

5.2.4. Photochemical sensing properties of free indolizine with ester and amino phenyl side groups (16)

For comparison free indolizine molecule (**16**) (2.09 x 10^{-7} M), synthesised using a literature procedure,[255,259] was titrated with the guest molecules (**19-25**) (1 x 10^{-4} M). Figure 5-14 shows the change in the fluorescence intensity of (**16**) in the presence of (**22**) with a volume of 2, 4, 6, 8, 10, 15, 20, 25, 50, 75, 100, 200 μL, respectively. The results provided for free indolizine (**16**) are in close agreement with the results obtained for the indolizine functionalised SWNTs (**17**).

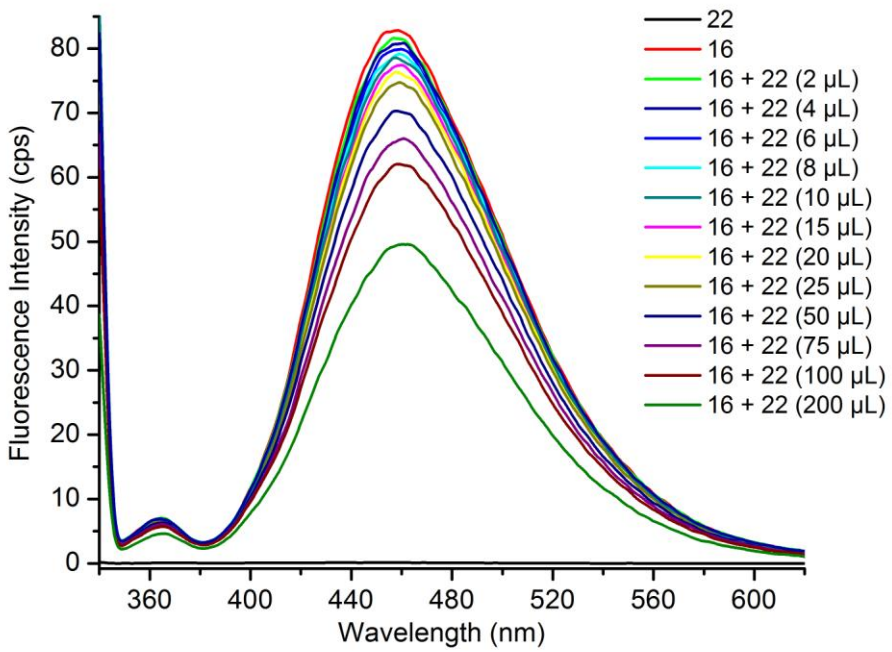

Figure 5- 14 Change in the fluorescence intensity of (**16**) in the presence of (**22**) with a volume of 2, 4, 6, 8, 10, 15, 20, 25, 50, 75, 100, 200 µL.

A Stern-Volmer plot of the emission data (polynomial fitted) provided by the addition of guest molecule (**22**) to the fluorescent host molecule (**16**), Figure 5-15, also displayed a slightly upward curvature in the range of 15 to 200 µL addition, Scheme 5-4.[349]

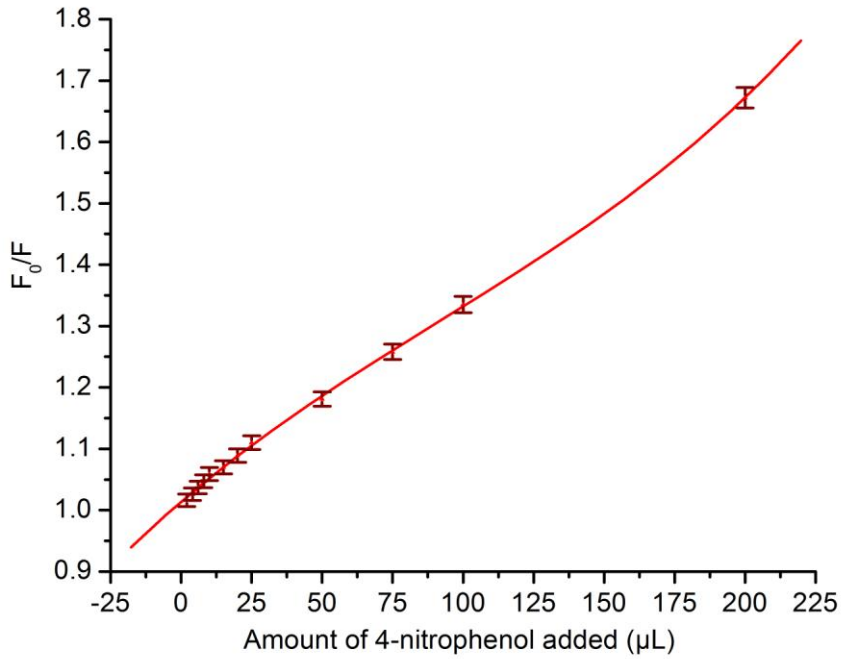

Figure 5- 15 Stern-Volmer plot of the emission data provided by the addition of 2, 4, 6, 8, 10, 15, 20, 25, 50, 75, 100, 200 µL equivalent of 4-nitrophenol (**22**) dissolved in CH_3CN to the free indolizine (**16**).

In order to probe the possible interactions between host and guest molecules FTIR and NMR spectra of the individual compounds (**16** and **22**) and the mixture (**16:22**) were also recorded as before. Stock solutions of (**16**) (10.64 mg, 3.28 x 10^{-2} mmol) and (**22**) (4.5 mg, 3.28 x 10^{-2} mmol) in $CDCl_3$ were prepared as in the case of free indolizine (**15a**). Figure 5-16 shows the ^{1}H NMR spectra of (**16**), (**22**) and the mixture (**16:22**). The ^{1}H NMR spectrum of the guest compound (**22**) shows that the aromatic protons undergo upfield shifting (H_c, -0.14 ppm; H_b, -0.12 ppm) while the hydroxyl proton (H_a) shifts to downfield by 0.84 ppm upon mixing. The appearance of the new broad signal at *ca.* 6.57 ppm might be explained by H-bonding between hydroxyl proton and ester carbonyls, amino group or water present in $CDCl_3$, or proton transfer from hydroxyl group to carbonyl.[354-359,361,362]

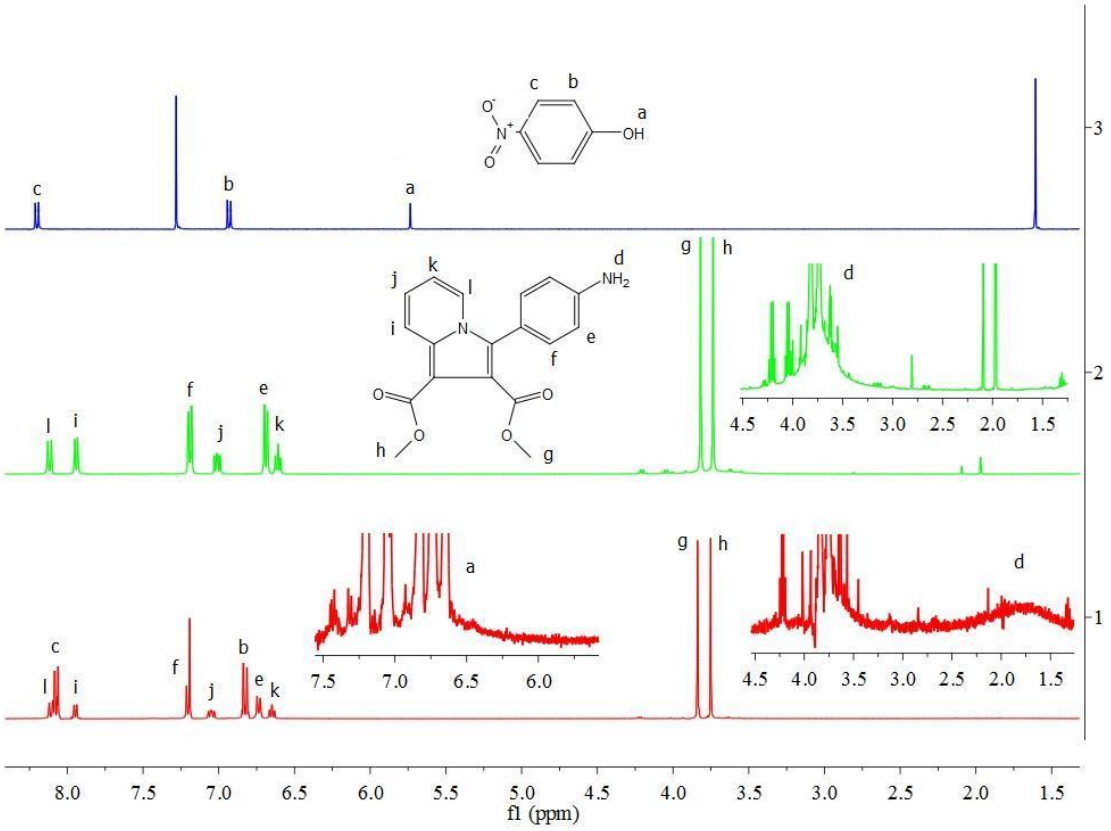

Figure 5- 16 ^{1}H NMR spectra of free indolizine (**16**), 4-nitrophenol (**22**) and the formed complex(s) (**16:22**).

Upfield and downfield shifts indicate that the compound (**22**) interacts with the indolizine aromatic ring system and/or amino benzene ring via π-π interactions and, H-bonding interaction between methoxy ester carbonyl (C=O) and/or amino benzene groups on free indolizine (**16**) and hydroxyl proton.[346,358,361,362] NH_2 protons (H_d) are not observed as an individual signal but integration of the two strong signals at *ca.* 3.70-3.80 ppm reveals that two more hydrogens are present under the methyl hydrogen signals (H_g and H_h). It was also noticed that the amino protons were no longer present at *ca.* 3.70-3.80 ppm upon the addition of 4-nitrophenol (**22**). However a new broad signal, which is probably due to the interaction of the amino protons with the hydroxyl proton of guest molecule, appeared at *ca.* 1.81 ppm as an indicative of the H-bonding or proton transfer from 4-nitrophenol to $–NH_2$ group.[357-359,361,362]

FTIR spectroscopy was also performed to elucidate proton transfer or the H-bonding interaction between ester carbonyls, amino protons and the hydroxyl group of the guest molecule.[356-359,361,362] Figure 5-17 shows the FTIR spectra of free indolizine (**16**), 4-nitrophenol (**22**) and the mixture (**16:22**).

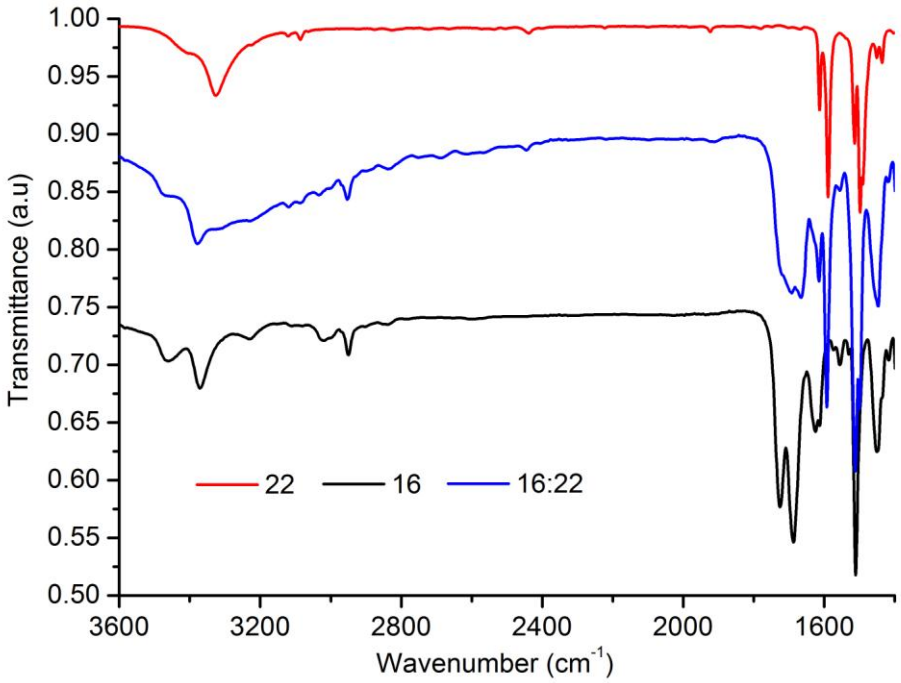

Figure 5- 17 FTIR spectra of free indolizine (**16**), 4-nitrophenol (**22**) and the mixture (**16:22**).

FTIR spectrum of the free indolizine (**16**) displayed two $\nu_{C=O}$ stretching vibrations at 1725 and 1686 cm^{-1} due to the presence of methoxy ester carbonyls and two ν_{N-H} stretching vibrations at 3467 and 3372 cm^{-1} which are characteristic bands for aromatic amines. The FTIR spectrum of the mixture prepared adding equimolar amount of host (**16**) and guest (**22**) compounds showed a broad $\nu_{C=O}$ stretching at 1690 cm^{-1} confirming that the ester carbonyls interacted with hydroxyl groups via either H-bonding or proton transfer when compared with the FTIR spectrum of free indolizine (**16**).[346,357-359,361,362] The shape and intensity of the $\nu_{C=O}$ stretching vibration at 1725 cm^{-1} significantly changed following the charge transfer complex formation as an

indicative of strong interaction like H-bonding or proton transfer.[346,357-359,361,362] It was also observed that the ν_{N-H} stretching vibrations shifted to high energy region and appeared at 3475 and 3379 cm^{-1}. FTIR spectrum of the guest molecule (**22**) displayed a sharp $\nu_{C=C}$ stretching band at 1589 cm^{-1} which shifts to 1594 cm^{-1} after mixing.

5.2.5. Effect of amino phenol side groups on the detection of 2,4-dinitrotoluene

Indolizine functionalised SWNTs (**17**) also showed enhanced sensitivity towards 4-nitrotoluene (**24**) and 2,4-dinitrotoluene (**25**) when compared with indolizine functionalised SWNTs (**14a**). Although the percentage decrease in fluorescent intensity upon the addition of guest compounds (**24-25**) to the indolizine functionalised SWNTs (**17**) is less than the percentage decrease recorded for the other guests (**20-22**) it was still detectable using fluorescence spectroscopy.

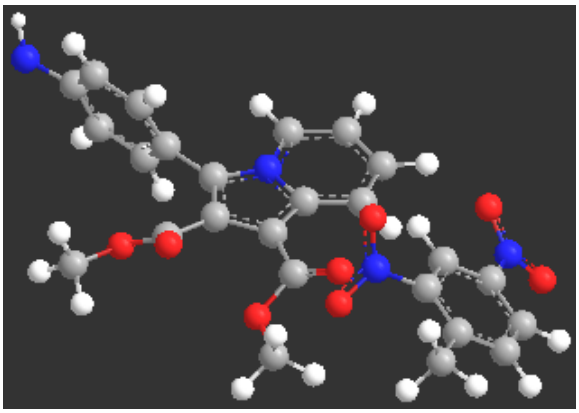

Scheme 5-5 MMFF94-minimized model of free indolizine (**16**) and guest compound (**25**). Color code: C, gray; H, white; N, blue; O, red.

This was perhaps expected due to the presence of the amino benzene ring attached to indolizine main skeleton. Since the interaction(s) mainly takes place on the amino benzene ring, indirect quenching of the fluorescence through the C-C bond between the amino benzene ring and main indolizine system occurs. As it is an indirect effect

on main fluorescent system only small decrease in fluorescent intensity of the indolizine ring system is observed, Scheme 5-5.

Binding titration results given in Appendix C (Figure C12) showed that fluorescence intensity of the host system (**17**) decreased uniformly in the presence of guest molecule (**25**) confirming the response of the host system (**17**) indicating that trace amount of 2,4-dinitrotoluene (**25**) could be detected using the photochemical sensor based on indolizine functionalised SWNTs (**17**) with a detection limit of 6.60 x 10^{-8} M. The Stern-Volmer plot of the emission data (polynomial fitted) displayed slight upward deviation from the linearity indicating that the quenching process is both dynamic and static (see Appendix C, Figure C13).[349] Control experiment carried out using the free indolizine (**16**) and guest molecule (**25**) were in close aggreement with the data provided for indolizine modified fluorescent SWNTs (**17**) (see Appendix C, Figure C14). Although the decrease in fluorescent intensity of free indolizine (**16**) was detectable by luminescence spectroscopy it was less than the fluorescent intensity decreases recorded upon the addition of guest molecules (**20**-**22**). This showed that the driving force causing a decrease in fluorescent intensity is mainly the H-bonding between ester carbonyls and hydroxyl groups on guest molecules (**20**-**22**) rather than π-π stacking. The Stern-Volmer plot of the emission data (polynomial fitted) displayed slight upward deviation from the linearity indicating the presence of both dynamic and static quenching processes (**25**) (see Appendix C, Figure C15).[349]

Figure 5-18 shows the FTIR spectra of free indolizine (**16**), 2,4-dinitrotouene (**25**) and the mixture formed (**16:25**).

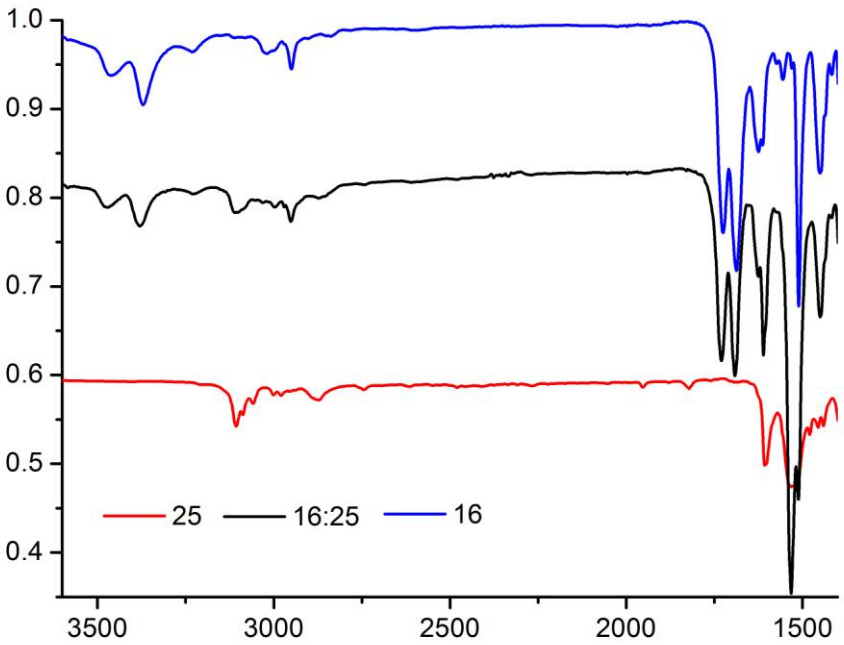

Figure 5- 18 FTIR spectra of free indolizine (**16**), 2,4-dinitrotoluene (**25**) and the complex (**16:25**).

FTIR spectrum of the free indolizine (**16**) displayed two $\nu_{C=O}$ stretching vibrations at 1725 and 1686 cm^{-1} due to the presence of methoxy ester carbonyls, and two ν_{N-H} stretching vibrations at 3467 and 3372 cm^{-1} which are characteristic bands for aromatic amines. FTIR spectrum of the mixture (**16:25**) displayed two $\nu_{C=O}$ bands shifted to 1729 and 1692 cm^{-1}. In contrast to guest compound (**22**), guest compound (**25**) had no significant effect on the band shape of carbonyl stretchings at 1729 and 1692 cm^{-1}. This revealed that there was no H-bonding interaction between ester carbonyls and guest molecule (**25**). However it was observed that the ν_{N-H} stretching vibrations shifted to high energy region and appeared at 3479 and 3383 cm^{-1} confirming the interaction of the NH_2 hydrogens with the guest compound (**25**) via probably H-bonding.[346] FTIR spectrum of the guest molecule (**25**) displayed a sharp $\nu_{C=C}$ stretching

band at 1605 cm^{-1} which shifts to 1612 cm^{-1} after complexation indicating a charge transfer from free indolizine to guest compound (**25**).

^{1}H NMR studies, Figure 5-19, carried out using free indolizine (**16**), 2,4-dinitrotoluene (**25**) and the possible complex formed (**16:25**) revealed that the guest compound (**25**) interacted both indolizine main skeleton and the amino benzene ring.[346]

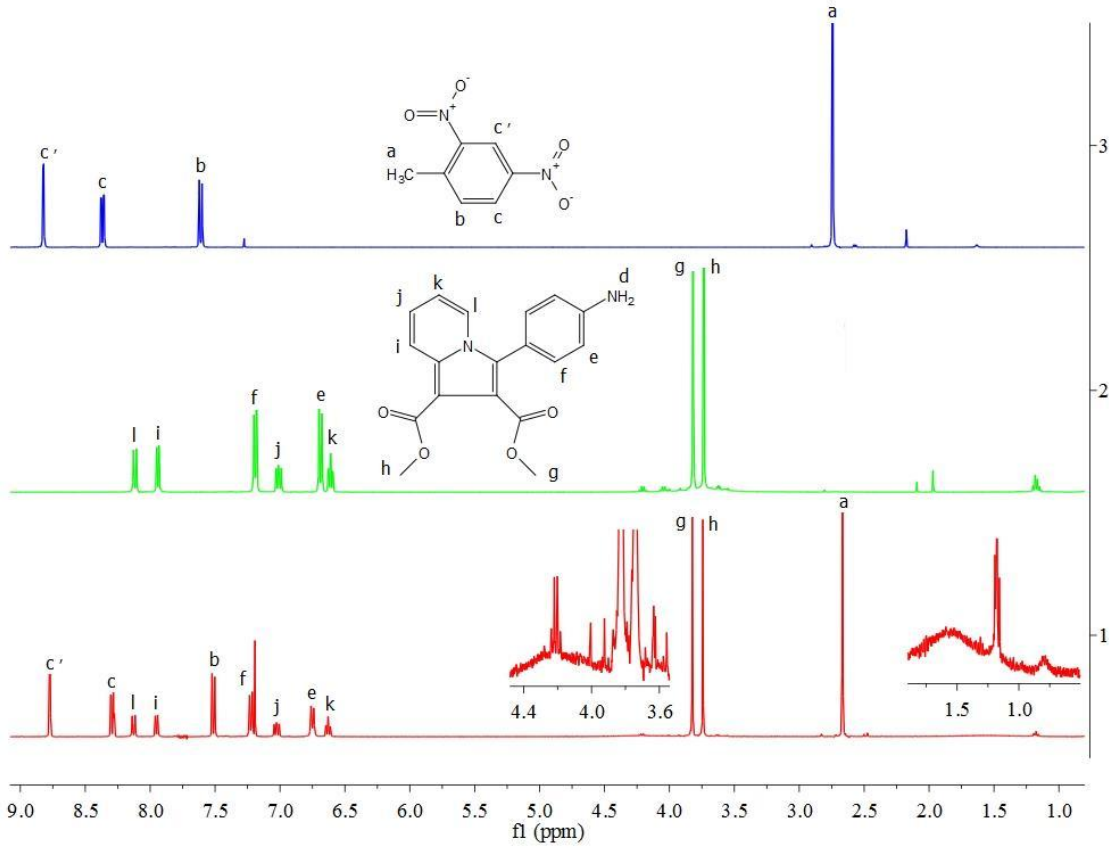

Figure 5- 19 ^{1}H NMR spectra of free indolizine (**16**), 2,4-dinitrotoluene (**25**) and the formed complex(s) (**16:25**)

NMR spectrum of the guest compound (**25**) shows that the aromatic protons (H_b, H_c and $H_{c'}$) and methyl protons (H_a) undergo upfield shifting (H_a, -0.08 ppm; H_b, -0.10 ppm; H_c, -0.08 ppm and $H_{c'}$, -0.05 ppm). NMR spectrum of free indolizine shows (**16**) eight different signals which correspond to aromatic ring ($H_{e\text{-}f}$ and $H_{i\text{-}k}$) and methyl ester ($H_{g\text{-}h}$) protons. Although there was no single signal for amino group protons

integration of the signals at *ca.* 3.70-3.80 ppm confirms the presence of the NH_2 protons (H_d) showing eight protons.

^{1}H NMR spectrum of the mixture (**16:25**) indicates that both the aromatic protons on indolizine main skeleton and amino benzene ring interacted with the guest compound (**25**) undergoing down field shifting (H_l, 0.01 ppm; H_i, 0.01 ppm; H_f, 0.03 ppm; H_j, 0.02 ppm; H_e, 0.06 ppm and H_k, 0.02 ppm). Integration studies also showed that the amino protons (H_d) at *ca.* 3.70-3.80 ppm disappeared following the complex formation. However two new broad signals which could be due to NH_2 protons (H_d) appeared at *ca.* 4.20 and 1.50 ppm. This might be due to the H-bonding between NH_2 protons and the NO_2 groups. Overall NMR data together with FTIR results revealed that 2,4-dinitrotoluene (**25**) could interact the indolizine compound (**16**) via π-π stacking through the main indolizine skeleton and amino benzene ring and H-bonding with NH_2 protons, Scheme 5-5.[346]

5.3. Solid state photochemical sensing properties of indolizine modified SWNTs

In addition to the solution phase photochemical sensing properties of the indolizine modified SWNTs (**14a** and **17**) it was also possible to investigate the solid state photophysical properties of the modified SWNTs (**14a** and **17**) before and after exposing to 4-nitrophenol (**22**) using a commercial spectrofluorimeter coupled with a PTFE-coated integrating sphere since the fluorescent SWNTs could be directly deposited on a suitable surface without needing a further support material. Fluorimetry experiments to determine photoluminescence quantum yield (PLQY) and the response of indolizine modified SWNTs (**14a** and **17**) to 4-nitrophenol (**22**) were performed following the procedure reported by Palsson *et al.* using a quartz substrate coated with fluorescent SWNTs and an excitation wavelength of 340 nm since the sensitivity of the

measurement was low below the selected wavelength.[363] PLQY of the modified SWNTs (**14a** and **17**) was determined using the formalism outlined by de Mello where Φ_{PL} is PLQY, $E_i(\lambda)$ and $E_0(\lambda)$ are, respectively, the integrated luminesence as a result of direct excitation of SWNTs and secondary excitation, $L_i(\lambda)$ and $L_0(\lambda)$ are the integrated excitation when SWNTs are directly excited and the excitation light first hits the sphere wall, respectively and, $L_e(\lambda)$ is the integrated excitation profile for an empty sphere.[364]

$$\phi_{PL} = \frac{E_i(\lambda) - (1-A)E_0(\lambda)}{L_e(\lambda)A} \qquad A = \frac{L_0(\lambda) - L_i(\lambda)}{L_0(\lambda)}$$

From the equation PLQY of the indolizine modified SWNTs (**14a** and **17**) was calculated as 0.9 and 0.3 %, respectively. However the PLQY of the modified SWNTs was less than the free indolizines (**15a** and **16**, see Chapter IV) with PLQY of 5.5 and 3.5 %, respectively. This was to be expected since the indolizines were covalently attached to SWNT sidewall and there could be charge transfer from the electron rich indolizine system to the electron poor SWNTs. Decrease in PLQY due to interaction between attached side groups and the walls of SWNT was also reported by Aprile and colleagues where they showed that the emission quantum yield of 2,4,6-triphenylpyrylium functionalized SWNTs (Φ = 1%) was lower than 2,4,6-triphenylpyrylium alone (Φ = 33%).[365] The absorption (1 – T) of the corresponding indolizine modified SWNTs were used to evaluate the photochemical response of the fluorescent SWNTs to 4-nitrophenol vapor. The absorption of the indolizine modified SWNTs (**14a** and **17**) before exposing to 4-nitrophenol (**22**) vapor were 0.62 and 0.79, respectively and, decreased to 0.57 and 0.78, recpectively, after exposing fluorescent SWNTs to the vapor of 4-nitrophenol indicating response of the fluorescent SWNTs to the vapor of 4-nitrophenol. In addition the PLQY of the corresponding modified materials (**14a** and **17**) slightly increased to 1.1 and 0.4 %, respectively following 4-

nitrophenol exposure. Preliminary solid state photophysical data revealed that indolizine modifed SWNTs (**14a** and **17**) might be capable of sensing 4-nitrophenol vapor at room temperature on solid substrate and, the photochemical sensor fabrication using the films of the indolizine modified SWNTs could be developed in future.

5.4. Conclusion

It has been demonstrated that the SWNTs having the fluorescent indolizine groups could be used as a potential photochemical sensor for detection of aromatic nitro compounds in both solution phase with a detection limit of 6.66×10^{-8} M and solid phase. Fluorescence spectroscopy studies revealed that the aromatic nitrophenols (**20-22**) could be detected efficiently using indolizine functionalised SWNTs (**14a and 17**) while aromatic nitrotoluene derivatives (**24** and **25**) might only be detected accurately using the indolizine modified SWNTs (**17**). FTIR and ^{1}H NMR studies of the host systems (**15a and 16**), guest compounds (**22** and **25**) and mixtures formed (**15a:2**, **16:2**, **16:25)** displayed that the intermolecular π-π interactions, H-bonding between host and guest system and, proton transfer could be main factors for the detection of the aromatic nitrophenol and nitrotoluene derivatives. Since nitroaromatics are present in explosive warfare agents including TNT and ammonium picrate, and pollute the environment, detection of trace amount of nitroaromatic compounds is important both in terms of homeland security and environmental monitoring. An attempt to investigate the solid state response of the indolizine system confirmed that the fluorescent SWNTs could be used as sensing devices in the UV-vis range without needing a further support material which is potentially important in future device fabrication. The indolizine modified SWNTs with reactive ester side groups could even be used for the detection of a variety of inclusion compounds such as

adamantanols, sodium cholotes, xylene derivatives by replacing the side groups with cyclodextrins or calixarenes.

6. REDUCTIVE ALKYLATION FOLLOWED BY ELECTROPHILE ADDITION

6.1. Introduction

Covalent modification has been thought to be one of the most likely methods to change the properties of nanotubes for more than a decade. The main advantage gained upon functionalisation of nanotubes is a considerable increase in their solubility. The existence of a great diversity of synthetic methods combined with the high number of chemical reactions has led to the formation of a wide variety of functionalised nanotubes[105,109-113,115-120,122,123,191] (see section 1.7). The special characteristics of the added groups, coupled with the unique structural, chemical, and electronic properties of nanotubes, have aided the development of new materials with tremendous potential in fascinating and widespread technological applications including field-effect transistors,[31-33] nano-tweezers,[34] high resolution atomic probes,[35] chemical probes,[36] mechanical actuators,[37] hydrogen storage,[38] non-volatile random access memory,[39] field-emission displays,[40] data storage devices,[41] and chemical sensors.[42]

Organolithium compounds including *n*-butyllithium, *sec*-butyllithium and *t*-butyllithium have widely been used to generate negatively charged SWNT intermediates which can be used to produce new functional groups (alkyl, aryl and carbonyl) or polymer chains on nanotube sidewalls. Viswanathan *et al.* have used *sec*-butyllithium to generate SWNT carboanions which initiate the polymerization of styrene at 48 ^{o}C under sonication.[124] Blake has reported the lithiation of MWNTs using *n*-butyllithium in THF and the further reaction of the negatively charged nanotube intermediate using chlorinated polypropylene to yield nanotubes covalently

bonded to chlorinated polypropylene.[125] Chen and colleagues have shown that the treatment of SWNTs with sec-butylithium and subsequently with carbon dioxide affords SWNTs modified with both alkyl and carboxyl groups.[126] Pekker *et al.* have reported that it was possible to produce carboanionic SWNTs using a metallic lithium or sodium in the presence of methanolic ammonia.[127] Similarly, Penicaud and co-workers[128] showed that lithium/sodium naphthalenide could be used to produce negatively charged SWNT intermediates which were easily alkylated with alkyl halides. Graupner *et al.* have caried out a new reductive alkylation of SWNTs using *t*-butyllithium in benzene followed by re-oxidation of carbanionic intermediate with air and it was reported that metallic tubes were more reactive than semiconducting tubes.[129] Recently, Wunderlich *et al.* have reported both reductive hydrogenation and alkylation of SWNTs using the Billups reaction and reductive alkylation of SWNTs using organolithium compounds in cyclohexane.[130,131] Once again the reactions favored the functionalisation of metallic over semiconducting tubes. The benefits, in terms of reduced toxicity of cyclohexane over benzene were also highlighted.[130,131] Similarly, Roubeau and co-workers have shown the use of methyllithium in THF under inert atmosphere to generate carbanionic SWNTs and the addition of several alkyl halides to the SWNT sidewalls.[366]

Although several modification methods have been reported on the reductive alkylation of SWNTs and the reactions of reactive carbanionic intermediates with alkyl halides there is still no report discussing both the reactivity of negatively charged SWNT intermediates with the reactive electrophilic groups having a sp^2 hybridized reactive carbon center.

Here we report a versatile method for the formylation, methyl formyl addition and benzyl formyl addition to SWNT surface following reductive alkylation using *n*-butyllithium in cylohexane under an argon atmosphere. Modified SWNTs were

characterized using several methods including FTIR, UV-vis-NIR, Raman spectroscopy, TGA-MS, AFM, fluorescence spectroscopy and optical microscopy.

6.2. Synthesis and properties of formyl and ester functionalized SWNTs

In general the reductive alkylation followed by electrophile addition was a two step reaction. The first step involves the generation of negatively charged SWNT intermediates, and the second step involves the reaction of carbanionic intermediates with *N*-formylpiperidine (NFP), methyl chloroformate (MCF), and benzyl chloroformate (BCF), Scheme 6-1. The electrophiles NFP, MCF and BCF are known to undergo facile formyl, methyl formyl, benzyl formyl transfer to organolithium and Grignard reagents, resulting in formation of functionalised molecules in very high yields.[367-370] All reactions were carried out under argon atmosphere at room temperature and purified SWNTs were dried at 100 ^{o}C in a schlenk apparatus under vacuum prior to the reaction with *n*-butyllithium. Anhydrous cyclohexane bubbled with argon for 30 min was transferred to the schlenk apparatus containing purified SWNTs and sonicated for 15 minutes as stated in Wunderlich's work.[130] It was observed that SWNTs were agglomerated when sonication stopped. After the addition of *n*-butyllithium to the SWNT dispersion, complete exfoliation of nanotubes was observed due to the formation of negatively charged SWNT intermediates which repel each other as reported by Graupner *et al.*.[159] The SWNT dispersion was further stirred for 30 min followed by 30 min sonication at room temperature and left for stirring overnight at room temperature. An excess amount of freshly distilled NFP, MCF or BCF under argon atmosphere was cannulated to quench the reaction intermediate (**26**) (*n*-Bu$_n$SWNT^{n-}).

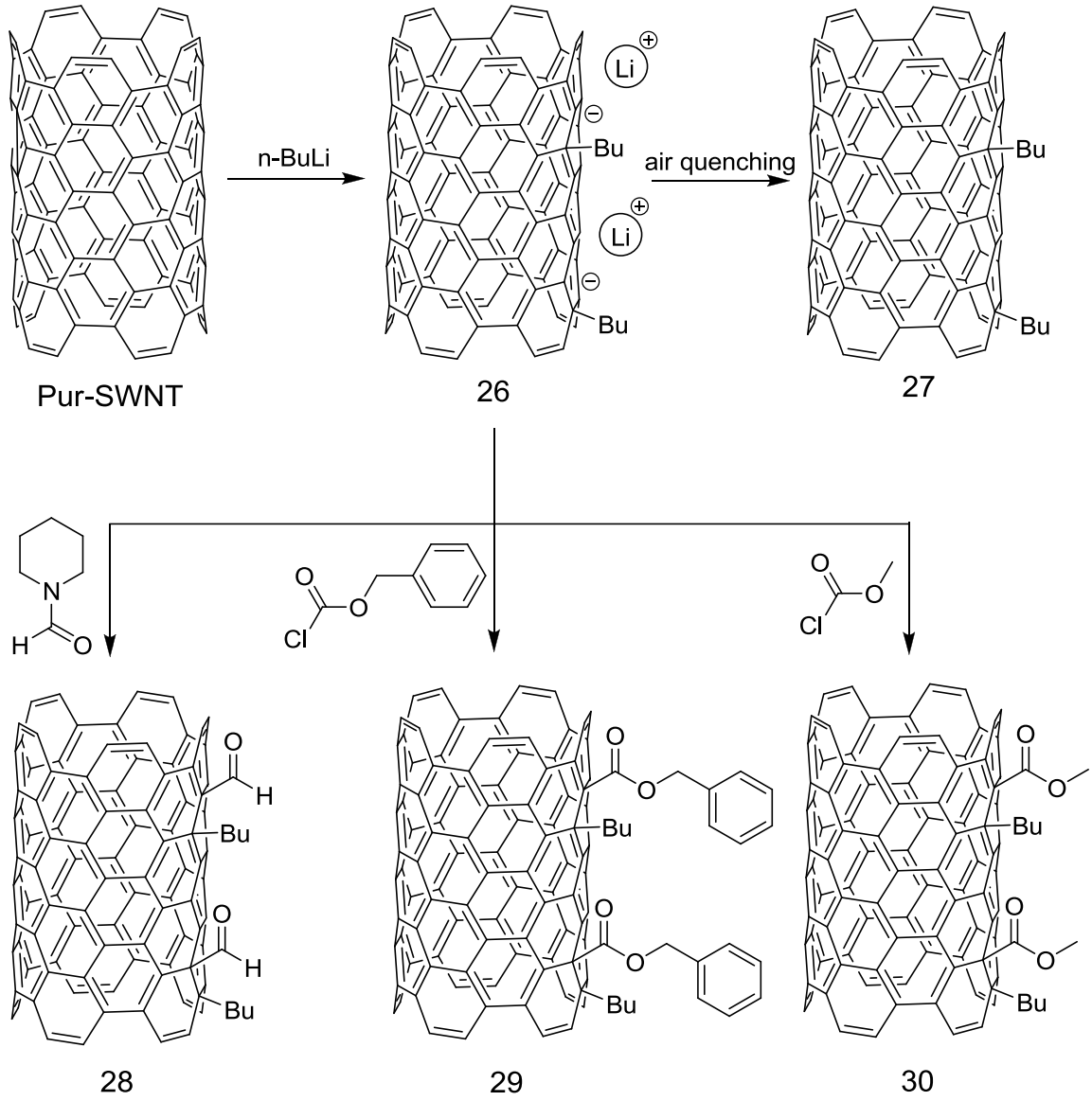

Scheme 6- 1 Schematic represantation of the n-butyllithium addition to the SWNTs surface followed by electrophilic substitution

For comparision the reactive SWNT intermediate (**26**) was also quenched by air following the literature method,[130] Scheme 6-1. Modified SWNTs were isolated and dried in a vacuum oven at 60 ^{o}C. All the modified SWNTs (**27**), (**28**), (**29**) and (**30**) were observed to spontaneously exfoliate without needing long ultrasonic treatment.

6.2.1. Effect of functional group addition on solubility

The normalized UV-vis-NIR spectra of the modified SWNTs (**27-30**), Figure 6-1, showed the expected suppression of the bands due to the conversion of sp^2 hybridized carbons to sp^3 hybridized carbon indicating that functionalisation had taken place.[80,169,198-200]

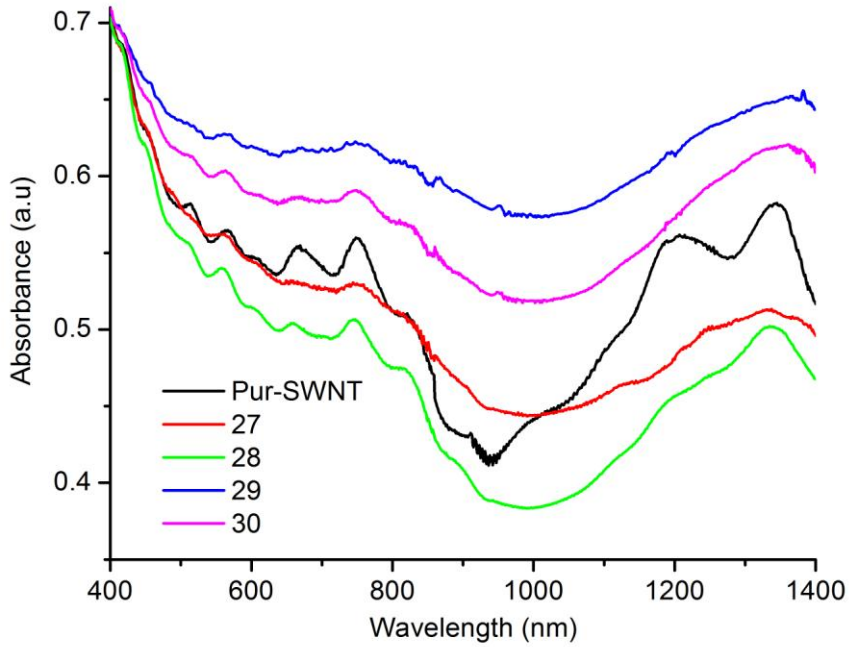

Figure 6- 1 Normalized (at 400 nm) UV-vis-NIR spectra, recorded in DMF, of purified SWNTs (black), butyl modified SWNTs (**27**) prepared by air quenching (red), butyl-formyl modified SWNTs (**28**) prepared by the addition of *N*-formylpiperidine (green), butyl-benzyl formyl modified SWNTs (**29**) prepared by the addition of benzylchloroformate (blue), and butyl-methyl formyl modified SWNTs (**30**) prepared by the addition of methylchloroformate (magenta).

A stable dispersion of purified SWNTs in DMF had a concentration of 7 μg mL^{-1}, calculated using Beer's law and an extinction coefficient of 30 mL mg^{-1} cm^{-1} and absorption values at λ=700 nm[209], which increased to 11 μg mL^{-1} upon the addition of

n-butyllithium followed by air quenching (**27**) which again increased to 49, 19 and 25 μg mL^{-1} when the butylated reactive intermediate quenched with NFP (**28**), BCF (**29**) and MCF (**30**), respectively.

6.2.2. Probing the selectivity of reductive alkylation of SWNTs using UV-vis-NIR and Raman spectroscopies

In order to investigate the selectivity and reactivity of *n*-butyllithium addition to the metallic and semiconducting SWNTs a simple kinetic study was performed. The reduction of SWNTs with alkyl lithium reagents and subsequent re-oxidation is thought, based on Raman spectroscopy and NIR fluorescence, to be selective for metallic SWNTs over semiconducting tubes with reactivity inversely proportional to diameter.[130,131] This is confirmed by the work here using UV-vis-NIR spectroscopy to monitor the rate of reaction of metallic versus semiconducting SWNTs with *n*-butyllithium. A stable dilute dispersion of purified SWNTs in dry DMF under inert atmosphere was filtered through cotton wool and cannulated into the UV-vis-NIR cuvette. The UV-vis-NIR spectrum of the purified SWNTs was recorded under inert atmosphere at room temperature. 100 μL *n*-butyllithium (1.6 M in cyclohexane) was added to SWNT dispersion. Absorption spectra were then recorded 9 times in the range of 300-1700 nm over a period of 45 minutes. The normalized UV-vis-NIR spectra of purified SWNTs and the modified SWNTs after the addition of *n*-butyllithium at 450 nm are shown in Figure 6-2. As expected, the electronic bands at *ca.* 500 nm (M11), 800 nm (S22) and 1200 nm (S11) for modified SWNTs (**26**) were suppressed when compared with the unmodified SWNTs confirming the covalent addition of the butyl groups to the nanotubes. However no clear distinction of the rate of *n*-butyllithium addition to metallic SWNTs and semiconducting was observed.

Reduction in the intensity of the bands revealed that both the metallic and the semiconducting SWNTs reacted with *n*-butyllithium under the conditions used.

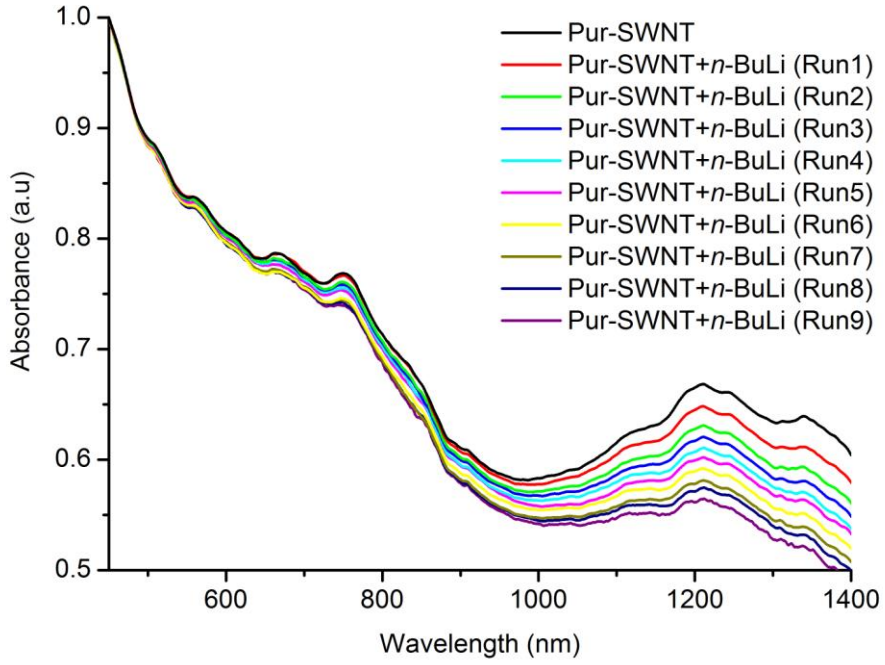

Figure 6- 2 Normalized (at 450 nm) UV-vis-NIR spectra of purified SWNTs (black), carbanionic intermediate (**26**) after the addition of 100 µL *n*-butyllithium (red), 5 minutes after the addition (green), 10 minutes after the addition (blue), 15 minutes after the addition (cyan), 20 minutes after the addition (magenta), 25 minutes after the addition (yellow), 30 minutes after the addition (olive), 35 minutes after the addition (navy) and 40 minutes after the addition (violet).

Therefore, a time drive experiment was carried out to evaluate the rate of the *n*-butyllithium addition towards the metallic and the semiconducting SWNTs. In order to monitor the change in absorbance intensities at 508 (M11), 747 (S22) and 1200 nm (S11), associated with transitions between the van Hove singularities,[139] absorption maximum was recorded over time following the addition of 100 µL *n*-butyllithium to the stable dispersion of purified SWNTs in dry DMF under argon. Figure 6-3 shows

the fitted lines of the absorbance change during 20 minutes at the wavelengths 508, 747 and 1200 nm, respectively. Close inspection of the change in absorption intensity with time revealed that the bands associated with metallic SWNTs were decreasing in intensity at a much faster rate than the bands associated with semiconducting nanotubes demonstrating that the metallic SWNTs are more reactive towards reduction with *n*-butyllithium as evidenced by the gradient of the fitted line. This agrees with Wunderlich's work where it has been shown that SWNTs exhibited more selectivity towards smaller diameter metallic nanotubes than semiconducting ones.[130,131]

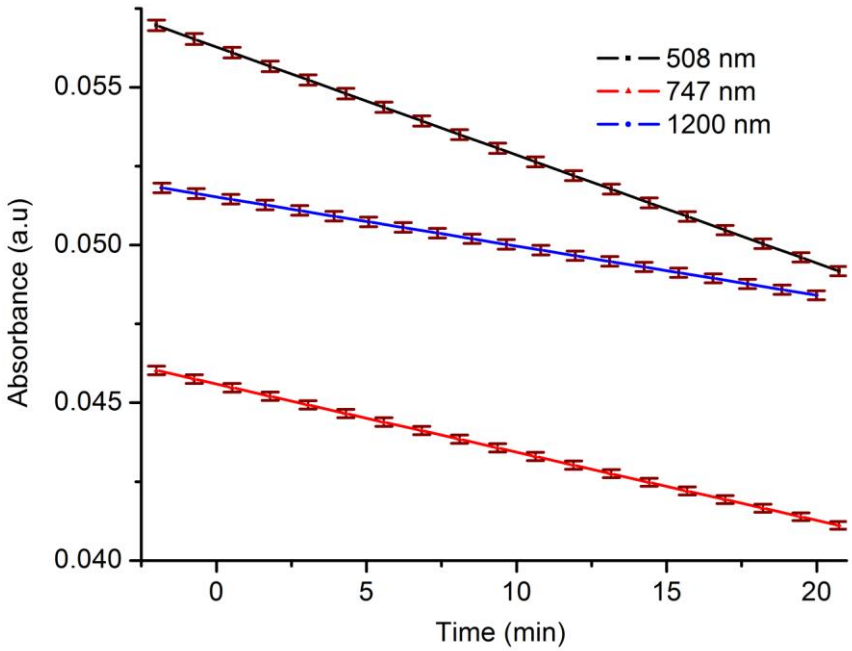

Figure 6- 3 Change in absorbance values of the corresponding metallic and semiconducting bands positioned at 508 nm (black), 747 nm (red) and 1200 nm (blue) with time.

Resonance Raman spectroscopy was used to provide a direct evidence for the covalent sidewall modification of SWNTs. [103,113,115,116,124,131,142,146,154,164,168,182,194,197,201] The Raman spectra (excited at 632.8 nm (1.96 eV) and normalized to the G-band intensity) of purified SWNTs, butyl modified SWNTs (**27**), butyl-formyl modified SWNTs (**28**),

butyl-benzyl formyl modified SWNTs (**29**) and butyl-methyl formyl modified SWNTs (**30**) are shown in Figure 6-4.

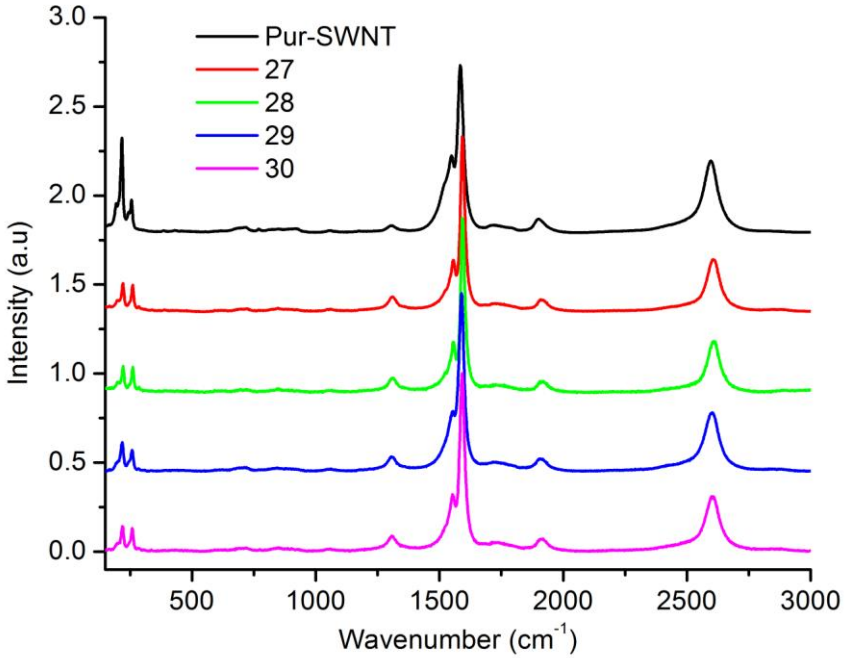

Figure 6- 4 Raman spectra (632.8 nm, 1.96 eV) of purified SWNTs (black), butyl modified SWNTs (**27**) prepared by air quenching (red), and butyl-formyl modified SWNTs (**28**) prepared by the addition of *N*-formylpiperidine (green), butyl-benzyl formyl modified SWNTs (**29**) prepared by the addition of benzylchloroformate (blue), and butyl-methyl formyl modified SWNTs (**30**) prepared by the addition of methylchloroformate (magenta) normalized and offset at the G-band.

As expected the functionalised SWNTs (**27**-**30**) displayed an increased D-band at ~1300 cm^{-1} when compared with unmodified purified SWNTs (A_D/A_G=0.024 ± 5.7×10^{-4}), with an A_D/A_G ratio of 0.158±0.002, 0.135±0.003, 0.140±0.001 and 0.167±0.003 respectively, indicating the groups are covalently bonded to the nanotube surface. The change in G-band intensity and line shape revealed that there was a small change in the electronic structure of the modified SWNTs (**27**-**30**). The Raman spectra

of purified SWNTs and modified (**27-30**) SWNTs excited at 532 nm (2.33 eV) and 785 nm (1.58 eV) are also given in Appendix D (Figure D1 and Figure D2) for comparision. From the spectra it is clear to see that the D band is shifted in frequency with changing laser excitation energy as the D band is dispersive. The Raman spectra of the modified SWNTs (**27-30**) excited at 532 nm showed a tangential mode (G-band) having a characteristic band shape at lower frequency owing to the Breit-Wigner-Fano (BWF) resonance of metallic nanotubes.[202] Excitation of modified SWNTs (**27-30**) at 785 nm (1.58 eV) showed a tangential mode splited into two bands, higher (G^+) and lower (G^-) frequency, are attributed to semiconducting SWNTs[130] and, the intensity change in band corresponded to the lower frequency showed a significant decrease in modified SWNTs (**27-30**) when compared with the unmodified SWNTs as an indicative of reaction of semiconducting nanotubes.[202,371] A_D/A_G ratio of the modified SWNTs (**27-30**) at 532 and 785 nm excitation is given in Table 6-1.

	Pur-SWNT	**27**	**28**	**29**	**30**
532 nm	0.064±0.001	0.189±0.002	0.174±0.006	0.173±0.004	0.201±0.004
785 nm	0.038±0.004	0.279±0.003	0.208±0.002	0.233±0.001	0.193±0.001

Table 6- 1 A_D/A_G of the modified SWNTs at 532 and 785 nm excitation.

The radial breathing modes (RBMs) in the Raman spectra exhibited considerable differences between the covalently modified (**27-30**) and pristine SWNTs as a result of covalent modification showing selectivity towards metallic and semiconducting nanotubes. Figure 6-5 displays the RBM region Raman spectra of the pristine and modified (**27** and **28**) SWNTs excited at 632.8 nm (1.96 eV).

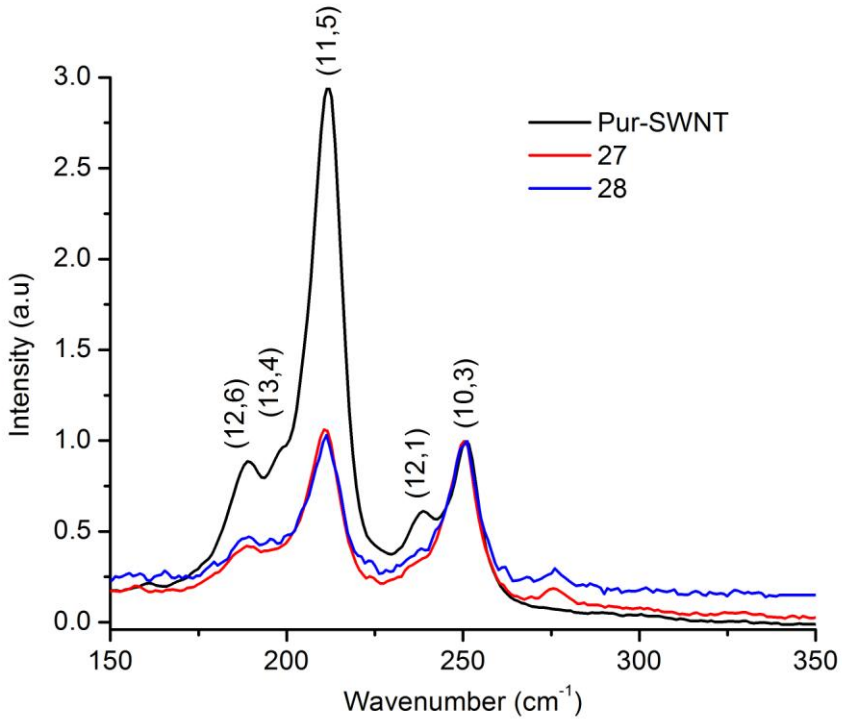

Figure 6- 5 RBM region of the Raman spectra (632.8 nm, 1.96 eV) of purified SWNTs (black), butyl modified SWNTs (**27**) prepared by air quenching (red), and butyl-formyl modified SWNTs (**28**) prepared by the addition of *N*-formylpiperidine (blue) normalized at 250 cm^{-1}.

Five main peaks at ~189, 199, 211, 239 and 250 cm^{-1} which correspond to (12,6), (13,4), (11,5), (12,1) and (10,3) SWNTs with diameter of 1.266, 1.198, 1.125, 0.986 and 0.941 nm respectively, can be assigned from the spectrum of unmodified SWNTs. Using the modified Kataura plots of Strano[142] the first three are denoted as metallic and the remaining two semiconducting. The semiconducting band at ~250 cm^{-1} in the spectra of unmodified and modified (**27** and **28**) SWNTs was selected as reference band since it was mainly unchanged. By normalizing the spectra at ~250 cm^{-1} it was seen that there was a significant decrease in the intensity of the band at ~211 cm^{-1} associated with (11,5) SWNTs while the band at ~239 cm^{-1} associated with (12,6) is decreasing slightly. Significant change in intensity of metallic bands indicated that the

n-butyllithium mainly reacted with metallic SWNTs despite showing affinity toward semiconducting SWNTs as well.

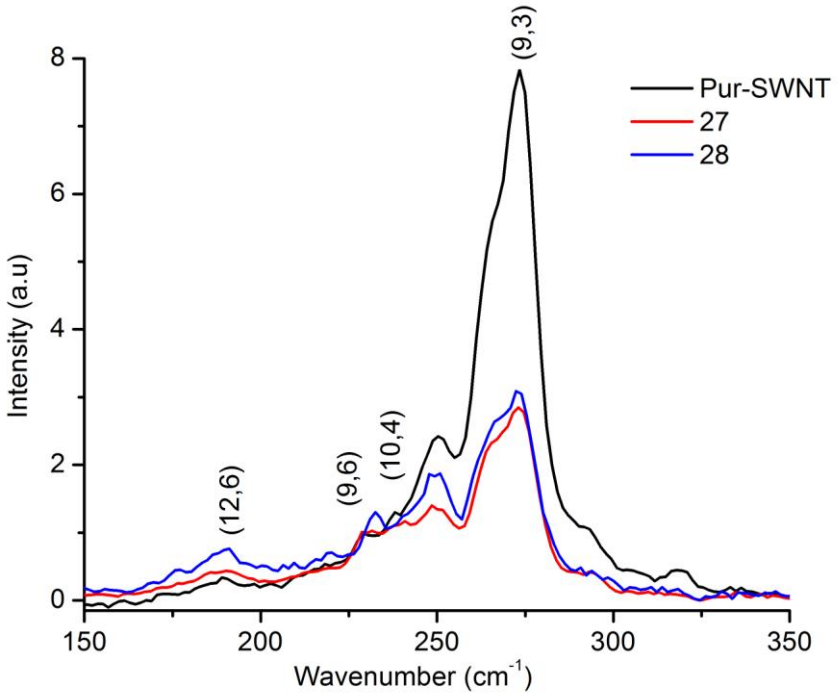

Figure 6- 6 RBM region of the Raman spectra (532 nm, 2.33 eV) of purified SWNTs (black), butyl modified SWNTs (**27**) prepared by air quenching (red), and butyl-formyl modified SWNTs (**28**) prepared by the addition of *N*-formylpiperidine (blue) normalized at 229 cm^{-1}.

The RBM region Raman spectrum of the unmodified purified SWNTs excited at 532 nm (2.33 eV), Figure 6-6, shows a strong band at 273 cm^{-1} which can be assigned to (9,3); the three possible weak bands at 191, 229 and 239 cm^{-1} having chirality indices (12,6), (9,6) and (10,4) respectively,[130] are ignored. The diameter of the nanotubes are 0.857, 0.986, 1.032 and 1.252 nm, respectively. The RBMs in Raman spectra, normalized at 229 cm^{-1}, of the modified SWNTs (**27** and **28**), Figure 6-6, show a significant decrease in the band at 273 cm^{-1} assigned to smaller diameter metallic SWNTs confirming the reactivity of small diameter metallic tubes.

Figure 6-7 shows the RBM region Raman spetrum, excited at 785 nm, of unmodified SWNTs with five bands at 202, 212, 224, 231 and 265 cm^{-1} which can be assigned (9,8), (9,7), (10,5), (11,3) and (10,2) respectively, with diameter of 1.179, 1.120, 1.056, 1.022 and 0.885 nm respectively,[130,191] the possible weak band at 245 cm^{-1} is ignored.

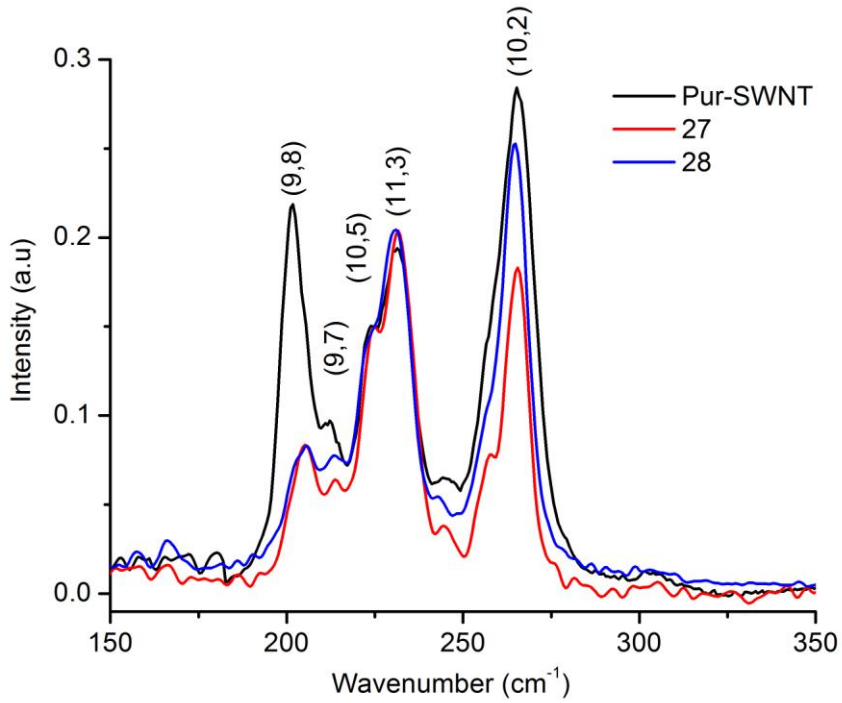

Figure 6- 7 RBM region of the Raman spectra (785 nm, 1.58 eV) of purified SWNTs (black), butyl modified SWNTs (**27**) prepared by air quenching (red), and butyl-formyl modified SWNTs (**28**) prepared by the addition of *N*-formylpiperidine (blue) normalized at 224 cm^{-1}.

The RBM Raman spectra of functionalised SWNTs (**27**) and (**28**), Figure 6-7, normalized at 224 cm^{-1}, show a considerable decrease in band at 202 cm^{-1} assigned to larger diameter semiconducting SWNTs and a somewhat smaller decrease in band at 265 cm^{-1} attributed to smaller diameter semiconducting SWNTs. Excitation at 632.8 nm showed that the *n*-butyllithium addition to nanotube surface was selective for metallic SWNTs where 532 nm excitation showed that selectivity was towards smaller

diameter metallic SWNTs. Moreover excitation at 785 nm showed that the reaction was not limited to metallic SWNTs displaying selectivity towards the smallest and larger diameter semiconducting SWNTs.

6.2.3. Characterisation of surface functional groups

Although Raman and UV-vis-NIR data for the modified SWNTs (**27-30**) give convincing evidence for the reductive butylation of SWNTs, they do not show significant differences to confirm the presence of the formyl, benzyl formyl and the methyl formyl groups. In order to obtain detailed information of the presence of formyl, benzyl formyl and methyl formyl groups attached to SWNTs surface the use of FTIR, TGA-MS, AFM, fluorescence spectroscopy and optical microscopy are curucial.

Figure 6-8 shows the FTIR spectra of the purified SWNTs and the modified SWNTs (**27-30**). FTIR spectrum of the butyl-formyl modified SWNTs (**28**) displays the presence of the formyl group ($\nu_{(CO)}$ 1720 cm^{-1}) and three bands characteristic for butyl chain at 2900, 1560 and 1425 cm^{-1} which are also present in the spectrum of butyl modified SWNTs (**27**) when compared to purified SWNTs.[372] The FTIR spectra of modified SWNTs (**29** and **30**) suggest that the SWNTs are functionalised with groups showing a carbonyl stretching at ~1770 cm^{-1} when compared with the spectrum of butyl modified SWNTs (**27**). Nevertheless the spectrum of modified SWNTs (**29**) shows a sharp peak located at ~2960 cm^{-1} which is due to the C-H stretching of aromatic ring protons as compared with the aliphatic C-H stretching located at ~2920 cm^{-1} in the spectrum of both (**27**) and (**28**) .

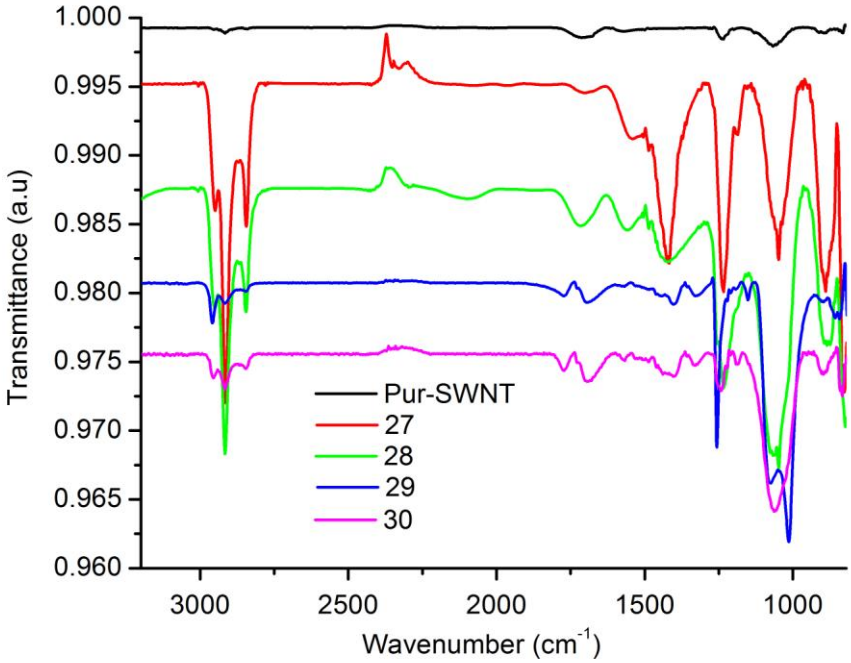

Figure 6- 8 Normalized and offset FTIR spectra of purified SWNTs (black), butyl modified SWNTs (**27**) prepared by air quenching (red), and butyl-formyl modified SWNTs (**28**) prepared by the addition of *N*-formylpiperidine (green), butyl-benzyl formyl modified SWNTs (**29**) prepared by the addition of benzylchloroformate (blue), and butyl-methyl formyl modified SWNTs (**30**) prepared by the addition of methylchloroformate (magenta).

Thermogravimetric analysis (TGA) was applied to detect the degree of functionalisation. TGA-MS of the modified SWNTs (**27-30**) showed a weight loss of ~20±0.005, 25±0.005, 47±0.005, 26±0.005 %, respectively, at 600 ^{o}C compared to ~5±0.005% for purified SWNTs, Figure 6-9. Calculations revealed the presence of ~1 butyl group for every 27 (3.72 atomic%) carbon atoms for the modified SWNTs (**27**), ~1 butyl-formyl group for every 29 (3.49 atomic%) carbon atoms for the modified SWNTs (**28**), ~1 butyl-benzylformyl group for every 22 (4.53 atomic%) carbon atoms for the modified SWNTs (**29**) and ~1 butyl-methylformyl group for every 36 (2.75 atomic%) carbon atoms for the modified SWNTs (**30**).

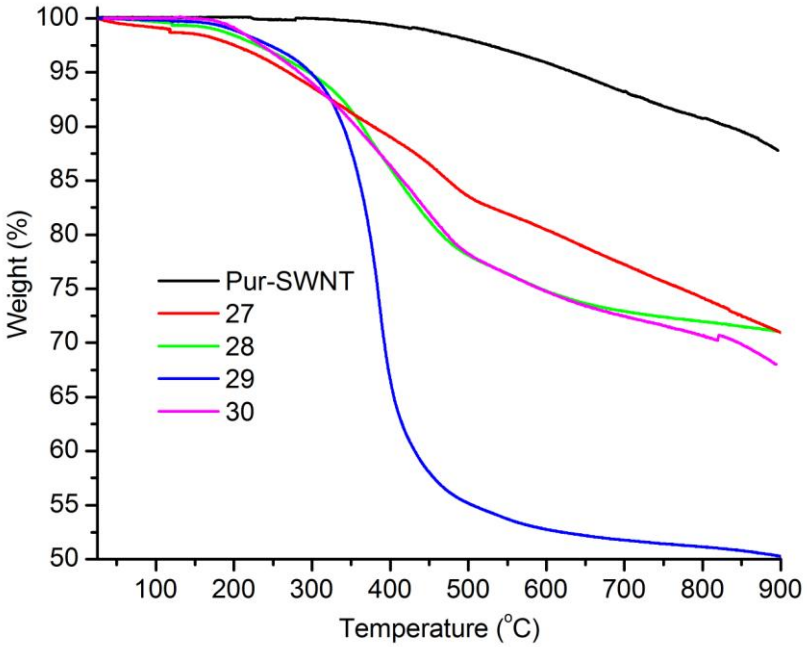

Figure 6- 9 TGA data (10 ^{o}C min^{-1}) of purified SWNTS (black), butyl modified SWNTs (**27**) (red), and butyl-formyl modified SWNTs (**28**) (green), butyl-benzyl formyl modified SWNTs (**29**) (blue), and butyl-methyl formyl modified SWNTs (**30**) (magenta).

The derivative of the TGA curves of the modified SWNTs (**27-30**), Figure 6-10, revealed that the mass loss started at ~200 ^{o}C and reached its maximum at ~400-450 ^{o}C while heating the modified SWNTs by 10 ^{o}C min^{-1}. From Figure 6-10 it is clear that the intensity of derivative curve of modified SWNTs (**29**) is greater when compared with modified SWNTs (**27**, **28** and **30**). Intensity change in derivative curves reveals that the weight loss in modified SWNTs (**29**) is higher than modified SWNTs (**27**, **28** and **30**) at ~400-450 ^{o}C since it has considerably bulky benzoxy group.

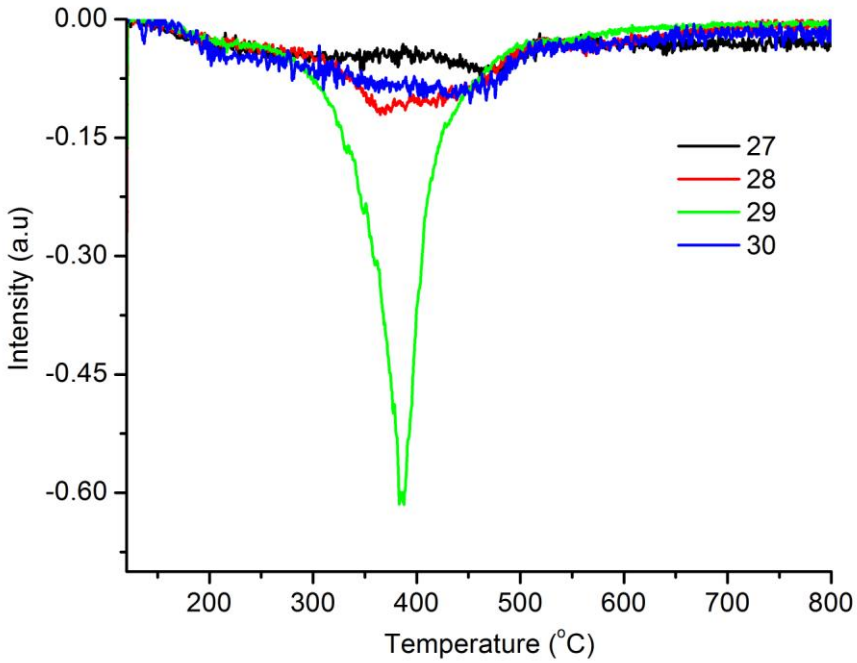

Figure 6- 10 TGA derivative of butyl modified SWNTs (**27**) (black), butyl-formyl modified SWNTs (**28**) (red), butyl-benzyl formyl modified SWNTs (**29**) (green) and butyl-methyl formyl modified SWNTs (**30**) (blue).

Mass spectrometry coupled with the TGA is very informative for the groups fragmented during the heating of the modified SWNTs till 900 ^{o}C. Figure 6-11 shows the mass fragmentations of the modified SWNTs (**27** and **28**) given off during the heating. Masses fragmented for the modified SWNTs (**27**) at ~200 ^{o}C, Figure 6-11, correspond to the butyl group (C_4H_{10}, 58 amu), propyl group (C_3H_7, 43 amu) and ethyl group (C_2H_5, 29 amu), respectively. In addition to the masses eliminated at ~200 ^{o}C another fragmentation which could correspond to formyl group (29 amu) was observed at ~400-450 ^{o}C for the butyl-formyl modified SWNTs (**28**), Figure 6-11, as an indicative of formyl functionalisation. The temperature at which the formyl group comes off was in close agreement with the given derivative curve for the butyl-formyl modified SWNTs (**28**) in Figure 6-10.

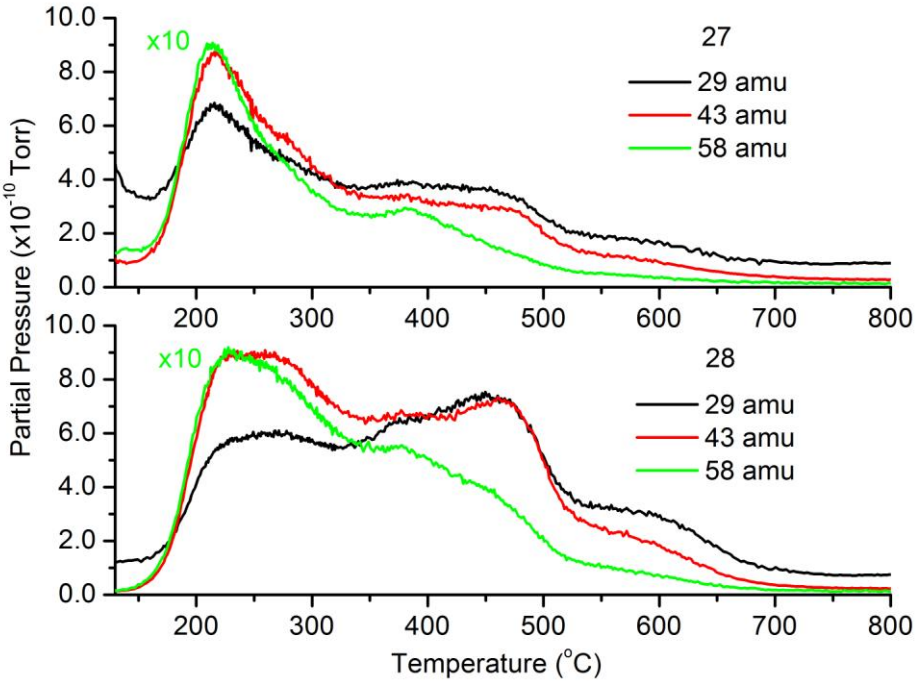

Figure 6- 11 Top: Mass trace (black) of ethyl (29 amu), (red) propyl (43 amu) and (green) butyl (58 amu) fragment given off during the heating of butyl modified SWNTs (**27**). Bottom: Mass trace (black) of ethyl (29 amu), (red) propyl (43 amu) and (green) butyl (58 amu) fragment given off during the heating of butyl-formyl modified SWNTs (**28**).

Figure 6-12 shows the mass fragmentations of (**29**) and (**30**) given off during the heating of modified nanotubes by 10 ^{o}C min^{-1} to 900 ^{o}C. Masses fragmented for the modified SWNTs (**29** and **30**) at ~200 ^{o}C are attributed to the butyl (C_4H_{10}, 58 amu) and propyl groups (C_3H_7, 43 amu). Mass fragmentations for the modified SWNTs (**29**) at ~400 ^{o}C correspond to benzoxy group (107 amu), phenyl group (78 amu) and benzyl group (91 amu), respectively, as an indicative of the presence of benzyl formyl group. The temperature at which the benzyl formyl fragmentations come off is in close agreement with the given derivative curve for benzyl-formyl modified SWNTs (**29**) in Figure 6-10. In the case of (**30**) mass fragmentation observed between 300-400 ^{o}C for

methoxy group (31 amu) reveals that the methyl formyl group is also present on nanotube surface.

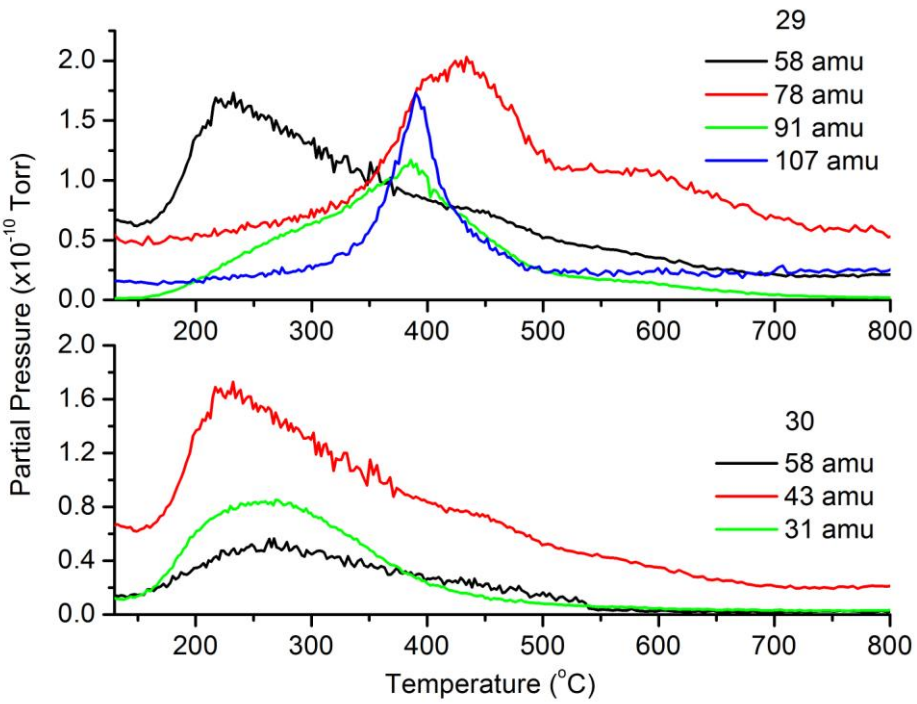

Figure 6- 12 Mass trace (black) of butyl (58 amu), (red) phenyl (78 amu), (green) benzyl (91 amu) and (blue) benzoxy (107 amu) fragment given off during the heating of butyl-benzylformyl modified SWNTs (**29**). Bottom: Mass trace (black) of butyl (58 amu), (red) propyl (43 amu) and (green) methoxy (31 amu) fragment given off during the heating of butyl-methylformyl modified SWNTs (**30**).

6.2.4. Tagging of functional groups for fluorescence spectroscopy studies and AFM visualisation

Due to the physical properties and low solubility of the SWNTs it is very hard to assign the attached organic side groups using known organic characterization techniques. Therefore several methodologies have been applied for probing the presence and the distribution of groups on surface. Chemical tagging is being

increasingly used to probe the covalently anchored side groups using microscopic or spectroscopic techniques.

It is known that the aldehydes undergo a reaction with both hydrazines and amines to produce hydrazones and imines, respectively. Scheme 2-2 shows the possible experimental pathway to tag formyl group on modified SWNTs (**28**) using a fluorescent dye, fluorescein-5-thiosemicarbazide (FTSC).

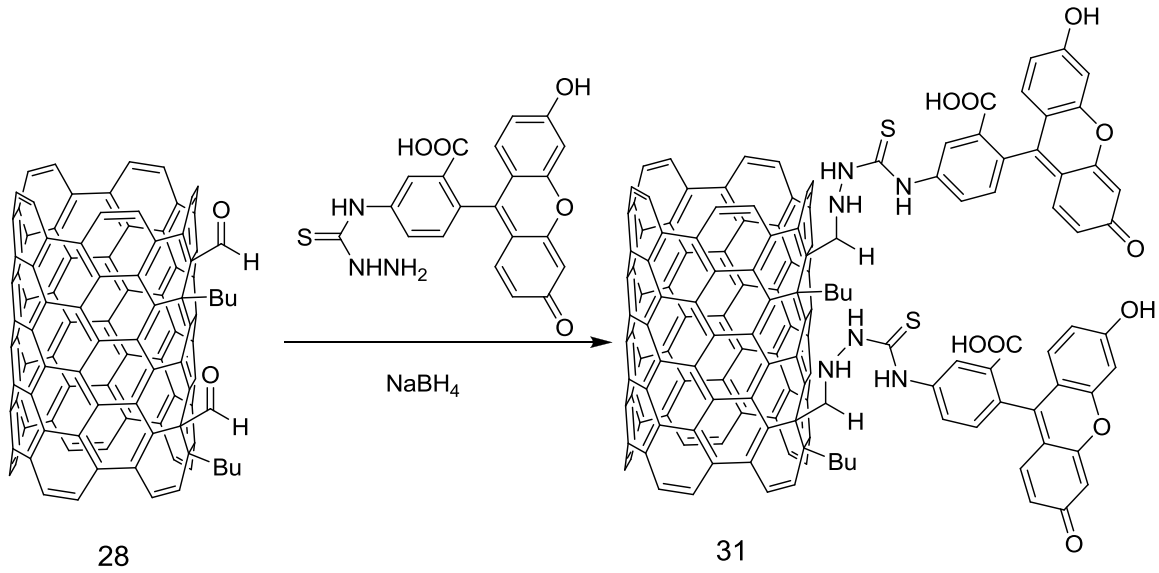

Scheme 6- 2 Schematic representation of the chemical tagging of formyl groups on modified SWNTs (**28**) using fluorescein-5-thiosemicarbazide (FTSC) dye.

Tagging with dye is used to image the tagged SWNTs (**31**) under optical microscope and record solution phase fluorescence spectrum of the material. In order to synthesize the modifed SWNTs having FTSC groups (**31**) on the surface a modified procedure reported by Thomson and co-workers[373] was followed. Reaction of FTSC with modifed SWNTs (**28**) involves the formation of hydrozone linkage in the presence of acid catalyst and the subsequent reduction of the hydrozone linkage using a mild reducing agent ($NaBH_4$) to yield comparatively more stable form of the product (**31**).

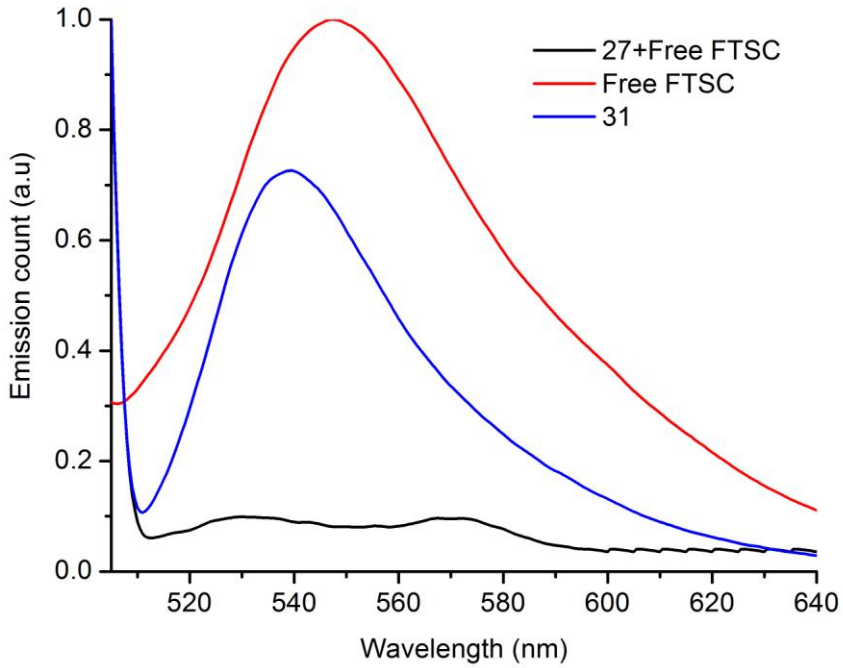

Figure 6-13 Normalized and offset fluorescence spectra of the modified SWNTs (**27**) mechanically mixed with free FTSC and washed with water, acetone and ethanol (black), free FTSC (red) and modified SWNTs tagged with FTSC dye (**31**) (blue).

In addition to the FTSC tagging experiment, a control was performed to ensure that the emission was not as a result of the adsorbed FTSC on the SWNT surface. This included mechanically mixing FTSC dye with the modified SWNTs (**27**) followed by water, ethanol and acetone washing. Figure 6-13 displays the fluoresence spectra of free FTSC, modified SWNTs tagged with FTSC (**31**) and modified SWNTs (**27**) mechanically mixed with free FTSC and washed by water, ethanol and acetone.

It is clear that the excitation of a stable dilute dispersion of FTSC tagged modified SWNTs (**31**) in DMF at 492 nm shows a green emission at ~540 nm compared with the free FTSC emited at ~547 nm in DMF. The emission taken due to the FTSC groups on modified SWNTs (**28**) surface at ~540 nm confirms the presence of the

formyl group on SWNTs surface. The control experiment carried out by mixing free FTSC with modified SWNTs (**27**) showed no sign of fluoresence.

The presence of the formyl group was also confirmed by recording the white light optical image and the epi-fluoresence image of both modified SWNTs (**27**), mechanically mixed with free FTSC and washed by water, acetone and ethanol, and modified SWNTs tagged with FTSC dye (**31**). Fluorescence images were recorded using excitation light transmitted through a 420 to 480 nm excitation filter and fluorescence observed after passage through a 500 nm emission filter (Olympus CX-DMB-2 cube). Figure 6-14 and Figure 6-15 display the white light optical and the epi-fluoresence image of the modified SWNTs (**27**) mechanically mixed with FTSC followed by washing and the FTSC modified SWNTs (**31**), respectively, which were deposited and dried on a glass microscope slide.

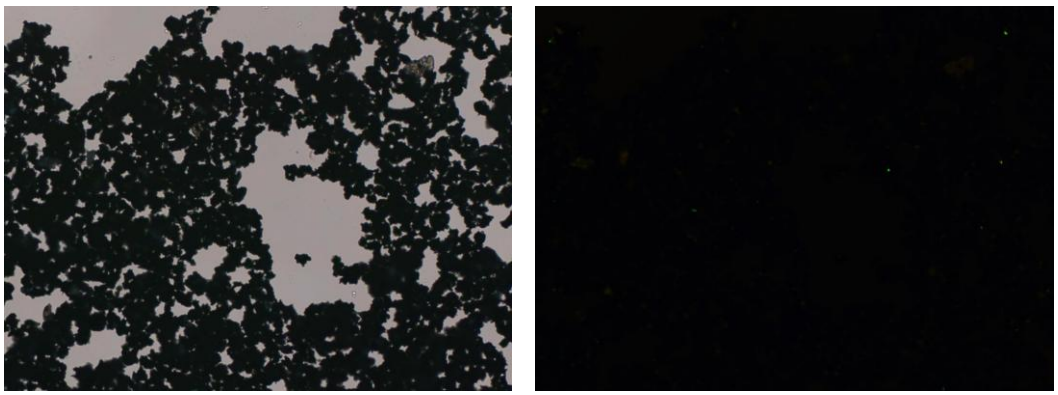

Figure 6- 14 White light optical image (left) and epi-fluorescence image (right) of the modified SWNTs (**27**) mechanically mixed with FTSC followed by water, acetone and ethanol washing (718 x 533 μm).

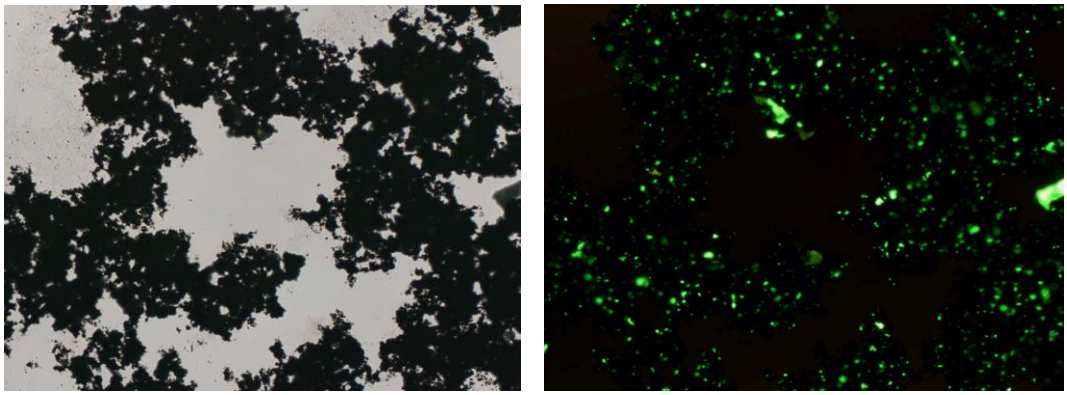

Figure 6- 15 White light optical image (left) and epi-fluorescence image (right) of the FTSC modified SWNTs (**31**) (718 x 533 μm).

Although white light optical images of both modified SWNTs (**27**) mechanically mixed with FTSC and FTSC modified SWNTs (**31**) look similar, the epi-fluorescence image of the FTSC modified SWNTs (**31**) displays visible green spots revealing the presence of the FTSC tagged formyl groups on the nanotube surface. Distribution of the green spots states that the yield of hydrazone formation reaction is sufficiently high for visualisation and imaging.

Besides the fluorescence spectroscopy and optical microscopy, it was also possible to assign the location and distribution of groups using atomic force microscopy (AFM) Scheme 2-3 shows the chemical pathway for tagging of aldehyde groups for AFM visualization.

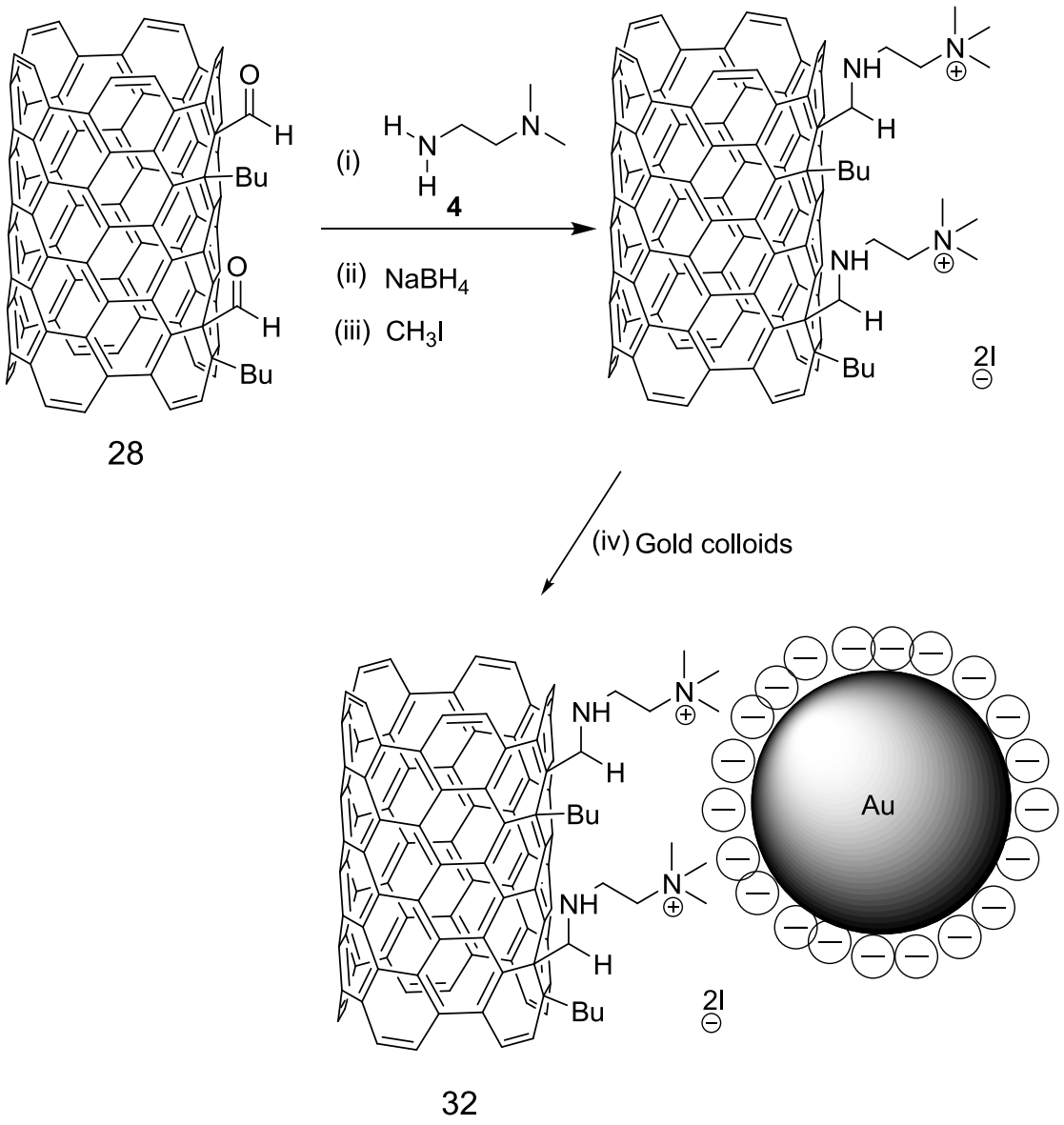

Scheme 6- 3 Schematic representation of the electrostatic interaction of gold colloids with formyl functionalised SWNTs (**28**) for AFM functional group tagging experiments.

The aldehyde functional groups on modified SWNTs (**28**) were converted to the imine with a terminal tertiary amine, by reaction with *N*,*N*-dimethylethylenediamine, which was subsequently hydrogenated using a mild reducing agent ($NaBH_4$) to prevent the decomposition of less stable imine linkage. After the quaternization of the tertiary amine on SWNTs surface using iodomethane, positively charged SWNTs were deposited on a mica surface, where they were exposed to citrate stabilized freshly

prepared gold colloids 4-6 nm in diameter. The mica surface was washed several times using high purity water to remove excess gold colloids adsorbed on surface. After drying the substrate at 80 ^{o}C for 2 hours data was recorded using tapping mode AFM. Figure 6-16 shows the AFM height image of the formyl-butyl modified SWNT with positively charged tertiary amines after exposing to citrate stabilized Au colloids (**32**).

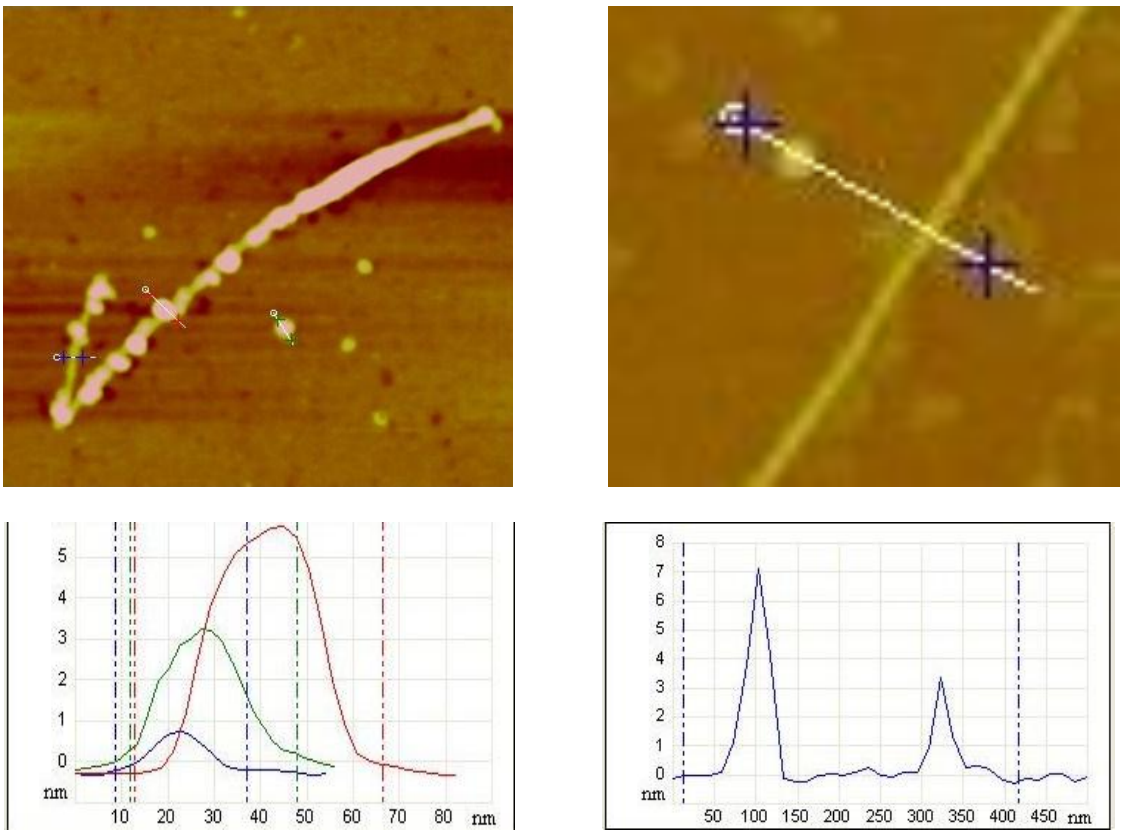

Figure 6- 16 A typical tapping mode AFM height image of the formyl-butyl modified SWNT (**28**) with positively charged tertiary amines (720 x 720 nm) (Top left) and butyl modified SWNT (**27**) (730 x 730 nm) (Top right) after exposure to citrate stabilized Au colloids (4-6 nm). z scale is 0-5 nm. The section analysis of the gold decorated individualized modified SWNT (**32**) (Bottom left) and butyl modified SWNTs (**27**) (Bottom right).

The presence of the gold nanoparticles on SWNT surface displays the electrostatic interaction of positively charged SWNTs with the negatively charged gold colloids revealing the availability and distribution of the formyl group on nanotube surface. The height analysis shows that the SWNTs were individualized after functionalisation. Control experiments carried out exposing the butyl modified SWNTs (**27**) with negatively charged gold colloids after treating with N,N-dimethylethylenediamine showed no gold nanoparticles along the SWNT surface, Figure 6-16. However there were a few gold nanoparticles which are not in contact with the SWNT surface.

It was also possible to tag the methyl formyl modified SWNTs (**30**) using the gold nanoparticles to provide futher evidences for the covalent modification of methyl formyl group to the nanotube surface. Scheme 2-4 shows the reaction pathway for the chemical tagging of ester groups on modified SWNTs (**30**).

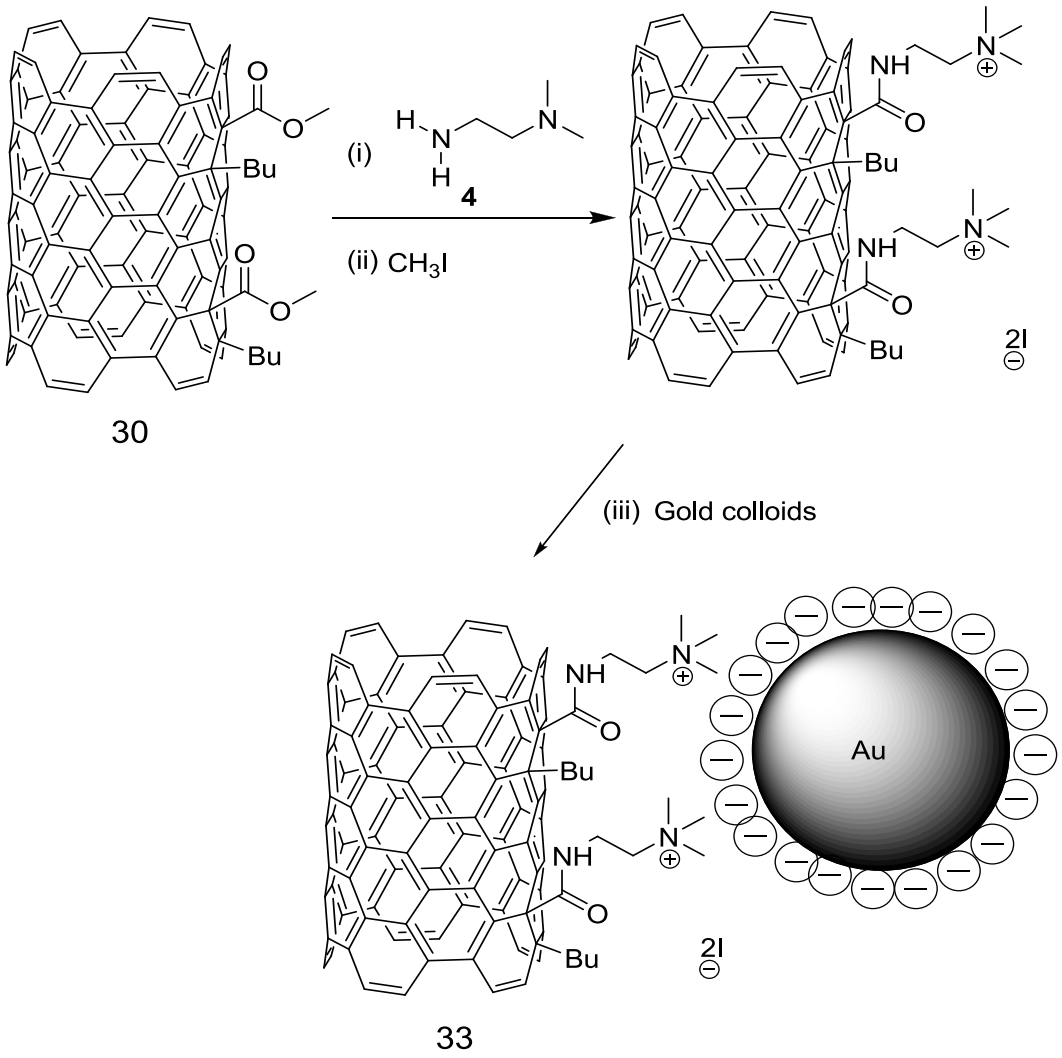

Scheme 6- 4 Schematic representation of the electrostatic interaction of gold colloids with methyl formyl functionalised SWNTs (**30**) for AFM functional group tagging experiments.

Methyl ester groups covalently attached to nanotube surface were converted into an amide by reaction with *N*,*N*-dimethylethylenediamine at 100 ^{o}C, which was quaternized by reaction with methyl iodide. Low reaction temperature ensures that nanotube surface was not functionalized by amine groups.[260] Positively charged SWNTs deposited on mica surface were exposed to citrate stabilized negatively

charged gold colloids 4-6 nm in diameter to image them under AFM. Figure 6-17 shows gold decorated SWNTs as light features indicating the presence and distribution of the methyl ester functional groups on nanotube surface. The section analysis reveals that the functionalisation causes individualization of SWNTs.

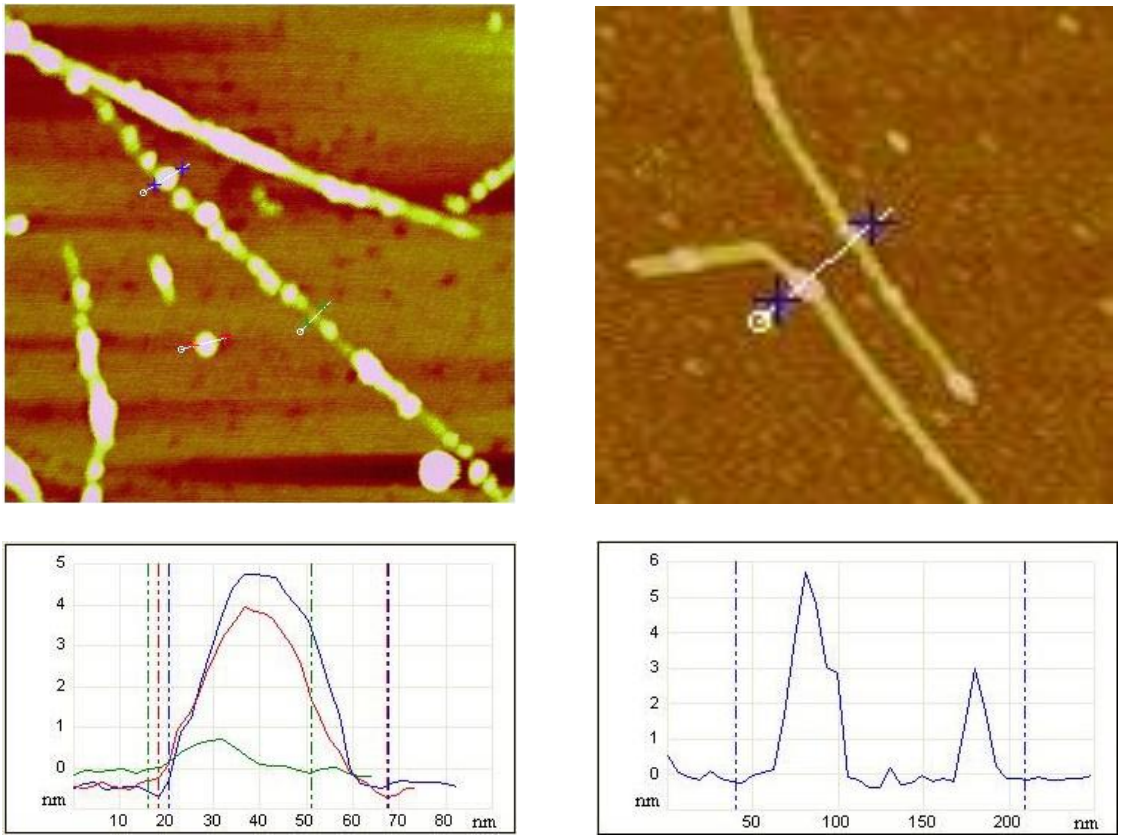

Figure 6- 17 A typical tapping mode AFM height image of the butyl- methyl formyl modified SWNT (**30**) with positively charged tertiary amines (740 x 740 nm) (Top left) and butyl modified SWNT (740 x 740 nm) (Top right) after exposure to citrate stabilized Au colloids (4-6 nm). z scale is 0-5 nm. The section analysis of the gold decorated individualized modified SWNT (**33**) (Bottom left) and butyl modified SWNT (**27**) (Bottom right).

Control experiments performed exposing the butyl modified SWNTs (**27**), treated with *N*,*N*-dimethylethylenedimaine at 100 ^{o}C, with negatively charged gold colloids

displayed a small number of gold nanoparticles in contact with the SWNT surface, Figure 6-17. This could be as a result of the carboxylic acid groups which may be present on the SWNT surface which can also react with amine to produce amide. However the distribution of the gold nanoparticles indicates that the number of carboxylic acid groups present is very small.

6.3. Conclusion

It has been demonstrated that purified SWNTs could be functionalised with groups having a sp^2 hybridized reactive carbon center following reductive alkylation. The selectivity of the reaction could be probed using UV-vis-NIR which has advantages over Raman spectroscopy which requires the use of multiple laser excitation and NIR fluorescence where only the semiconducting nanotubes can be probed. UV-vis-NIR spectroscopy results revealed that *n*-butyllithium addition to SWNT sidewall was selective for both metallic and semiconducting SWNTs showing a comparatively higher reaction rate for metallic nanotubes. Raman spectroscopy showed that *n*-butyllithium addition to nanotube surface was selective for smaller diameter metallic and smaller and larger diameter semiconducting SWNTs. The findings were very important since selective functionalisation of SWNTs can be a tool for the separation of the metallic nanotubes from semiconductings to use in electronic aplications. Introducing reactive aldehyde and ester groups can be very useful to extend the surface chemistry by forming hydrazone or imine linkages via formyl groups and amide or new ester linkages with methoxy and benzoxy ester groups to improve solubility and processibility of SWNTs. The only limitation of the process was the use of solvent, cyclohexane, whic had limited solvation capability. Therefore cyclohexane soluble reactants, especially liquids, were preferred to obtain high yields. The solubilities of the formylated (**28**) and ester functionalised (**29** and **30**) SWNTs were higher than

purified and butyl functionalised (**27**) SWNTs. TGA results showed that the electrophile addition to the butyl modified reactive SWNT intermediate is an efficient process to produce nanotubes having different functionalities. Fluorescent tagging experiments showed that aldehyde groups could be reacted with either hydrazines or terminal amines to yield hydrazone or imine linkages respectively, which allow nanotubes to be visualised by optical microscopy. AFM tagging experiments displaying the electrostatic interaction of citrate stabilized gold nanoparticles with aldehydes (**28**) and esters (**30**) which were postively charged showed that the functional groups were present on the entire length of the carbon nanotubes.

7. EXPERIMENTAL

7.1. Characterisation of modified SWNTs

AFM. Samples for AFM analysis were produced by drop deposition onto freshly cleaved mica of the corresponding solution of SWNTs (ca. 0.005 mg mL^{-1}) in *N*,*N*-dimethylformamide produced by sonication in an ultrasonic bath (Ultrawave U50, 30 – 40 kHz) for 15 mins. Samples were dried in air before imaging in tapping mode using a Digital Instruments Multimode AFM with a Nanoscope IV controller.

XPS. XPS studies were performed at NCESS, Daresbury laboratory using a Scienta ESCA 300 hemispherical analyser with a base pressure under 3×10^{-9} mbar. The analysis chamber was equipped with a monochromated Al Kα X-ray source ($h\nu$= 1486.6 eV). Charge compensation was achieved (if required) by supplying low energy (<3 eV) electrons to the samples. XPS data were referenced with respect to the corresponding C 1s binding energy of 284.5 eV which is typical for carbon nanotubes.[17] Photoelectrons were collected at a 45 degree take-off angle, and the analyser pass energy was set to 150 eV giving an overall energy resolution of 0.4 eV. Analysis of XPS data were performed using CasaXPS software. Shirley was used as background type while deconvoluting the XPS spectra.

TGA-MS. Thermogravimetric analysis – mass spectrometry (TGA-MS) data were recorded on 1–3 mg of sample using a Perkin Elmer Pyris I coupled to a Hiden HPR20 mass spectrometer. Data were recorded in flowing He (20 mL min^{-1}) at a ramp rate of 10 °C min^{-1} to 900 °C after being held at 120 °C for 30 mins to remove any residual solvent.

UV-vis-NIR Spectroscopy. The UV-vis-NIR absorption spectra were recorded on a Perkin Elmer Lambda 900 spectrometer. The samples were prepared by dispersing the nanotube material in *N*,*N*-dimethylformamide, ethanol or water by sonication in an ultrasonic bath (Ultrawave U50, 30 – 40 kHz) for 5 mins followed by filtration through a plug of cotton wool to remove particulates after allowing the solution to stand for 2 h.

Raman Spectroscopy. Raman spectra were recorded using a Jobin Yvon Horiba LabRAM spectrometer in a back scattered confocal configuration using He/Ne (632.8 nm, 1.96 eV), Nd:YAG (532 nm, 2.33 eV) or diode (785 nm, 1.58 eV) laser excitation. All spectra were recorded on solid samples over several regions and were referenced to the silicon line at 520 cm^{-1}.

FTIR Spectroscopy. Infrared spectra were recorded on thick films using a Perkin Elmer Spectrum 100 equipped with a Pike ATR fitted with a Ge crystal. FTIR spectra of SWNT free organic compounds were recorded as neat or powder.

Fluorescence Spectroscopy. Fluorescence spectra were recorded on a Perkin Elmer LS55 luminescence spectrometer using an excitation wavelength of 330 nm. SWNT samples were prepared by dispersing SWNTs in DMF (0.1 mg mL^{-1}) or acetonitrile (~10^{-4} M) and allowing them to settle for 8h followed by filtration. Free indolizine compounds were dissolved in acetonitrile.

Optical Microscopy. Samples were prepared dispersing the SWNT material in a volatile solvent. A few drops of SWNT dispersion were dropped on a microscope slide and dried. Fluorescence images were recorded using excitation light transmitted through a 420 to 480 nm excitation filter and fluorescence observed after passage through a 500 nm emission filter (Olympus CX-DMB-2 cube).

Fluorimeter. Luminesence spectra of the indolizine modified SWNTs (solid sample) were recorded using a Jobin Yvon Horiba Fluoromax-3 coupled wth a PTFE-coated integrating sphere (Glen Spectra). The sample material was drop-dried onto a 10 mm diameter quartz substrate and mounted about 20 mm into the sphere from a holder in the entry port facing the excitation light beam. The measured spectra were background corrected by subtracting the spectrum obtained using a blank substrate and subsequently corrected for the wavelength sensitivity of the fluorimeter and spectral response of the sphere. The spectral response of the sphere was determined using a calibrated tungsten lamp (Ocean Optic) and the fluorimeter as detector.[363]

Rheometer. Rheology measurements were conducted on a TA Instruments AR2000 using a parallel plate geometry with 40 mm diameter plates and a gap of 1 mm. A frequency sweep from 0.01 to 100 Hz was carried out in controlled strain mode with a strain amplitude of 5%.

7.2. Purification of SWNTs

Purified SWNTs produced by the HiPco method and supplied by Unidym, USA, were further purified by heating in air at 400 °C, then soaking in 6 M HCl overnight, followed by filtration over a polycarbonate membrane (0.2 μm), and washing with copious amounts of high-purity water until pH-neutral. The purified SWNTs were annealed under vacuum (10^{-2} mbar) at 900 °C to remove residual carboxylic acid functional groups and any adsorbed gases or solvents.

7.3. Synthesis of pyridine functionalised SWNTs

4-aminopyridine and sodium nitrite were purchased from Aldrich and used as received.

SWNT-Pyridine (2). A cooled solution (0 °C) of $NaNO_2$ (0.490 g, 7.10 mmol) dissolved in 0.7 mL of water was added drop wise to 4-aminopyridine (0.658 g, 6.99 mmol) dissolved in 5 mL of HCl (4 M) cooled to 0 °C. The resulting yellow solution was stirred for 30 min and maintained at 0 °C. A cooled solution (0 °C) of purified SWNTs (10 mg) dispersed in *N*,*N*-dimethylformamide (20 mL), using an ultrasonic bath (Ultrawave U50, 30 – 40 kHz) for 5 mins, was then added drop wise. The reaction mixture was held at 0 °C and stirred for 4 h after which time it was allowed to warm to room temperature and stirred for a further 15 h. The SWNTs were filtered through a nylon membrane (0.2 μm, Whatman), re-dispersed in 2 M HCl (100 mL), filtered and washed with copious amount of water until pH neutral. The resulting solid material was dispersed in 2 M NaOH (100 mL) and stirred overnight to ensure deprotonation of the pyridinium salt to pyridine. The functionalised SWNTs were then isolated by filtration through a nylon membrane (0.2 μm, Whatman) and washed with water until pH neutral and re-dispersed and filtered using THF (2 × 30 mL), acetone (2 × 30 mL) and ethanol (2 × 30 mL), respectively and dried overnight at 80 °C to afford SWNT-pyridine (**2**).

7.4. Synthesis of indolizine functionalised SWNTs

Pyridine, ethyl-2-bromoacetate, p-nitrobenzyl bromide, benzylamine, oleum, hydrogen bromide in acetic acid were purchased from Aldrich and used as received.

N-(Ethoxycarbonylmethyl)-pyridinium Bromide (4). The pyridinium salt (**4**) was prepared following a modified literature procedure.[255] Pyridine (100 mmol) was added to ethyl 2-bromoacetate (110 mmol) and the mixture stirred for 12 h at room temperature. The resulting off-white solid was washed with diethyl ether (3 × 20 mL) to remove excess pyridine and ethyl 2-bromoacetate to afford the pyridinium bromide

salt **(4)** (22.64 g, 92%) as confirmed by FTIR, ^{1}H and ^{13}C NMR and mass spectrometry. IR (neat) (ν(C=O) cm^{-1}) : 1737, (ν(C=N) cm^{-1}) 1637, (ν(C=C) cm^{-1}) 1577; ^{1}H NMR (400 MHz, $CDCl_3$,): 9.49-9.55 (d, *J*=6.06 Hz, 2H), 8.62-8.53 (t, *J*=7.81 Hz, 2H), 8.16-8.09 (t, *J*=7.80 Hz, 1H), 6.34 (s, 2H), 4.33-4.25 (q, *J*=7.14 Hz, 2H), 1.35-1.28 (t, *J*=7.05 Hz, 3H); ^{13}C NMR (400MHz, $CDCl_3$): 165.8, 146.7, 146.1, 127.7, 63.4, 61.1, 14.1.

Sodium 4-(bromomethyl)benzenesulfonate. Salt was prepared following the literature procedure (12.6 g, 93 %).[256] IR (ATR) (ν(SO) cm^{-1}) : 1195 (sym); ^{1}H NMR (400 MHz, D_2O,): 7.64-7.72 (d, *J*=8.0 Hz, 2H), 7.44-7.54 (d, *J*=8.0 Hz, 2H), 4.65-4.85 (s, 2H); ^{13}C NMR (400MHz, $CDCl_3$): 142.3, 141.8, 129.6, 126.0, 32.6.

N-(4-methylbenzenesulfonic acid)-pyridinium bromide (5). The pyridinium salt (**5**) was prepared following a modified literature procedure.[255] Pyridine (50 mmol) was added to sodium 4-(bromomethy1)benzenesulfonate (45 mmol) and the mixture stirred for 12 h at room temperature. The resulting off-white solid was washed with diethyl ether (3 × 20 mL), methanol (3 × 20 mL) and acetone (3 × 20 mL) to remove excess pyridine and sodium 4-(bromomethy1)benzenesulfonate to afford the pyridinium bromide salt **(5)** (14.26 g, 90%) as confirmed by FTIR, ^{1}H and ^{13}C NMR and mass spectrometry. IR (ATR) (ν(SO) cm^{-1}) : 1210 (sym); ^{1}H NMR (400 MHz, D_2O,): 8.75-8.88 (d, *J*=5.6 Hz, 2H), 8.42-8.52 (t, *J*=7.6 Hz, 1H), 7.92-8.04 (t, *J*=6.8 Hz, 2H); 7.7-7.8 (d, *J*=8.0 Hz, 2H); 7.4-7.5 (d, *J*=8.4 Hz, 2H); 5.72-5.82 (s, 2H) ^{13}C NMR (400MHz, $CDCl_3$): 146.28, 144.54, 143.71, 135.94, 129.45, 128.55, 126.53, 63.81.

N-(4-nitrobenzyl)-pyridinium bromide (6). The pyridinium salt (**6**) was prepared following a modified literature procedure.[255] Pyridine (50 mmol) was added to *p*-nitrobenzyl bromide (45 mmol) and the mixture stirred for 12 h at room temperature. The resulting off-white solid was washed with diethyl ether (3 × 20 mL), ethanol (3 × 20 mL) and acetone (3 × 20 mL) to remove excess pyridine and *p*-nitrobenzyl bromide to afford the pyridinium bromide salt **(6)** (11.68 g, 88 %) as confirmed by FTIR, ^{1}H and ^{13}C NMR and mass spectrometry. IR (ATR) (ν(NO) cm^{-1}) : 1520 (sym), (ν(NO) cm^{-1}) 1345 (asym); ^{1}H NMR (400 MHz, D_2O,): 8.86-8.96 (d, 2H), 8.52-8.58 (t, 1H), 8.12-8.20 (d, 2H); 8.02-8.10 (d, 2H); 7.52-7.60 (d, 2H); 5.86-5.94 (s, 2H) ^{13}C NMR (400MHz, $CDCl_3$): 148.23, 146.62, 144.79, 139.89, 129.86, 128.77, 124.51, 63.45.

SWNT-Indolizine (Conventional Heating) (7a). SWNTs (10 mg) were dispersed in *N*,*N*-dimethylformamide (15 mL) using mild sonication in an ultrasonic bath (Ultrawave U50, 30-40 kHz) for 5 min and the dispersion heated to 140 °C. The pyridinium salt (**4**) (1.026 g, 4.17 mmol) was then added to the dispersion followed by triethylamine (0.58 mL, 4.17 mmol) after 30 min. The reaction mixture was refluxed for 5 days, and the functionalised SWNTs were collected via filtration through a PTFE membrane (0.2 μm). The solid SWNTs were then transferred to a cellulose thimble, and impurities and unreacted reagents were removed by Soxhlet extraction using acetonitrile for 18 h. The SWNTs were then dispersed in deionized water (50 mL) and filtered through a PTFE membrane (0.2 μm), dispersed in acetone (50 mL) and filtered through a PTFE membrane (0.2 μm), and finally dispersed in ethanol (50 mL) and filtered through a PTFE membrane (0.2 μm) and dried overnight at 120 °C to afford SWNT-indolizine (**7a**).

SWNT-Indolizine (Microwave Heating) (7b). SWNTs (10 mg) were dispersed in *N*,*N*-dimethylformamide (15 mL) using mild sonication in an ultrasonic bath (Ultrawave U50, 30 - 40 kHz) for 5 min. The pyridinium salt **(4)** (1.026 g, 4.17 mmol) and triethylamine (0.58 mL, 4.177 mmol) were then added to the dispersion. The reaction mixture was then heated to 150 °C at 2 bar pressure, in a heat and pressure resistant vessel, with microwaves for 1 h (150 W for 5 min followed by 20 W for 50 min at 2.54 GHz) using a Biotage Initiator Sixty. The SWNTs were washed and isolated as described in conventional heating procedure to afford SWNT-indolizine (**7b**).

SWNT-Indolizine (Microwave Heating) (8). SWNTs (10 mg) were dispersed in *N*,*N*-dimethylformamide (15 mL) using mild sonication in an ultrasonic bath (Ultrawave U50, 30 - 40 kHz) for 5 min. The pyridinium salt **(5)** (1.468 g, 4.17 mmol) and triethylamine (0.58 mL, 4.177 mmol) was then added to the dispersion. The reaction mixture was then heated to 150 °C at 2 bar pressure, in a heat and pressure resistant vessel, with microwaves for 1 h (150 W for 5 min followed by 20 W for 50 min at 2.54 GHz) using a Biotage Initiator Sixty. The functionalised SWNTs were collected via filtration through a PTFE membrane (0.2 μm). The solid SWNTs were then transferred to a cellulose thimble, and impurities and unreacted reagents were removed by Soxhlet extraction using acetonitrile for 18 h. The SWNTs were then dispersed in deionized (50 mL) and filtered through a PTFE membrane (0.2 μm), dispersed in acetone (50 mL) and filtered through a PTFE membrane (0.2 μm), and finally dispersed in ethanol (50 mL) and filtered through a PTFE membrane (0.2 μm) and dried overnight at 120 °C to afford SWNT-indolizine (**8**).

SWNT-Indolizine (Microwave Heating) (9). SWNTs (10 mg) were dispersed in *N*,*N*-dimethylformamide (15 mL) using mild sonication in an ultrasonic bath (Ultrawave U50, 30 - 40 kHz) for 5 min. The pyridinium salt **(6)** (1.230 g, 4.17 mmol) and triethylamine (0.58 mL, 4.177 mmol) was then added to the dispersion. The reaction mixture was then heated to 150 °C at 2 bar pressure, in a heat and pressure resistant vessel, with microwaves for 1 h (150 W for 5 min followed by 20 W for 50 min at 2.54 GHz) using a Biotage Initiator Sixty. The SWNTs were washed and isolated as described in conventional heating procedure to afford SWNT-indolizine (**9**).

Transesterification with decanol (10). Ethoxy groups on indolizine modified SWNTs (**7b**) were converted into the decoxy groups via the addition of excess decanol (0.5 mL) to the dispersion of 3 mg of (**7b**) in DMF (15 mL) followed by overnight stirring at room temperature. The resulting mixture was filtered through the nylon membrane and washed with copious amount of acetone (3 × 40 mL) to afford the decanol modified indolizine-SWNTs (**10**).

Preparation of quaternary salt of indolizine-SWNTs (11). Indolizine modified SWNTs (**7b**) (5 mg in 10 mL DMF) were refluxed with 3 mL of *N*,*N*-dimethylethylenediamine at 100 ^{o}C for 15 h. The mixture was dispersed in acetone (50 mL) and filtered through the nylon membrane (0.2 μm), dispersed in ethanol (50 mL) and filtered through nylon membrane (0.2 μm) and dried at 80 ^{o}C. The resulting amide modified indolizine-SWNTs with tertiary amine groups were stirred with iodomethane (10 mL) for 15 h to afford quaternary ammonium salts of indolizine-SWNTs (**11**). The resulting mixture was filtered through the nylon membrane (0.2 μm) and washed with copious amount of acetone (3 × 40 mL) and dried at room temperature.

SWNT-Pyridinium Ester (13a). To a dispersion of SWNT-Pyridine (**2**) (5 mg) in dry *N*,*N*-dimethylformamide (10 mL), dispersed using an ultrasonic bath (Ultrawave U50, 30 – 40 kHz) for 5 mins, was added ethyl-2-bromoacetate (5 mL, 45.09 mmol) and the reaction mixture stirred at room temperature for 12 hours. The SWNTs were then filtered through a nylon membrane (0.2 μm, Whatman), re-dispersed in acetone (30 mL), filtered and washed with acetone (2 × 30 mL) and dried overnight at 80 °C to afford SWNT-pyridinium ester (**13a**).

SWNT-Pyridinium Ester (13b). To a dispersion of SWNT-Pyridine (**2**) (5 mg) in dry *N*,*N*-dimethylformamide (10 mL), dispersed using an ultrasonic bath (Ultrawave U50, 30 – 40 kHz) for 5 mins, was added p-nitrobenzyl bromide (5.4 g, 25 mmol) and the reaction mixture stirred at room temperature for 12 hours. The SWNTs were then filtered through a nylon membrane (0.2 μm, Whatman), re-dispersed in acetone (30 mL), filtered and washed with THF (2 × 30 mL), acetone (2 × 30 mL) and dried overnight at 80 °C to afford SWNT-pyridinium ester (**13b**).

PEG$_{400}$-yl 2-bromoacetate. PEG$_{400}$-yl 2-bromoacetate was prepared following a literature procedure[285] and characterized using FTIR, ^{1}H and ^{13}C NMR. IR (ATR) (ν(C=O) cm^{-1}) : 1739, (ν(C-H) cm^{-1}) 2870, (ν(H$_2$C-O-CH$_2$) cm^{-1}) 1100; ^{1}H NMR (400 MHz, $CDCl_3$,): 4.2-4.4 (t, $COOCH_2$), 3.8-3.9 (s, CH_2Br), 3.6-3.7 (m, OCH_2CH_2O; ^{13}C NMR (100MHz, $CDCl_3$): 167.8 (COOR), 71.2 (OCH_2CH_2O), 26.1 (CH_2Br).

PEG$_{2000}$-yl 2-bromoacetate. PEG$_{2000}$-yl 2-bromoacetate was prepared following a literature procedure[285] and characterized using FTIR, ^{1}H and ^{13}C NMR. IR (ATR) (ν(C=O) cm^{-1}) : 1745, (ν(C-H) cm^{-1}) 2885, (ν(H$_2$C-O-CH$_2$) cm^{-1}) 1096; ^{1}H NMR

(400 MHz, $CDCl_3$,): 4.3-4.4 (t, $COOCH_2$), 3.8-3.9 (s, CH_2Br), 3.6-3.7 (m, PEG chain protons), 3.4-3.5 (m, CH_2OH), 3.3-3.4 (s, OH; ^{13}C NMR (100MHz, $CDCl_3$): 167.9 (COOR), 71.4 (OCH_2CH_2O), 26.2 (CH_2Br).

SWNT-Pyridinium Ester (13c). To a dispersion of SWNT-Pyridine (**2**) (5 mg) in dry *N*,*N*-dimethylformamide (10 mL), dispersed using an ultrasonic bath (Ultrawave U50, 30 – 40 kHz) for 5 mins, was added PEG_{400}-yl 2-bromoacetate (3.11 g, 5 mmol) and the reaction mixture stirred at room temperature for 12 hours. The SWNTs were then filtered through a nylon membrane (0.2 μm, Whatman), re-dispersed in acetone (30 mL), filtered and washed with THF (2 × 30 mL), acetone (2 × 30 mL), ethanol (2 × 30 mL) and dried overnight at 80 °C to afford SWNT-pyridinium ester (**13c**).

SWNT-Pyridinium Ester (13d). To a dispersion of SWNT-Pyridine (**2**) (5 mg) in dry *N*,*N*-dimethylformamide (10 mL), dispersed using an ultrasonic bath (Ultrawave U50, 30 – 40 kHz) for 5 mins, was added PEG_{2000}-yl 2-bromoacetate (11.1 g, 5 mmol) and the reaction mixture stirred at room temperature for 12 hours. The SWNTs were then filtered through a nylon membrane (0.2 μm, Whatman), re-dispersed in acetone (30 mL), filtered and washed with THF (2 × 30 mL), acetone (2 × 30 mL), ethanol (2 × 30 mL) and dried overnight at 80 °C to afford SWNT-pyridinium ester (**13d**).

SWNT-Indolizine (14a). To a dispersion of SWNT-Pyridinium ester (**13a**) (5 mg) in dry *N*,*N*-dimethylformamide (10 mL), dispersed using an ultrasonic bath (Ultrawave U50, 30 – 40 kHz) for 5 mins, was added dimethyl acetylenedicarboxylate (5 mL, 40.67 mmol). The reaction mixture was stirred at room temperature for 1 h and then triethylamine (1 mL, 7.17 mmol) added and the reaction stirred for a further 5 h at

room temperature and then 15 h at 60°C. The reaction was quenched by the addition of high purity water (50 mL) and the mixture filtered through a PTFE membrane (0.2 μm, Whatman). The SWNTs were re-dispersed and filtered through a PTFE membrane using THF (2 × 30 mL), acetone (2 × 30 mL) and ethanol (2 × 30 mL), respectively to remove any residual organic material and dried overnight at 80 °C to afford SWNT-indolizine (**14a**).

SWNT-Indolizine (14b). SWNT-Pyridinium ester (**13b**) (5 mg) in dry *N*,*N*-dimethylformamide (10 mL) was dispersed using an ultrasonic bath (Ultrawave U50, 30 – 40 kHz) for 10 mins and heated to 80 ^{o}C in an oil bath. Dimethylacetylene dicarboxylate (5 mL, 40.67 mmol) and triethylamine (1 mL, 7.17 mmol) were then added to nanotube dispersion, respectively. The reaction mixture was stirred for 15 h at 80 °C. The reaction was quenched by the addition of high purity water (50 mL) and the mixture filtered through a nylon membrane (0.2 μm, Whatman). The SWNTs were re-dispersed and filtered through a nylon membrane using THF (2 × 30 mL), acetone (2 × 30 mL) and ethanol (2 × 30 mL), respectively to remove any residual organic material and dried overnight at 80 °C to afford SWNT-indolizine (**14b**).

SWNT-Indolizine (17). SWNT-indolizine (**14b**) was reduced using the given literature procedure.[290] The SWNTs were re-dispersed and filtered through a nylon membrane using THF (2 × 30 mL), acetone (2 × 30 mL) and ethanol (2 × 30 mL), respectively to remove any residual organic material and dried overnight at 80 °C to afford SWNT-indolizine (**17**).

SWNT-Indolizine (14c). SWNT-Pyridinium ester (**13c**) (5 mg) in dry *N*,*N*-dimethylformamide (10 mL) was dispersed using an ultrasonic bath (Ultrawave U50, 30 – 40 kHz) for 10 mins and heated to 80 ^{o}C in an oil bath. Dimethylacetylene dicarboxylate (5 mL, 40.67 mmol) and triethylamine (1 mL, 7.17 mmol) were then added to nanotube dispersion, respectively. The reaction mixture was stirred for 15 h at 80 °C. The reaction was quenched by the addition of high purity water (50 mL) and the mixture filtered through a nylon membrane (0.2 μm, Whatman). The SWNTs were re-dispersed and filtered through a nylon membrane using THF (2 × 30 mL), acetone (2 × 30 mL) and ethanol (2 × 30 mL), respectively to remove any residual organic material and dried overnight at 80 °C to afford SWNT-indolizine (**14c**).

SWNT-Indolizine (14d). SWNT-Pyridinium ester (**13d**) (5 mg) in dry *N*,*N*-dimethylformamide (10 mL) was dispersed using an ultrasonic bath (Ultrawave U50, 30 – 40 kHz) for 10 mins and heated to 80 ^{o}C in an oil bath. Dimethylacetylene dicarboxylate (5 mL, 40.67 mmol) and triethylamine (1 mL, 7.17 mmol) were then added to nanotube dispersion, respectively. The reaction mixture was stirred for 15 h at 80 °C. The reaction was quenched by the addition of high purity water (50 mL) and the mixture filtered through a nylon membrane (0.2 μm, Whatman). The SWNTs were re-dispersed and filtered through a nylon membrane using THF (2 × 30 mL), acetone (2 × 30 mL) and ethanol (2 × 30 mL), respectively to remove any residual organic material and dried overnight at 80 °C to afford SWNT-indolizine (**14d**).

3-ethyl 1,2-dimethyl indolizine-1,2,3-tricarboxylate (15a). Pyridine (7.91g, 100 mmol) was added to ethyl bromoacetate (18.37g, 110 mmol) and the mixture stirred for 12 h at room temperature. The resulting off-white solid was washed with diethyl ether (3 x 20 mL) to afford the pyridinium bromide salt N-(ethoxycarbonylmethyl)-

pyridinium bromide (22.64 g, 92%). At room temperature with vigorous stirring, $N(CH_2CH_3)_3$ (0.283g, 2.8 mmol) was added to the pyridinium bromide salt (0.689g, 2.8 mmol) in 10 mL $CHCl_3$ followed by drop wise addition of dimethylacetylene dicarboxylate (DMAD) (0.308g, 2.8 mmol). After solvent removal, the product was eluted with chloroform and crystallized from diethylether. Yield 75% (0.596 g); mp 115.5-116.5 °C; R_f 0.47 ($CHCl_3$); IR (neat, υ(CO) cm^{-1}): 1740, 1708; ^1H NMR (400MHz, $CDCl_3$): 9.47 (d, *J*=7.15 Hz, 1H), 8.26 (d, *J*=9.05 Hz, 1H), 7.31 (m, *J*=8.04 Hz, 1H), 6.97 (m, *J*=7.01 Hz, 1H), 4.30 (q, *J*=7.20 Hz, 2H), 3.92 (s, 3H), 3.82 (s, 3H), 1.32 (t, *J*=7.12 Hz, 3H). ^{13}C NMR (100MHz, $CDCl_3$): 165.2, 162.3, 159.1, 151.3, 136.8, 129.5, 126.9, 125.6, 118.9, 114.3, 101.9, 59.9, 51.7, 50.6, 13.1; *m/z (ES+)*: 305 (M^+, 100 %).

Dimethyl 3-(4-nitrophenyl)indolizine-1,2-dicarboxylate (15b). Pyridine (50 mmol) was added to *p*-nitrobenzyl bromide (45 mmol) and the mixture stirred for 12 h at room temperature. The resulting off-white solid was washed with diethyl ether (3 × 20 mL), ethanol (3 × 20 mL) and acetone (3 × 20 mL) to remove excess pyridine and to *p*-nitrobenzyl bromide to afford the pyridinium bromide salt (11.68 g, 88 %). At reflux temperature with vigorous stirring, $N(CH_2CH_3)_3$ (0.283g, 2.8 mmol) was added to the pyridinium bromide salt (0.826g, 2.8 mmol) in 10 mL $CHCl_3$ followed by drop wise addition of dimethylacetylene dicarboxylate (DMAD) (0.308g, 2.8 mmol). After solvent removal, the product was eluted with EtOAc/hexane (2:1) and crystallized from diethylether. Yield 37% (0.366 g); R_f 0.58 (EtOAc/Hexane); IR (neat, υ(CO) cm^{-1}): 1723, 1702, υ(NO_2) 1505, 1340; ^1H NMR (400MHz, $CDCl_3$): 8.39 (d, *J*=9.16 Hz, 2H), 8.30 (d, *J*=9.06 Hz, 1H), 8.10 (d, *J*=7.12 Hz, 1H), 7.75 (d, *J*=8.93 Hz, 1H), 7.22 (t, *J*=7.94 Hz, 1H), 6.85 (t, *J*=6.87 Hz, 1H), 3.94 (s, 3H), 3.86 (s, 3H). ^{13}C NMR (100MHz, $CDCl_3$): 166.29, 163.83, 147.69, 135.99, 135.91, 130.44, 124.40, 124.30,

123.45, 123.03, 122.25, 120.76, 114.37, 103.08, 52.70, 51.48 ; *m/z (ES+)*: 354 (M^+, 100 %).

Dimethyl 3-(4-aminophenyl)indolizine-1,2-dicarboxylate (16). Dimethyl 3-(4-nitrophenyl)indolizine-1,2-dicarboxylate (**15b**) was reduced into dimethyl 3-(4-aminophenyl)indolizine-1,2-dicarboxylate (**16**) using the given literature procedure.[290] After solvent removal, the product was eluted with EtOAc/hexane (2:1) and crystallized from diethylether. IR (neat, cm^{-1}): υ(NH_2) 3457, 3369 υ(CO) 1726, 1686; ^1H NMR (400MHz, $CDCl_3$): 8.12 (d, *J*=9.17 Hz, 1H), 7.93 (d, *J*=7.16 Hz, 1H), 7.19 (d, *J*=8.5 Hz, 2H), 7.01 (t, *J*=7.89 Hz, 1H), 6.69 (d, *J*=8.48 Hz, 2H), 6.61 (t, *J*=6.79 Hz, 1H), 3.82 (s, 3H), 3.74 (s, 5H). ^{13}C NMR (100MHz, $CDCl_3$): 167.16, 164.38, 147.17, 134.98, 131.20, 125.65, 123.76, 123.32, 121.45, 120.22, 118.23, 115.29, 113.17, 101.48, 52.43, 51.25; *m/z (ES+)*: 324 (M^+, 100 %).

7.5. Sensing properties of indolizine modified SWNTs

Phenol, 2-nitrophenol, 3-nitrophenol, 4-nitrophenol, 2-nitrosotoluene, 4-nitrotoluene and 2,4-dinitrotoluene were purchased from Aldrich and used as received.

General procedure for solution sensing. A stock solution of **14a** and **17** (~1.50 μg/mL, ~1.25 x 10^{-4} M in terms of carbon), (**15a**) and (**16**) (2.09 x 10^{-7} M), and the guest molecules (**19-25**) (1 x 10^{-4} M) were prepared in acetonitrile (CH_3CN) for fluorescence spectral analysis. Each time a 3 mL solution of corresponding indolizine (**14a**, **17**, **15a** or **16**) was filled in a quartz cell of 1cm optical path length, and different stock solutions of guest molecules (**19-25**) were added into quartz cell portion wise (2, 2, 2, 2, 2, 5, 5, 5, 25, 25, 25, 100 μL) using a micropipette. An excitation

wavelength of 330 nm and a temperature of 25 ^{o}C were employed in all experiments. Emission spectra were recorded after each addition.

7.6. Reductive alkylation followed by electrophile addition

N-formylpiperidine, methyl chloroformate, benzyl chloroformate, *n*-butyllithium (1.6 M solution in hexane), sodium borohydride, *N*,*N*-dimethylethylenediamine, FTSC and iodomethane were purchased from Aldrich and used as received.

Butyl modified SWNT reactive intermediate (26). SWNTs (60 mg, 5 mmol) was weighed in a Schlenk flask with a stirring bar and dried overnight in a vacuum oven at 120 ^{o}C. Anhydrous cyclohexane (200 mL) bubbled with argon for 30 min was cannulated under argon to the schlenk flask containing purified SWNTs and sonicated for 15 minutes in an ultrasonic bath (Ultrawave U50, 30 – 40 kHz). To this dispersion *n*-butyllithium (25 mmol) (1.6 M solution in hexanes, Aldrich) was added dropwise over a 30 min period. The resulting dispersion was then stirred for 30 min at room temperature followed by 30 min sonication in an ultrasonic bath (Ultrawave U50, 30 – 40 kHz) and left for stirring 2 days at room temperature. The homogeneous stable black dispersion was cannulated into four different vacuum dried and argon purged schlenk flasks that contain 50 mL of stable reactive intermediate (*n*-Bu$_n$SWNT^{n-}) (**26**).

Butyl modified SWNTs (27). The butyl modified SWNTs (**27**) were prepared following a modified literature procedure.[131] Stable dispersion of SWNT reactive intermediate (**26**) was quenched by air for 5h and diluted with HCl (0.5 M, 100 mL) to dissolve the excess metal salts. Resulting heterogeneous mixture was stirred for 1 h and filtered through a nylon membrane (0.2 μm, Whatman), re-dispersed in 0.5 M HCl (100 mL), filtered and washed with copious amount of water until pH neutral. The

functionalised SWNTs were than re-dispersed and filtered using ethanol (2 x 30 mL), acetonitrile (2 x 30 mL), THF (2 x 30 mL) and acetone (2 x 30 mL), respectively and dried overnight at 80 ^{o}C to afford butyl modified SWNTs (**27**).

Butyl-formyl modified SWNTs (28). 4 mL of *N*-formylpiperidine (3.6 mmol) distilled under argon was cannulated to the stable dispersion of SWNT reactive intermediate (**26**) under argon atmosphere and the resulting mixture was stirred overnight at room temperature. 100 mL dilute HCl (0.5 M) was then added to the dispersion to dissolve the excess metal salts. Resulting heterogeneous mixture was stirred for 1 h and filtered through a nylon membrane (0.2 μm, Whatman), re-dispersed in 0.5 M HCl (100 mL), filtered and washed with copious amount of water until pH neutral. The functionalised SWNTs were than re-dispersed and filtered using ethanol (2 x 30 mL), acetonitrile (2 x 30 mL), THF (2 x 30 mL) and acetone (2 x 30 mL), respectively and dried overnight at 80 ^{o}C to afford butyl-formyl modified SWNTs (**28**).

Butyl-benzyl formyl modified SWNTs (29). Benzyl chloroformate (5.2 mL, 3.6 mmol) distilled under argon was cannulated to the stable dispersion of SWNT reactive intermediate (**26**) under argon atmosphere and the resulting mixture was stirred overnight at room temperature. 100 mL dilute HCl (0.5 M) was then added to the dispersion to dissolve the excess metal salts. Resulting heterogeneous mixture was stirred for 1 h and filtered through a nylon membrane (0.2 μm, Whatman), re-dispersed in 0.5 M HCl (100 mL), filtered and washed with copious amount of water until pH neutral. The functionalised SWNTs were than re-dispersed and filtered using ethanol (2 x 30 mL), acetonitrile (2 x 30 mL), THF (2 x 30 mL) and acetone (2 x 30 mL),

respectively and dried overnight at 80 ^{o}C to afford butyl-benzyl formyl modified SWNTs (**29**).

Butyl-methyl formyl modified SWNTs (30). Methyl chloroformate (2.8 mL, 3.6 mmol) distilled under argon was cannulated to the stable dispersion of SWNT reactive intermediate (**26**) under argon atmosphere and the resulting mixture was stirred overnight at room temperature. 100 mL dilute HCl (0.5 M) was then added to the dispersion to dissolve the excess metal salts. Resulting heterogeneous mixture was stirred for 1 h and filtered through a nylon membrane (0.2 μm, Whatman), re-dispersed in 0.5 M HCl (100 mL), filtered and washed with copious amount of water until pH neutral. The functionalised SWNTs were than re-dispersed and filtered using ethanol (2 x 30 mL), acetonitrile (2 x 30 mL), THF (2 x 30 mL) and acetone (2 x 30 mL), respectively and dried overnight at 80 ^{o}C to afford butyl-methyl formyl modified SWNTs (**30**).

FTSC-dyed butyl-formyl modified SWNTs (31). The FTSC tagging was performed following a modified literature procedure.[373] Butyl-formyl modified SWNTs (**28**) (3 mg, 0.25 mmol) was dispersed in dry DMF (10 mL) using an ultrasonic bath (Ultrawave U50, 30 – 40 kHz) for 10 min under nitrogen. FTSC (4.2 mg, 0.01 mmol) dissolved in dry DMF (10 mL) was then cannulated to the SWNT dispersion at room temperature. HCl (1 μL, 12.06 M) was added as catalyst and mixture was stirred overnight at room temperature. The resulting SWNT dispersion was filtered through a nylon membrane (0.2 μm, Whatman) and briefly washed with DMF (50 mL), re-dispersed in DMF (15 mL) and treated with $NaBH_4$ (0.125 mmol) for 4 h. FTSC-dyed butyl-formyl modified SWNTs were filtered through a nylon membrane and washed with DMF (50 mL) and acetone (50 mL). Resulting solid was dispersed in

acetonitrile, transferred to a cellulose extraction thimble and extracted with a soxhlet apparatus overnight. Extracted solid modified SWNTs were dispersed in acetonitrile and filtered through a nylon membrane. The functionalised SWNTs were then re-dispersed and filtered using water (2 x 30 mL), ethanol (2 x 30 mL), THF (2 x 30 mL) and acetone (2 x 30 mL), respectively and dried overnight at 80 ^{o}C to afford FTSC-dyed butyl-formyl modified SWNTs (**31**).

Control experiment for FTSC-dyed butyl-formyl modified SWNTs. Butyl modified SWNTs (**27**) (3 mg, 0.25 mmol) was dispersed in dry DMF (10 mL) using an ultrasonic bath (Ultrawave U50, 30 – 40 kHz) for 10 min under nitrogen. FTSC (4.2 mg, 0.01 mmol) dissolved in dry DMF (10 mL) was then cannulated to the SWNT dispersion at room temperature. HCl (1 μL, 12.06 M) was added as catalyst and mixture was stirred overnight at room temperature. The resulting SWNT dispersion was filtered through a nylon membrane (0.2 μm, Whatman) and briefly washed with DMF (50 mL), re-dispersed in DMF (15 mL) and treated with $NaBH_4$ (0.125 mmol) for 4 h. Black dispersion was filtered through a nylon membrane and washed with DMF (50 mL) and acetone (50 mL). Resulting solid was dispersed in acetonitrile, transferred to a cellulose extraction thimble and extracted with a soxhlet apparatus overnight. Extracted solid modified SWNTs were dispersed in acetonitrile and filtered through a nylon membrane. Resulting solid SWNTs were then re-dispersed and filtered using water (2 x 30 mL), ethanol (2 x 30 mL), THF (2 x 30 mL) and acetone (2 x 30 mL), respectively and dried overnight at 80 ^{o}C to afford control product.

Tagging of formyl groups for AFM visualization (32). Butyl-formyl modified SWNTs (**28**) (3 mg, 0.25 mmol) was dispersed in dry DMF (10 mL) using an ultrasonic bath (Ultrawave U50, 30 – 40 kHz) for 10 min under nitrogen. *N*,*N*-

dimethylethylenediamine (200 μL, 1.85 mmol) and HCl (3 μL, 12.06 M) were added to the SWNT dispersion at room temperature and dispersion was stirred overnight under nitrogen at room temperature. The resulting SWNT dispersion was filtered through a nylon membrane (0.2 μm, Whatman) and briefly washed with ethanol (50 mL), vacuum dried, re-dispersed in DMF (15 mL) and treated with ($NaBH_4$) (5.3 mmol, 0.2 g) for 4 h. SWNT mixture was filtered through a nylon membrane and washed with ethanol (50 mL). The functionalised SWNTs were then re-dispersed and filtered using water (2 x 30 mL), ethanol (2 x 30 mL), THF (2 x 30 mL) and acetone (2 x 30 mL), respectively and dried overnight at 80 ^{o}C to afford terminal tertiary amine functionalised SWNTs. Modified SWNTs was then dispersed in iodomethane, stirred overnight at room temperature, diluted with acetone, filtered through a nylon membrane and washed with acetone to yield positively charged quaternarized ammonium salt of butyl-formyl modified SWNTs which interacts with gold colloids to produced gold decorated modified nanotubes (**32**).

Control experiment for tagging of formyl groups for AFM visualization. Butyl modified SWNTs (**27**) (3 mg, 0.25 mmol) was dispersed in dry DMF (10 mL) using an ultrasonic bath (Ultrawave U50, 30 – 40 kHz) for 10 min under nitrogen. *N*,*N*-dimethylethylenediamine (200 μL, 1.85 mmol) and HCl (3 μL, 12.06 M) were added to the SWNT dispersion at room temperature and dispersion was stirred overnight under nitrogen at room temperature. The resulting SWNT dispersion was filtered through a nylon membrane (0.2 μm, Whatman) and briefly washed with ethanol (50 mL), vacuum dried, re-dispersed in DMF (15 mL) and treated with ($NaBH_4$) (5.3 mmol, 0.2 g) for 4 h. SWNT mixture was filtered through a nylon membrane and washed with ethanol (50 mL). The functionalised SWNTs were then re-dispersed and filtered using water (2 x 30 mL), ethanol (2 x 30 mL), THF (2 x 30 mL) and acetone (2

x 30 mL), respectively and dried overnight at 80 ^{o}C. Modified SWNTs was then dispersed in iodomethane, stirred overnight at room temperature, diluted with acetone , filtered through a nylon membrane and washed with acetone to use as a control sample.

Tagging of methyl formyl groups for AFM visualization (33). Butyl-methyl formyl modified SWNTs (**30**) (3 mg, 0.25 mmol) was dispersed in dry DMF (10 mL) using an ultrasonic bath (Ultrawave U50, 30 – 40 kHz) for 10 min under nitrogen. *N*,*N*-dimethylethylenediamine (2 mL, 18.5 mmol) was added to the SWNT dispersion at room temperature. Dispersion was heated to 100 ^{o}C and stirred for 15 h under nitrogen to produce amide linkages. The resulting SWNT dispersion was filtered through a nylon membrane (0.2 μm, Whatman) and washed with ethanol (50 mL). The functionalised SWNTs were then re-dispersed and filtered using water (2 x 30 mL), ethanol (2 x 30 mL), THF (2 x 30 mL) and acetone (2 x 30 mL), respectively and dried overnight at 80 ^{o}C to afford terminal tertiary amine functionalised SWNTs. Modified SWNTs was then dispersed in iodomethane, stirred for 15 h at room temperature, diluted with acetone, filtered through a nylon membrane and washed with acetone to yield positively charged quaternarized ammonium salt of butyl-methyl formyl modified SWNTs which interacts with gold colloids to produced gold decorated modified nanotubes (**33**).

Control experiment for tagging of methyl formyl groups for AFM visualization. Butyl modified SWNTs (**27**) (3 mg, 0.25 mmol) was dispersed in dry DMF (10 mL) using an ultrasonic bath (Ultrawave U50, 30 – 40 kHz) for 10 min under nitrogen. *N*,*N*-dimethylethylenediamine (2 mL, 18.5 mmol) was added to the SWNT dispersion at room temperature. Dispersion was heated to 100 ^{o}C and stirred for 15 h under

nitrogen to produce amide linkages. The resulting SWNT dispersion was filtered through a nylon membrane (0.2 μm, Whatman) and washed with ethanol (50 mL). The functionalised SWNTs were then re-dispersed and filtered using water (2 x 30 mL), ethanol (2 x 30 mL), THF (2 x 30 mL) and acetone (2 x 30 mL), respectively and dried overnight at 80 ^{o}C. Modified SWNTs was then dispersed in iodomethane, stirred for 15 h at room temperature, diluted with acetone, filtered through a nylon membrane and washed with acetone to use as a control sample.

Appendix A : Additional information of Chapter III

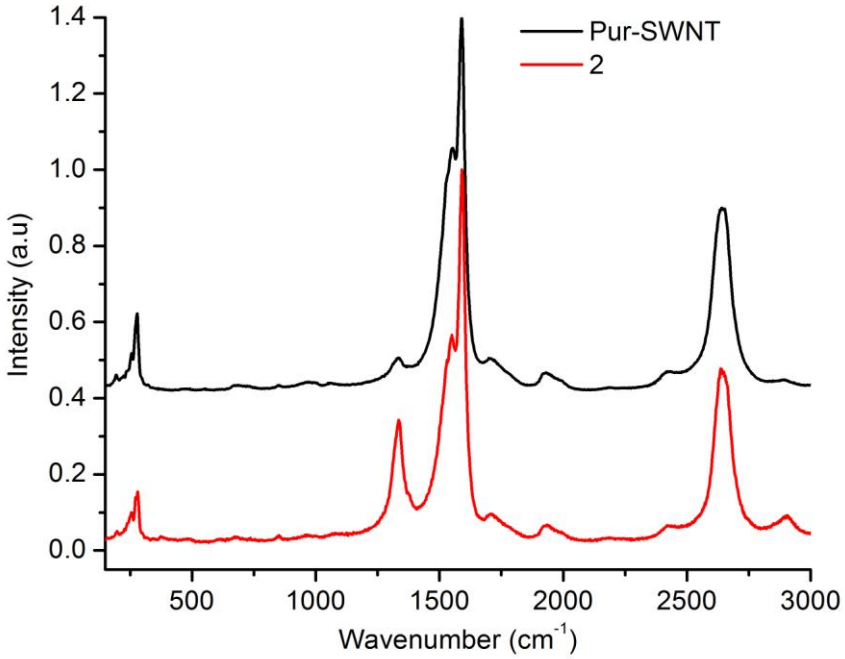

Figure A1 Raman spectra (532 nm, 2.33 eV) of purified SWNTs (black) and pyridine functionalised SWNTs (**2**) (red) normalized at the G-band.

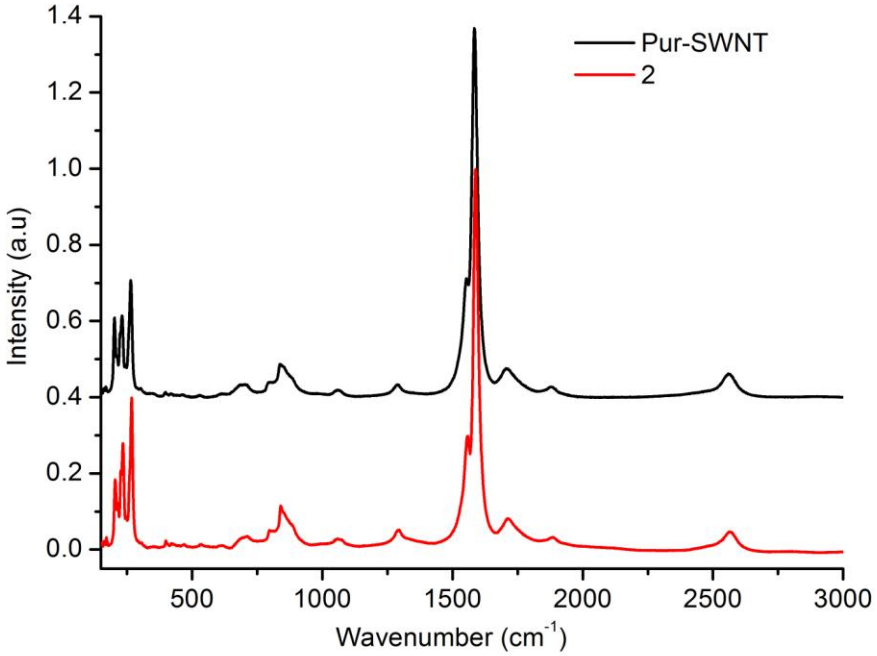

Figure A2 Raman spectra (785 nm, 1.58 eV) of purified SWNTs (black) and pyridine functionalised SWNTs (**2**) (red) normalized at the G-band.

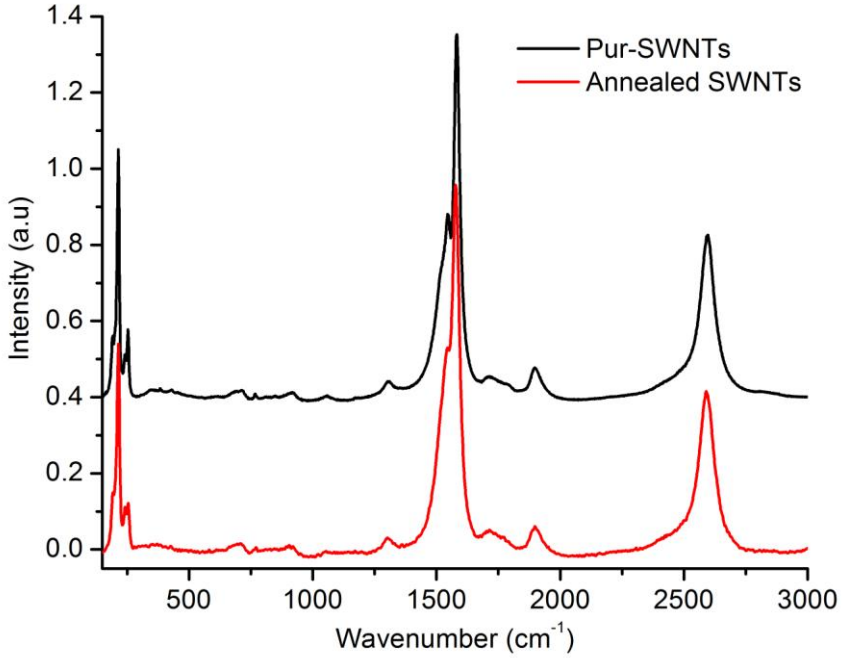

Figure A3 Raman spectra (632.8 nm, 1.96 eV) of purified SWNTs (black) and annealed pyridine functionalised SWNTs (red) normalized at the G-band.

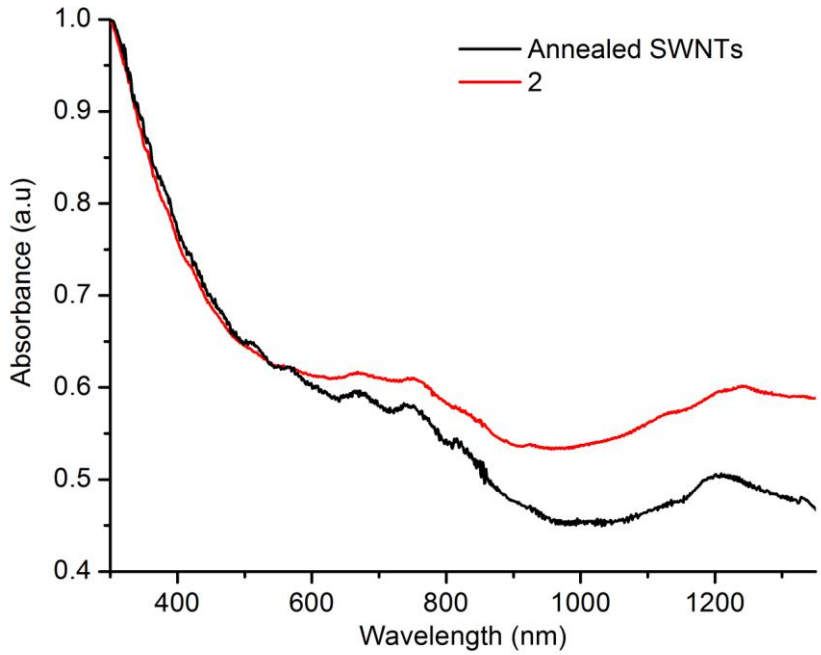

Figure A4 Normalized (at 300 nm) UV-vis-NIR spectra of annealed pyridine functionalised SWNTs at 900 ^{o}C (black) and pyridine functionalised SWNTs (**2**) (red) recorded in *N*,*N*-dimethylformamide.

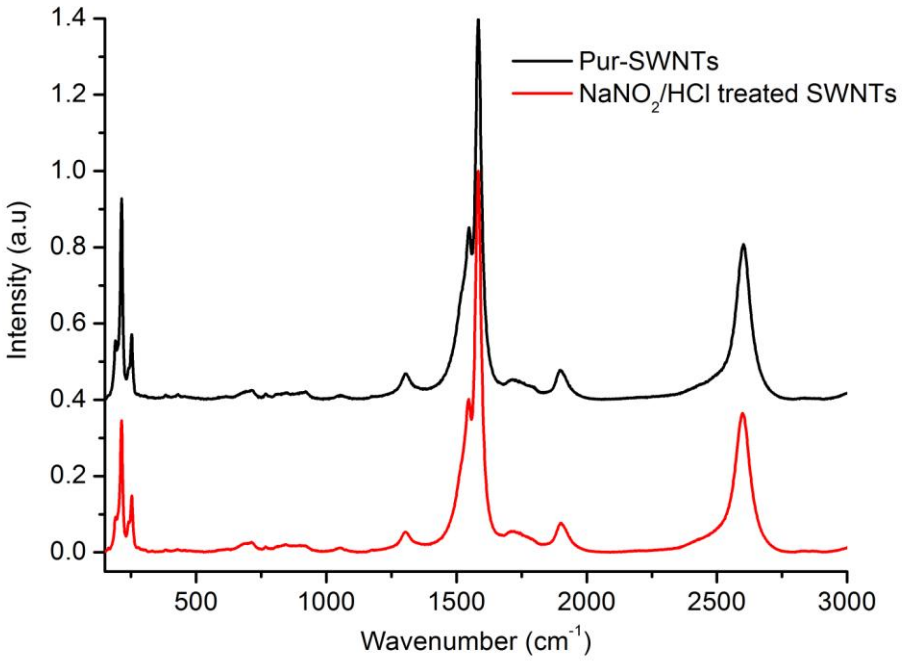

Figure A5 Offset Raman spectra (632.8 nm, 1.96 eV) of purified SWNTs (black) and $NaNO_2$/HCl treated SWNTs (red) normalized at the G-band.

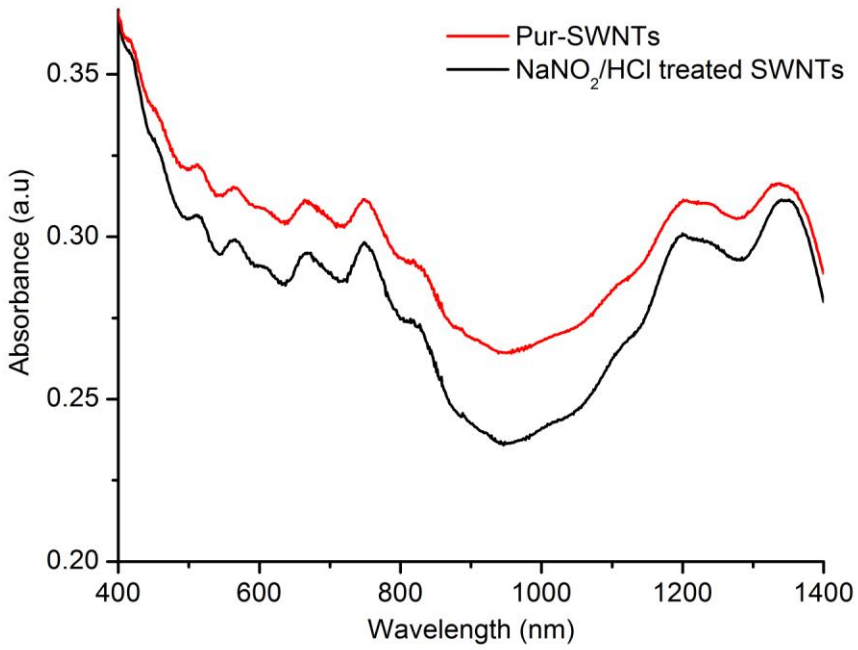

Figure A6 Normalized (at 400 nm) UV-vis-NIR spectra of purified SWNTs (black) and $NaNO_2$/HCl treated SWNTs (red) recorded in *N*,*N*-dimethylformamide.

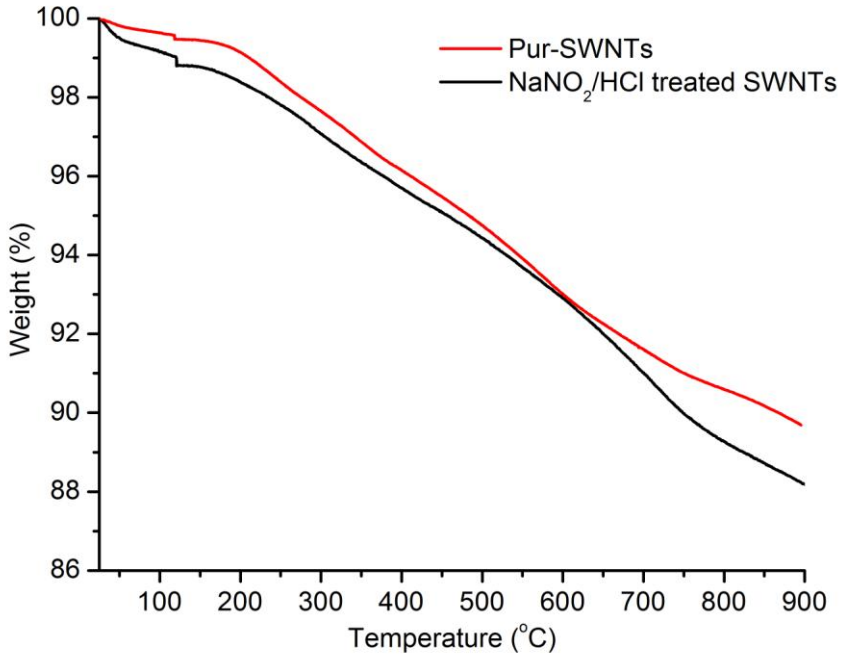

Figure A7 TGA plot (10 °C min^{-1}) of purified SWNTs (black) and $NaNO_2$/HCl treated SWNTs (red).

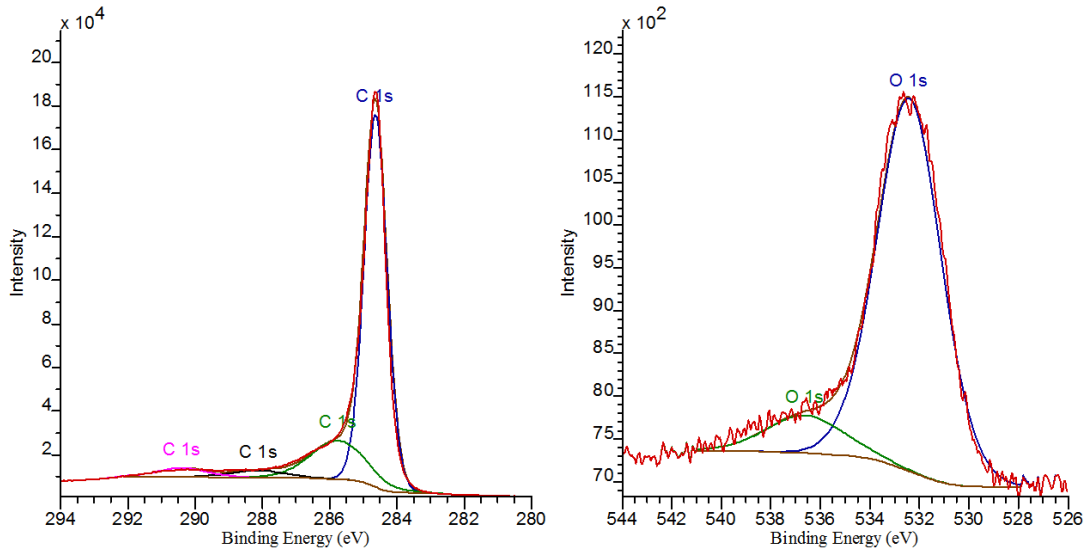

Figure A8 Left: C1s XPS spectrum of the purified SWNTs with four components *ca.* 284.6 (blue), 285.7 (green), 288.1 (black) and 290.3 (magenta) eV; Right: O1s XPS spectrum of the purified SWNTs with two components *ca.* 532.4 (blue) and 536.4 (green) eV.

Appendix B : Additional information of Chapter IV

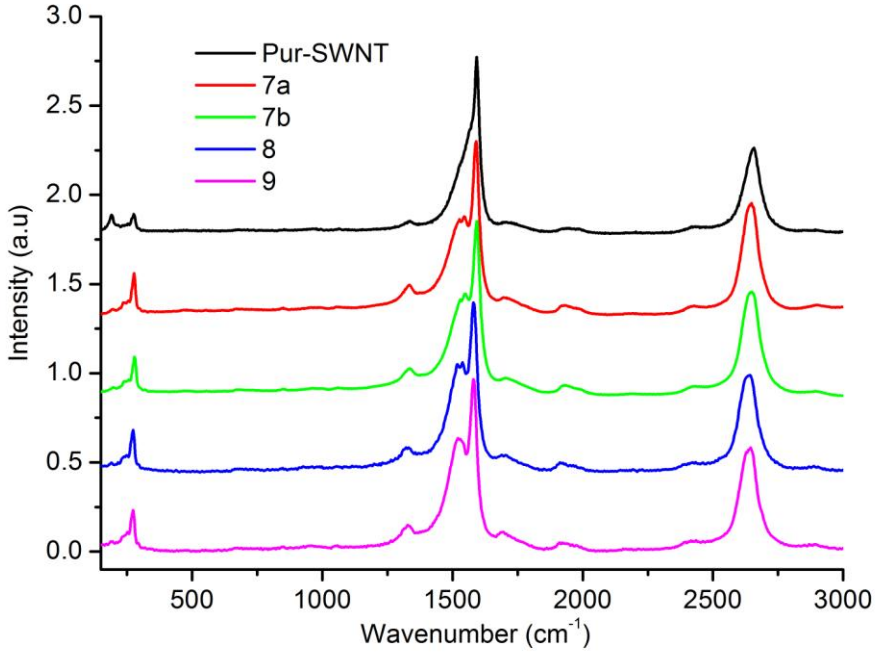

Figure B1 Raman spectra (532 nm, 2.33 eV) of purified SWNTs (black), indolizine functionalised SWNTs (**7a**) prepared by conventional heating using *N*-(ethoxycarbonylmethyl)-pyridinium bromide (**4**) (red) and indolizine functionalised SWNTs (**7b**) prepared by microwave heating using *N*-(ethoxycarbonylmethyl)-pyridinium bromide (**4**) (green), indolizine functionalised SWNTs (**8**) prepared by microwave heating using *N*-(4-methyl sodium benzenesulfonate)-pyridinium bromide (**5**) (blue) and indolizine functionalised SWNTs (**9**) prepared by microwave heating using *N*-(4-nitrobenzyl)-pyridinium bromide (**6**) (magenta) normalised at the G-band.

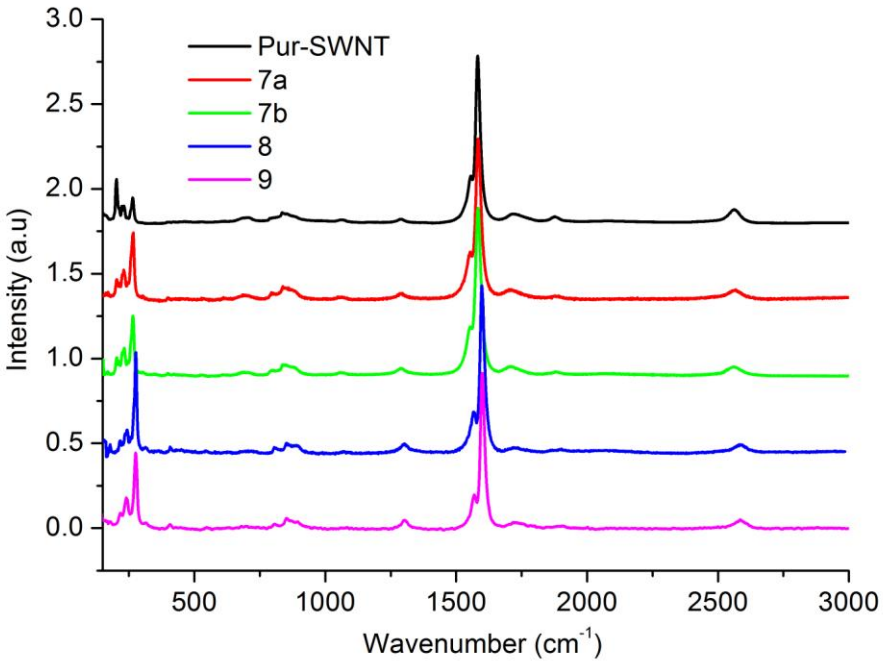

Figure B2 Raman spectra (785 nm, 1.58 eV) of purified SWNTs (black), indolizine functionalised SWNTs (**7a**) prepared by conventional heating using *N*-(ethoxycarbonylmethyl)-pyridinium bromide (**4**) (red) and indolizine functionalised SWNTs (**7b**) prepared by microwave heating using *N*-(ethoxycarbonylmethyl)-pyridinium bromide (**4**) (green), indolizine functionalised SWNTs (**8**) prepared by microwave heating using *N*-(4-methyl sodium benzenesulfonate)-pyridinium bromide (**5**) (blue) and indolizine functionalised SWNTs (**9**) prepared by microwave heating using *N*-(4-nitrobenzyl)-pyridinium bromide (**6**) (magenta) normalised at the G-band.

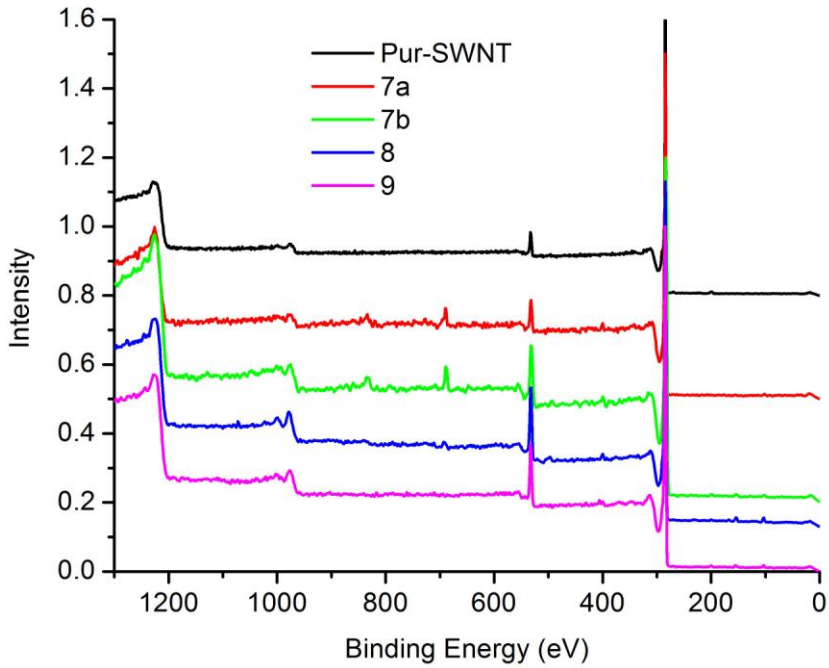

Figure B3 Normalised and offset XPS survey spectra of purified SWNTs (black), indolizine functionalised SWNTs (**7a**) prepared by conventional heating using *N*-(ethoxycarbonylmethyl)-pyridinium bromide (**4**) (red) and indolizine functionalised SWNTs (**7b**) prepared by microwave heating using *N*-(ethoxycarbonylmethyl)-pyridinium bromide (**4**) (green), indolizine functionalised SWNTs (**8**) prepared by microwave heating using *N*-(4-methyl sodium benzenesulfonate)-pyridinium bromide (**5**) (blue) and indolizine functionalised SWNTs (**9**) prepared by microwave heating using *N*-(4-nitrobenzyl)-pyridinium bromide (**6**) (magenta) normalised at the G-band.

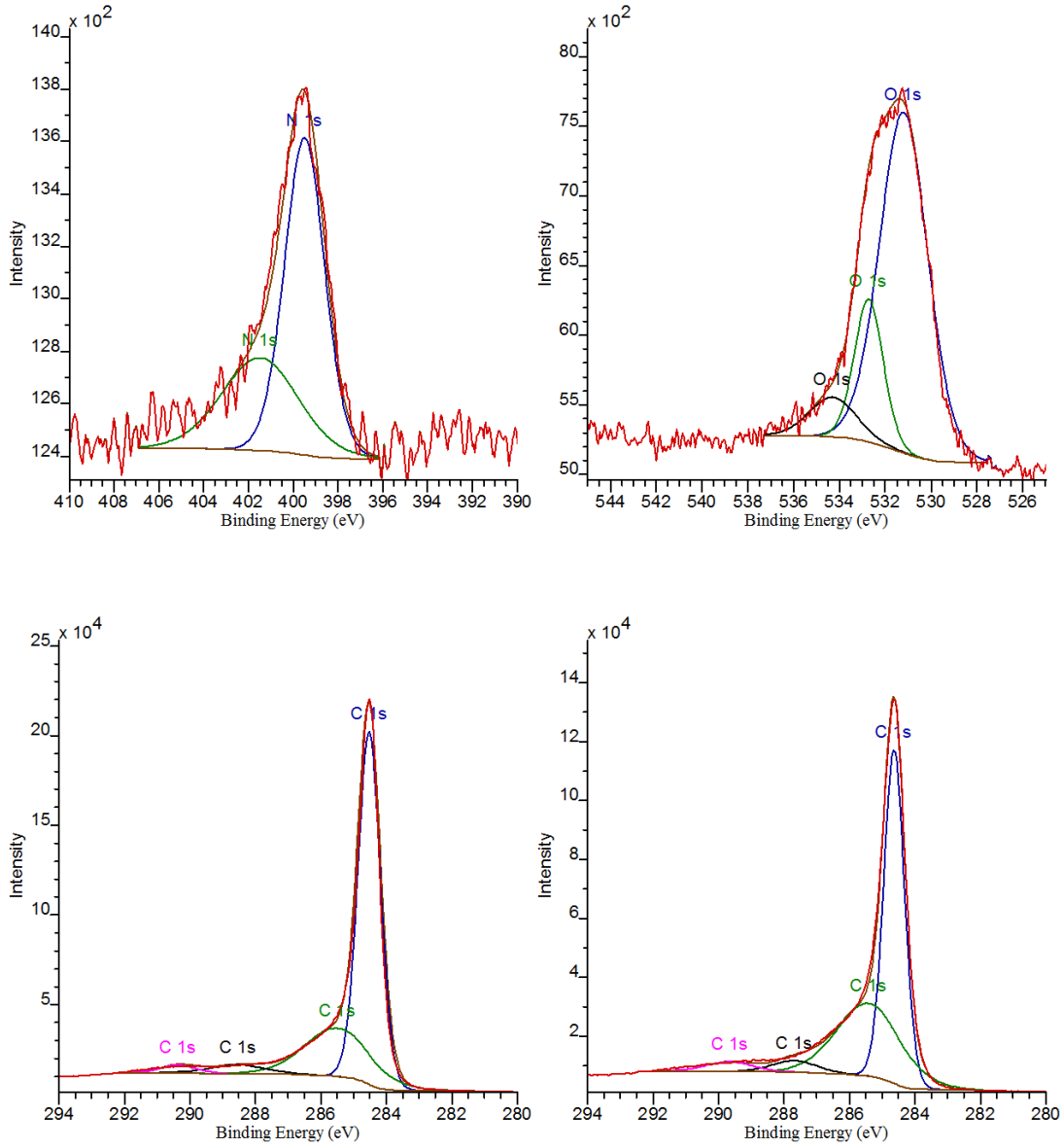

Figure B4 Left: N1s XPS spectrum of the indolizine modified SWNTs (**7a**) with two components *ca.* 399.4 (blue) and 401.4 (green) eV; Right: O1s XPS spectrum of the indolizine modified SWNTs (**7a**) with three components 531.2 (blue), 532.7 (green) and 534.3 (black) eV; Bottom Left: C1s XPS spectrum of the indolizine modified SWNTs (**7a**) with four components *ca.* 284.5 (blue), 285.5 (green), 288.5 (black) and 290.3 (magenta) eV; Bottom Right: C1s XPS spectrum of the indolizine modified SWNTs (**7b**) with four components *ca.* 284.6 (blue), 285.4 (green), 287.6 (black) and 289.6 (magenta) eV .

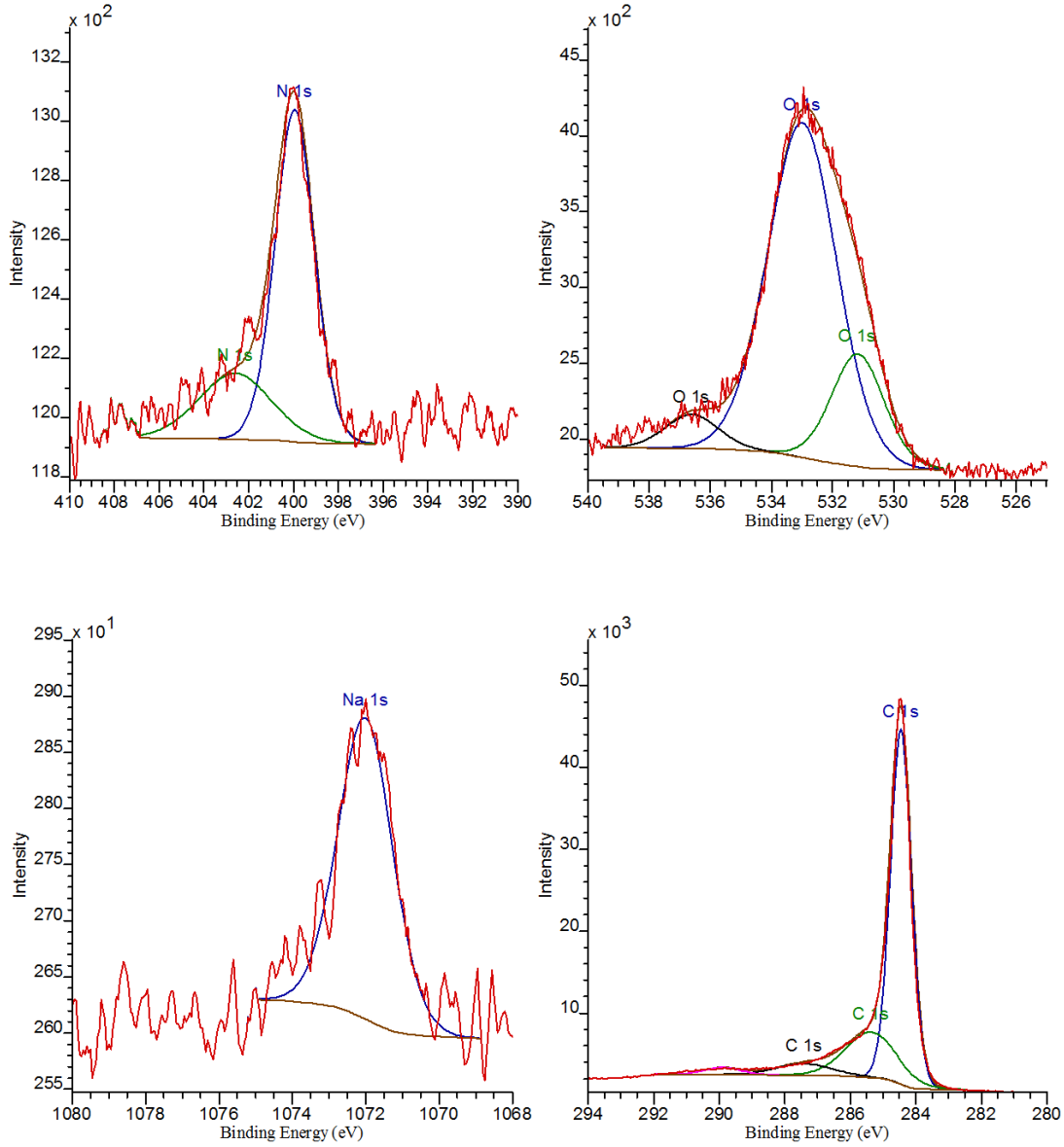

Figure B5 Top Left: N1s XPS spectrum of the indolizine modified SWNTs (**8**) with two components *ca.* 399.9 (blue) and 402.4 (green) eV; Top Right: O1s XPS spectrum of the indolizine modified SWNTs (**8**) with three components *ca.* 531.2 (green), 532.9 (blue) and 536.6 (black) eV; Bottom Left: Na1s XPS spectrum of the indolizine modified SWNTs (**8**) with one component *ca.* 1072 (blue) eV; Bottom Right: C1s XPS spectrum of the indolizine modified SWNTs (**8**) with four components *ca.* 284.5 (blue), 285.4 (green), 287.4 (black) and 289.9 (magenta) eV.

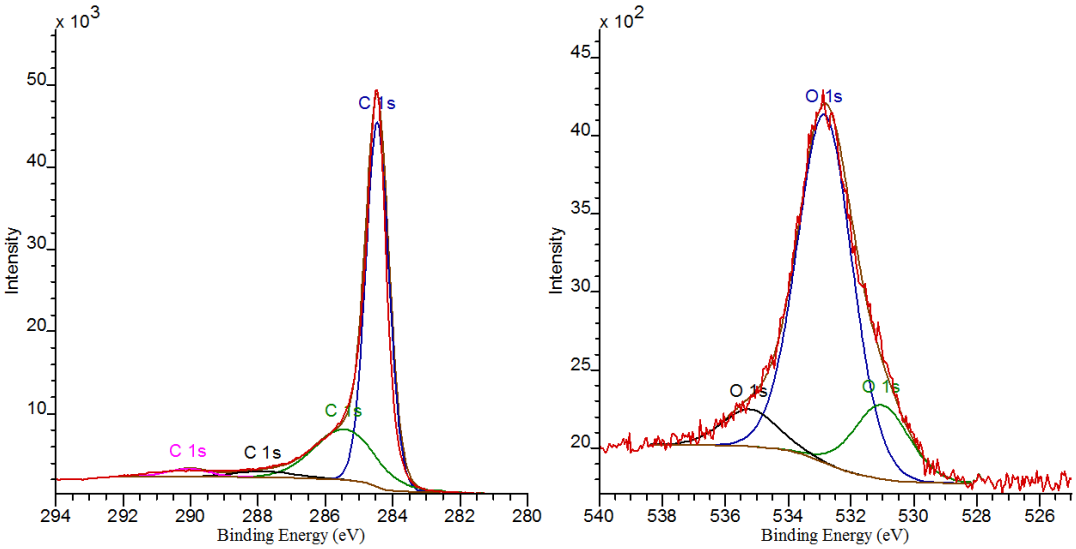

Figure B6 Left: C1s XPS spectrum of the indolizine modified SWNTs (**9**) with four components *ca.* 284.5 (blue), 285.4 (green), 287.8 (black) and 290.0 (magenta) eV; Right: O1s XPS spectrum of the indolizine modified SWNTs (**9**) with three components *ca.* 531.0 (green), 532.8 (blue) and 535.2 (black) eV.

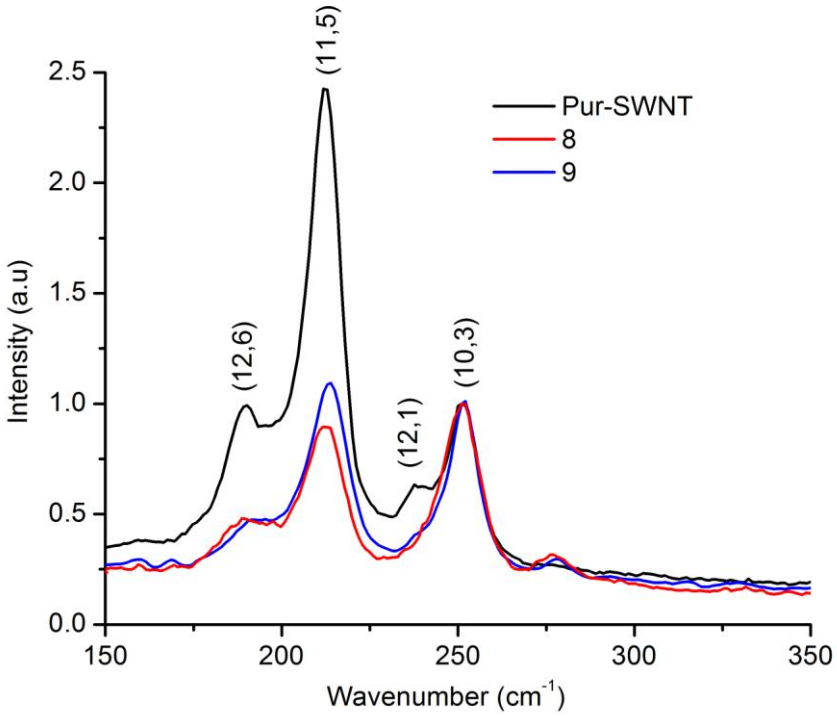

Figure B7 RBM region of the Raman spectra (632.8 nm, 1.96 eV) of purified SWNTs (black), indolizine functionalised SWNTs (**8**) prepared by microwave heating using *N*-(4-methyl sodium benzenesulfonate)-pyridinium bromide (**5**) (red) and indolizine functionalised SWNTs (**9**) prepared by microwave heating using *N*-(4-nitrobenzyl)-pyridinium bromide (**6**) (blue) normalized at 251 cm^{-1}.

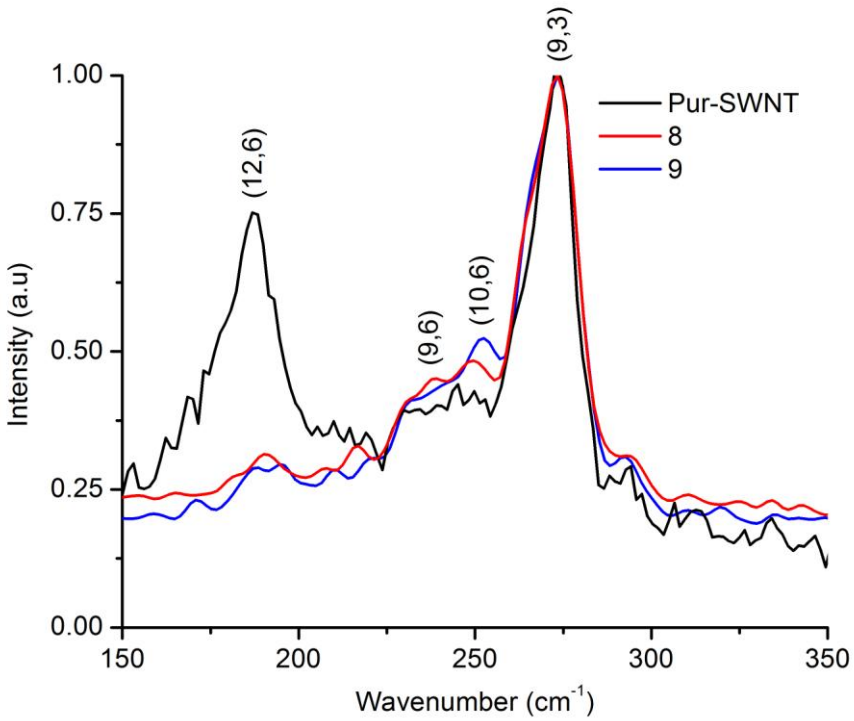

Figure B8 RBM region of the Raman spectra (532 nm, 2.33 eV) of purified SWNTs (black), indolizine functionalised SWNTs (**8**) prepared by microwave heating using *N*-(4-methyl sodium benzenesulfonate)-pyridinium bromide (**5**) (red) and indolizine functionalised SWNTs (**9**) prepared by microwave heating using *N*-(4-nitrobenzyl)-pyridinium bromide (**6**) (blue) normalized at 273 cm^{-1}.

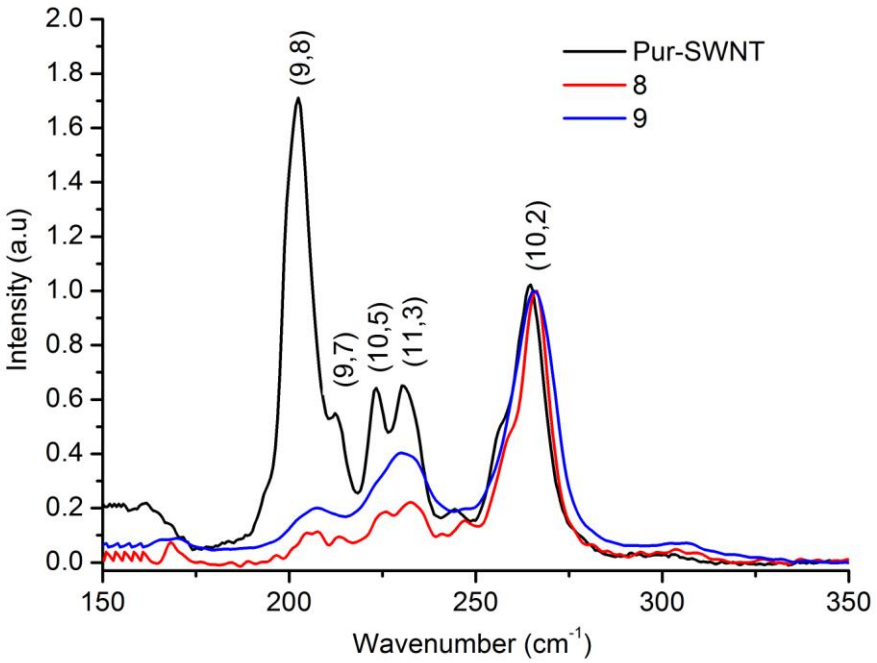

Figure B9 RBM region of the Raman spectra (785 nm, 1.58 eV) of purified SWNTs (black), indolizine functionalised SWNTs (**8**) prepared by microwave heating using *N*-(4-methyl sodium benzenesulfonate)-pyridinium bromide (**5**) (red) and indolizine functionalised SWNTs (**9**) prepared by microwave heating using *N*-(4-nitrobenzyl)-pyridinium bromide (**6**) (blue) normalized at 265 cm^{-1}.

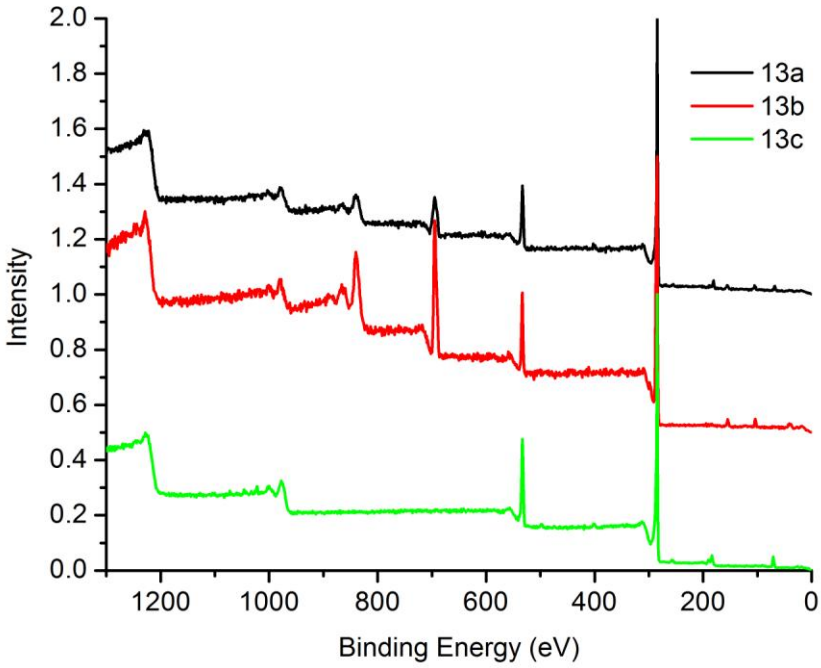

Figure B10 Normalized and offset XPS survey spectra of the pyridinium salt functionalised SWNTs (**13a**) prepared by ethyl-2-bromoacetate (black), pyridinium salt functionalised SWNTs (**13b**) prepared by p-nitrobenzylbromide (red) and pyridinium salt functionalised SWNTs (**13c**) prepared by PEG_{400}-yl 2-bromoacetate (green).

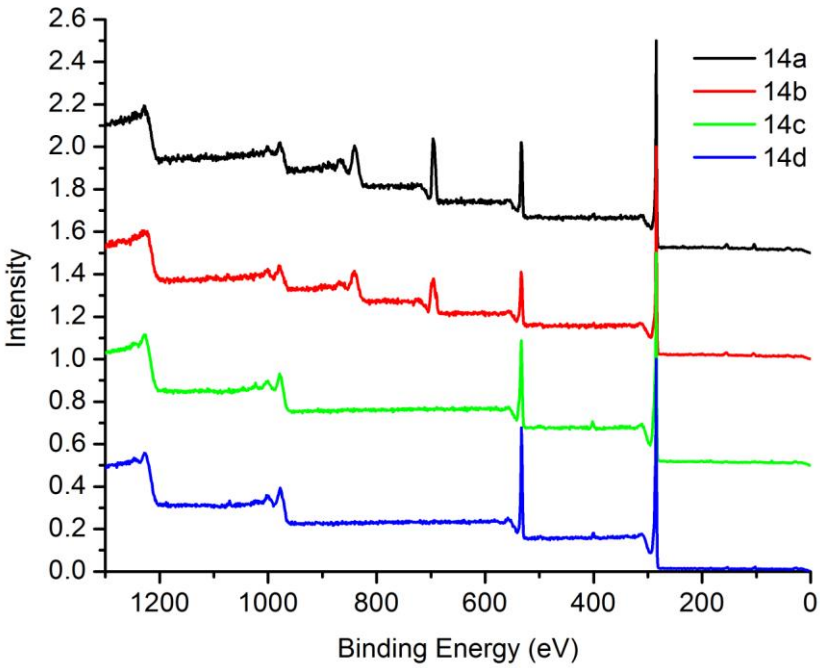

Figure B11 Normalized and offset XPS survey spectra of the indolizine functionalised SWNTs (**14a**) prepared by ethyl-2-bromoacetate (black), indolizine functionalised SWNTs (**14b**) prepared by p-nitrobenzylbromide (red), indolizine functionalised SWNTs (**14c**) prepared by PEG_{400}-yl 2-bromoacetate (green) and indolizine functionalised SWNTs (**14d**) prepared by PEG_{2000}-yl 2-bromoacetate (blue).

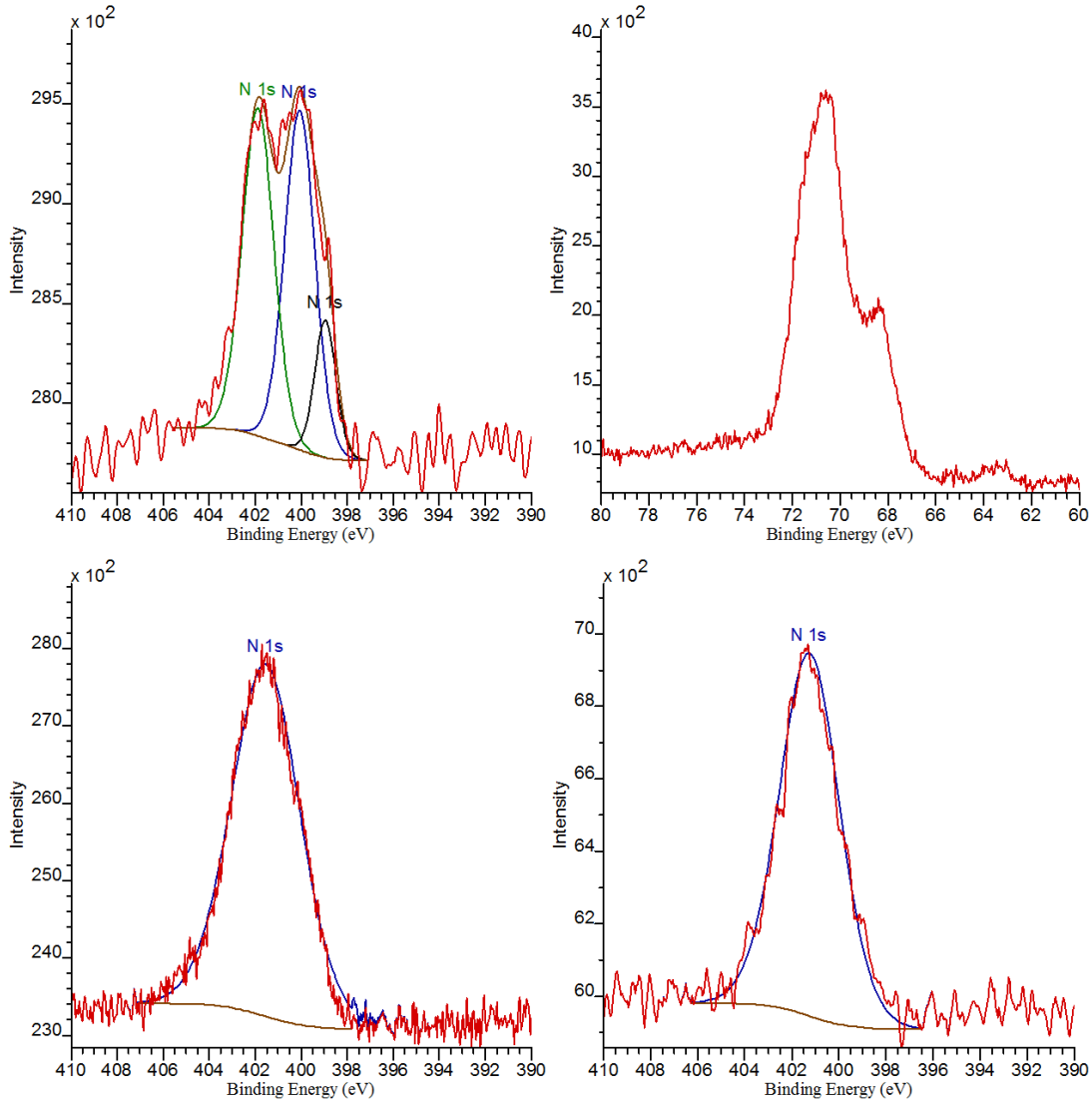

Figure B12 Top Left: N1s XPS spectrum of the pyridinium salt modified SWNTs (**13c**) prepared by PEG_{400}-yl 2-bromoacetate with three components *ca.* 398.9 (black), 400.4 (blue) and 401.9 (green) eV; Top Right: Br3d XPS spectrum of the pyridinium salt modified SWNTs (**13c**) prepared by PEG_{400}-yl 2-bromoacetate *ca.* 68.2-70.7 eV; Bottom Left: N1s XPS spectrum of the indolizine modified SWNTs (**14c**) prepared by PEG_{400}-yl 2-bromoacetate with one component *ca.* 401.5 (blue) eV; Bottom Right: N1s XPS spectrum of the indolizine modified SWNTs (**14d**) prepared by PEG_{2000}-yl 2-bromoacetate with one component *ca.* 401.2 (blue) eV.

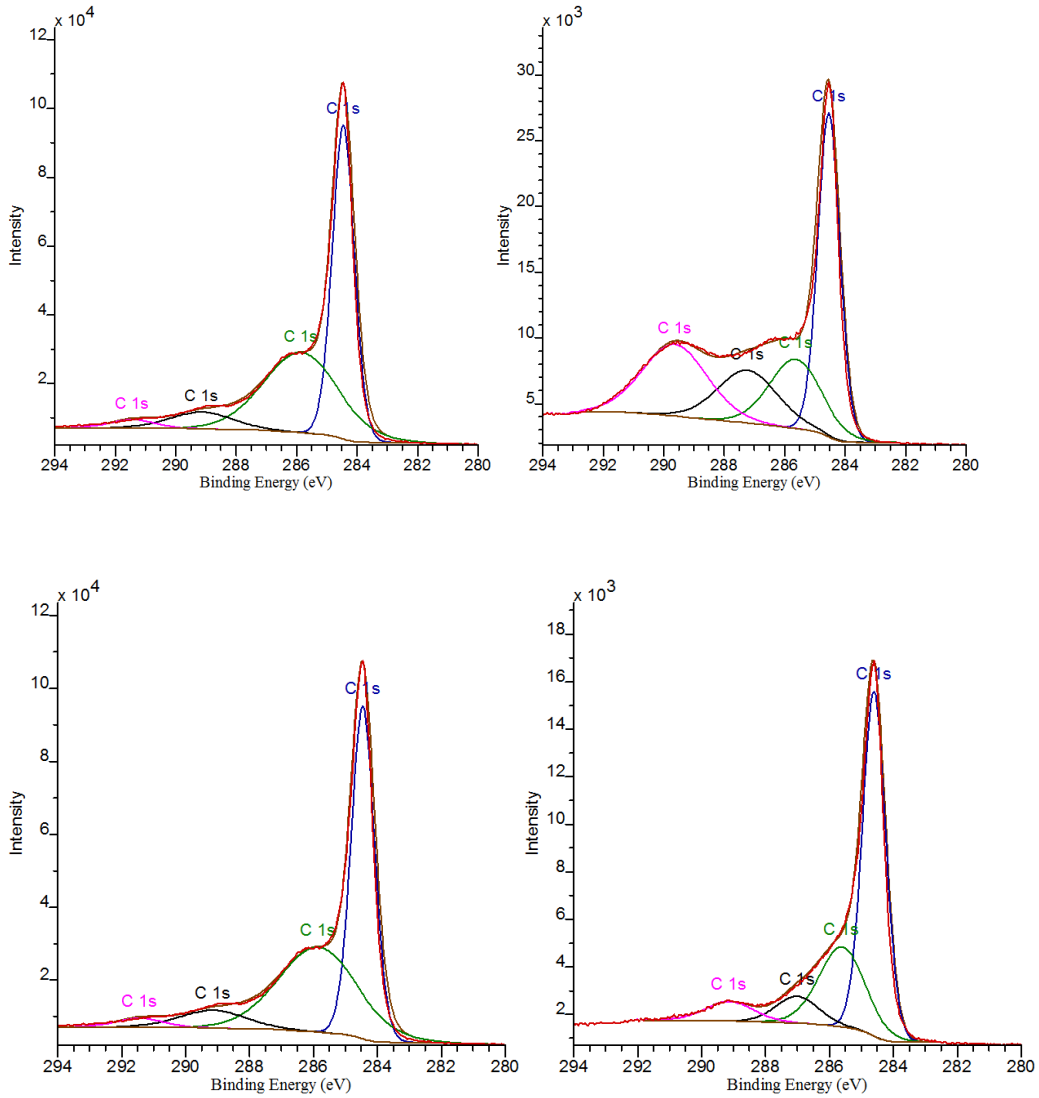

Figure B13 Top Left: C1s XPS spectrum of the pyridinium salt modified SWNTs (**13a**) prepared by ethyl-2-bromoacetate with four components *ca.* 284.5 (blue), 285.8 (green), 289.1 (black) and 291.4 (magenta) eV; Top right: C1s XPS spectrum of the pyridinium salt modified SWNTs (**13b**) prepared by p-nitrobenzylbromide with four components *ca.* 284.5 (blue), 285.6 (green), 287.2 (black) and 289.6 (magenta) eV; Bottom Left: C1s XPS spectrum of the pyridinium salt modified SWNTs (**13c**) prepared by PEG_{400}-yl 2-bromoacetate with four components *ca.* 284.5 (blue), 285.8 (green), 289.1 (black) and 291.4 (magenta) eV; Bottom right: C1s XPS spectrum of the indolizine modified SWNTs (**17**) prepared by p-nitrobenzylbromide with four components *ca.* 284.6 (blue), 285.6 (green), 286.9 (black) and 289.1 (magenta) eV.

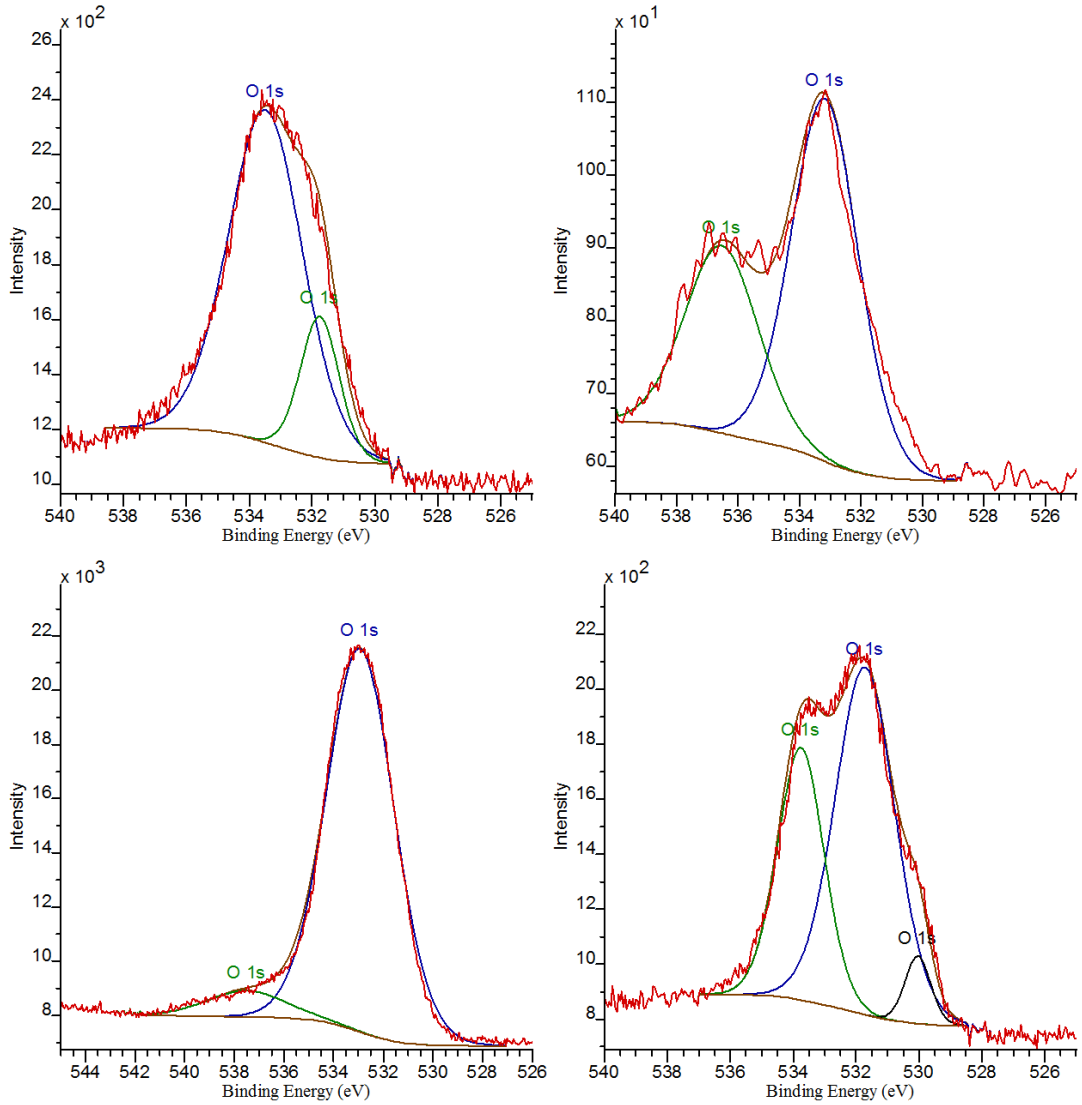

Figure B14 Top Left: O1s XPS spectrum of the pyridinium salt modified SWNTs (**13a**) prepared by ethyl-2-bromoacetate with two components *ca.* 531.8 (green) and 533.6 (blue) eV; Top Right: O1s XPS spectrum of the pyridinium salt modified SWNTs (**13b**) prepared by p-nitrobenzylbromide with two components *ca.* 531.1 (blue) and 536.5 (green) eV; Bottom Left: O1s XPS spectrum of the pyridinium salt modified SWNTs (**13c**) prepared by PEG_{400}-yl 2-bromoacetate with two components *ca.* 532.9 (green) and 537.4 (blue) eV; Bottom right: O1s XPS spectrum of the indolizine modified SWNTs (**17**) prepared by p-nitrobenzylbromide with three components *ca.* 530.0 (black), 531.7 (blue) and 533.7 (green) eV.

Appendix C : Additional information for Chapter V

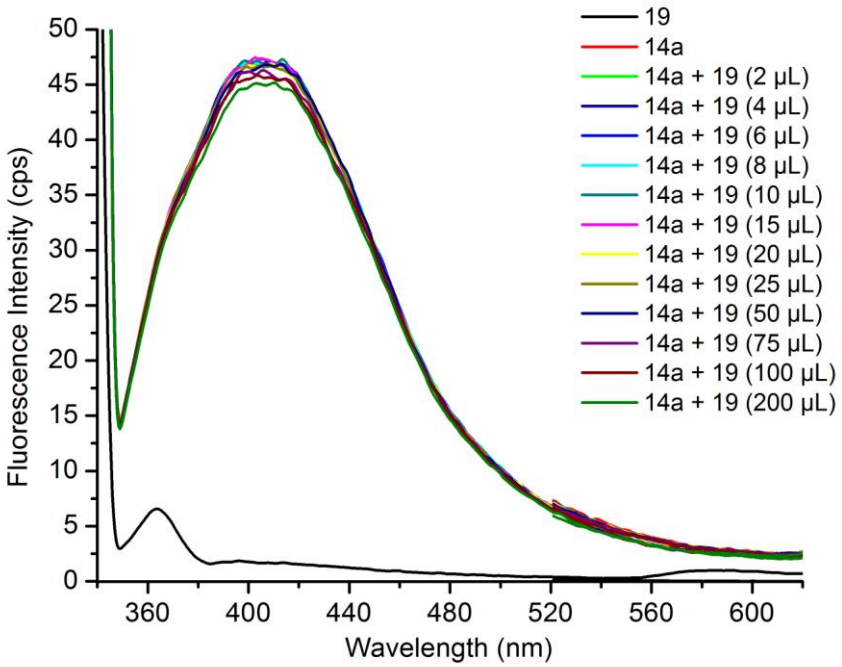

Figure C1 Change in fluorescence spectra of **14a** (1.25×10^{-4} M) excited at 330 nm in the presence of 2, 4, 6, 8, 10, 15, 20, 25, 50, 75, 100, 200 µL equivalent of phenol (**19**) (1×10^{-4} M) dissolved in CH_3CN.

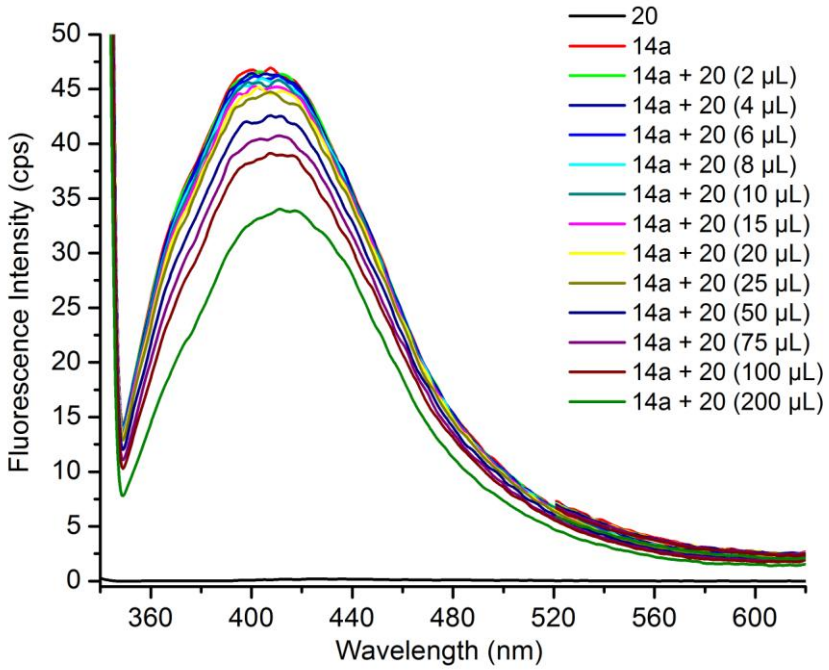

Figure C2 Change in fluorescence spectra of **14a** (1.25×10^{-4} M) excited at 330 nm in the presence of 2, 4, 6, 8, 10, 15, 20, 25, 50, 75, 100, 200 µL equivalent of 2-nitrophenol (**20**) (1×10^{-4} M) dissolved in CH_3CN.

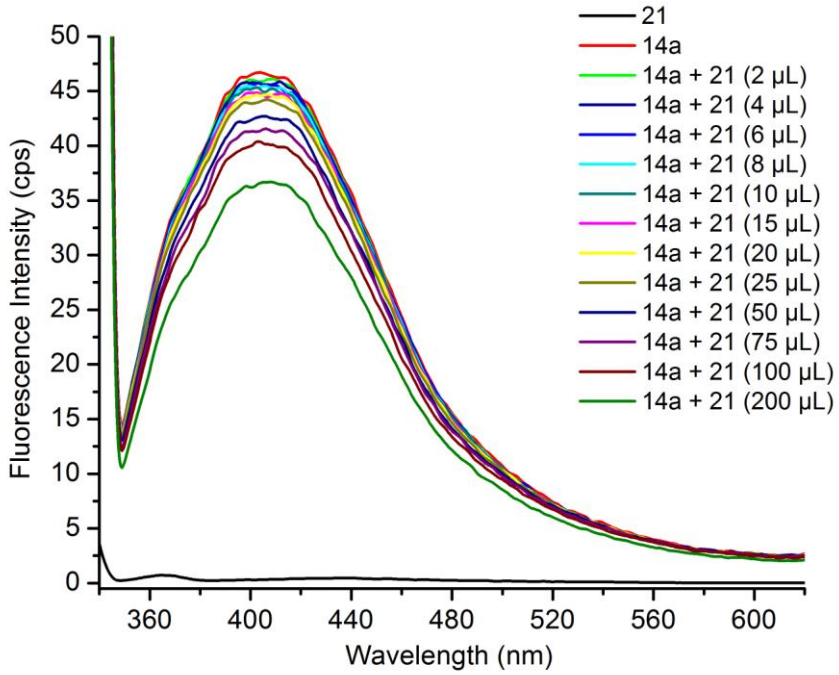

Figure C3 Change in fluorescence spectra of **14a** (1.25×10^{-4} M) excited at 330 nm in the presence of 2, 4, 6, 8, 10, 15, 20, 25, 50, 75, 100, 200 µL equivalent of 3-nitrophenol (**21**) (1×10^{-4} M) dissolved in CH_3CN.

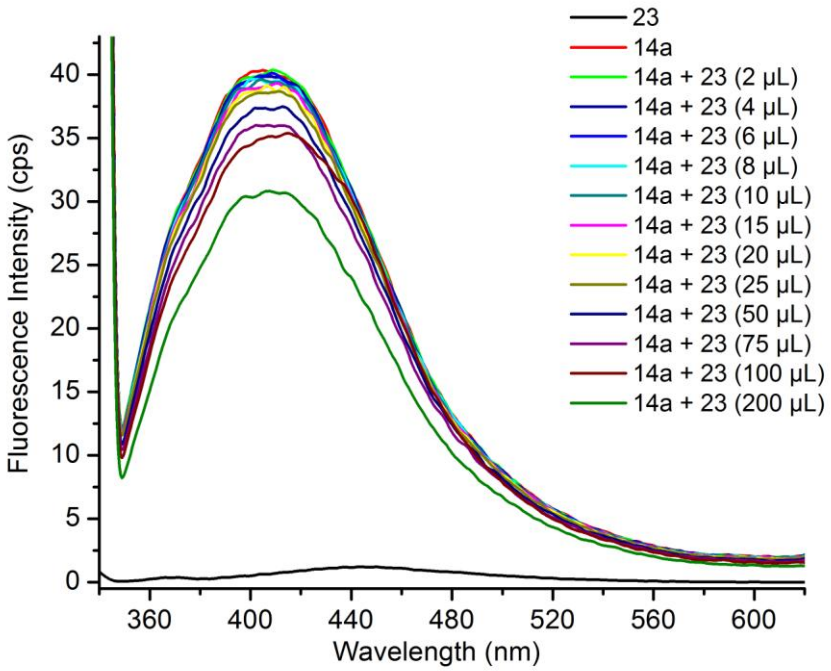

Figure C4 Change in fluorescence spectra of **14a** (1.25×10^{-4} M) excited at 330 nm in the presence of 2, 4, 6, 8, 10, 15, 20, 25, 50, 75, 100, 200 µL equivalent of 2-nitrosotoluene (**23**) (1×10^{-4} M) dissolved in CH_3CN.

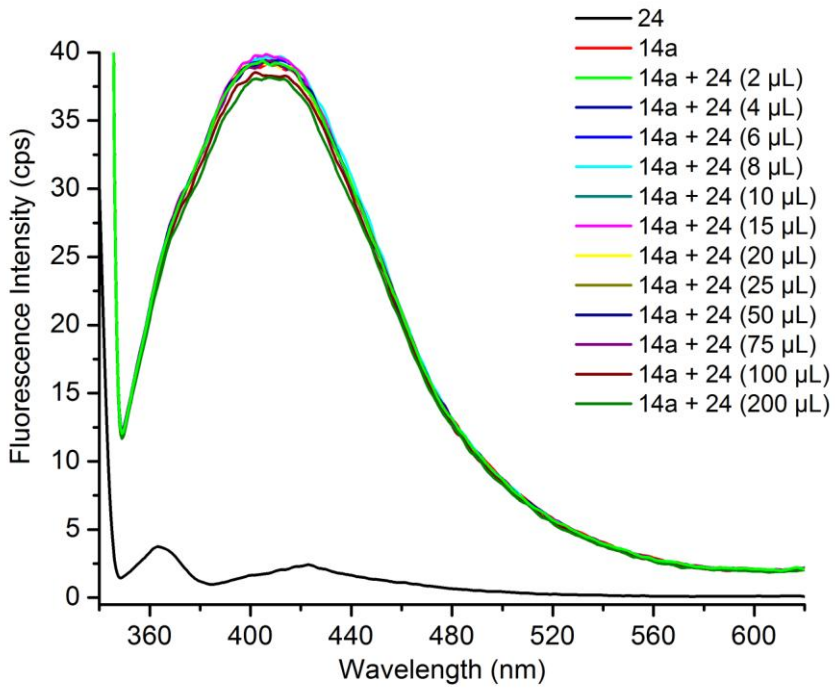

Figure C5 Change in fluorescence spectra of **14a** (1.25×10^{-4} M) excited at 330 nm in the presence of 2, 4, 6, 8, 10, 15, 20, 25, 50, 75, 100, 200 µL equivalent of 4-nitrotoluene (**24**) (1×10^{-4} M) dissolved in CH_3CN.

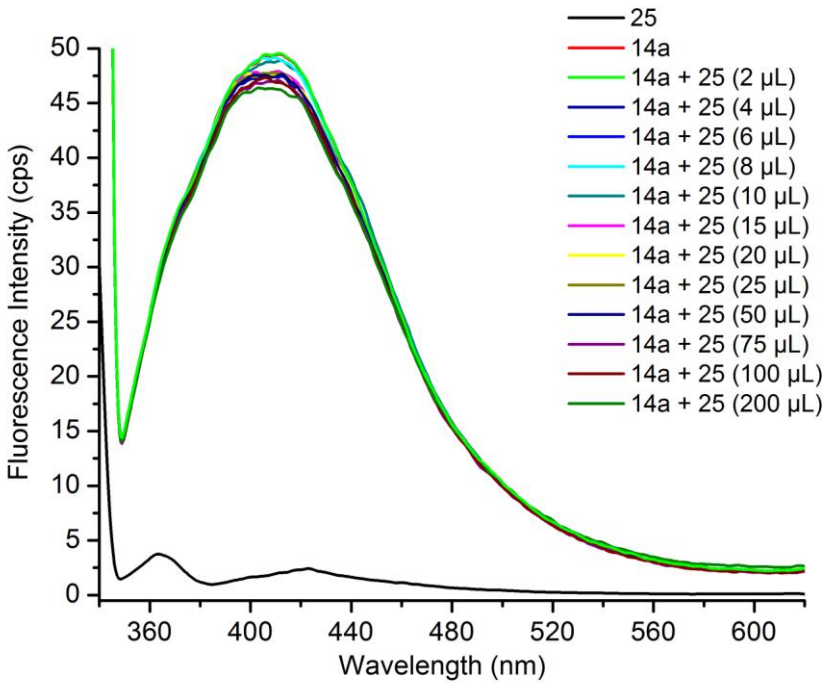

Figure C6 Change in fluorescence spectra of **14a** (1.25×10^{-4} M) excited at 330 nm in the presence of 2, 4, 6, 8, 10, 15, 20, 25, 50, 75, 100, 200 µL equivalent of 2,4-dinitrotoluene (**25**) (1×10^{-4} M) dissolved in CH_3CN.

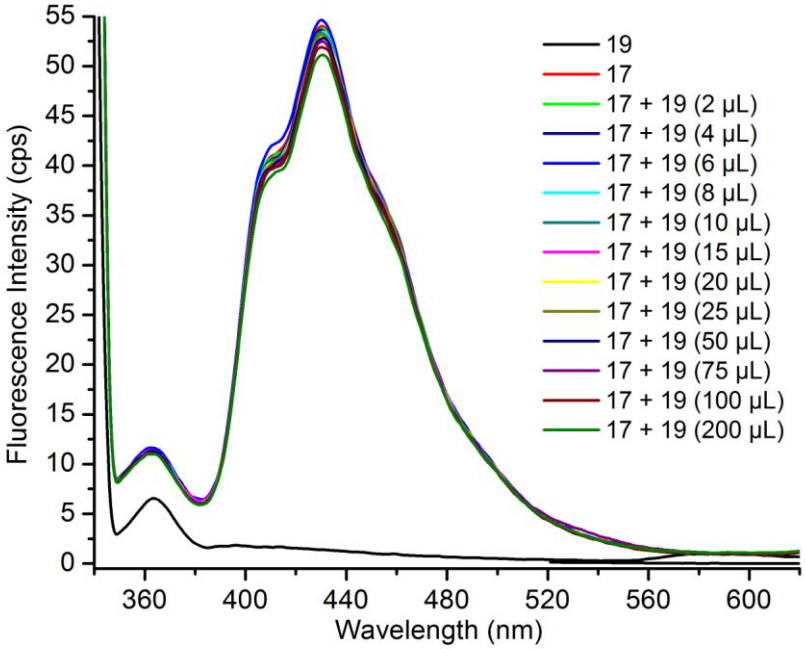

Figure C7 Change in fluorescence spectra of **17** (1.25×10^{-4} M) excited at 330 nm in the presence of 2, 4, 6, 8, 10, 15, 20, 25, 50, 75, 100, 200 µL equivalent of phenol (**19**) (1×10^{-4} M) dissolved in CH_3CN.

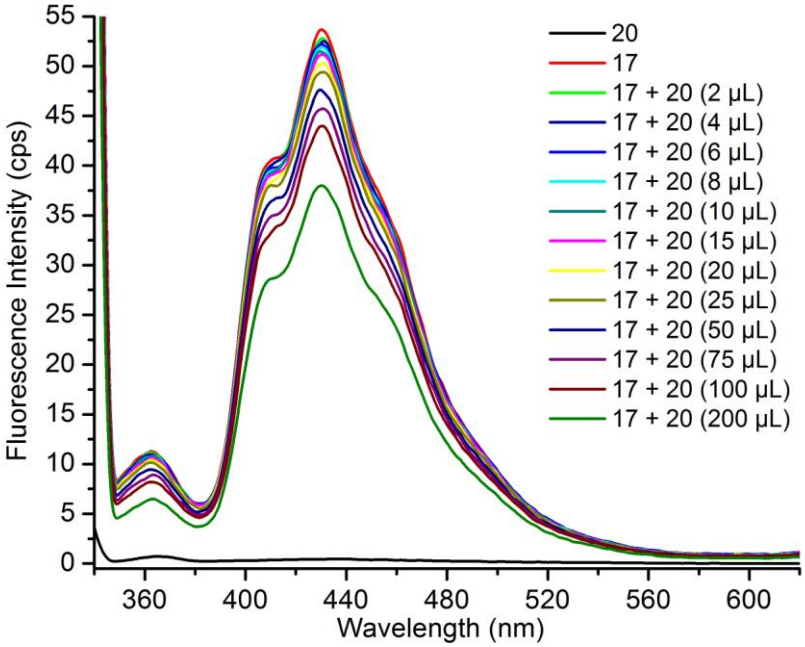

Figure C8 Change in fluorescence spectra of **17** (1.25×10^{-4} M) excited at 330 nm in the presence of 2, 4, 6, 8, 10, 15, 20, 25, 50, 75, 100, 200 µL equivalent of 2-nitrophenol (**20**) (1×10^{-4} M) dissolved in CH_3CN.

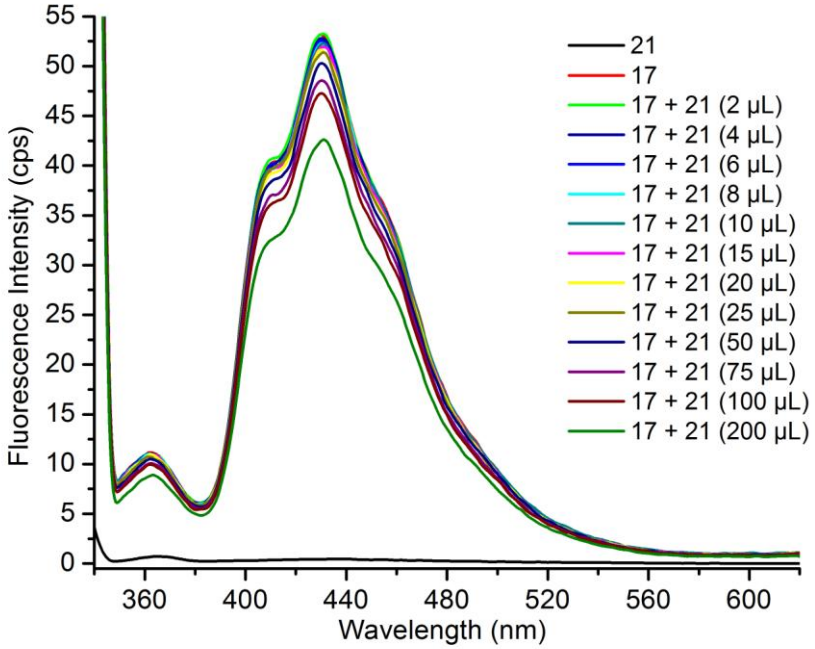

Figure C9 Change in fluorescence spectra of **17** (1.25 x 10^{-4} M) excited at 330 nm in the presence of 2, 4, 6, 8, 10, 15, 20, 25, 50, 75, 100, 200 µL equivalent of 3-nitrophenol (**21**) (1 x 10^{-4} M) dissolved in CH_3CN.

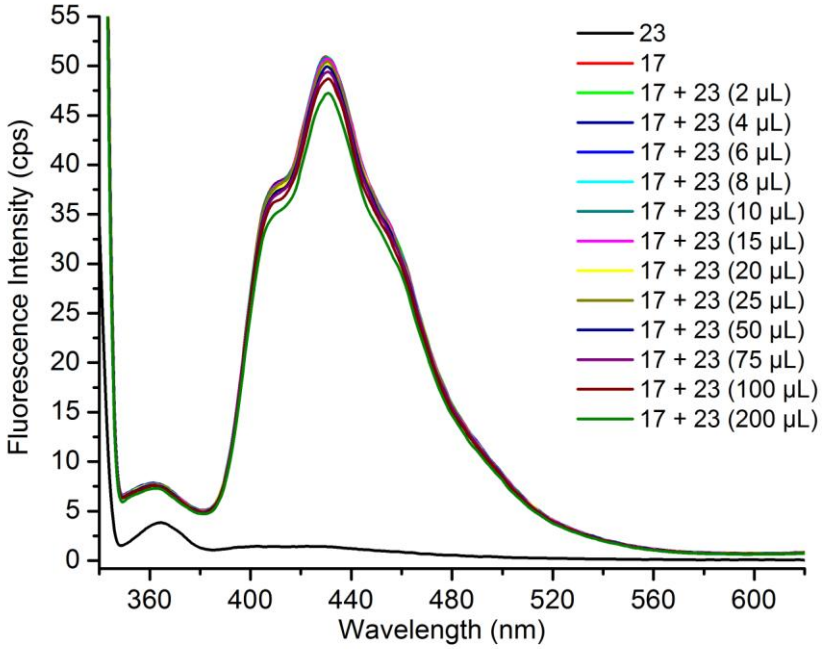

Figure C10 Change in fluorescence spectra of **17** (1.25×10^{-4} M) excited at 330 nm in the presence of 2, 4, 6, 8, 10, 15, 20, 25, 50, 75, 100, 200 µL equivalent of 2-nitrosotoluene (**23**) (1×10^{-4} M) dissolved in CH_3CN.

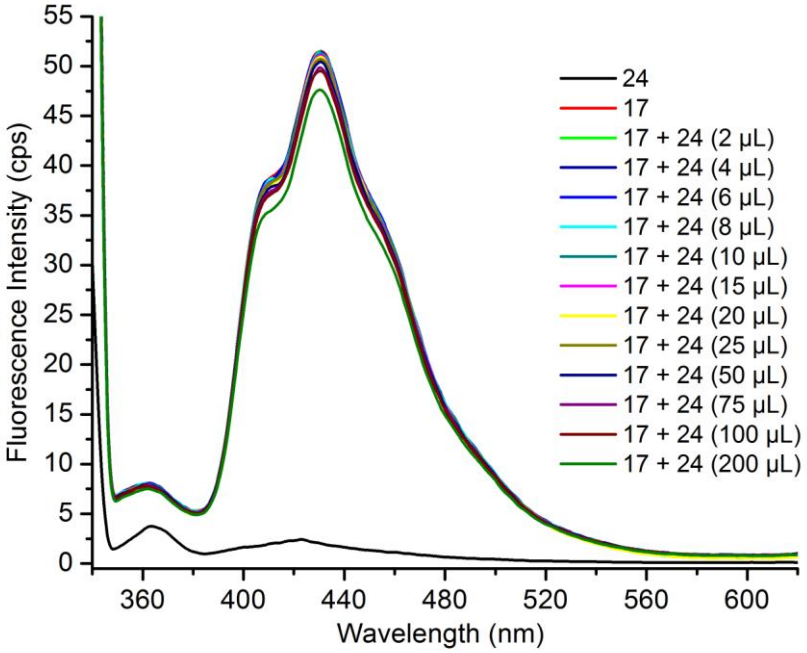

Figure C11 Change in fluorescence spectra of **17** (1.25×10^{-4} M) excited at 330 nm in the presence of 2, 4, 6, 8, 10, 15, 20, 25, 50, 75, 100, 200 µL equivalent of 4-nitrotoluene (**24**) (1×10^{-4} M) dissolved in CH_3CN.

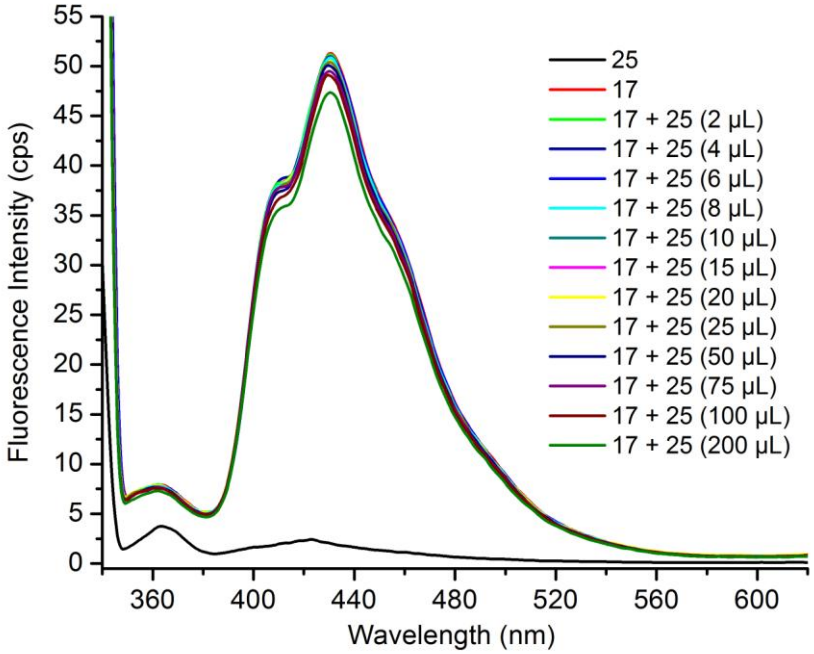

Figure C12 Change in fluorescence spectra of **17** (1.25×10^{-4} M) excited at 330 nm in the presence of 2, 4, 6, 8, 10, 15, 20, 25, 50, 75, 100, 200 µL equivalent of 2,4-dinitrotoluene (**25**) (1×10^{-4} M) dissolved in CH_3CN.

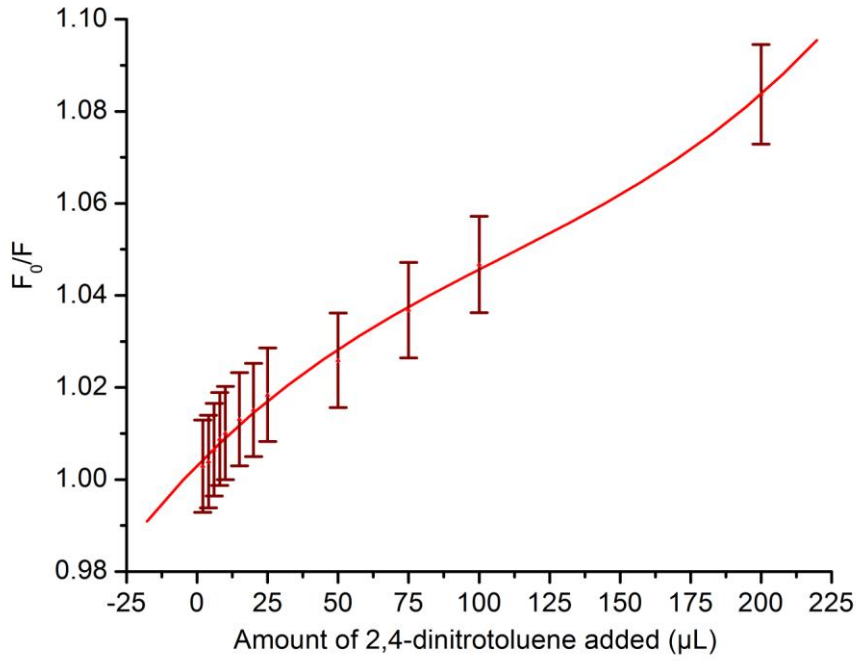

Figure C13 Stern-Volmer plot of the emission data (polynomial fitted) provided by the addition of 2, 4, 6, 8, 10, 15, 20, 25, 50, 75, 100, 200 µL equivalent of 2,4-dinitrotoluene (**25**) dissolved in CH_3CN to the indolizine functionalised SWNTs (**17**).

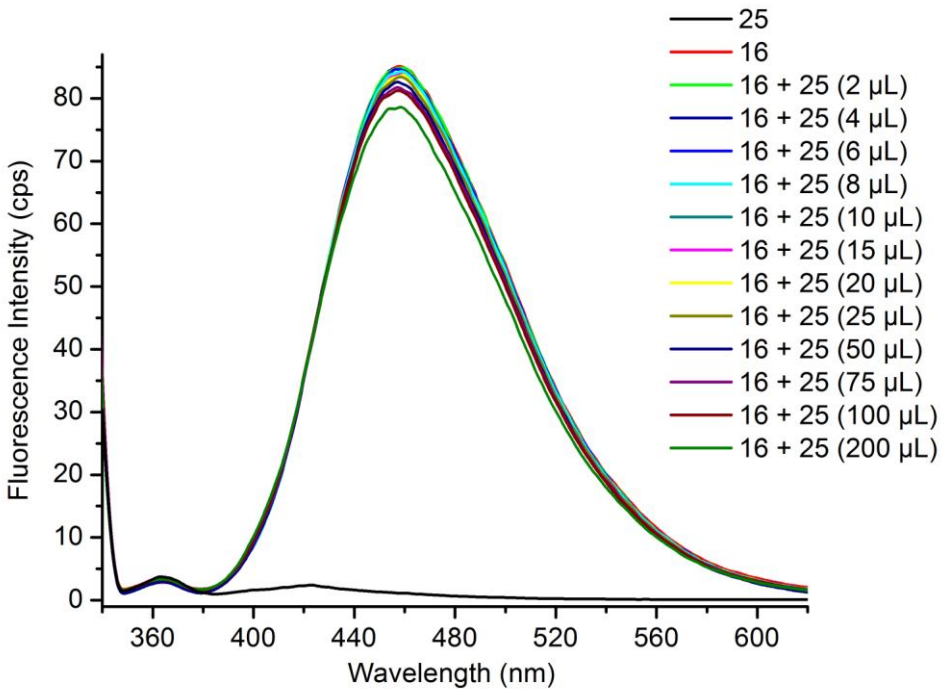

Figure C14 Change in fluorescence spectra of **16** (2.09×10^{-7} M) excited at 330 nm in the presence of 2, 4, 6, 8, 10, 15, 20, 25, 50, 75, 100, 200 µL equivalent of 2,4-dinitrotoluene (**25**) (1×10^{-4} M) dissolved in CH_3CN.

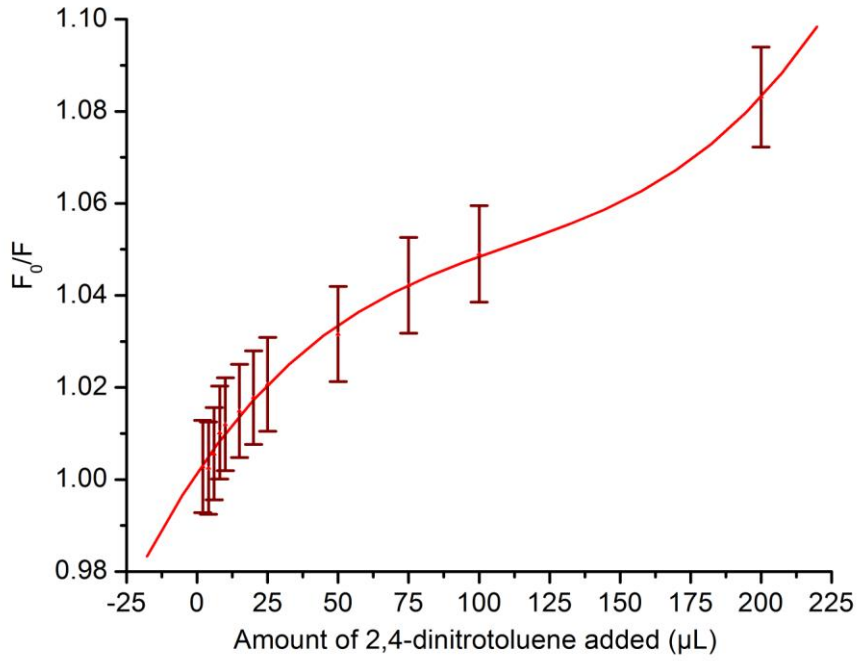

Figure C15 Stern-Volmer plot of the emission data (polynomial fitted) provided by the addition of 2, 4, 6, 8, 10, 15, 20, 25, 50, 75, 100, 200 μL equivalent of 2,4-dinitrotoluene (**25**) dissolved in CH_3CN to the free indolizine (**16**).

Appendix D : Additional information for Chapter VI

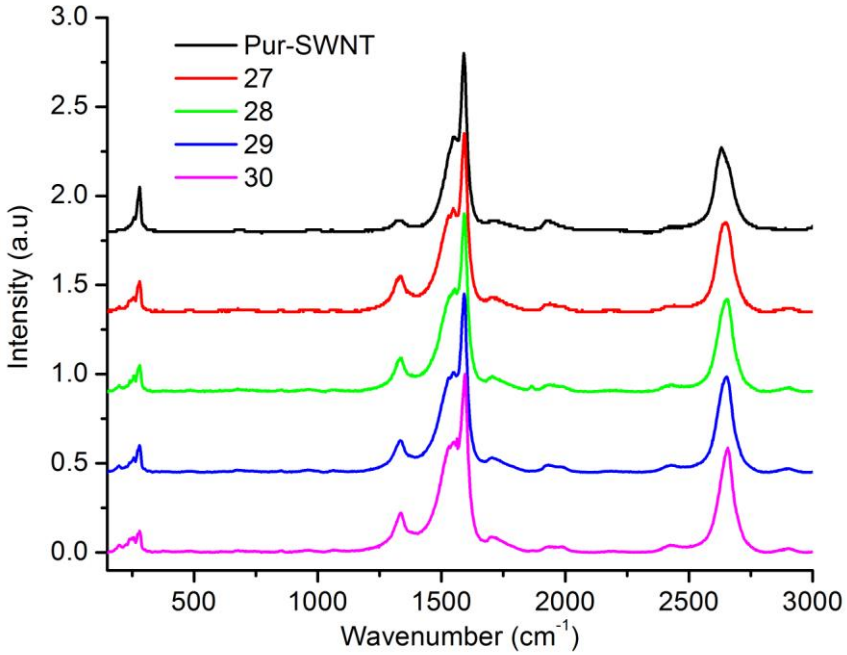

Figure D1 Raman spectra (532 nm, 2.33 eV) of purified SWNTs (black), butyl modified SWNTs (**27**) prepared by air quenching (red), and butyl-formyl modified SWNTs (**28**) prepared by the addition of N-formylpiperidine (green), butyl-benzyl formyl modified SWNTs (**29**) prepared by the addition of benzylchloroformate (blue), and butyl-methyl formyl modified SWNTs (**30**) prepared by the addition of methylchloroformate (magenta) normalized and offset at the G-band.

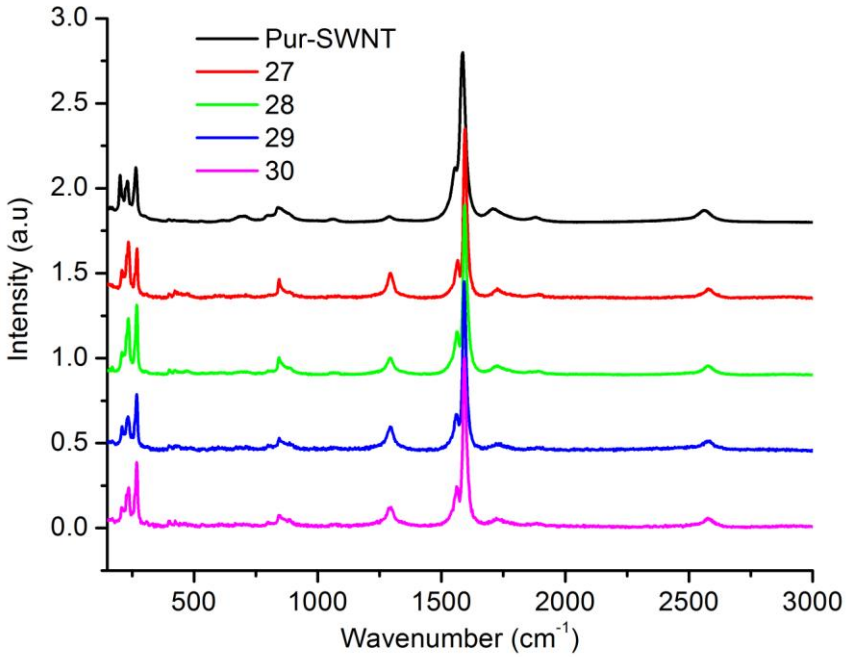

Figure D2 Raman spectra (785 nm, 1.58 eV) of purified SWNTs (black), butyl modified SWNTs (**27**) prepared by air quenching (red), and butyl-formyl modified SWNTs (**28**) prepared by the addition of *N*-formylpiperidine (green), butyl-benzyl formyl modified SWNTs (**29**) prepared by the addition of benzylchloroformate (blue), and butyl-methyl formyl modified SWNTs (**30**) prepared by the addition of methylchloroformate (magenta) normalized and offset at the G-band.

Appendix E : Published Articles

P1. Bayazit, M. K.; Coleman, K. S., Fluorescent Single-Walled Carbon Nanotubes Following the 1,3-Dipolar Cycloaddition of Pyridinium Ylides. *Journal of the American Chemical Society* **2009,** 131, (30), 10670-10676.

Abstract: Pyridinium ylides generated from simple Kro¨hnke salts undergo a 1,3-dipolar cycloaddition to single-walled carbon nanotubes (SWNTs) offering a simple and convenient method for the covalent modification of carbon nanotubes. The indolizine functionalized SWNTs generated, emit blue light when excited at 335 nm. The location and distribution of the functional groups was determined by AFM using electrostatic interactions with gold nanoparticles. While resonance Raman spectroscopy showed that the 1,3-dipolar cylcloaddition of the pyridinium ylides to the nanotube surface was selective for metallic and large diameter semiconducting SWNTs. The indolizine functionalized SWNTs were further characterized using FTIR, UV-vis-NIR, TGA-MS, and XPS.

P2. Bayazit, M. K.; Suri, A.; Coleman, K. S., Formylation of single-walled carbon nanotubes. *Carbon* **2010,** 48, (12), 3412-3419.

Abstract: Formyl or aldehyde groups are transferred to the surface of single-walled carbon nanotubes (SWCNTs) by reaction of reduced carbon nanotubes with N-formylpiperidine. This could open the way for more versatile chemical modification reactions of carbon nanotubes than is currently possible using functionalization methods reported to date. The formylated SWCNTs were characterized by thermogravimetric analysis–mass spectrometry and Raman, UV–vis–NIR and FTIR

spectroscopy. The location and distribution of the functional groups was determined by AFM using electrostatic interactions with gold nanoparticles. The formylated SWCNTs were further derivatized with a fluorescent dye and studied using fluorescence spectroscopy.

References

(1) Kroto, H. W.; Heath, J. R.; Obrien, S. C.; Curl, R. F.; Smalley, R. E. *Nature* **1985**, *318*, 162-163.

(2) Radushkevich, L. V.; Lukyanovich, V. M. *Zurn Fisic Chim* **1952**, 88-95.

(3) Monthioux, M.; Kuznetsov, V. L. *Carbon* **2006**, *44*, 1621-1623.

(4) Iijima, S. *Nature* **1991**, *354*, 56-58.

(5) Odom, T. W.; Huang, J. L.; Kim, P.; Lieber, C. M. *Journal of Physical Chemistry B* **2000**, *104*, 2794-2809.

(6) Lau, K. T.; Hui, D. *Composites Part B-Engineering* **2002**, *33*, 263-277.

(7) Meyyappan, M. In *Eds., In : Carbon Nanotubes Science and Applications, Boca Raton London, New York, Washington, D.C: CRC Press LLC,Chapter 1,* **2005**.

(8) Hirsch, A. *Angewandte Chemie-International Edition* **2002**, *41*, 1853-1859.

(9) Bethune, D. S.; Kiang, C. H.; Devries, M. S.; Gorman, G.; Savoy, R.; Vazquez, J.; Beyers, R. *Nature* **1993**, *363*, 605-607.

(10) Iijima, S.; Ichihashi, T. *Nature* **1993**, *363*, 603-605.

(11) Dresselhaus, M. S., Dresselhaus, G., and Eklund, P., *Science of Fullerenes and Carbon Nanotubes, Academic Press, San Diego,*, **1996**.

(12) Hamada, N.; Sawada, S.; Oshiyama, A. *Physical Review Letters* **1992**, *68*, 1579-1581.

(13) Saito, R.; Fujita, M.; Dresselhaus, G.; Dresselhaus, M. S. *Applied Physics Letters* **1992**, *60*, 2204-2206.

(14) Dai, H. J. *Surface Science* **2002**, *500*, 218-241.

(15) Mintmire, J. W.; Dunlap, B. I.; White, C. T. *Physical Review Letters* **1992**, *68*, 631-634.

(16) Dresselhaus, M. S.; Dresselhaus, G.; Saito, R. *Physical Review B* **1992**, *45*, 6234-6242.

(17) Tanaka, K.; Okahara, K.; Okada, M.; Yamabe, T. *Chemical Physics Letters* **1992**, *191*, 469-472.

(18) Wildoer, J. W. G.; Venema, L. C.; Rinzler, A. G.; Smalley, R. E.; Dekker, C. *Nature* **1998**, *391*, 59-62.

(19) *Carbon Nanotubes: Synthesis, S., Properties and Applications*; Dresselhaus, M. S.; Dresselhaus, G.; Avouris, Ph., Eds.; Springer: Berlin, 2001.

(20) Odom, T. W.; Huang, J. L.; Kim, P.; Lieber, C. M. *Nature* **1998**, *391*, 62-64.

(21) Terrones, M. *International Materials Reviews* **2004**, *49*, 325-377.

(22) Dai, H. J. *Accounts of Chemical Research* **2002**, *35*, 1035-1044.

(23) Dai, H. J. In *Carbon Nanotubes*; Springer-Verlag Berlin: Berlin, 2001; Vol. 80, p 29-53.

(24) Liu, J.; Fan, S. S.; Dai, H. J. *Mrs Bulletin* **2004**, *29*, 244-250.

(25) O'Connell, M. J. *Eds., In : Carbon Nanotubes Properties and Applications, Boca, Raton London, New York, CRC, Taylor & Francis Group, LLC, Chapter 2, ,* **2006**.

(26) Thess, A.; Lee, R.; Nikolaev, P.; Dai, H. J.; Petit, P.; Robert, J.; Xu, C. H.; Lee, Y. H.; Kim, S. G.; Rinzler, A. G.; Colbert, D. T.; Scuseria, G. E.; Tomanek, D.; Fischer, J. E.; Smalley, R. E. *Science* **1996**, *273*, 483-487.

(27) Dal, H. J.; Rinzler, A. G.; Nikolaev, P.; Thess, A.; Colbert, D. T.; Smalley, R. E. *Chemical Physics Letters* **1996**, *260*, 471-475.

(28) Nikolaev, P.; Bronikowski, M. J.; Bradley, R. K.; Rohmund, F.; Colbert, D. T.; Smith, K. A.; Smalley, R. E. *Chemical Physics Letters* **1999**, *313*, 91-97.

(29) Vander Wal, R. L.; Ticich, T. M.; Curtis, V. E. *Chemical Physics Letters* **2000**, *323*, 217-223.

(30) Vander Wal, R. L.; Ticich, T. M.; Curtis, V. E. *Journal of Physical Chemistry A* **2000**, *104*, 7209-7217.

(31) Deheer, W. A.; Chatelain, A.; Ugarte, D. *Science* **1995**, *270*, 1179-1180.

(32) Bockrath, M.; Cobden, D. H.; McEuen, P. L.; Chopra, N. G.; Zettl, A.; Thess, A.; Smalley, R. E. *Science* **1997**, *275*, 1922-1925.

(33) Tans, S. J.; Verschueren, A. R. M.; Dekker, C. *Nature* **1998**, *393*, 49-52.

(34) Kim, P.; Lieber, C. M. *Science* **1999**, *286*, 2148-2150.

(35) Dai, H. J.; Hafner, J. H.; Rinzler, A. G.; Colbert, D. T.; Smalley, R. E. *Nature* **1996**, *384*, 147-150.

(36) Wong, S. S.; Joselevich, E.; Woolley, A. T.; Cheung, C. L.; Lieber, C. M. *Nature* **1998**, *394*, 52-55.

(37) Baughman, R. H.; Cui, C. X.; Zakhidov, A. A.; Iqbal, Z.; Barisci, J. N.; Spinks, G. M.; Wallace, G. G.; Mazzoldi, A.; De Rossi, D.; Rinzler, A. G.; Jaschinski, O.; Roth, S.; Kertesz, M. *Science* **1999**, *284*, 1340-1344.

(38) Dillon, A. C.; Jones, K. M.; Bekkedahl, T. A.; Kiang, C. H.; Bethune, D. S.; Heben, M. J. *Nature* **1997**, *386*, 377-379.

(39) Rueckes, T.; Kim, K.; Joselevich, E.; Tseng, G. Y.; Cheung, C. L.; Lieber, C. M. *Science* **2000**, *289*, 94-97.

(40) Choi, W. B.; Chung, D. S.; Kang, J. H.; Kim, H. Y.; Jin, Y. W.; Han, I. T.; Lee, Y. H.; Jung, J. E.; Lee, N. S.; Park, G. S.; Kim, J. M. *Applied Physics Letters* **1999**, *75*, 3129-3131.

(41) Cooper, E. B.; Manalis, S. R.; Fang, H.; Dai, H.; Matsumoto, K.; Minne, S. C.; Hunt, T.; Quate, C. F. *Applied Physics Letters* **1999**, *75*, 3566-3568.

(42) Kong, J.; Franklin, N. R.; Zhou, C. W.; Chapline, M. G.; Peng, S.; Cho, K. J.; Dai, H. J. *Science* **2000**, *287*, 622-625.

(43) Krishnan, A.; Dujardin, E.; Ebbesen, T. W.; Yianilos, P. N.; Treacy, M. M. J. *Physical Review B* **1998**, *58*, 14013-14019.

(44) Lu, J. P. *Physical Review Letters* **1997**, *79*, 1297-1300.

(45) Popov, V. N.; Van Doren, V. E.; Balkanski, M. *Physical Review B* **2000**, *61*, 3078-3084.

(46) Yu, M. F.; Lourie, O.; Dyer, M. J.; Moloni, K.; Kelly, T. F.; Ruoff, R. S. *Science* **2000**, *287*, 637-640.

(47) Yu, M. F.; Files, B. S.; Arepalli, S.; Ruoff, R. S. *Physical Review Letters* **2000**, *84*, 5552-5555.

(48) Treacy, M. M. J.; Ebbesen, T. W.; Gibson, J. M. *Nature* **1996**, *381*, 678-680.

(49) Wong, E. W.; Sheehan, P. E.; Lieber, C. M. *Science* **1997**, *277*, 1971-1975.

(50) Falvo, M. R.; Clary, G. J.; Taylor, R. M.; Chi, V.; Brooks, F. P.; Washburn, S.; Superfine, R. *Nature* **1997**, *389*, 582-584.

(51) Shaffer, M. S. P.; Windle, A. H. *Advanced Materials* **1999**, *11*, 937-+.

(52) Zhang, X. F.; Liu, T.; Sreekumar, T. V.; Kumar, S.; Moore, V. C.; Hauge, R. H.; Smalley, R. E. *Nano Letters* **2003**, *3*, 1285-1288.

(53) Cooper, C. A.; Ravich, D.; Lips, D.; Mayer, J.; Wagner, H. D. *Composites Science and Technology* **2002**, *62*, 1105-1112.

(54) Benoit, J. M.; Corraze, B.; Chauvet, O. *Physical Review B* **2002**, *65*, 4.

(55) Bhattacharyya, A. R.; Sreekumar, T. V.; Liu, T.; Kumar, S.; Ericson, L. M.; Hauge, R. H.; Smalley, R. E. *Polymer* **2003**, *44*, 2373-2377.

(56) Biercuk, M. J.; Llaguno, M. C.; Radosavljevic, M.; Hyun, J. K.; Johnson, A. T.; Fischer, J. E. *Applied Physics Letters* **2002**, *80*, 2767-2769.

(57) Kim, B.; Lee, J.; Yu, I. S. *Journal of Applied Physics* **2003**, *94*, 6724-6728.

(58) Sandler, J. K. W.; Kirk, J. E.; Kinloch, I. A.; Shaffer, M. S. P.; Windle, A. H. *Polymer* **2003**, *44*, 5893-5899.

(59) Sennett, M.; Welsh, E.; Wright, J. B.; Li, W. Z.; Wen, J. G.; Ren, Z. F. *Applied Physics a-Materials Science & Processing* **2003**, *76*, 111-113.

(60) Dalton, A. B.; Collins, S.; Munoz, E.; Razal, J. M.; Ebron, V. H.; Ferraris, J. P.; Coleman, J. N.; Kim, B. G.; Baughman, R. H. *Nature* **2003**, *423*, 703-703.

(61) Sreekumar, T. V.; Liu, T.; Min, B. G.; Guo, H.; Kumar, S.; Hauge, R. H.; Smalley, R. E. *Advanced Materials* **2004**, *16*, 58-+.

(62) Ajayan, P. M.; Zhou, O. Z. In *Carbon Nanotubes*; Springer-Verlag Berlin: Berlin, 2001; Vol. 80, p 391-425.

(63) Roukes, M. *Physics World* **2001**, *14*, 25-31.

(64) Cho, A. *Science* **2003**, *299*, 36-37.

(65) Schwab, K.; Henriksen, E. A.; Worlock, J. M.; Roukes, M. L. *Nature* **2000**, *404*, 974-977.

(66) Sazonova, V.; Yaish, Y.; Ustunel, H.; Roundy, D.; Arias, T. A.; McEuen, P. L. *Nature* **2004**, *431*, 284-287.

(67) Schwab, K. C.; Roukes, M. L. *Physics Today* **2005**, *58*, 36-42.

(68) Roukes, M. *Scientific American* **2001**, *285*, 48-+.

(69) Tohji, K.; Takahashi, H.; Shinoda, Y.; Shimizu, N.; Jeyadevan, B.; Matsuoka, I.; Saito, Y.; Kasuya, A.; Ito, S.; Nishina, Y. *Journal of Physical Chemistry B* **1997**, *101*, 1974-1978.

(70) Huang, S. M.; Dai, L. M. *Journal of Physical Chemistry B* **2002**, *106*, 3543-3545.

(71) Chiang, I. W.; Brinson, B. E.; Smalley, R. E.; Margrave, J. L.; Hauge, R. H. *Journal of Physical Chemistry B* **2001**, *105*, 1157-1161.

(72) Bandow, S.; Rao, A. M.; Williams, K. A.; Thess, A.; Smalley, R. E.; Eklund, P. C. *Journal of Physical Chemistry B* **1997**, *101*, 8839-8842.

(73) Niyogi, S.; Hu, H.; Hamon, M. A.; Bhowmik, P.; Zhao, B.; Rozenzhak, S. M.; Chen, J.; Itkis, M. E.; Meier, M. S.; Haddon, R. C. *Journal of the American Chemical Society* **2001**, *123*, 733-734.

(74) Murphy, R.; Coleman, J. N.; Cadek, M.; McCarthy, B.; Bent, M.; Drury, A.; Barklie, R. C.; Blau, W. J. *Journal of Physical Chemistry B* **2002**, *106*, 3087-3091.

(75) O'Connell, M. J.; Boul, P.; Ericson, L. M.; Huffman, C.; Wang, Y. H.; Haroz, E.; Kuper, C.; Tour, J.; Ausman, K. D.; Smalley, R. E. *Chemical Physics Letters* **2001**, *342*, 265-271.

(76) Suri, A.; Chakraborty, A. K.; Coleman, K. S. *Chemistry of Materials* **2008**, *20*, 1705-1709.

(77) Banerjee, S.; Kahn, M. G. C.; Wong, S. S. *Chemistry-a European Journal* **2003**, *9*, 1899-1908.

(78) Tasis, D.; Tagmatarchis, N.; Bianco, A.; Prato, M. *Chemical Reviews* **2006**, *106*, 1105-1136.

(79) Niyogi, S.; Hamon, M. A.; Hu, H.; Zhao, B.; Bhowmik, P.; Sen, R.; Itkis, M. E.; Haddon, R. C. *Accounts of Chemical Research* **2002**, *35*, 1105-1113.

(80) Bahr, J. L.; Tour, J. M. *Journal of Materials Chemistry* **2002**, *12*, 1952-1958.

(81) Liu, J.; Rinzler, A. G.; Dai, H. J.; Hafner, J. H.; Bradley, R. K.; Boul, P. J.; Lu, A.; Iverson, T.; Shelimov, K.; Huffman, C. B.; Rodriguez-Macias, F.; Shon, Y. S.; Lee, T. R.; Colbert, D. T.; Smalley, R. E. *Science* **1998**, *280*, 1253-1256.

(82) Duesberg, G. S.; Burghard, M.; Muster, J.; Philipp, G.; Roth, S. *Chemical Communications* **1998**, 435-436.

(83) Islam, M. F.; Rojas, E.; Bergey, D. M.; Johnson, A. T.; Yodh, A. G. *Nano Letters* **2003**, *3*, 269-273.

(84) Matarredona, O.; Rhoads, H.; Li, Z. R.; Harwell, J. H.; Balzano, L.; Resasco, D. E. *Journal of Physical Chemistry B* **2003**, *107*, 13357-13367.

(85) Liu, A. H.; Honma, I.; Ichihara, M.; Zhou, H. S. *Nanotechnology* **2006**, *17*, 2845-2849.

(86) Zou, Y. B.; Feng, Y. C.; Wang, L.; Liu, X. B. *Carbon* **2004**, *42*, 271-277.

(87) Baskaran, D.; Mays, J. W.; Bratcher, M. S. *Chemistry of Materials* **2005**, *17*, 3389-3397.

(88) Bandyopadhyaya, R.; Nativ-Roth, E.; Regev, O.; Yerushalmi-Rozen, R. *Nano Letters* **2002**, *2*, 25-28.

(89) Star, A.; Steuerman, D. W.; Heath, J. R.; Stoddart, J. F. *Angewandte Chemie-International Edition* **2002**, *41*, 2508-+.

(90) Tsang, S. C.; Guo, Z. J.; Chen, Y. K.; Green, M. L. H.; Hill, H. A. O.; Hambley, T. W.; Sadler, P. J. *Angewandte Chemie-International Edition in English* **1997**, *36*, 2198-2200.

(91) Guo, Z. J.; Sadler, P. J.; Tsang, S. C. *Advanced Materials* **1998**, *10*, 701-703.

(92) Azamian, B. R.; Davis, J. J.; Coleman, K. S.; Bagshaw, C. B.; Green, M. L. H. *Journal of the American Chemical Society* **2002**, *124*, 12664-12665.

(93) Balavoine, F.; Schultz, P.; Richard, C.; Mallouh, V.; Ebbesen, T. W.; Mioskowski, C. *Angewandte Chemie-International Edition* **1999**, *38*, 1912-1915.

(94) Zheng, M.; Jagota, A.; Strano, M. S.; Santos, A. P.; Barone, P.; Chou, S. G.; Diner, B. A.; Dresselhaus, M. S.; McLean, R. S.; Onoa, G. B.; Samsonidze, G. G.; Semke, E. D.; Usrey, M.; Walls, D. J. *Science* **2003**, *302*, 1545-1548.

(95) Zheng, M.; Jagota, A.; Semke, E. D.; Diner, B. A.; McLean, R. S.; Lustig, S. R.; Richardson, R. E.; Tassi, N. G. *Nature Materials* **2003**, *2*, 338-342.

(96) Chen, R. J.; Zhang, Y. G.; Wang, D. W.; Dai, H. J. *Journal of the American Chemical Society* **2001**, *123*, 3838-3839.

(97) Tagmatarchis, N.; Prato, M.; Guldi, D. M. *Physica E-Low-Dimensional Systems & Nanostructures* **2005**, *29*, 546-550.

(98) Paloniemi, H.; Aaritalo, T.; Laiho, T.; Liuke, H.; Kocharova, N.; Haapakka, K.; Terzi, F.; Seeber, R.; Lukkari, J. *Journal of Physical Chemistry B* **2005**, *109*, 8634-8642.

(99) Tomonari, Y.; Murakami, H.; Nakashima, N. *Chemistry-a European Journal* **2006**, *12*, 4027-4034.

(100) Ivanov, V.; Fonseca, A.; Nagy, J. B.; Lucas, A.; Lambin, P.; Bernaerts, D.; Zhang, X. B. *Carbon* **1995**, *33*, 1727-1738.

(101) Fu, K. F.; Huang, W. J.; Lin, Y.; Riddle, L. A.; Carroll, D. L.; Sun, Y. P. *Nano Letters* **2001**, *1*, 439-441.

(102) Hamon, M. A.; Hui, H.; Bhowmik, P.; Itkis, H. M. E.; Haddon, R. C. *Applied Physics a-Materials Science & Processing* **2002**, *74*, 333-338.

(103) Chen, J.; Hamon, M. A.; Hu, H.; Chen, Y. S.; Rao, A. M.; Eklund, P. C.; Haddon, R. C. *Science* **1998**, *282*, 95-98.

(104) Hamon, M. A.; Chen, J.; Hu, H.; Chen, Y. S.; Itkis, M. E.; Rao, A. M.; Eklund, P. C.; Haddon, R. C. *Advanced Materials* **1999**, *11*, 834-+.

(105) Bahr, J. L.; Yang, J. P.; Kosynkin, D. V.; Bronikowski, M. J.; Smalley, R. E.; Tour, J. M. *Journal of the American Chemical Society* **2001**, *123*, 6536-6542.

(106) Moore, V. C.; Strano, M. S.; Haroz, E. H.; Hauge, R. H.; Smalley, R. E.; Schmidt, J.; Talmon, Y. *Nano Letters* **2003**, *3*, 1379-1382.

(107) Shim, M.; Kam, N. W. S.; Chen, R. J.; Li, Y. M.; Dai, H. J. *Nano Letters* **2002**, *2*, 285-288.

(108) O'Connell, M. J.; Bachilo, S. M.; Huffman, C. B.; Moore, V. C.; Strano, M. S.; Haroz, E. H.; Rialon, K. L.; Boul, P. J.; Noon, W. H.; Kittrell, C.; Ma, J. P.; Hauge, R. H.; Weisman, R. B.; Smalley, R. E. *Science* **2002**, *297*, 593-596.

(109) Dyke, C. A.; Tour, J. M. *Nano Letters* **2003**, *3*, 1215-1218.

(110) Bahr, J. L.; Tour, J. M. *Chemistry of Materials* **2001**, *13*, 3823-+.

(111) Hudson, J. L.; Casavant, M. J.; Tour, J. M. *Journal of the American Chemical Society* **2004**, *126*, 11158-11159.

(112) Dyke, C. A.; Tour, J. M. *Journal of the American Chemical Society* **2003**, *125*, 1156-1157.

(113) Mickelson, E. T.; Huffman, C. B.; Rinzler, A. G.; Smalley, R. E.; Hauge, R. H.; Margrave, J. L. *Chemical Physics Letters* **1998**, *296*, 188-194.

(114) Khabashesku, V. N.; Billups, W. E.; Margrave, J. L. *Accounts of Chemical Research* **2002**, *35*, 1087-1095.

(115) Ying, Y. M.; Saini, R. K.; Liang, F.; Sadana, A. K.; Billups, W. E. *Organic Letters* **2003**, *5*, 1471-1473.

(116) Liang, F.; Sadana, A. K.; Peera, A.; Chattopadhyay, J.; Gu, Z. N.; Hauge, R. H.; Billups, W. E. *Nano Letters* **2004**, *4*, 1257-1260.

(117) Georgakilas, V.; Kordatos, K.; Prato, M.; Guldi, D. M.; Holzinger, M.; Hirsch, A. *Journal of the American Chemical Society* **2002**, *124*, 760-761.

(118) Holzinger, M.; Abraha, J.; Whelan, P.; Graupner, R.; Ley, L.; Hennrich, F.; Kappes, M.; Hirsch, A. *Journal of the American Chemical Society* **2003**, *125*, 8566-8580.

(119) Coleman, K. S.; Bailey, S. R.; Fogden, S.; Green, M. L. H. *Journal of the American Chemical Society* **2003**, *125*, 8722-8723.

(120) Kamaras, K.; Itkis, M. E.; Hu, H.; Zhao, B.; Haddon, R. C. *Science* **2003**, *301*, 1501-1501.

(121) Chen, Y.; Haddon, R. C.; Fang, S.; Rao, A. M.; Lee, W. H.; Dickey, E. C.; Grulke, E. A.; Pendergrass, J. C.; Chavan, A.; Haley, B. E.; Smalley, R. E. *Journal of Materials Research* **1998**, *13*, 2423-2431.

(122) Holzinger, M.; Vostrowsky, O.; Hirsch, A.; Hennrich, F.; Kappes, M.; Weiss, R.; Jellen, F. *Angewandte Chemie-International Edition* **2001**, *40*, 4002-+.

(123) Nakamura, T.; Ishihara, M.; Ohana, T.; Tanaka, A.; Koga, Y. *Chemical Communications* **2004**, 1336-1337.

(124) Viswanathan, G.; Chakrapani, N.; Yang, H. C.; Wei, B. Q.; Chung, H. S.; Cho, K. W.; Ryu, C. Y.; Ajayan, P. M. *Journal of the American Chemical Society* **2003**, *125*, 9258-9259.

(125) Blake, R.; Gun'ko, Y. K.; Coleman, J.; Cadek, M.; Fonseca, A.; Nagy, J. B.; Blau, W. J. *Journal of the American Chemical Society* **2004**, *126*, 10226-10227.

(126) Chen, S. M.; Shen, W. M.; Wu, G. Z.; Chen, D. Y.; Jiang, M. *Chemical Physics Letters* **2005**, *402*, 312-317.

(127) Pekker, S.; Salvetat, J. P.; Jakab, E.; Bonard, J. M.; Forro, L. *Journal of Physical Chemistry B* **2001**, *105*, 7938-7943.

(128) Penicaud, A.; Poulin, P.; Derre, A.; Anglaret, E.; Petit, P. *Journal of the American Chemical Society* **2005**, *127*, 8-9.

(129) Graupner, R.; Abraham, J.; Wunderlich, D.; Vencelova, A.; Lauffer, P.; Rohrl, J.; Hundhausen, M.; Ley, L.; Hirsch, A. *Journal of the American Chemical Society* **2006**, *128*, 6683-6689.

(130) Wunderlich, D.; Hauke, F.; Hirsch, A. *Chemistry-a European Journal* **2008**, *14*, 1607-1614.

(131) Wunderlich, D.; Hauke, F.; Hirsch, A. *Journal of Materials Chemistry* **2008**, *18*, 1493-1497.

(132) Avouris, P. *Accounts of Chemical Research* **2002**, *35*, 1026-1034.

(133) Vostrowsky, O.; Hirsch, A. *Angewandte Chemie-International Edition* **2004**, *43*, 2326-2329.

(134) Dyke, C. A.; Tour, J. M. *Journal of Physical Chemistry A* **2004**, *108*, 11151-11159.

(135) Hirsch, A.; Vostrowsky, O. *Functional Molecular Nanostructures* **2005**, *245*, 193-237.

(136) Chen, Z. F.; Thiel, W.; Hirsch, A. *Chemphyschem* **2003**, *4*, 93-+.

(137) Kataura, H.; Kumazawa, Y.; Maniwa, Y.; Umezu, I.; Suzuki, S.; Ohtsuka, Y.; Achiba, Y. *Synthetic Metals* **1999**, *103*, 2555-2558.

(138) Bachilo, S. M.; Strano, M. S.; Kittrell, C.; Hauge, R. H.; Smalley, R. E.; Weisman, R. B. *Science* **2002**, *298*, 2361-2366.

(139) Strano, M. S.; Dyke, C. A.; Usrey, M. L.; Barone, P. W.; Allen, M. J.; Shan, H. W.; Kittrell, C.; Hauge, R. H.; Tour, J. M.; Smalley, R. E. *Science* **2003**, *301*, 1519-1522.

(140) Strano, M. S.; Doorn, S. K.; Haroz, E. H.; Kittrell, C.; Hauge, R. H.; Smalley, R. E. *Nano Letters* **2003**, *3*, 1091-1096.

(141) Saini, R. K.; Chiang, I. W.; Peng, H. Q.; Smalley, R. E.; Billups, W. E.; Hauge, R. H.; Margrave, J. L. *Journal of the American Chemical Society* **2003**, *125*, 3617-3621.

(142) Strano, M. S. *Journal of the American Chemical Society* **2003**, *125*, 16148-16153.

(143) Wang, C. J.; Cao, Q.; Ozel, T.; Gaur, A.; Rogers, J. A.; Shim, M. *Journal of the American Chemical Society* **2005**, *127*, 11460-11468.

(144) Kim, W. J.; Usrey, M. L.; Strano, M. S. *Chemistry of Materials* **2007**, *19*, 1571-1576.

(145) Kim, W. J.; Nair, N.; Lee, C. Y.; Strano, M. S. *Journal of Physical Chemistry C* **2008**, *112*, 7326-7331.

(146) Nair, N.; Kim, W. J.; Usrey, M. L.; Strano, M. S. *Journal of the American Chemical Society* **2007**, *129*, 3946-3954.

(147) Fantini, C.; Usrey, M. L.; Strano, M. S. *Journal of Physical Chemistry C* **2007**, *111*, 17941-17946.

(148) Doyle, C. D.; Rocha, J. D. R.; Weisman, R. B.; Tour, J. M. *Journal of the American Chemical Society* **2008**, *130*, 6795-6800.

(149) Brunetti, F. G.; Herrero, M. A.; Munoz, J. D. M.; Giordani, S.; Diaz-Ortiz, A.; Filippone, S.; Ruaro, G.; Meneghetti, M.; Prato, M.; Vazquez, E. *Journal of the American Chemical Society* **2007**, *129*, 14580-+.

(150) Brunetti, F. G.; Herrero, M. A.; Munoz, J. D.; Diaz-Ortiz, A.; Alfonsi, J.; Meneghetti, M.; Prato, M.; Vazquez, E. *Journal of the American Chemical Society* **2008**, *130*, 8094-8100.

(151) Menard-Moyon, C.; Izard, N.; Doris, E.; Mioskowski, C. *Journal of the American Chemical Society* **2006**, *128*, 6552-6553.

(152) Harnon, M. A.; Stensaas, K. L.; Sugar, M. A.; Tumminello, K. C.; Allred, A. K. *Chemical Physics Letters* **2007**, *447*, 1-4.

(153) Banerjee, S.; Wong, S. S. *Journal of the American Chemical Society* **2004**, *126*, 2073-2081.

(154) Banerjee, S.; Wong, S. S. *Nano Letters* **2004**, *4*, 1445-1450.

(155) An, K. H.; Park, J. S.; Yang, C. M.; Jeong, S. Y.; Lim, S. C.; Kang, C.; Son, J. H.; Jeong, M. S.; Lee, Y. H. *Journal of the American Chemical Society* **2005**, *127*, 5196-5203.

(156) Yang, C. M.; Park, J. S.; An, K. H.; Lim, S. C.; Seo, K.; Kim, B.; Park, K. A.; Han, S.; Park, C. Y.; Lee, Y. H. *Journal of Physical Chemistry B* **2005**, *109*, 19242-19248.

(157) Seo, K.; Park, K. A.; Kim, C.; Han, S.; Kim, B.; Lee, Y. H. *Journal of the American Chemical Society* **2005**, *127*, 15724-15729.

(158) Hemraj-Benny, T.; Wong, S. S. *Chemistry of Materials* **2006**, *18*, 4827-4839.

(159) Graupner, R.; Abraham, J.; Wunderlich, D.; Vencelova, A.; Lauffer, P.; Rohrl, J.; Hundhausen, M.; Ley, L.; Hirsch, A. *Journal of the American Chemical Society* **2006**, *128*, 6683-6689.

(160) Muller, M.; Maultzsch, J.; Wunderlich, D.; Hirsch, A.; Thomsen, C. *Physica Status Solidi B-Basic Solid State Physics* **2008**, *245*, 1957-1960.

(161) Pekker, A.; Wunderlich, D.; Kamaras, K.; Hirsch, A. *Physica Status Solidi B-Basic Solid State Physics* **2008**, *245*, 1954-1956.

(162) Fernando, K. A. S.; Lin, Y.; Wang, W.; Cao, L.; Meziani, M. J.; Wang, X.; Veca, M. L.; Zhang, P. Y.; Quinn, R. A.; Allard, L. F.; Sun, Y. P. *Journal of Physical Chemistry C* **2007**, *111*, 10254-10259.

(163) Krupke, R.; Hennrich, F.; von Lohneysen, H.; Kappes, M. M. *Science* **2003**, *301*, 344-347.

(164) Chattopadhyay, D.; Galeska, L.; Papadimitrakopoulos, F. *Journal of the American Chemical Society* **2003**, *125*, 3370-3375.

(165) Joselevich, E. *Angewandte Chemie-International Edition* **2004**, *43*, 2992-2994.

(166) Joselevich, E. *Chemphyschem* **2004**, *5*, 619-624.

(167) Kim, U. J.; Furtado, C. A.; Liu, X. M.; Chen, G. G.; Eklund, P. C. *Journal of the American Chemical Society* **2005**, *127*, 15437-15445.

(168) Stevens, J. L.; Huang, A. Y.; Peng, H. Q.; Chiang, L. W.; Khabashesku, V. N.; Margrave, J. L. *Nano Letters* **2003**, *3*, 331-336.

(169) Hu, H.; Zhao, B.; Hamon, M. A.; Kamaras, K.; Itkis, M. E.; Haddon, R. C. *Journal of the American Chemical Society* **2003**, *125*, 14893-14900.

(170) Pompeo, F.; Resasco, D. E. *Nano Letters* **2002**, *2*, 369-373.

(171) Burghard, M. *Surface Science Reports* **2005**, *58*, 1-109.

(172) Jorio, A.; Souza, A. G.; Dresselhaus, G.; Dresselhaus, M. S.; Swan, A. K.; Unlu, M. S.; Goldberg, B. B.; Pimenta, M. A.; Hafner, J. H.; Lieber, C. M.; Saito, R. *Physical Review B* **2002**, *65*.

(173) Dresselhaus, M. S.; Dresselhaus, G.; Hofmann, M. *Vibrational Spectroscopy* **2007**, *45*, 71-81.

(174) Liu, X.; Pichler, T.; Knupfer, M.; Golden, M. S.; Fink, J.; Kataura, H.; Achiba, Y. *Physical Review B* **2002**, *66*.

(175) Campidelli, S.; Sooambar, C.; Diz, E. L.; Ehli, C.; Guldi, D. M.; Prato, M. *Journal of the American Chemical Society* **2006**, *128*, 12544-12552.

(176) Peng, H. Q.; Alemany, L. B.; Margrave, J. L.; Khabashesku, V. N. *Journal of the American Chemical Society* **2003**, *125*, 15174-15182.

(177) Zhang, L.; Zhang, J.; Schmandt, N.; Cratty, J.; Khabashesku, V. N.; Kelly, K. F.; Barron, A. R. *Chemical Communications* **2005**, 5429-5431.

(178) Fan, Y. W.; Burghard, M.; Kern, K. *Advanced Materials* **2002**, *14*, 130-+.

(179) Giordani, S.; Bergin, S. D.; Nicolosi, V.; Lebedkin, S.; Kappes, M. M.; Blau, W. J.; Coleman, J. N. *Journal of Physical Chemistry B* **2006**, *110*, 15708-15718.

(180) Azamian, B. R.; Coleman, K. S.; Davis, J. J.; Hanson, N.; Green, M. L. H. *Chemical Communications* **2002**, 366-367.

(181) DeBorde, T.; Joiner, J. C.; Leyden, M. R.; Minot, E. D. *Nano Letters* **2008**, *8*, 3568-3571.

(182) Plank, N. O. V.; Jiang, L. D.; Cheung, R. *Applied Physics Letters* **2003**, *83*, 2426-2428.

(183) Liang, F.; Alemany, L. B.; Beach, J. M.; Billups, W. E. *Journal of the American Chemical Society* **2005**, *127*, 13941-13948.

(184) Coleman, K. S.; Chakraborty, A. K.; Bailey, S. R.; Sloan, J.; Alexander, M. *Chemistry of Materials* **2007**, *19*, 1076-1081.

(185) Dresselhaus, M. S.; Dresselhaus, G.; Jorio, A. *Journal of Physical Chemistry C* **2007**, *111*, 17887-17893.

(186) Kelly, K. F.; Chiang, I. W.; Mickelson, E. T.; Hauge, R. H.; Margrave, J. L.; Wang, X.; Scuseria, G. E.; Radloff, C.; Halas, N. J. *Chemical Physics Letters* **1999**, *313*, 445-450.

(187) Wu, H. L.; Yang, Y. Y.; Ma, C. C. M.; Kuan, H. C. *Journal of Polymer Science Part a-Polymer Chemistry* **2005**, *43*, 6084-6094.

(188) Zeng, L. L.; Zhang, L.; Barron, A. R. *Nano Letters* **2005**, *5*, 2001-2004.

(189) Singh, P.; Campidelli, S.; Giordani, S.; Bonifazi, D.; Bianco, A.; Prato, M. *Chemical Society Reviews* **2009**, *38*, 2214-2230.

(190) Spectroscopy Volume Two; Straughan, B. P., Walker S., Eds.; Chapman and Hall: London, 1976., Ed.

(191) Bayazit, M. K.; Coleman, K. S. *Journal of the American Chemical Society* **2009**, *131*, 10670-10676.

(192) Mukherjee, A.; Combs, R.; Chattopadhyay, J.; Abmayr, D. W.; Engel, P. S.; Billups, W. E. *Chemistry of Materials* **2008**, *20*, 7339-7343.

(193) Kim, U. J.; Liu, X. M.; Furtado, C. A.; Chen, G.; Saito, R.; Jiang, J.; Dresselhaus, M. S.; Eklund, P. C. *Physical Review Letters* **2005**, *95*.

(194) Cai, L. T.; Bahr, J. L.; Yao, Y. X.; Tour, J. M. *Chemistry of Materials* **2002**, *14*, 4235-4241.

(195) Mawhinney, D. B.; Naumenko, V.; Kuznetsova, A.; Yates, J. T.; Liu, J.; Smalley, R. E. *Journal of the American Chemical Society* **2000**, *122*, 2383-2384.

(196) Rao, A. M.; Richter, E.; Bandow, S.; Chase, B.; Eklund, P. C.; Williams, K. A.; Fang, S.; Subbaswamy, K. R.; Menon, M.; Thess, A.; Smalley, R. E.; Dresselhaus, G.; Dresselhaus, M. S. *Science* **1997**, *275*, 187-191.

(197) Dyke, C. A.; Stewart, M. P.; Tour, J. M. *Journal of the American Chemical Society* **2005**, *127*, 4497-4509.

(198) Boul, P. J.; Liu, J.; Mickelson, E. T.; Huffman, C. B.; Ericson, L. M.; Chiang, I. W.; Smith, K. A.; Colbert, D. T.; Hauge, R. H.; Margrave, J. L.; Smalley, R. E. *Chemical Physics Letters* **1999**, *310*, 367-372.

(199) Kazaoui, S.; Minami, N.; Jacquemin, R.; Kataura, H.; Achiba, Y. *Physical Review B* **1999**, *60*, 13339-13342.

(200) Kazaoui, S.; Minami, N.; Kataura, H.; Achiba, Y. *Synthetic Metals* **2001**, *121*, 1201-1202.

(201) Banerjee, S.; Wong, S. S. *Journal of Physical Chemistry B* **2002**, *106*, 12144-12151.

(202) Brown, S. D. M.; Jorio, A.; Corio, P.; Dresselhaus, M. S.; Dresselhaus, G.; Saito, R.; Kneipp, K. *Physical Review B* **2001**, *63*, 8.

(203) Cooper, C. A.; Young, R. J.; Halsall, M. *Composites Part a-Applied Science and Manufacturing* **2001**, *32*, 401-411.

(204) Dresselhaus, M. S.; Jorio, A.; Hofmann, M.; Dresselhaus, G.; Saito, R. *Nano Letters*, *10*, 751-758.

(205) Spectroscopy Volume Three; Straughan, B. P., Walker S., Eds.; Chapman and Hall: London, 1976., Ed.

(206) Itkis, M. E.; Niyogi, S.; Meng, M. E.; Hamon, M. A.; Hu, H.; Haddon, R. C. *Nano Letters* **2002**, *2*, 155-159.

(207) Choi, N.; Kimura, M.; Kataura, H.; Suzuki, S.; Achiba, Y.; Mizutani, W.; Tokumoto, H. *Japanese Journal of Applied Physics Part 1-Regular Papers Short Notes & Review Papers* **2002**, *41*, 6264-6266.

(208) Zhao, W.; Song, C. H.; Zheng, B.; Liu, J.; Viswanathan, T. *Journal of Physical Chemistry B* **2002**, *106*, 293-296.

(209) Landi, B. J.; Ruf, H. J.; Worman, J. J.; Raffaelle, R. P. *Journal of Physical Chemistry B* **2004**, *108*, 17089-17095.

(210) Arai, T.; Nobukuni, S.; Sandanayaka, A. S. D.; Ito, O. *Journal of Physical Chemistry C* **2009**, *113*, 14493-14499.

(211) Ehli, C.; Rahman, G. M. A.; Jux, N.; Balbinot, D.; Guldi, D. M.; Paolucci, F.; Marcaccio, M.; Paolucci, D.; Melle-Franco, M.; Zerbetto, F.; Campidelli, S.; Prato, M. *Journal of the American Chemical Society* **2006**, *128*, 11222-11231.

(212) Chochos, C. L.; Stefopoulos, A. A.; Campidelli, S.; Prato, M.; Gregoriou, V. G.; Kallitsis, J. K. *Macromolecules* **2008**, *41*, 1825-1830.

(213) Ehli, C.; Guldi, D. M.; Herranz, M. A.; Martin, N.; Campidelli, S.; Prato, M. *Journal of Materials Chemistry* **2008**, *18*, 1498-1503.

(214) Ballesteros, B.; Campidelli, S.; de la Torre, G.; Ehli, C.; Guldi, D. M.; Prato, M.; Torres, T. *Chemical Communications* **2007**, 2950-2952.

(215) Pehrsson, P. E.; Zhao, W.; Baldwin, J. W.; Song, C. H.; Liu, J.; Kooi, S.; Zheng, B. *Journal of Physical Chemistry B* **2003**, *107*, 5690-5695.

(216) Plank, N. O. V.; Cheung, R.; Andrews, R. J. *Applied Physics Letters* **2004**, *85*, 3229-3231.

(217) Plank, N. O. V.; Forrest, G. A.; Cheung, R.; Alexander, A. J. *Journal of Physical Chemistry B* **2005**, *109*, 22096-22101.

(218) Chakraborty, A. K.; Coleman, K. S.; Dhanak, V. R. *Nanotechnology* **2009**, *20*.

(219) Huang, W. J.; Taylor, S.; Fu, K. F.; Lin, Y.; Zhang, D. H.; Hanks, T. W.; Rao, A. M.; Sun, Y. P. *Nano Letters* **2002**, *2*, 311-314.

(220) Stephenson, J. J.; Hudson, J. L.; Azad, S.; Tour, J. M. *Chemistry of Materials* **2006**, *18*, 374-377.

(221) Schmidt, G.; Gallon, S.; Esnouf, S.; Bourgoin, J. P.; Chenevier, P. *Chemistry-a European Journal* **2009**, *15*, 2101-2110.

(222) Itkis, M. E.; Perea, D. E.; Jung, R.; Niyogi, S.; Haddon, R. C. *Journal of the American Chemical Society* **2005**, *127*, 3439-3448.

(223) Usrey, M. L.; Lippmann, E. S.; Strano, M. S. *Journal of the American Chemical Society* **2005**, *127*, 16129-16135.

(224) Pels, J. R.; Kapteijn, F.; Moulijn, J. A.; Zhu, Q.; Thomas, K. M. *Carbon* **1995**, *33*, 1641-1653.

(225) Lindberg, B. J.; Hedman, J. *Chemica Scripta* **1975**, *7*, 155-166.

(226) Actis, P.; Caulliez, G.; Shul, G.; Opallo, M.; Mermoux, M.; Marcus, B.; Boukherroub, R.; Szunerits, S. *Langmuir* **2008**, *24*, 6327-6333.

(227) Sampanthar, J. T.; Neoh, K. G.; Ng, S. W.; Kang, E. T.; Tan, K. L. *Advanced Materials* **2000**, *12*, 1536-1539.

(228) Chen, G. L.; Li, Y.; Lin, J.; Huan, C. H. A.; Guo, Y. P. *Journal of Physics D-Applied Physics* **1999**, *32*, 195-199.

(229) Yuan, W. Z.; Sun, J. Z.; Dong, Y. Q.; Haussler, M.; Yang, F.; Xu, H. P.; Qin, A. J.; Lam, J. W. Y.; Zheng, Q.; Tang, B. Z. *Macromolecules* **2006**, *39*, 8011-8020.

(230) Star, A.; Liu, Y.; Grant, K.; Ridvan, L.; Stoddart, J. F.; Steuerman, D. W.; Diehl, M. R.; Boukai, A.; Heath, J. R. *Macromolecules* **2003**, *36*, 553-560.

(231) Grunlan, J. C.; Liu, L.; Kim, Y. S. *Nano Letters* **2006**, *6*, 911-915.

(232) Strano, M. S. *Nature Materials* **2006**, *5*, 433-434.

(233) Grunlan, J. C.; Liu, L.; Regev, O. *Journal of Colloid and Interface Science* **2008**, *317*, 346-349.

(234) Yang, D.; Hu, J. H.; Wang, C. C. *Carbon* **2006**, *44*, 3161-3167.

(235) Tian, Y.; He, Q.; Cui, Y.; Tao, C.; Li, J. B. *Chemistry-a European Journal* **2006**, *12*, 4808-4812.

(236) Ferry, J. D. *Viscoelastic Properties of Polymers*; New York: Wiley, **1980**.

(237) Liu, C. Y.; Zhang, J.; He, J. S.; Hu, G. H. *Polymer* **2003**, *44*, 7529-7532.

(238) Vaysse, M.; Khan, M. K.; Sundararajan, P. *Langmuir* **2009**, *25*, 7042-7049.

(239) Shi, J. H.; Guo, Z. X.; Zhan, B. H.; Luo, H. X.; Li, Y. F.; Zhu, D. B. *Journal of Physical Chemistry B* **2005**, *109*, 14789-14791.

(240) Homenick, C. M.; Sheardown, H.; Adronov, A. *Journal of Materials Chemistry*, *20*, 2887-2894.

(241) Ogoshi, T.; Takashima, Y.; Yamaguchi, H.; Harada, A. *Journal of the American Chemical Society* **2007**, *129*, 4878-+.

(242) Tagmatarchis, N.; Prato, M. *Journal of Materials Chemistry* **2004**, *14*, 437-439.

(243) Prato, M.; Kostarelos, K.; Bianco, A. *Accounts of Chemical Research* **2008**, *41*, 60-68.

(244) Pantarotto, D.; Briand, J. P.; Prato, M.; Bianco, A. *Chemical Communications* **2004**, 16-17.

(245) Kostarelos, K.; Lacerda, L.; Pastorin, G.; Wu, W.; Wieckowski, S.; Luangsivilay, J.; Godefroy, S.; Pantarotto, D.; Briand, J. P.; Muller, S.; Prato, M.; Bianco, A. *Nature Nanotechnology* **2007**, *2*, 108-113.

(246) Georgakilas, V.; Bourlinos, A.; Gournis, D.; Tsoufis, T.; Trapalis, C.; Mateo-Alonso, A.; Prato, M. *Journal of the American Chemical Society* **2008**, *130*, 8733-8740.

(247) Zhang, W.; Swager, T. M. *Journal of the American Chemical Society* **2007**, *129*, 7714-+.

(248) Alvaro, M.; Atienzar, P.; la Cruz, P.; Delgado, J. L.; Troiani, V.; Garcia, H.; Langa, F.; Palkar, A.; Echegoyen, L. *Journal of the American Chemical Society* **2006**, *128*, 6626-6635.

(249) Alvaro, M.; Atienzar, P.; de la Cruz, P.; Delgado, J. L.; Garcia, H.; Langa, F. *Journal of Physical Chemistry B* **2004**, *108*, 12691-12697.

(250) Wang, Y. B.; Iqbal, Z.; Mitra, S. *Carbon* **2005**, *43*, 1015-1020.

(251) Gundersen, L. L.; Malterud, K. E.; Negussie, A. H.; Rise, F.; Teklu, S.; Ostby, O. B. *Bioorganic & Medicinal Chemistry* **2003**, *11*, 5409-5415.

(252) Sonnenschein, H.; Hennrich, G.; Resch-Genger, U.; Schulz, B. *Dyes and Pigments* **2000**, *46*, 23-27.

(253) Padwa, A.; Austin, D. J.; Precedo, L.; Zhi, L. *Journal of Organic Chemistry* **1993**, *58*, 1144-1150.

(254) Mahon, J.; Mehta, L. K.; Middleton, R. W.; Parrick, J.; Rami, H. K. *Journal of Chemical Research-S* **1992**, 362-363.

(255) Henrick, C. A.; Ritchie, E.; Taylor, W. C. *Australian Journal of Chemistry* **1967**, *20*, 2441-&.

(256) Hubbuch, A.; Bindewald, R.; Fohles, J.; Naithani, V. K.; Zahn, H. *Angewandte Chemie-International Edition in English* **1980**, *19*, 394-396.

(257) Li, S.; Kurtz, H.; Korambath, P.; Li, Y. S. *Journal of Molecular Structure* **2000**, *550*, 235-244.

(258) Retaru, A. V.; Druta, I. D.; Oeser, T.; Muller, T. J. J. *Helvetica Chimica Acta* **2005**, *88*, 1798-1812.

(259) Henrick, C. A.; Ritchie, E.; Taylor, W. C. *Australian Journal of Chemistry* **1967**, *20*, 2467-&.

(260) Basiuk, E. V.; Monroy-Pelaez, M.; Puente-Lee, I.; Basiuk, V. A. *Nano Letters* **2004**, *4*, 863-866.

(261) Basiuk, E. V.; Gromovoy, T. Y.; Datsyuk, A. M.; Palyanytsya, B. B.; Pokrovskiy, V. A.; Basiuk, V. A. *Journal of Nanoscience and Nanotechnology* **2005**, *5*, 984-990.

(262) Yang, C. M.; Kaneko, K.; Yudasaka, M.; Iijima, S. *Physica B-Condensed Matter* **2002**, *323*, 140-142.

(263) Kikuma, J.; Yoneyama, K.; Nomura, M.; Konishi, T.; Hashimoto, T.; Mitsumoto, R.; Ohuchi, Y.; Seki, K. *Journal of Electron Spectroscopy and Related Phenomena* **1998**, *88*, 919-925.

(264) Tarabek, J.; Kavan, L.; Dunsch, L.; Kallbac, M. *Journal of Physical Chemistry C* **2008**, *112*, 13856-13861.

(265) Felten, A.; Bittencourt, C.; Pireaux, J. J. *Nanotechnology* **2006**, *17*, 1954-1959.

(266) Papagelis, K.; Kalyva, M.; Tasis, D.; Parthenios, I.; Siokou, A.; Galiotis, C. *Physica Status Solidi B-Basic Solid State Physics* **2007**, *244*, 4046-4050.

(267) Aradhya, S. V.; Garimella, S. V.; Fisher, T. S. *Journal of the Electrochemical Society* **2008**, *155*, K161-K165.

(268) Rajumon, M. K.; Hegde, M. S.; Rao, C. N. R. *Solid State Communications* **1986**, *60*, 267-270.

(269) Camalli, M.; Caruso, F.; Mattogno, G.; Rivarola, E. *Inorganica Chimica Acta* **1990**, *170*, 225-231.

(270) Jurewicz, K.; Babel, K.; Pietrzak, R.; Delpeux, S.; Wachowska, H. *Carbon* **2006**, *44*, 2368-2375.

(271) Hulicova, D.; Yamashita, J.; Soneda, Y.; Hatori, H.; Kodama, M. *Chemistry of Materials* **2005**, *17*, 1241-1247.

(272) Masarapu, C.; Wei, B. Q. *Langmuir* **2007**, *23*, 9046-9049.

(273) Raffa, V.; Ciofani, G.; Nitodas, S.; Karachalios, T.; D'Alessandro, D.; Masini, M.; Cuschieri, A. *Carbon* **2008**, *46*, 1600-1610.

(274) Rosenthal, D.; Ruta, M.; Schlogl, R.; Kiwi-Minsker, L. *Carbon*, *48*, 1835-1843.

(275) Xu, J.; Yao, P.; Li, X.; He, F. *Materials Science and Engineering B-Advanced Functional Solid-State Materials* **2008**, *151*, 210-219.

(276) Sayes, C. M.; Liang, F.; Hudson, J. L.; Mendez, J.; Guo, W. H.; Beach, J. M.; Moore, V. C.; Doyle, C. D.; West, J. L.; Billups, W. E.; Ausman, K. D.; Colvin, V. L. *Toxicology Letters* **2006**, *161*, 135-142.

(277) Swartz, W. E.; Wynne, K. J.; Hercules, D. M. *Analytical Chemistry* **1971**, *43*, 1884-&.

(278) Lee, H. U.; Park, S. Y.; Kang, Y. H.; Jeong, S. Y.; Choi, S. H.; Jahng, K. Y.; Cho, C. R. *Acta Biomaterialia*, *6*, 519-525.

(279) Feng, J. C.; Wen, G.; Huang, W.; Kang, E. T.; Neoh, K. G. *Polymer Degradation and Stability* **2006**, *91*, 12-20.

(280) Wildgoose, G. G.; Hyde, M. E.; Lawrence, N. S.; Leventis, H. C.; Jiang, L.; Jones, T. G. J.; Compton, R. G. *Langmuir* **2005**, *21*, 4584-4591.

(281) Toupin, M.; Belanger, D. *Langmuir* **2008**, *24*, 1910-1917.

(282) Toupin, M.; Belanger, D. *Journal of Physical Chemistry C* **2007**, *111*, 5394-5401.

(283) Vlahovici, A.; Druta, I.; Andrei, M.; Cotlet, M.; Dinica, R. *Journal of Luminescence* **1999**, *82*, 155-162.

(284) Becuwe, M.; Landy, D.; Delattre, F.; Cazier, F.; Fourmentin, S. *Sensors* **2008**, *8*, 3689-3705.

(285) Yue, G. H.; Wan, Y. D.; Song, S. J.; Yang, G. C.; Chen, Z. X. *Bioorganic & Medicinal Chemistry Letters* **2005**, *15*, 453-458.

(286) Nandivada, H.; Jiang, X. W.; Lahann, J. *Advanced Materials* **2007**, *19*, 2197-2208.

(287) Li, H. M.; Cheng, F. O.; Duft, A. M.; Adronov, A. *Journal of the American Chemical Society* **2005**, *127*, 14518-14524.

(288) Guo, Z.; Liang, L.; Liang, J. J.; Ma, Y. F.; Yang, X. Y.; Ren, D. M.; Chen, Y. S.; Zheng, J. Y. *Journal of Nanoparticle Research* **2008**, *10*, 1077-1083.

(289) Campidelli, S.; Ballesteros, B.; Filoramo, A.; Diaz, D. D.; de la Torre, G.; Torres, T.; Rahman, G. M. A.; Ehli, C.; Kiessling, D.; Werner, F.; Sgobba, V.; Guldi, D. M.; Cioffi, C.; Prato, M.; Bourgoin, J. P. *Journal of the American Chemical Society* **2008**, *130*, 11503-11509.

(290) Bellamy, F. D.; Ou, K. *Tetrahedron Letters* **1984**, *25*, 839-842.

(291) Zhang, C.; Lai, Z. G.; Lu, F. C. *Polymer* **1991**, *32*, 3075-3079.

(292) Cen, L.; Neoh, K. G.; Cai, Q.; Kang, E. T. *Journal of Colloid and Interface Science* **2006**, *300*, 190-199.

(293) Pantea, D.; Darmstadt, H.; Kaliaguine, S.; Roy, C. *Journal of Analytical and Applied Pyrolysis* **2003**, *67*, 55-76.

(294) Jiang, H. J.; Zhu, L. B.; Moon, K. S.; Wong, C. P. *Carbon* **2007**, *45*, 655-661.

(295) Chiang, Y. C.; Lee, C. Y. *Journal of Materials Science* **2009**, *44*, 2780-2791.

(296) Moreno-Castilla, C.; Lopez-Ramon, M. V.; Carrasco-Marin, F. *Carbon* **2000**, *38*, 1995-2001.

(297) Pantea, D.; Darmstadt, H.; Kaliaguine, S.; Roy, C. *Applied Surface Science* **2003**, *217*, 181-193.

(298) Worley, C. M.; Vannet, M. D.; Ball, G. L.; Moddeman, W. E. *Surface and Interface Analysis* **1987**, *10*, 273-279.

(299) Estrade-Szwarckopf, H. *Carbon* **2004**, *42*, 1713-1721.

(300) Silva, A. R.; Freire, C.; de Castro, B.; Freitas, M. M. A.; Figueiredo, J. L. *Microporous and Mesoporous Materials* **2001**, *46*, 211-221.

(301) Gao, Z.; Bandosz, T. J.; Zhao, Z.; Han, M.; Liang, C.; Qiu, J. *Langmuir* **2008**, *24*, 11701-11710.

(302) Goworek, J.; Swiatkowski, A.; Biniak, S. *Langmuir* **1997**, *13*, 1225-1228.

(303) Shibata, M.; Kimura, Y.; Yaginuma, D. *Polymer* **2004**, *45*, 7571-7577.

(304) Ginder, J. M.; Epstein, A. J.; Macdiarmid, A. G. *Solid State Communications* **1989**, *72*, 987-990.

(305) Yamaguchi, I.; Shigesue, S.; Sato, M. *Reactive & Functional Polymers* **2009**, *69*, 91-96.

(306) Brant, P.; Feltham, R. D. *Journal of Organometallic Chemistry* **1976**, *120*, C53-C57.

(307) Burger, K.; Tschimarov, F.; Ebel, H. *Journal of Electron Spectroscopy and Related Phenomena* **1977**, *10*, 461-465.

(308) Phanthong, C.; Somasundrum, M. *Electroanalysis* **2008**, *20*, 1024-1027.

(309) Jin, H.; Heller, D. A.; Kim, J. H.; Strano, M. S. *Nano Letters* **2008**, *8*, 4299-4304.

(310) Liu, Y.; Wu, S.; Ju, H. X.; Xu, L. *Electroanalysis* **2007**, *19*, 986-992.

(311) McAlpine, M. C.; Ahmad, H.; Wang, D. W.; Heath, J. R. *Nature Materials* **2007**, *6*, 379-384.

(312) Rivas, G. A.; Rubianes, M. D.; Pedano, M. L.; Ferreyra, N. F.; Luque, G. L.; Rodriguez, M. C.; Miscoria, S. A. *Electroanalysis* **2007**, *19*, 823-831.

(313) Salimi, A.; Noorbakhsh, A.; Mamkhezri, H.; Ghavami, R. *Electroanalysis* **2007**, *19*, 1100-1108.

(314) Salimi, A.; Izadi, M.; Hallaj, R.; Rashidi, M. *Electroanalysis* **2007**, *19*, 1668-1676.

(315) Zhang, M. G.; Smith, A.; Gorski, W. *Analytical Chemistry* **2004**, *76*, 5045-5050.

(316) Merkoci, A.; Pumera, M.; Llopis, X.; Perez, B.; del Valle, M.; Alegret, S. *Trac-Trends in Analytical Chemistry* **2005**, *24*, 826-838.

(317) Balasubramanian, K.; Burghard, M. *Analytical and Bioanalytical Chemistry* **2006**, *385*, 452-468.

(318) Kang, I. P.; Schulz, M. J.; Kim, J. H.; Shanov, V.; Shi, D. L. *Smart Materials & Structures* **2006**, *15*, 737-748.

(319) Li, Z. L.; Dharap, P.; Nagarajaiah, S.; Barrera, E. V.; Kim, J. D. *Advanced Materials* **2004**, *16*, 640-+.

(320) Hierold, C.; Jungen, A.; Stampfer, C.; Helbling, T. *Sensors and Actuators a-Physical* **2007**, *136*, 51-61.

(321) Barone, P. W.; Baik, S.; Heller, D. A.; Strano, M. S. *Nature Materials* **2005**, *4*, 86-U16.

(322) Zhao, W.; Song, C. H.; Pehrsson, P. E. *Journal of the American Chemical Society* **2002**, *124*, 12418-12419.

(323) Heller, D. A.; Jeng, E. S.; Yeung, T. K.; Martinez, B. M.; Moll, A. E.; Gastala, J. B.; Strano, M. S. *Science* **2006**, *311*, 508-511.

(324) Gruner, G. *Analytical and Bioanalytical Chemistry* **2006**, *384*, 322-335.

(325) Heller, D. A.; Baik, S.; Eurell, T. E.; Strano, M. S. *Advanced Materials* **2005**, *17*, 2793-+.

(326) Wang, F.; Gu, H. W.; Swager, T. M. *Journal of the American Chemical Society* **2008**, *130*, 5392-+.

(327) Collins, P. G.; Bradley, K.; Ishigami, M.; Zettl, A. *Science* **2000**, *287*, 1801-1804.

(328) Pengfei, Q. F.; Vermesh, O.; Grecu, M.; Javey, A.; Wang, O.; Dai, H. J.; Peng, S.; Cho, K. J. *Nano Letters* **2003**, *3*, 347-351.

(329) Snow, E. S.; Perkins, F. K.; Houser, E. J.; Badescu, S. C.; Reinecke, T. L. *Science* **2005**, *307*, 1942-1945.

(330) Allen, B. L.; Kichambare, P. D.; Star, A. *Advanced Materials* **2007**, *19*, 1439-1451.

(331) Liu, N. Y.; Cai, X. P.; Zhang, Q.; Lei, Y.; Chan-Park, M. B. *Electroanalysis* **2008**, *20*, 558-562.

(332) Jeng, E. S.; Nelson, J. D.; Prather, K. L. J.; Strano, M. S. *Small*, *6*, 40-43.

(333) Barone, P. W.; Strano, M. S. *J Diabetes Sci Technol* **2009**, *3*, 242-52.

(334) Ju, S. Y.; Kopcha, W. P.; Papadimitrakopoulos, F. *Science* **2009**, *323*, 1319-1323.

(335) Kauffman, D. R.; Shade, C. M.; Uh, H.; Petoud, S.; Star, A. *Nature Chemistry* **2009**, *1*, 500-506.

(336) Kim, J. H.; Heller, D. A.; Jin, H.; Barone, P. W.; Song, C.; Zhang, J.; Trudel, L. J.; Wogan, G. N.; Tannenbaum, S. R.; Strano, M. S. *Nature Chemistry* **2009**, *1*, 473-481.

(337) Zhao, Y. L.; Hu, L. B.; Gruener, G.; Stoddart, J. F. *Journal of the American Chemical Society* **2008**, *130*, 16996-17003.

(338) Dong, Z. P.; Yang, B.; Jin, J.; Li, J.; Kang, H. W.; Zhong, X.; Li, R.; Ma, J. T. *Nanoscale Research Letters* **2009**, *4*, 335-340.

(339) Dong, Z. P.; Jin, J.; Zhao, W. F.; Geng, H. M.; Zhao, P.; Li, R.; Ma, J. T. *Applied Surface Science* **2009**, *255*, 9526-9530.

(340) Zhang, L. B.; Tao, L.; Li, B. L.; Jing, L.; Wang, E. K. *Chemical Communications*, *46*, 1476-1478.

(341) Delattre, F.; Cazier, F.; Tine, A. *Current Analytical Chemistry* **2009**, *5*, 48-52.

(342) Surpateanu, G. G.; Becuwe, M.; Lungu, N. C.; Dron, P. I.; Fourmentin, S.; Landy, D.; Surpateanu, G. *Journal of Photochemistry and Photobiology a-Chemistry* **2007**, *185*, 312-320.

(343) Delattre, F.; Woisel, P.; Surpateanu, G.; Bria, M.; Cazier, F.; Decock, P. *Tetrahedron* **2004**, *60*, 1557-1562.

(344) Weidner, C. H.; Wadsworth, D. H.; Bender, S. L.; Beltman, D. J. *Journal of Organic Chemistry* **1989**, *54*, 3660-3664.

(345) Okada, S.; Sawada, K.; Kuroda, A.; Watanabe, S.; Tanaka, H.; Fujisawa Pharmaceutical Co., Ltd.: 1998, p 1884.

(346) She, N. F.; Gao, M.; Cao, L. P.; Wu, A. X.; Isaacs, L. *Organic Letters* **2009**, *11*, 2603-2606.

(347) Lei, Y.; Mulchandani, P.; Chen, W.; Wang, J.; Mulchandani, A. *Electroanalysis* **2003**, *15*, 1160-1164.

(348) Gui, Y. H.; Xie, C. S.; Xu, J. Q.; Wang, G. Q. *Journal of Hazardous Materials* **2009**, *164*, 1030-1035.

(349) Principles of Fluorescence Spectroscopy; Lakowicz, J. R., third ed.; Springer: Newyork, 2006.

(350) Evale, B. G.; Hanagodimath, S. M. *Journal of Luminescence* **2009**, *129*, 1174-1180.

(351) Evale, B. G.; Hanagodimath, S. M. *Journal of Luminescence*, *130*, 1330-1337.

(352) Zhao, F.; Liu, L.; Xiao, F.; Li, J.; Yan, R.; Fan, S.; Zeng, B. *Electroanalysis* **2007**, *19*, 1387-1393.

(353) Yu, H. T.; Colucci, W. J.; McLaughlin, M. L.; Barkley, M. D. *Journal of the American Chemical Society* **1992**, *114*, 8449-8454.

(354) Lommerse, J. P. M.; Price, S. L.; Taylor, R. *Journal of Computational Chemistry* **1997**, *18*, 757-774.

(355) Yoshimi, Y.; Maeda, H.; Sugimoto, A.; Mizuno, K. *Tetrahedron Letters* **2001**, *42*, 2341-2343.

(356) Dharmalingam, K.; Ramachandran, K.; Sivagurunathan, P. *Spectrochimica Acta Part a-Molecular and Biomolecular Spectroscopy* **2007**, *66*, 48-51.

(357) Hojo, M.; Hasegawa, H.; Mizobe, A.; Ohkawa, Y.; Miimi, Y. *Journal of Physical Chemistry* **1995**, *99*, 16609-16615.

(358) Dasgupta, P. K.; Moulik, S. P.; Das, A. R. *Bulletin of the Chemical Society of Japan* **1991**, *64*, 3156-3159.

(359) Oncescu, T.; Oancea, A. M.; Demaeyer, L. *Journal of Physical Chemistry* **1989**, *93*, 3526-3531.

(360) Hanagodimath, S. M.; Evale, B. G.; Manohara, S. R. *Spectrochimica Acta Part a-Molecular and Biomolecular Spectroscopy* **2009**, *74*, 943-948.

(361) Murthy, A. S. N.; Reddy, A. R. *Advances in Molecular Relaxation and Interaction Processes* **1982**, *22*, 199-221.

(362) Ilczyszyn, M. *Journal of the Chemical Society-Faraday Transactions* **1994**, *90*, 1411-1414.

(363) Palsson, L. O.; Monkman, A. P. *Advanced Materials* **2002**, *14*, 757-758.

(364) deMello, J. C.; Wittmann, H. F.; Friend, R. H. *Advanced Materials* **1997**, *9*, 230-&.

(365) Aprile, C.; Martin, R.; Alvaro, M.; Garcia, H.; Scaiano, J. C. *Chemistry of Materials* **2009**, *21*, 884-890.

(366) Roubeau, O.; Lucas, A.; Penicaud, A.; Derre, A. *Journal of Nanoscience and Nanotechnology* **2007**, *7*, 3509-3513.

(367) Olah, G. A.; Arvanaghi, M. *Angewandte Chemie-International Edition in English* **1981**, *20*, 878-879.

(368) Kolotuchin, S. V.; Meyers, A. I. *Journal of Organic Chemistry* **2000**, *65*, 3018-3026.

(369) Palomo, C.; Aizpurua, J. M.; Benito, A.; Cuerdo, L.; Fratila, R. M.; Miranda, J. I.; Linden, A. *Journal of Organic Chemistry* **2006**, *71*, 6368-6373.

(370) Reed, M. W.; Moore, H. W. *Journal of Organic Chemistry* **1988**, *53*, 4166-4171.

(371) Kukovecz, A.; Pichler, T.; Pfeiffer, R.; Kramberger, C.; Kuzmany, H. *Physical Chemistry Chemical Physics* **2003**, *5*, 582-587.

(372) Heaps, D. A.; Griffiths, P. R. *Analytical Chemistry* **2005**, *77*, 5965-5972.

(373) Thomson, C. I.; Lowe, R. M.; Ragauskas, A. J. *Carbohydrate Polymers* **2007**, *69*, 799-804.